# Journal of Engineering

A Scientific Refereed Journal
Published by College of
Engineering University of
Baghdad

August

2014

Number 8

Volume 20

# ENGINEERING

**College of Engineering**                    **University of Baghdad**

## List of Contents

# The Effective Width in Composite Steel Concrete Beams at Ultimate Loads

**Dr. Mohannad Husain   Mohsen**
Instructor
College of Engineering-University of Baghdad
email:mhnd7@yahoo.com

**Salam Naseer Mohammed***
M.Sc. student
College of Engineering-University of Baghdad
email:salamnaseer@yahoo.com

## ABSTRACT

A composite section is made up of a concrete slab attached to a steel beam by means of shear connectors. Under positive and negative bending moment, part of the slab will act as a flange of the beam, resisting the longitudinal compression or tension force. When the spacing between girders becomes large, it is evident that the simple beam theory does not strictly apply because the longitudinal stress in the flange will vary with distance from the girder web, the flange being more highly stressed over the web than in the extremities. This phenomenon is termed "shear lag".

In this paper, a nonlinear three-dimensional finite element analysis is employed to evaluate and determine the actual effective slab width of the composite steel-concrete beams by using the Analysis System computer program (ANSYS 11.0).

The of elements were used (SOLID65, LINK8, SHELL143, COMBIN39, TARGE170 and CONTA174) to model the concrete slab, the steel reinforcing bars, the steel girder, the shear connectors (including uplift and dowel action), and the interface between top flange of the steel girder and concrete slab, respectively.

Comparisons with experimental tests have been performed to validate the finite element analysis results. In general, excellent agreement between the finite element solution and the experimental results has been obtained. The maximum difference in ultimate load is about (2.9%).

Finally, parametric studies have been carried out to investigate the effect of some important parameters; these parameters include the degree of interaction, slab thickness, slab width, concrete compressive strength ($f_c'$), distribution of shear connectors, reinforcement of slab, type of loading, and boundary conditions. The effect of changing these parameters causes variety in the effective slab width and the maximum stress reaches 40.7% and 28.5%, respectively.

**Keywords:** shear lag, effective width, composite beams, partial interaction, nonlinear analysis

### العرض الفعال في العتبات المركبة من الفولاذ والخرسانة عند الحمل الاقصى

**د. مهند حسين محسن**
مدرس
كلية الهندسة – جامعة بغداد

**سلام نصير محمد**
ماجستير
كلية الهندسة – جامعة بغداد

### الخلاصة

ان المقطع المركب يتكون من شفة خرسانية مربوطة بعارضة فولاذية بواسطة روابط القص. تحت عزم الإنحناء الموجب والسالب جزء من البلاطة يعمل كجزء من العتبة لمقاومة الشد أو الانضغاط الطولي. عندما تصبح المسافة بين العوارض الفولاذية كبيرة،فان نظرية العتبة البسيطة لا تنطبق بدقة لأن الإجهاد الطولي في الحافات سيتفاوت حسب المسافة من وترة العارضة. حيث ان مناطق الشفة القريبة من الوترة تكون تحت إجهادات أكبر من الحافة البارزة،فان هذه الظاهرة تسمى "تخلف القص".

اعتمدت هذه الرسالة تحليل لاخطي ثلاثي الأبعاد ، بإستخدام طريقة العناصر المحددة ، لتقييم وتحديد عرض الشفة الفعال للعتبة الفولاذية الخرسانية المركبة بأستخدام برنامج الحاسوب (ANSYS 11.0).

SOLID65, LINK8, SHELL143, COMBIN39, TARGE170 ) أستخدمت عناصر محددة مختلفة
CONTA174) لتمثيل البلاطة الخرسانية وحديد التسليح والعارضة الفولاذية وروابط القص (متضمناً الانفصال والانزلاق)
والمنطقة البينية.

للتحقق من صحة التمثيل تم إجراء مقارنة مع فحوصات عملية لأعتاب مركبة. وقد كانت النتائج متوافقة بشكل ممتاز.
وأكبر نسبة فرق في التحمل الأقصى كانت 2.9%.

أخيراً، لقد أجريت عدة دراسات لتحري تأثير بعض المتغيرات المهمة. زمن تلك المتغيرات تأثيردرجـة الارتبـاط وتأثير سمك
البلاطة وتـاثير عرض الشفة وتأثير مقاومـة الانضـغاط للخرسـانة وتـأثير توزيـع رابطـات القص وتـأثير كميـة حديـد التسـليح فـي
البلاطة وتأثير نوع الإسناد والتحميل. إن تأثير التغاير في هذه المتغيرات قد سبب إختلاف عرض الشفة الفعـال و أعظم إجهـاد
فيها بمقدار 40.7% و 28.5% على التوالي.

## 1. INTRODUCTION
Composite steel-concrete structures are used widely in bridge and building construction. A composite member is formed when a steel component, such as an I-section beam, is attached to a concrete component, such as a floor slab or bridge deck. The fact that each material is used to take advantage of its best attributes makes composite steel-concrete construction very efficient and economical. However, the real attraction of composite construction is based on having an efficient connection of the steel to the concrete, and it is this connection that allows a transfer of forces and given composite member unique behavior [Oehlers and Bradford, 1999]. Although the word composite may refer to all kinds of different materials connected together, in this study the term composite construction means steel girder attached to a reinforced concrete slab by means of mechanical connectors, **Fig. 1**. The functions of these connectors are to transfer horizontal and normal forces between the two components, thus sustaining the composite action.

## 2. SHEAR LAG
The thin slab of cellular and beam and slab decks can be thought of as flanges of I- or T-beams. When such I- or T-beam are flexed, the compression/tension force in each flange near mid span is injected into the flange by longitudinal edge shear forces. Under the action of the axial compression and eccentric edge shear flows, the flange distorts as shown in **Fig. 2** and does not compress as assumed in simple beam theory with plane sections remaining plane. The amount of distortion depends on both the shape of the flange in plane and on the distribution of shear flow along its edge. As is shown in **Fig. 2**, a narrow flange distorts little and its behavior approximates to that assumed in simple beam theory. In contrast, the wide flanges distort seriously because the compression induced by the edge shears does not flow very far from the loaded edge, and much of each wide flange is ineffective. The decrease in flange compression away from the loaded edge due to shear distortion is called (shear lag) ,**Hamply, 1976**.
Shear lag has long been of interest to researches. **Adekola, 1974,** formulated and solved constitutive equations which relate partial interaction with shear lag by series solutions for deflections and in-plane stress in the slab to satisfy all the known boundary conditions. **Foutch** and **Chang, 1982,** investigated the effects of shear lag and shear deformation on the static and dynamic response of tapered thin-walled box beams. **Dezi et al. 2001** proposed a model for analyzing the shear-lag effect in composite beams with flexible shear connection. **Sun and Bursi, 2005,** proposed displacement-based and two-filed mixed beam elements for the linear analysis of steel–concrete composite beams with shear lag and deformable shear connection. **Chiewanichakorn et al. 2004,** introduced a three-dimensional non-linear finite element analysis to evaluate and determine the actual effective slab width of steel-composite bridge girders. **Aref et al. 2007,** investigated the behavior of steel–concrete composite girders mainly under applied negative moment to develop and apply an appropriate effective slab width definition. **Zhou 2011,** presented a new F.E.M. to be proposed for the analysis of shear lag effect in box girders under prestressing.

## 3. EFFECTIVE SLAB WIDTH
Effective width definition has traditionally been based on the distribution of longitudinal stress across the slab width. This definition takes effective width as the equivalent width of slab having a constant stress distribution across it and sustaining a force that is equal to interaction axial force in each of the elements of

the composite system. The magnitude of the constant stress is taken as the peak longitudinal stress in the slab at the slab-beam junction [Adekola, 1974[b]], as shown in **Fig. 3**.

Many researchers, **Mackey, 1961**; **Adekola, 1968**; **Ansourian, 1975**; **Heins, 1976**; **Elkelish, 1986**; and **Oehlers** and **Bradford, 1999**, used Eq. (1) to calculate the effective slab width in composite beams.

$$2\bar{b} = \frac{2\int_0^b \sigma_y \, dx}{(\sigma_y)_{max}} \tag{1}$$

Where ($2\bar{b}$) is the effective width of the concrete slab, ($b$) is a half slab width, ($\sigma_y$) represent the normal stress in the longitudinal direction in the slab at top surface, and ($\sigma_y)_{max}$ is the maximum normal stress between $0 \leq x \leq b$  **Fig. 4**.

The numerator of the Eq. (1) was calculated by an approximate method using trapezoidal rule; these calculations were done by MATLAB (R2010a) computer program.

### 3.1 Effective Width in Codes of Practice
The effective width concept has been widely recognized and implemented into different codes of practice around the world. The formulas used by various codes are shown in **Table 1**.

## 4. BRIDGE DESIGN SPECIFICATIONS
### 4.1 British Specification [BSI 1979, BSI 1982]
In part 5 of BS5400, the effective slab width ratios are defined in three Tables, which cover simply supported, cantilever, and internal spans for continuous girders. For each case, effective slab width ratios for mid-span, quarter span, and support are specified based on girder spacing to span length ratios (*s/l*). Different ratios are separately specified for uniformly distributed and concentrated load.

### 4.2 Canadian Specification [CSA 2000, CSA 2001]
In calculating flexural resistances and stresses in slab- on girder and box girder bridges with a concrete slab, whether girders are steel or concrete, a reduced cross-section defined by the following effective slab width criteria, i.e. Eqs. (2) and (3), shall be used. $2\bar{b}$ is the effective slab width, *s/2* is half girder spacing and *l* is the span length.

$$\frac{\bar{b}}{s/2} = 1 - \left\{ 1 - \frac{l}{15s/2} \right\}^3 \qquad for \quad \frac{l}{s/2} \leq 15 \tag{2}$$

$$\frac{\bar{b}}{s/2} = 1 \qquad for \quad \frac{l}{s/2} > 15 \tag{3}$$

### 4.3 Japanese Specification [JRA 1996]
In Japan, one-side effective slab width, $\lambda$, is used to calculate strength and stiffness of the girders. One-side effective slab width ($\lambda$) for uniformly distributed load and concentrate load can be computed using Eqs. (4) and (5), respectively.

$$\lambda = s/2 \qquad for \quad \frac{s/2}{l} \leq 0.05$$
$$= \left[ 1.1 - 2\left(\frac{s/2}{l}\right) \right] s/2 \qquad for \quad 0.05 < \frac{s/2}{l} < 0.3 \tag{4}$$
$$= 0.15l \qquad for \quad 0.3 \leq \frac{s/2}{l} \quad EU$$

$$\lambda = s/2 \qquad for \quad \frac{s/2}{l} \leq 0.02$$
$$= \left[ 1.06 - 3.2\left(\frac{s/2}{l}\right) + 4.5\left(\frac{s/2}{l}\right)^2 \right] s/2 \qquad for \quad 0.05 < \frac{s/2}{l} < 0.3 \tag{5}$$
$$= 0.15l \qquad for \quad 0.3 \leq \frac{s/2}{l}$$

#### 4.4 Eurocode 4 [Eurocode 4 1992, eurocode4 1997]

In Eurocode 4, the one side effective slab width shall be taken as the distance from the centerline of the girder to the center of the outstand shear connectors plus one-eighth of the effective span length but not greater than half of the geometric slab width.

#### 4.5 Australia Standard [AS 2327.1, 1996]

The effective width ( $2\bar{b}$ ) shall be calculated as the sum of the distances $2\bar{b}/2$, measured on each side of the center-line of the steel beam, where $2\bar{b}/2$ are in each case the smallest of:

a) **L/8**, where **L** is the span of the beam.
b) In the case of a concrete slab with a free edge (i.e. an edge beam situation). Either the perpendicular distance to the edge measured from the center-line of the beam, or 6 times the overall depth ($h_c$) of the concrete slab plus half the width of the steel beam flange ($b_f$).
c) In the case of a concrete slab which spans between two steel beams (i.e. either an edge beam or internal beam situation), either half the center-to-center distance between the steel beams or 8 times the overall depth ($h_c$) of the concrete slab plus half the width of the steel beam flange ($b_f$).

It must be noted that the Australian code takes into account the slab thickness in the effective slab width computations.

#### 5. ANSYS FINITE ELEMENT MODEL

ANSYS 11.0 is a comprehensive general-purpose finite element computer program. It is capable of performing static and dynamic analysis. It is a very powerful and impressive engineering tool that may be used to solve a variety of problems.

#### 5.1 Finite Element Model

A three-dimensional eight-node solid element (SOLID65) is used to model the concrete slab, while the steel reinforcement bar is modeled by a spar element (LINK8). The steel beam is modeled by a four-node shell element (SHELL143). A spar element (LINK8) is used to model shear connector to resist uplift; while the dowel action of shear connector is modeled by combine element (COMBIN39), in the modeling of interface between two surfaces a contact element (CONTA174) and target element (TARGE170) is used, as shown in **Fig. 6,** and the geometry of these elements is shown **Fig. 5.**

#### 6. FINITE ELEMENT VERIFICATIONS

The verification of the finite element modeling described above can be accomplished and comparing the results generated by the finite element analysis program (ANSYS V.11) to those obtained from the experimental test. In this paper, yam and Chapman simply composite steel-concrete beam [**Yam and Chapman, 1968**] is used to verify the accuracy and performance of the finite element models used in this study.

The simply supported composite beam, tested by yam and Chapman, is one in a series of tested beams. The beam span was 5486 mm and subjected to a concentrated load at the midspan. In the present study the chosen specimen is designated as beam (E 11). The dimensions and reinforcement details of this beam are shown in **Fig. 7.**

#### 6.1 Finite Element Idealization and Material Properties

The three-dimensional finite element mesh for one half of the beam has been used by using ANSYS 11.0 computer program, as shown in **Fig.8**. Concrete slab is idealized by using (1792) eight node brick elements (SOLID65), and steel beam is idealized by using (364) four node shell elements (SHELL143). Reinforcement is idealized by using (510) link elements (LINK8). The interface between the concrete slab and the steel beam (sticking and friction) is idealized by (112) eight node contact elements (CONTA174) and (112) eight node target elements (TARGE170). Shear connectors are idealized by (100) link elements (LINK8) to resist uplift separation. The effect of dowel action of the shear connectors through the interface between top flange of steel beam and concrete slab is idealized by (50) combine elements (COMBIN39) to resist slip. The function used to idealize the load-slip relation is:

$$Q = 31.8(1 - e^{-4.7\,\gamma}) \qquad\qquad (6)$$

Where $Q$ is the load on shear connector in (kN) and $\gamma$ is the slip in (mm) [Yam and Chapman, 1968].

The total number of nodes resulting from the above idealization is (2871) nodes, and the total number of element is (3040) elements.

Material properties of the Yam and Chapman composite beam are summarized in **Table 2**. In this analysis the symmetry has been used by using half span of the beam. The boundary condition of this beam is shown in **Fig. 8**. The roller support is obtained by constrained displacement in y-axis, and at mid span the symmetry condition is used, the symmetry condition is obtained by constrained displacement in z-axis (longitudinal axis) for all nodes and rotations in x-axis for shell elements. The load applied (510 kN) at midspan is distributed on a rectangular area, as shown in **Fig. 8.**

The results obtained using the nonlinear finite element analysis carried out for the beam (E 11) are presented and compared with the experimental data, as shown in Table 3. The experimental and nonlinear analytical load-deflection curves are shown in **Fig. 9.**

## 7. PARAMETRIC STUDY

A simply supported steel-concrete composite beam tested by Yam and Chapman (E 11) has been selected to carry out the parametric study. The parameters studied can be summarized as follows:
1) Effect of Degree of Interaction.
2) Effect of Concrete Compressive Strength (f´$_c$).
3) Effect of Longitudinal Reinforcement.

The effect of partial interaction on Yam and Chapman composite beam has been investigated. To get full interaction, a large value for the stiffness of the shear connectors used by Yam and Chapman experimentally has been used by multiplying the stiffness value by $10^6$. While for partial interaction, the number of shear connectors used by Yam and Chapman experimentally has been reduced as a percentage from the number of studs that has been used experimentally.

In this work, the uniformly distributed Load ($UDL$ kN/m$^2$) (on the overall slab) is investigated

The nonlinear finite element analysis for the simply supported steel-concrete composite beam tested by Yam and Chapman (E 11) gave the ultimate load (500 kN) in case of ($CL$) and (190.5 kN/m$^2$) in case of ($UDL$). The distribution of longitudinal stresses in the slab has different shapes along the slab as shown in the **Fig. 10**. The distribution of the effective slab widths and longitudinal stresses for Yam and Chapman composite steel-concrete beam (E 11) for several stages of loading is shown in **Figs. 11 and 12.**

The effect of partial interaction on the effective slab width and the stress distribution at midspan, with various degrees of interaction, at ultimate load are shown in **Figs. 13 and 14.**

The effect of the degree of interaction on the effective slab width and maximum stress at midspan for this beam at ultimate load is listed in **Tables 4 and 5,** respectively. Comparison of effective slab width with design specifications at ultimate load is shown in **Table 6.** From the obtained results, it can be seen that when the degree of interaction increases from 24% to the used the effective slab width decreases by 10.8% and the maximum slab stress decreases by 25.6%.

The effect of concrete compressive strength on the effective slab width and maximum stress at midspan for this beam at ultimate load is listed in **Tables 7 and 8,** respectively. From the obtained results, it is seen that when the concrete compressive strength increases from (21 MPa) to (30 MPa), the effective slab width decreases by 24.5% **Fig. 15** and the maximum slab stress decreases by 28.5%, **Fig. 16**.

The effect of longitudinal reinforcement on the effective slab width and maximum stress at midspan for this beam at ultimate load is listed in **Tables 9 and 10,** respectively. From the obtained results, it is seen that when the diameter of longitudinal reinforcement increases from (Ø12 mm) to (Ø25 mm), the effective slab width increases by 40.7% , **Fig. 17** and the maximum slab stress increases by 19.7% **,Fig. 18.**

## 8. CONCLUSIONS

1) The results indicate good estimates of failure loads compared with experimental values. The maximum difference ratio in ultimate load is about 1.9%, while the maximum difference ratio in central deflection is about 4.7%  These results reveal the accuracy and efficiency of the selected elements in ANSYS 11.0 computer program in predicting the behavior and ultimate load of composite steel-concrete beams.
2) When the degree of interaction increases from 24% to the used the effective slab width decreases by 10.8% and the maximum slab stress decreases by 25.6%.

3) When the concrete compressive strength increases from (21 MPa) to (30 MPa), the effective slab width decreases by 24.5% and the maximum slab stress decreases by 28.5%.
4) When the diameter of longitudinal reinforcement increases from (Ø12 mm) to (Ø25 mm), the effective slab width increases by 40.7% and the maximum slab stress increases by 19.7%.

## REFERENCES

➢ AASHTO LRFD Bridge Design Specifications ,2004. A*merican Association of State Highway and Transportation Officials (AASHTO), 3rd Edition*, Washington, D.C.

➢ ACI Committee 318M-08, 2008. Building Code Requirements for Structural Concrete, ACI 318M-08 and Commentary, American Concrete Institute, pp. 473.

➢ Adekola, A. O. ,1974[a]. *The Dependence of Shear Lag on Partial Interaction in Composite Beams*, International Journal of Solids Structures, Vol.10, pp. 389-400.

➢ Adekola, A. O. ,1974[b]. *On Shear Lag Effects in Orthotropic Composite Beams*, International Journal of Solids and Structures, Vol. 10, pp. 735-754.

➢ AISC ,1986. *Load and Resistance Factor Design (LRFD), Manual of Steel Construction*, 1st Edition, American Institute of Steel Construction, pp. 1124.

➢ Ansourian, P. ,1975. *An Application of the Method of Finite Elements to the Analysis of Composite Floor Systems,* Proceedings of Institution of Civil Engineers, Vol. 59, pp. 699-725.

➢ ANSYS Manual, Version 10, 2005.

➢ Aref, A. J., Chiewanichakorn, M., Chen, S. S., and Ahn, S. 2007.*Effective Slab Width Definition for Negative Moment Regions of Composite Bridges*, Journal of Bridge Engineering, ASCE, Vol.12, No.3, May, pp. 339-349.

➢ Australia standard-composite structures, part 1: Simply Supported Beam (AS 2327.1:1996). Standards Association of Australia, New South Waels.

➢ BSI (1985), Structural Use of Concrete, Part 1: Code of Practice for Design and Construction, Part 2: Code of Practice for Special Circumstances, BS8110, British Standard Institution, London.

➢ Chiewanichakorn, M., Ahn, I-S, Aref, A. J., and Chen, S. S. , 2004.*The Development of Revised Effective Slab Width Criteria for Steel-Concrete Composite Bridges*," Structures Congress, George. E. Blandford-Editor, May, pp. 22-26.

➢ CSA ,2001. *Commentary on CAN/CSA-S6-00, Canadian Highway Bridge Design Code*, CSA International (cited according to Chiewanichakorn et al., 2004).

➢ Dezi, L., Gara, F., Leoni, G., and Tarantino, A. M. , 2001.*Time-Dependent Analysis of Shear Lag Effect in Composite Beams,* Journal of Engineering Mechanics, ASCE, Vol. 127, No. 1, January, pp. 71-79.

➢ Effective Slab width, 1978. Section 1.2.4, Report of Committee 41A, Monograph on Planning and Design of Tall Buildings, Vol. SB, Chap. SB-9, SACE.

➢ Elkelish, S., and Robinson, H. ,1986. *Effective Widths of Composite Beams with Ribbed Metal Deck,*" Canadian Journal of Civil Engineering, Vol. 13, pp. 575-582.

➢ Eurocode 4 ,1992. *Design of Composite Steel and Concrete Structures*, Part 1.1: general rules and rules for buildings (ENV 1994-1-1: 1992), European committee for standardization (Cited According to Chiewanichakorn et. al., 2004).

➢ Eurocode 4 ,1997. *Design of Composite Steel and Concrete Structures*, Part 2; Composite Bridges (ENV 1994-2: 1997), European Committee for Standardization (Cited According to Chiewanichakorn et. al., 2004).

➢ FIP-C and CA ,1970. *International Recommendations for the Design and Construction of Concrete Structures,* Cement and Concrete Association, London, England, pp. 39-40. Foutch, D. A., and Chang, P. C. (1982) "A Shear Lag Anomaly," Journal of the Structural Engineering, Vol. 108, No. 7, pp. 1653-1658.

➢ Hamply, E. C., 1976. *Bridge Deck Behavior, Chapman and Hall, London* EC4P 4EE, pp. 272.

➢ Heins, C. P., and Fan, H. M. ,1976. *Effective Composite Beam Width at Ultimate Load*, Journal of the Structural Division, Proceedings of the American Society of Civil Engineers, Vol. 102, No. ST 11, November, pp. 2163-2179.

➢ JRA ,1996. *Design Specifications for Highway Bridges (Part I- In General and Part III- Steel Bridges), Japan Road Association* (in Japanese) (cited According to Chiewanichakorn et al., 2004).

➢ Mackey, S. M. E., and Wong, F. K. C. ,1961.*The Effective Width of a Composite Tee-Beam Flange,* The Structural Engineer, Vol. 39, No. 9, September, pp. 277-285.

➢ Sun, F. F., and Bursi, O. S. , 2005. *Displacement-Based and Two-Filed Mixed Variational Formulation for Composite Beams with Shear Lag*, Journal of Engineering Mechanics, ASCE, Vol.131, No. 2, February, pp. 199-210.

➢ Yam, L. C. P., and Chapman, J. C. ,1968. *The Inelastic Behavior of Simply Supported Composite Beams of Steel and Concrete,* Proceedings of the Institute of Civil Engineers, Vol. 41, December, pp. 651-683.

## NOMENCLATURE
*The following symbols are used in this paper:-*

$b$ = one-side slab width

$\bar{b}$ = one-side effective slab width

$f'_c$ = ultimate compressive strength   (Cylinder Test)

$L$ = span length of the beam

$\sigma_y$ = normal stress in the longitudinal direction

$(\sigma_y)_{max}$ = maximum normal stress in the longitudinal direction

$b_f$ = steel beam flange width
$Q$ = shear force in one shear connector
$\gamma$ = slip at the interface
$s$ = spacing of beams
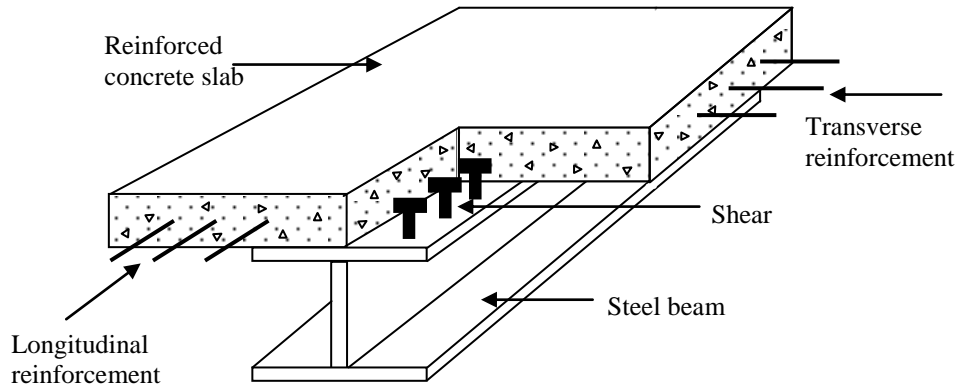


**Figure 1.** Composite beam components**.**
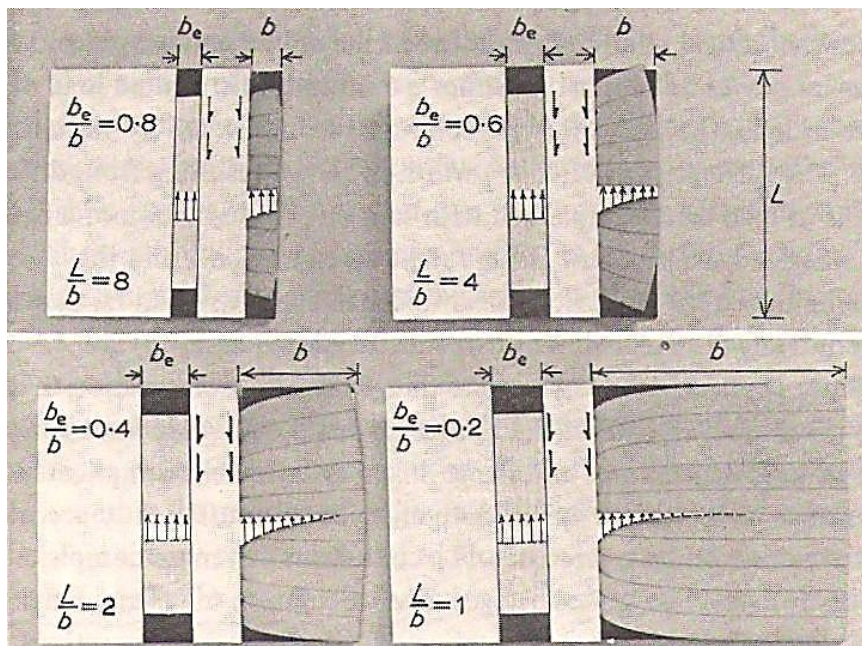


**Figure 2.** Shear lag distortion of flanges of various widths**.** [Hamply 1976].

**Figure 4.** Effective width Definition**.**

**Figure 3.** Effective slab width definition**.**
**Chiewanichakorn et al., 2004**[b]



**(a**



**(b)**



**(c)**



**(d)**



**(e)**

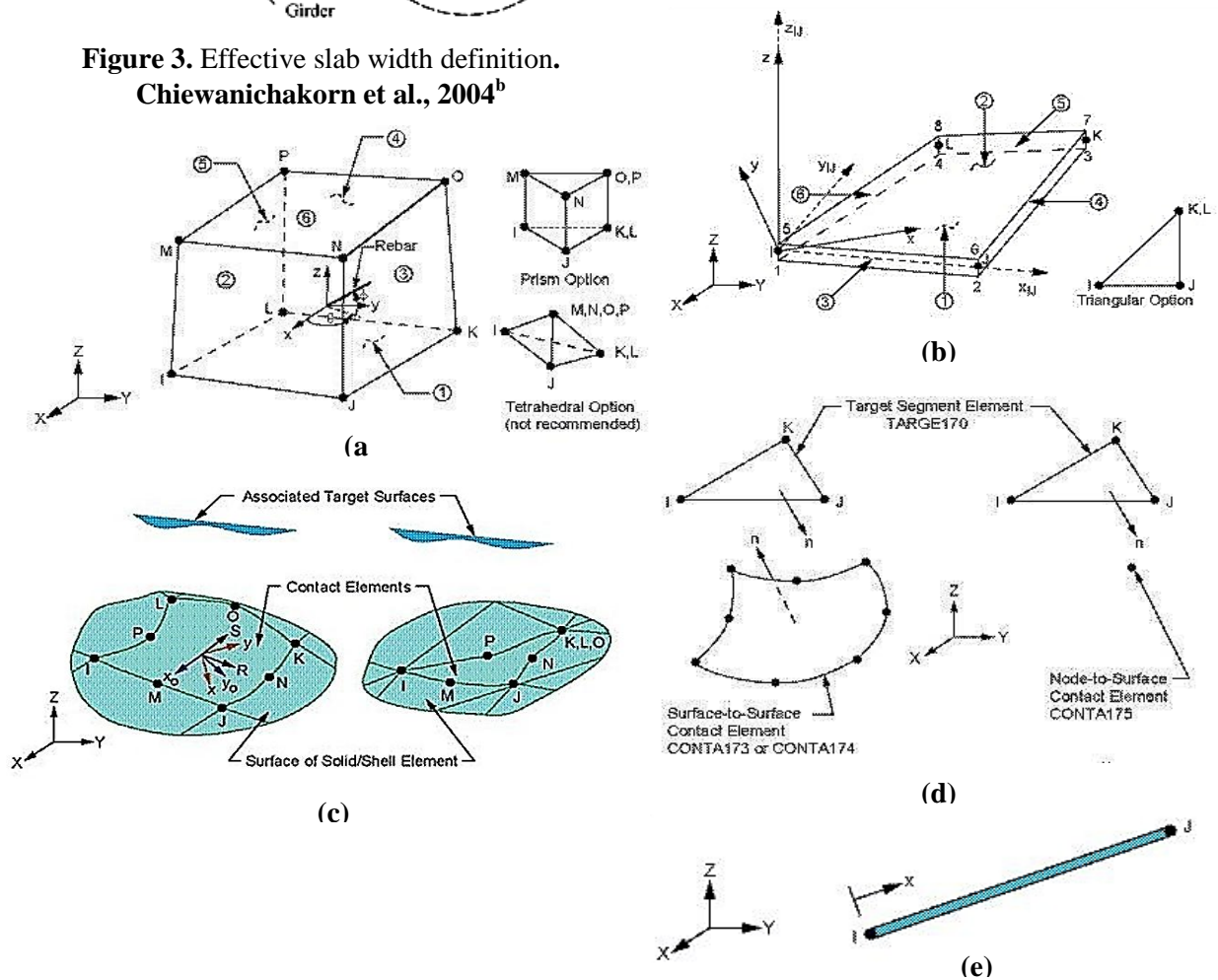**Figure 5.** Elements geometry.
(a)SOLID65 (b) SHELL143 (c) CONTA174 (d) TARGE170 (e) LINK8. [ANSYS Manual 2005]

**Table 1.** Effective width of the slab.

| Code | Formula |
|---|---|
| **AASHO [AASHO, 1944]** | $2\bar{b}$ (interior beams) is the least of:<br>**1. L/4**<br>**2. 12h$_c$ + greater of (h$_w$ or b$_f$/2)**<br>**3. average (s) of adjacent beams** |
| **AASHTO [Bowels, 1981]** | $2\bar{b}$ is least of:<br>**1. L/4**<br>**2. s**<br>**3. 12h$_c$** |
| **AASHTO-LRFD [AASHTO, 1998; AASHTO, 2004]** | $2\bar{b}$ (interior girder) is the least of:<br>**1. L/4**<br>**2. 12h$_c$ + greater of (h$_w$ or b$_f$/2)**<br>**3. average (s) of adjacent beams**<br>$2\bar{b}$ (exterior girder): ( $2\bar{b}$ (interior girder)/2) + the least of:<br>**1. L/8**<br>**2. 6h$_c$ + greater of (h$_w$/2 or top b$_f$/4)**<br>**3. overhang width** |
| **ACI [ACI 318M-08]** | $2\bar{b}$ (interior girder) is least of:<br>**1. L/4**<br>**2. s**<br>**3. b$_w$ + 16h$_c$**<br>$2\bar{b}$ (exterior girder) is least of:<br>**1. L/12+b$_w$**<br>**2. 6h$_c$+b$_w$**<br>**3. s/2+b$_w$/2** |
| **AISC [American institute of steel construction, 1999]** | $2\bar{b}$ is the least of:<br>**1. L/4**<br>**2. s**<br>**3. 2b$_e$** |
| **BS 8110 [BSI 8110 Part 1 and Part 2, 1985]** | $2\bar{b}$ is least of:<br>**1. L/5+b$_w$**<br>**2. s** |
| **CEB [FIP-C and CA, 1970]** | $2\bar{b}$ = L/8 for U.D.L.<br>$2\bar{b}$ = L/10 for point load. |
| **BS CP 117 [BSI Part 1, 1965]** | $2\bar{b}$ is least of:<br>**1. L/3**<br>**2. s**<br>**3. b$_f$ + 12h$_c$** |
| **BS CP 117 [BSI Part 2, 1967]** | **1. for s ≤ L/10:** $2\bar{b}$ = s<br>**2. for s > L/10:** $(s/2\bar{b})^2 = 1+12(s/L)^2$<br>but $2\bar{b}$ shall not be taken as less than L/10. |
| **Report of Committee 41A [Effective Slab Width, 1978]** | $2\bar{b}$ is the least of:<br>**1. L/4**<br>**2. s**<br>**3. 2b$_e$** |
| **Special Committee on Concrete and Reinforced Concrete [Special, 1916]** | $2\bar{b}$ is the least of:<br>**1. L/4**<br>**2. 12hc** |
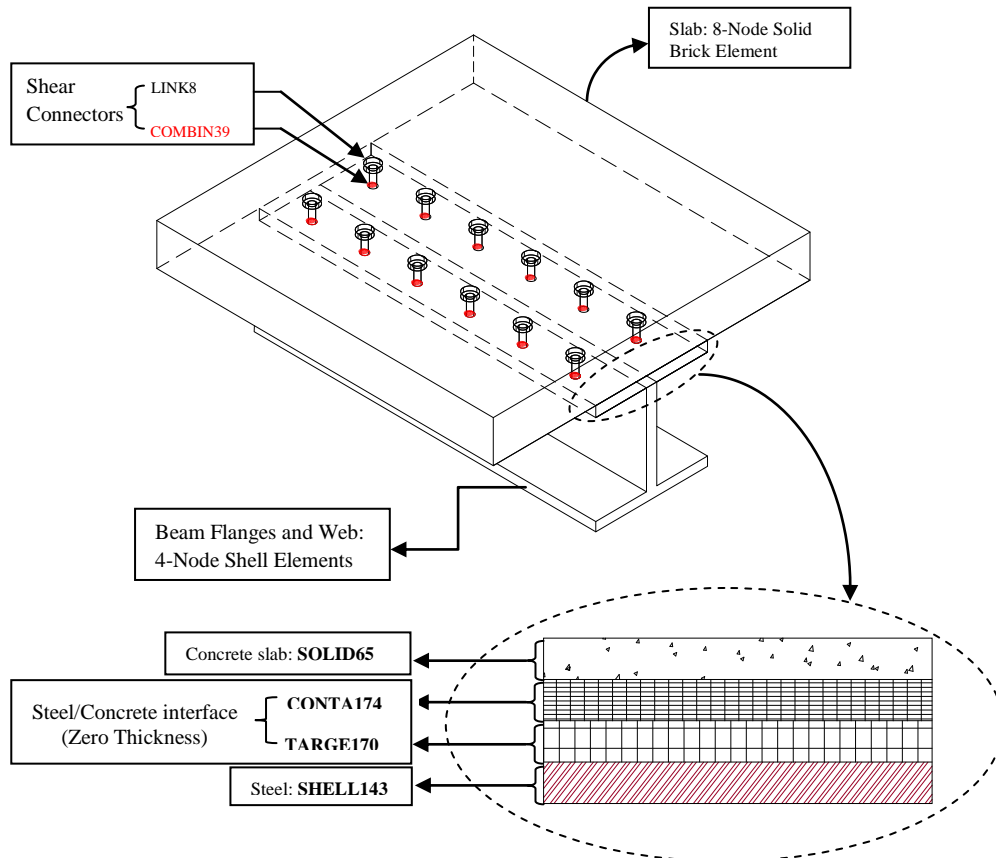
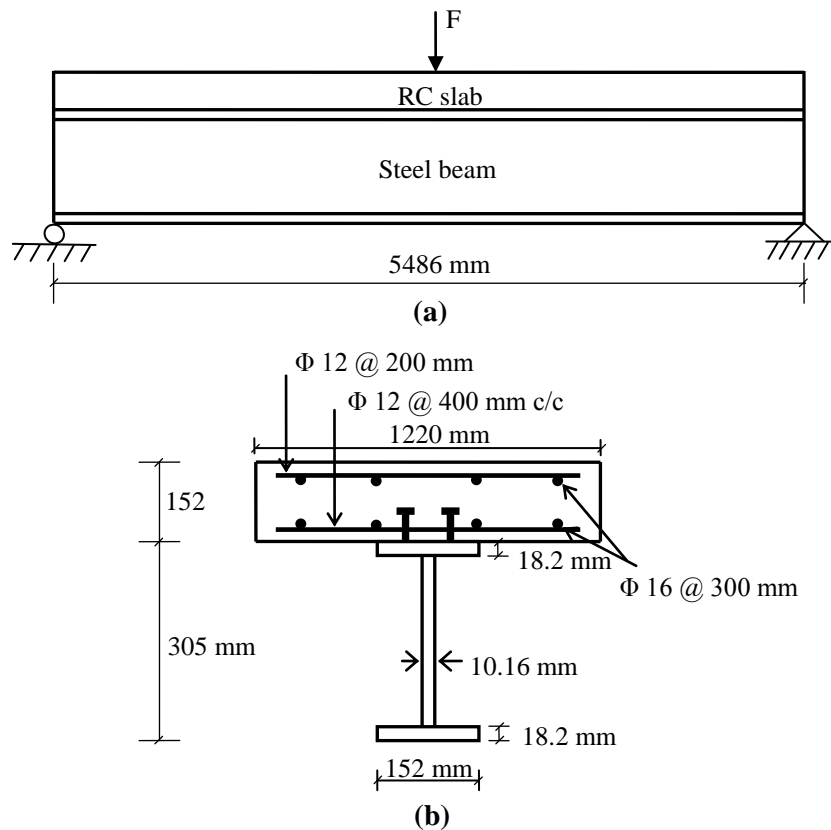**Figure 6.** Schematic drawing of finite element model for composite beam**.**



**Figure 7.** Yam and chapman test beam
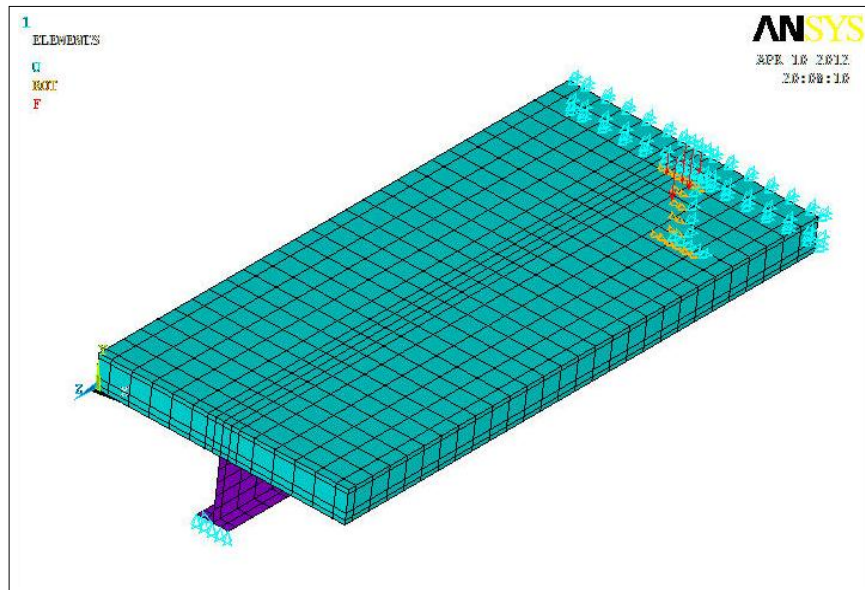(a) dimensions and loading arrangement of beam (e 11) (b) cross section**.**

**Figure 8.** Three-dimensional finite element mesh for yam and chapman
*composite steel-concrete beam (e 11).*

**Table 2.** Material properties used for yam and chapman composite steel-concrete beam (E 11).

|  | Symbol | Definition | Value |
|---|---|---|---|
| **Concrete** | $f'_c$ | **Compressive Strength (MPa)** | **50** |
| | $E_c$ | **Young's Modulus (MPa)** | **33234** |
| | $f_r$ | **Tensile Strength (MPa)** | **4.38** |
| | $v$ | **Poisson's Ratio** | **0.15\*** |
| | $\beta_o$ | **Shear Transfer Parameters** | **0.3\*** |
| | $\beta_c$ | | **0.83\*** |
| **Reinforcement** | $f_y$ | **Yield Stress (MPa)** | **265 (Ø16)** |
| | | | **265 (Ø12)** |
| | $E_s$ | **Young's Modulus (MPa)** | **205000** |
| | $v$ | **Poisson's Ratio** | **0.3** |
| | $E_w$ | **Steel Hardening Parameter (MPa)** | **4100** |
| **Steel Beam** | $f_y$ | **Yield Stress (MPa)** | **265** |
| | $E_s$ | **Young's Modulus (MPa)** | **205000** |
| | $E_w$ | **Steel Hardening Parameter (MPa)** | **4100** |
| **Shear Connector** | $H$ | **Overall Height (mm)** | **50** |
| | $\phi$ | **Diameter (mm)** | **12** |
| | $S_{stud}$ | **Spacing (mm)** | **100** |
| | $N_f$ | **Number of Studs** | **100** |
| | $f_y$ | **Yield Stress (MPa)** | **265** |
| | $E_s$ | **Young's Modulus (MPa)** | **205000** |
| | $E_w$ | **Steel Hardening Parameter (MPa)** | **4100** |
| **Interface** | $\mu$ | **Coefficient of Friction** | **0.7[†]** |

 **\***assumed value, † [ACI 318M-08]

Note: $E_c = 4700\sqrt{f'_c}$ , $E_w = 0.02\,E_s$ , $f_r = 0.62\sqrt{f'_c}$
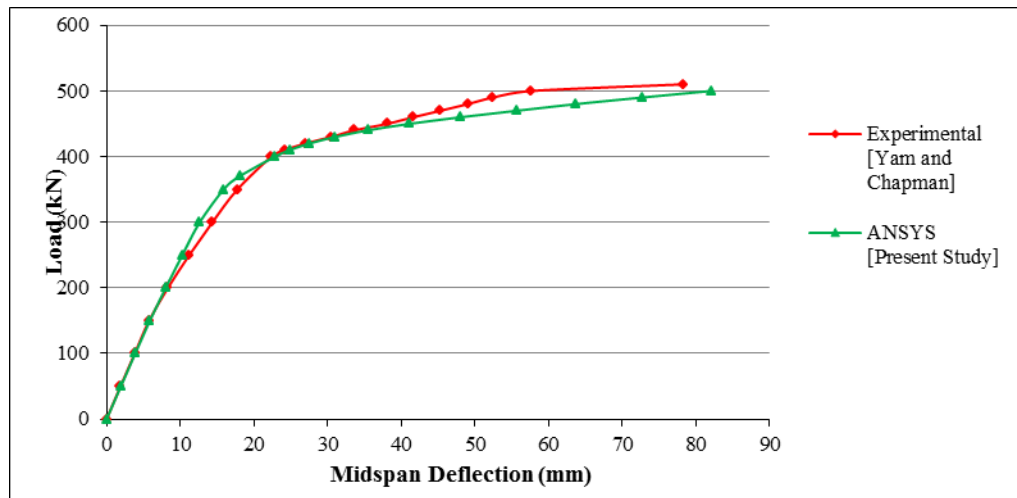
**Figure.9** Experimental and nonlinear analytical load-deflection curves for yam and chapman composite beam (e 11).

**Table 3**. Comparison between the experimental and analytical results of yam and chapman composite beam (e 11).

| | | |
|---|---|---|
| **Max. Central Defl. (mm)** | **Experimental** | **78.4** |
| | **Analytical** | **82.1** |
| **Ultimate Load (kN)** | **Experimental** | **510** |
| | **Analytical** | **500** |
| $\dfrac{\textbf{Pu (Analytical)}}{\textbf{Pu (Experimental)}}$ | | **0.98** |
| **Error in (Pu)** | | **-1.9%** |
| **Failure Mode** | | **Concrete Crushing** |



**Figure 10.** Slab top surface stress distribution for *udl* (190.5 kn/m$^2$).

**Figure 11.** Slab top surface stress distribution for several stages of loading for *udl* (190.5 kn/m$^2$) at mid span.



**Figure 12.** Effective width for several stages of loading for *udl* (190.5 kn/m$^2$).
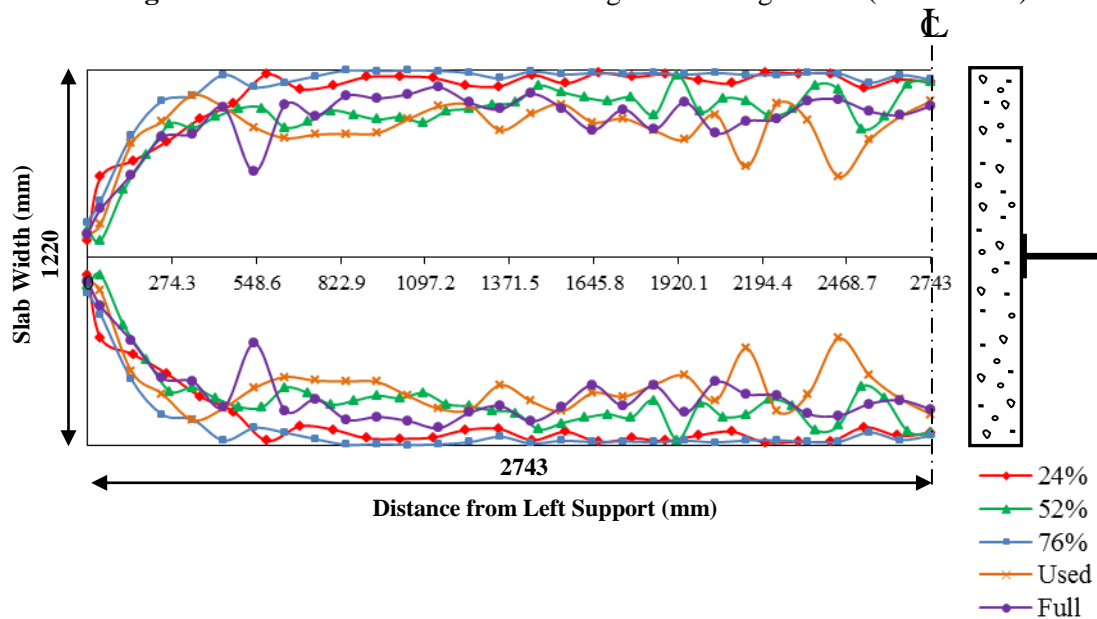


**Figure 13.** Effective width for various degrees of interaction at ultimate load for *UDL.*

14
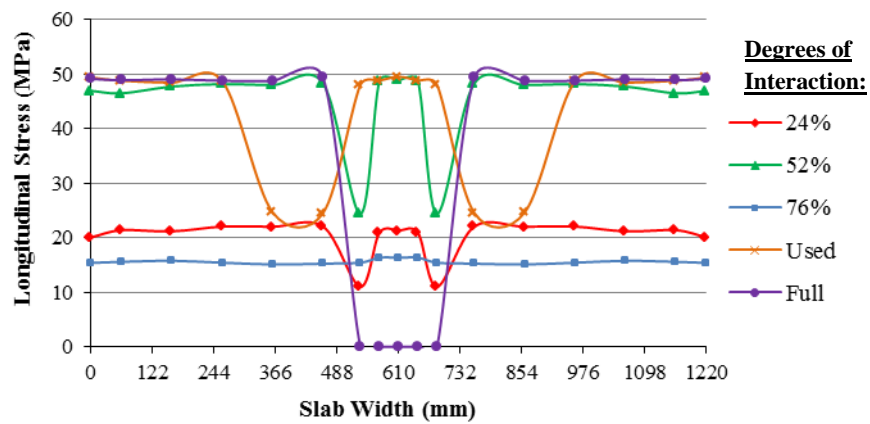
**Figure 14.** Effect of degree of interaction on the stress distribution in midspan section at ultimate load *UDL*.
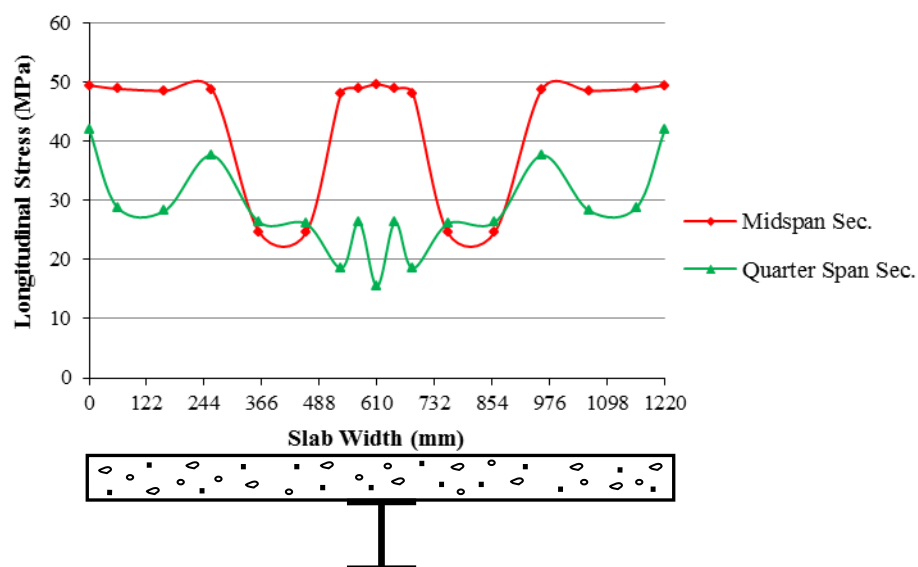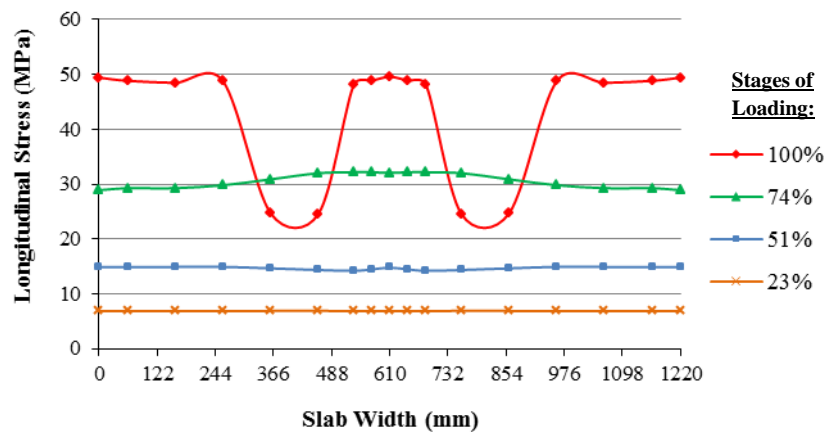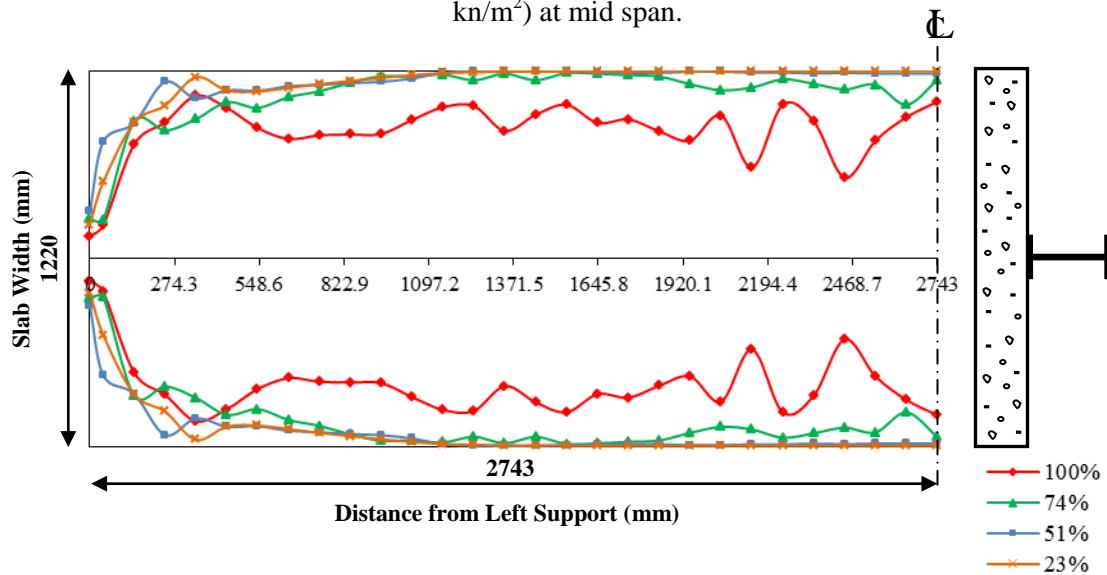
**Table 4.** Effect of degree of interaction on the maximum slab stress at ultimate load in midspan for *UDL*.

| Degree of Interaction (%) | Maximum Slab Stress Ratio ($\sigma_c/\sigma_{ca}$) |
|---|---|
| 24 | 0.753 |
| 52 | 0.396 |
| 76 | 0.431 |
| Used | 0.559 |
| Full | 0.560 |

**Table 5.** Effect of degree of interaction on the effective slab width ratio at ultimate load in midspan for *UDL*

| Degree of Interaction (%) | Effective Width Ratio ($\bar{b}/b$) |
|---|---|
| 24 | 0.934 |
| 52 | 0.934 |
| 76 | 0.948 |
| Used | 0.833 |
| Full | 0.808 |

**Table 6.** Comparison of effective slab width in midspan with design specifications at ultimate load for *UDL*

| Degree of Interaction (%) | $2\bar{b}$ (mm) | ASHTTO-LRFD | | ACI | | AISC | BS 8110 |
|---|---|---|---|---|---|---|---|
| | | Exterior | Interior | Exterior | Interior | | |
| 24 | 1139 | 1144 | 1220 | 609 | 1220 | 1220 | 1220 |
| 52 | 1140 | 1144 | 1220 | 609 | 1220 | 1220 | 1220 |
| 76 | 1156 | 1144 | 1220 | 609 | 1220 | 1220 | 1220 |
| Used | 1017 | 1144 | 1220 | 609 | 1220 | 1220 | 1220 |
| Full | 985 | 1144 | 1220 | 609 | 1220 | 1220 | 1220 |
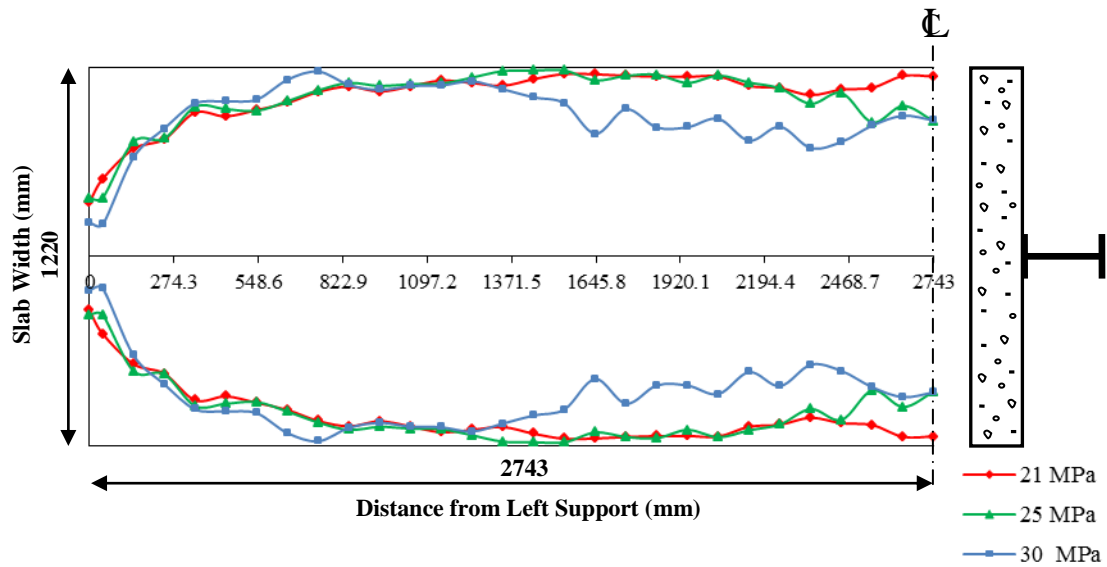
**Figure 15.** Effective width for various concrete strengths at ultimate load for *UDL*.
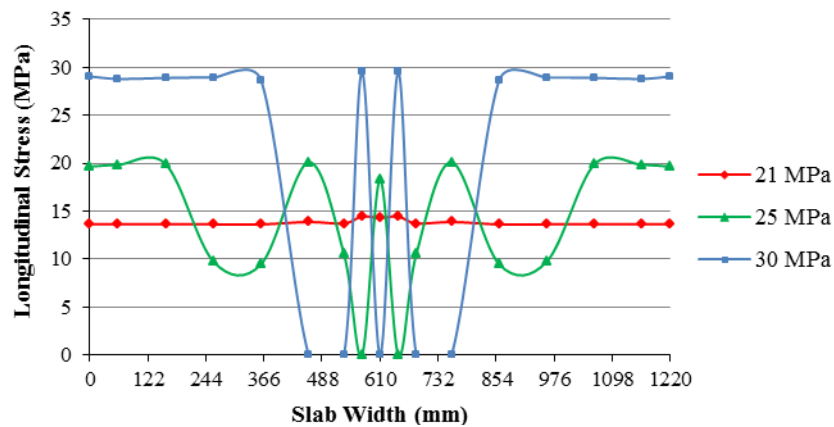


**Figure 16.** Effect of concrete strength on the stress distribution in midspan at ultimate load for *UDL*.

**Table 7.** Effect of concrete strength on the effective slab width ratio at ultimate load in midspan for *UDL*

| $f'_c$ (MPa) | Effective Width Ratio ($\bar{b}/b$) |
|---|---|
| 21 | 0.951 |
| 25 | 0.714 |
| 30 | 0.718 |

**Table 8.** Effect of concrete strength on the maximum slab stress at ultimate load in midspan for *UDL*

| $f'_c$ (MPa) | Maximum Slab Stress Ratio ($\sigma_c/\sigma_{ca}$) |
|---|---|
| 21 | |
| 25 | 0.875 |
| 30 | 0.837 |
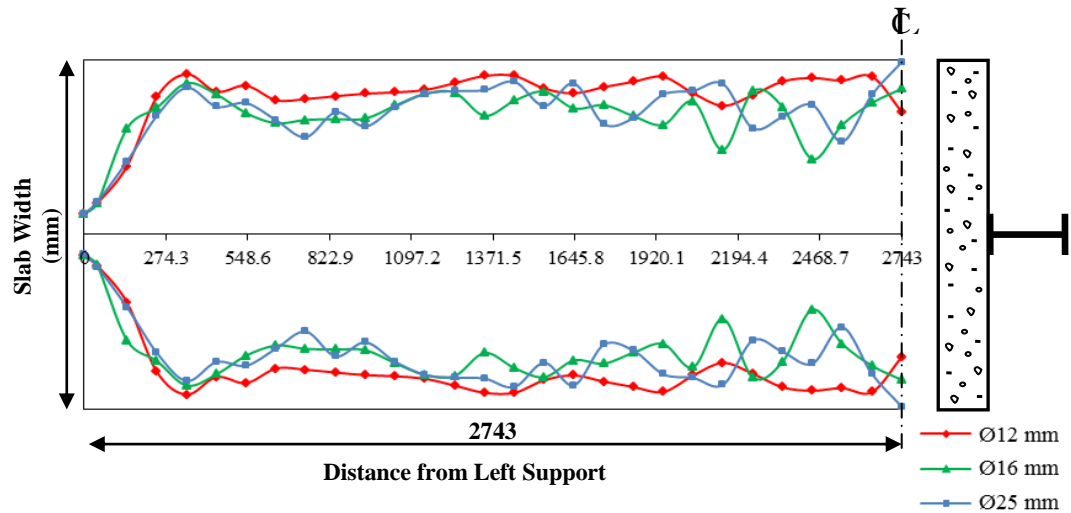
**Figure 17.** Effective width for various diameters of longitudinal reinforcement at ultimate load for *UDL*.
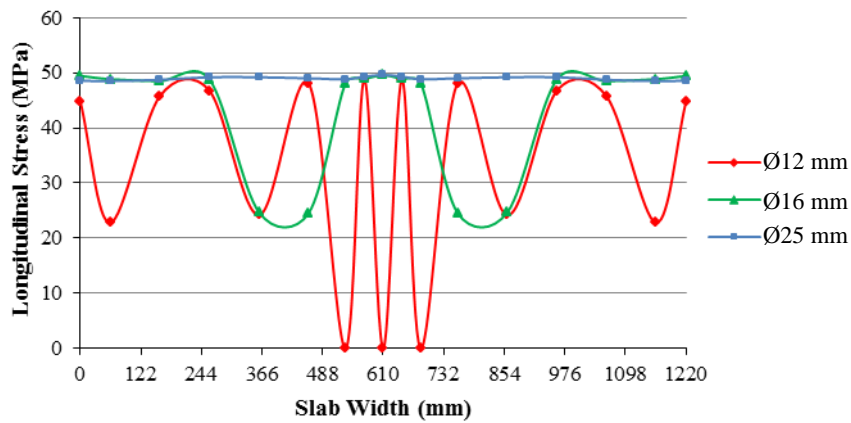


**Figure 18.** Effect of longitudinal reinforcement on the stress distribution in midspan at ultimate load for *UDL*.

**Table 9.** Effect of longitudinal reinforcement on the effective slab width ratio at ultimate load in midspan for *UDL*.

| Diameter of Longitudinal Reinforcement (mm) | Effective Width Ratio ($\bar{b}/b$) |
|:---:|:---:|
| Ø12 | 0.701 |
| Ø16 | 0.833 |
| Ø25 | 0.987 |

**Table 10.** Effect of longitudinal reinforcement on the maximum slab stress at ultimate load in midspan for *UDL*

| Diameter of Longitudinal Reinforcement (mm) | Maximum Slab Stress Ratio ($\sigma_c/\sigma_{ca}$) |
|:---:|:---:|
| Ø12 | 0.512 |
| Ø16 | 0.559 |
| Ø25 | 0.613 |

17

# PAPR Reduction of OFDM Signals Using Clipping and Coding

**Mohammed Kasim Al-Haddad**
Lecturer
Electronics and Communication Department
College of Engineering - Baghdad University
mkmih12@gmail.com

## ABSTRACT

The problem of the high peak to average ratio (PAPR) in OFDM signals is investigated with a brief presentation of the various methods used to reduce the PAPR with special attention to the clipping method. An alternative approach of clipping is presented, where the clipping is performed right after the IFFT stage unlike the conventional clipping that is performed in the power amplifier stage, which causes undesirable out of signal band spectral growth. In the proposed method, there is clipping of samples not clipping of wave, therefore, the spectral distortion is avoided. Coding is required to correct the errors introduced by the clipping and the overall system is tested for two types of modulations, the QPSK as a constant amplitude modulation and 16QAM as a varying amplitude modulation.

**Key words:** OFDM (orthogonal frequency division multiplexing), PAPR (peak to average power ratio), clipping, QPSK (quadrature phase shift keying) modulation, QAM (quadrature amplitude), channel coding.

## تخفيض قيمة PAPR لاشارات OFDM باستعمال القطع والترميز

**محمد قاسم محمد**
مدرس
قسم الالكترونيك والاتصالات
كلية الهندسة ـ جامعة بغداد

### الخلاصة

في هذا البحث دُرست مشكلة ارتفاع نسبة القمة الى المعدل القدرة PAPR في اشارات OFDM مع استعراض مختصر للطرق المختلفة المستعملة للتقليل الـ PAPR والتركيز على طريقة القطع. تم تقديم طريقة بديلة للقطع حيث يُجرى القطع بعد مرحلة الـ IFFT بعكس الطريقة التقليدية للقطع حيث يُجرى القطع في مرحلة مكبر القدرة والتي تولد نمو الطيف خارج الحزمة الخاصة بالاشارة. في الطريقة المقترحة تم قطع العينات وليس الموجة لذلك يتم تجنب تشويه الطيف. تكون الحاجة الى الترميز لاجل تصحيح الاخطاء المتولدة بسبب القطع وقد تم اختبار المنظومة ككل على تحميل QPSK الذي هو ذو سعة ثابتة وتحميل 16QAM الذي هو ذو سعة متغيرة.

**الكلمات الرئيسية:** التقسيم الترددي المتعامد، نسبة القمة الى معدل القدرة، القطع، تضمين الطور الربعي، تضمين السعة الربعي

## 1- INTRODUCTION

In modern communications the Orthogonal Frequency Division Multiplexing (OFDM) is becoming increasingly a widely used technique to transmit data due to its attractive advantages especially its immunity to multipath fading and impulsive noise, bandwidth efficiency and the fact that recent technology advancement made its complexity no longer an obstacle against implementation. This made it possible to have the OFDM to be adopted in many wireless communication systems like 802.11a, 802.11n, 802.16 and 4G mobile systems. Despite the wide spread applications of OFDM but this is mostly in systems where the high cost is affordable and non-battery operated devices, on the other hand OFDM still has limited application in mobile cell phones application because of the high peak to average power ratio (PAPR) of the OFDM signal. Such problem requires the power amplifier (PA) stage to have a relatively wide dynamic range to accommodate for the high peaks of the OFDM signal. This can lead to a low efficiency of the PA, **Reynaert, 2006** and **Hu, 2010**, and will cause a deleterious effect of the battery life which is a very undesirable to the user. There are many techniques that try to solve the high PAPR problem but each has its disadvantage; these techniques will be discussed later. Clipping is the direct and simplest technique to deal with the high PAPR problem, where the waveform is clipped whenever this waveform exceeds a specified threshold. This has the disadvantage of increasing the out of band spectral power due to the nonlinear effect on the waveform, and as it is so obvious to anyone who is involved in wireless communications, the bandwidth is becoming a very scarce resource and the OFDM is basically a solution to this problem and by using direct brutal clipping to the signal waveform, we are eliminating the advantage of OFDM that wireless communication is relying on. On the other hand regulatory authorities have strict requirements regarding radiation outside the subscriber's accommodated bandwidth. Filtering can be used to eliminate the out of band spectral growth due to clipping but this may reproduce the high peaks again, so, multistage of clipping and filtering may be required which is very demanding in terms of amount of calculation and/or cost. The traditional way of clipping where the OFDM signal is allowed to grow at a certain instance of time and then this signal is applied to a power amplifier with insufficient backoff input power which leads to clipping of the wave. In this work the clipping is made by software to the samples produced by the IFFT stage, therefore, this clipping will be referred to as the **sample clipping** as opposed to the wave clipping produced by the traditional clipping, see **Fig. 1**. Although sample clipping affects the certain sample values (that are higher than a certain threshold) and hence affects the transmitted data carrying symbols but it does not cause out of band spectral growth and does not distorts the in band spectrum. The modification of the sample value can be considered as an impulsive noise because from Eq. (4) there are N values of the data carrying symbol ck that depend on the value of a specific OFDM symbol $s(n)$.

## 2- OFDM AND THE PAPR

The idea of the OFDM transmission is that instead of sending a high rate data with rate $R_s=1/T_s$, where $T_s$ is the symbol duration, on a single carrier, the data are converted into a bank of N parallel subchannels each is transmitted by a different carrier with a fixed frequency separation given by ,**Rohling, 2011**.

$$f_s = 1/(NT_s) \tag{1}$$

where $T$ is the symbol duration, in this way the new symbol duration will be $NT$ and the new rate $R_m=1/(NT_s)$. Although the situation in terms of bandwidth seems the same because in the single carrier we are sending at rate $R_s=1/T_s$ while in the multicarrier $N$ carriers are sent with rate $R_m=1/(NT_s)$ so theoretically it is the same bandwidth, but actually wireless channels suffer from the multipath situation, where the signal arrives at different time delays at the receiver which makes different symbols to be added up at the same time at the receiver which causes what is commonly known as Inter Symbol Interference (ISI). Such channel is referred to as time dispersive channel and the amount of the ISI is considered negligible if the symbol time is much greater than the channel maximum delay spread $T_m$. So, in the single carrier situation it should be such that $T_s \gg T_m$ while in multi carrier it should be $NT_s \gg T_m$. From this it can be seen that the maximum delay spread $T_m$ is a limiting factor against increasing the symbol rate while in multicarrier transmission the condition can be met by increasing the number of carriers $N$.

The complex OFDM signal can be expressed as

$$s(t) = \sum_{k=0}^{N-1} c_k \exp(2\pi(f_o + kf_s)t) \quad 0 < t < NT \tag{2}$$

where $c_k$ is the data carrying symbol, it is a complex quantity and its values depend on the modulation and constellation shape, $f_o$ is the OFDM carrier frequency and $f_s$ is the separation frequency given by Eq. (1) which is a requirement to maintain orthogonality. In the receiver the received signal is sampled $N$ times within each OFDM symbol, that is within time equals $NT_s$ which according to Eq. (2) contains $N$ data symbols ($c_k$) this gives $N$ equations with $N$ unknowns that can be solved for the $c_k$'s. In practice this is not how it is done, returning to Eq. (2) if the carrier term is excluded and making the sampling at $t=nT_s$, the OFDM sampled signal will be

$$s(n) = \sum_{k=0}^{N-1} c_k \exp(2\pi nk / N) \quad (n=0,1,\ldots,N\text{-}1) \tag{3}$$

Eq. (3) looks so much like the Inverse Fourier Transform (IFFT) of the data symbols $c_k$. This is an important advantage of the OFDM because the IFFT can be implemented by efficient algorithms. In the receiver side the values of dada carrying symbols $c_k$ are obtained by Fast Fourier Transform (FFT) as in Eq. (4) below

$$c_k = \sum_{n=0}^{N-1} s(n) \exp(-2\pi nk / N) \quad (k=0,1,\ldots,N\text{-}1) \tag{4}$$

A simple block diagram featuring the main components of the OFDM transmitter-receiver is shown in **Fig. 2**. There are other component in the OFDM system which are not discussed here like the windowing and the cyclic prefix because they deal with the spectral shaping and equalization and these issues are not within the scope of this work and do not affect our treatment of the PAPR.

After this brief overview of the OFDM we turn our attention to the PAPR problem. The PAPR of a signal $s(t)$ can be expressed as ,**Bhad et al., 2012.**

$$PAPR = \frac{\max[s(t)]^2}{E\{[s(t)]^2\}} \tag{5}$$

where $\max[s(t)]^2$ is the maximum power, $E\{.\}$ is the expected value operator and $E\{[s(t)]^2\}$ is the average power of $s(t)$. From Eq. (2) it is clear that the OFDM signal is the sum of multiple sinusoids and it can happen that at certain instances these sinusoids add up constructively and lead to high

peak as shown in **Fig. 1**. The peak and average power of the OFDM symbol can be found from Eq. (3) as

$$P(n) = s(n)s^*(n)$$

$$P(n) = \left(\sum_{k=0}^{N-1} c_k \exp(j2\pi nk/N)\right)\left(\sum_{m=0}^{N-1} c_m^* \exp(-j2\pi nm/N)\right)$$

$$P(n) = \sum_{k=0}^{N-1}\sum_{m=0}^{N-1} c_k c_m^* \exp(j2\pi n(k-m)/N) \tag{6}$$

By making the change of variables *r=m-k* Eq. (6) becomes:

$$P(n) = \sum_{r}\sum_{m=0}^{N-1-r} c_{m-r} c_m^* \exp(-j2\pi r/N) \tag{7}$$

In the above equation the range of values of *r* in the outer summation is from –(*N*–1) to (*N*–1). The difference between the summations in Eqs. (6) and Eq. (7) can be viewed like summing elements of an *N*x*N* matrix; in Eq. (6) the summation is in row-column direction, while in Eq. (7) is in diagonals direction. The inner summation is called the aperiodic autocorrelation of *c* at displacement *r*. To find the average power the expected value of Eq. (7) is taken over the random variable *c* and it is assumed that the data symbols are independent and each has zero mean (because the constellations are usually symmetrically distributed) the terms in Eq. (7) vanish except when r=0, so the average power will be reduced to:

$$P_{av} = E[P(n)] = \sum_{m=0}^{N-1} E[|c_m|^2] \tag{8}$$

And since it is usually assumed without loss of generality that the constellation of any modulation scheme (QPSK or QAM) has normalized average power, then Eq. (8) reduces to simply

$$P_{av} = N \tag{9}$$

To find an upper bound of the expression in Eq. (7) it is known that the complex exponential term has the upper bound of 1 ($|e^{jx}|\le 1$) and the correlation term has an upper bound when all coefficients are equal to the maximum coefficient which we denote $c_M$, so from Eq. (7)

$$P(n) \le \sum_{r}\sum_{m=0}^{N-1-r} |c_M|^2 \text{ (1)} \tag{10}$$

Now the term inside the summation is constant (independent of *m* and *r*) and remember that the outer summation is over the values –(*N*–)≤ *r* ≤(*N*–1) so we will separate the case when r=0 and combine the two cases when r is positive and negative because the inner summation is the same, so, Eq. (10) will be:

$$P(n) \le |c_M|^2 N + 2\sum_{r=1}^{N-1}\sum_{m=0}^{N-1-r} |c_M|^2 = |c_M|^2 N + 2|c_M|^2 \sum_{r=1}^{N-1}(N-r)$$

$$P(n) \le |c_M|^2 N + 2|c_M|^2 \left(N(N-1) - N(N-1)/2\right)$$

$$P(n) \leq |c_M|^2 N^2 \tag{11}$$

In other words the peak power is proportional to $N^2$ with constant of proportionality equals the magnitude square of the data symbol of maximum amplitude. It should be noted that this constant equals unity for the MPSK modulation and depends on the constellation shape for the amplitude varying constellations like the QAM case. Hence we get from Eqs. (9) and (11) the peak to average power ratio

$$PAPR = N|c_M| \tag{12}$$

Sometimes this ratio is given in dB and its square root is called the crest factor. It can be seen that PAPR increases with the number of carriers and this makes the reduction of this ratio an important job.

## 3- TECHNIQUES FOR PAPR REDUCTION IN OFDM

In this section, an overview is presented for the different techniques used to reduce PAPR in OFDM. In general there is no single technique that is best in every aspect for PAPR reduction. Every technique has its own drawback in one or more of the following aspects:

1- Cost which is either in hardware or amount of calculations
2- Reduction in coding rate
3- Distortion
4- Increasing of transmission power
5- Transmission of side information

It is up to the designer to determine which of the above can be tolerated by the specific application. A brief description is presented her for the different techniques used for PAPR reduction.

### 3.1- Clipping and Filtering

Clipping is the simplest and the most straightforward technique for reducing PAPR, actually clipping alone can hardly be considered a technique because in this case the system is doing nothing and the high peaks of the OFDM signal are passed to the power amplifier that does not have enough input backoff which causes clipping of the high peaks. The clipped signal can be represented by **Joshi** and **Saini, 2011**.

$$\bar{s}(t) = \begin{cases} s(t) & |s(t)| \leq T \\ Te^{j\phi(t)} & |s(t)| > T \end{cases} \tag{13}$$

where $s(t)$ is the OFDM given by eq. (1), $T$ is the threshold and $\phi(t)$ is the phase of $s(t)$.
As a consequence the out of band spectrum will grow due to the signal distortion as shown in **Fig. 3**. Therefore, clipping is usually combined with filtering as in the work of **Bhad *et al*., 2012**, but the filtering will cause the clipped peaks to grow again so further clipping-filtering stages are usually required which in turn causes increase in cost.

### 3.2- Coding

The method of coding is based on the idea of choosing a forward error coding (FEC) scheme where the codewords have low PAPR. In this technique two goals are achieved; reducing the PAPR and providing more reliable transmission via coding. Many researches have been developed in this field

and most adopt Golay sequence to achieve low PAPR. Golay pairs are defined as the two sequences whose aperiodic autocorrelation add to zero i.e. if $a(n)$ and $b(n)$ are two sequences of length $N$ then

$$C_a(k) + C_b(k) = 0 \text{ for k=1, 2,... } N \tag{14}$$

Where

$$C_x(k) = \sum_{n=0}^{N-k-1} x(n)x(n+k) \tag{15}$$

Is called the aperiodic autocorrelation of the sequence $x(n)$. Any two sequences that satisfy Eq. (14) are called *Golay pairs* and either sequence is called a *Golay sequence*. It can be shown that Golay sequences when chosen as OFDM symbols will have PAPR of at most of 2 ($PAPR \leq 2$) irrespective of the sequence length $N$ ,**Davis** and **Jedwab, 1999**. In 1999 Davis and Jedwab devised an analytical scheme to produce Golay sequences and found a relationship between Golay sequences and Reed-Muller codes. Although their work was limited to MPSK signals up to 32 carriers it was considered a landmark that many other researchers like **Rößing *et al.*, 2001,** who expanded Davis and Jedwab work to 16QAM and archived *PAPR≤*3.6 or **Huang *et al.*, 2010,** who expanded to 64QAM achieving *PAPR≤*2.85, **Lee** and **Golomb, 2006** also expanded to 64QAM achieving *PAPR≤*4.66.

The problem with the coding method for reducing the PAPR is that the hamming distance between sequences that have low PAPR is not always high. Therefore, many sequences with low PAPR are excluded in order to satisfy the high hamming distance criteria of the coding scheme. Satisfying both conditions (low PMPR and high hamming distance) results in reduction of the coding rate and hence the information rate which strips the OFDM technique from its main advantage.

### 3.3- Selected Mapping

In selected mapping (SLM), each information sequence $D$ is mapped to $U$ different sequence blocks $X^u$ (where u=0,1,…U-1) in many cases the mapping is performed by multiplying the information sequence by random vector $B^u$ i.e.

$$X^u = B^u D \quad u = 0,1,....,U-1 \tag{16}$$

The effect of this mapping is supposed to introduce randomness in the new sequence $X^u$ such that the PAPR of $X^u$ will be lower than the PAPR of $D$ for some $u$. In other words selected mapping selects the vector $B^u$ such that $PAPR(X^u)$ is minimum over $u$ and sends the value of $u$ as a side information so that the receiver can extract the information sequence $D$. The advantage of the selected mapping is that it works for any type of modulation, while the disadvantage is that in order to find the minimum PAPR, the transmitter requires to perform the IFFT stage $U$ times and selects the output that with minimum PAPR, and this increase the cost requirement of the system. On the other hand, the requirement of sending side information is also a cost in terms of bandwidth requirement. There is another technique that is closely related to SLM which instead of the mapping used by Eq. (16), a set of interleavers is used to find one output whose PAPR is lowest to be selected for transmission. In literature, selected mapping received great deal of attention to improve performance especially in terms of computational cost, for example, **Ding** and **Lin-Bo, 2011** used a

method called Random Screening (RS-SLM) to find the mapping vector $B^u$ of Eq. (16) before the IFFT stage, so, only one IFFT stage is required. RS-SLM is based on calculating coefficients for each $X^u$ sequence, these coefficients are measures of randomness, periodicity, and period of the sequence and by using a special criterion, the sequence with the lowest PAPR can be found and sent to the IFFT stage. Although this method requires only one IFFT stage but it still requires some calculations and the authors only presented the results for limited parameters where the number of carriers $N$=64, the number of vectors $U$=8 and BPSK modulation type. **Breiling *et al*., 2001,** proposed a method that does not require explicit transmission of the side information (the mapping vector index $u$), in the traditional methods where the mapping vector index $u$ is explicitly transmitted, the whole information sequence can be lost if transmission error occurs in the value of $u$. Breiling proposed to concatenate the index $u$ at the beginning of the information sequence and feeding the resulting sequence to a scrambler, according to the value of $u$ different scrambled vectors are produced and fed to $U$ IFFT stages to choose the output with lowest PAPR. At the receiver, the received sequence is descrambled and if no transmission errors occurred, the information sequence is retrieved with the index $u$.

### 3.4- Partial Transmit Sequence

In Partial Transmit Sequence (PTS) method the signal block $X(k)$, of length $N$, is partitioned into M blocks, where $M$ is a divisor of $N$. New $M$ vectors $X^m(k)$ (m=1,2,…, M) are generated such that

$$X^m(k) = \begin{cases} X(k) & (m-1)L < k \le mL \\ 0 & otherwise \end{cases} \tag{17}$$

where $L=N/M$ is the length of the partition vector $X^m$(k). The signal block $X(k)$ can be expressed in terms of the partition vectors $X^m(k)$ by

$$X(k) = \sum_{m=1}^{M} X^m(k) \tag{18}$$

Now the vectors $X^m(k)$ are fed to $M$ IFFT stages to generate $M$ time-domain vectors $x^m(n)$ which are in turn each multiplied by a fixed phase shift number $b^m$. The sum is optimized by choosing the set of values of $b^m$ for the lowest PAPR, i.e.

$$x(n) = \sum_{m=1}^{M} b^m x^m(n) \tag{19}$$

where the values of $b^m$ are chosen from a set of phase shifts $b^m=e^{j2\pi h/W}$, where $h$=0,1,…$W$-1 and $W$ is a given integer whose value affects the performance. Eq. (19) says that the transmitted sequence is a linear combination of the outputs of the IFFT stages with each output phase-shifted by $b^m$. Now the system must make an exhaustive search for the values of $b^m$ that minimize the PAPR. In practice, without loss of performance, $b^1$=1 so the exhaustive search for the $M$-1 vectors from a set of W values gives a value of $W^{(M-1)}$ iterations and the size of the side information is $\lfloor \log_2(W^{(M-1)}) \rfloor$ where $\lfloor x \rfloor$ is the greatest integer less than or equal to $x$. In the receiver, performing the FFT to $x(n)$ results in

$$\text{FFT}[x(n)] = \sum_{m=1}^{m=M} b_m \text{FFT}[x_m(n)] = \sum_{m=1}^{m=M} b_m X_m(k) \tag{20}$$

And because of the special arrangement of $X^m(k)$ as in Eq. (17), the output of the FFT stage will be the signal vector $X(k)$ with each partition multiplied by the corresponding phase shift $b^m$ that are obtained from the transmitted side information. The main disadvantage of the PTS method is the large amount of iterations that depend of the values of $M$ and $W$, where increasing their values enhances the performance in terms of lowering the value of the PAPR while degrades the performance in terms of amount of computations **Han *et al.*, 2005**. The partitioning expressed by Eq. (17) is called adjacent partitioning and it is not the only way of partitioning, there is the interleaved and the pseudo random partitioning but the adjacent partitioning is the simplest to implement. **Lee *et al.*, 2012,** presented a tree-based method for reducing the number of iterations required to find the best phase vector, the performance is better than the exhaustive search in terms of number of iterations but it is suboptimal in terms of achieved PAPR values.

### 3.5-Tone Reservation
In tone reservation (TR) the frequency domain data sequence $D$ (of length $N$) is not composed entirely of data symbols, rather it has zero values at certain frequency indices on the other hand a sequence $A$, same length as sequence $D$, is composed of nonzero entries where $X$ has zero entry and a zero entry where $D$ has a nonzero entry. The overall sequence $X=D+A$ is fed to the IFFT stage such that

$$x(n)=\text{IFFT}[X]=\text{IFFT}[D]+\text{IFFT}[A] \tag{21}$$

The problem now become to find $A$ such that the time domain added signal IFFT[$A$] results in reduction of PAPR of the overall time domain signal $x(n)$. **Hu *et al*., 2010,** used TR and used iterative procedure in which the vector of the reserved tones is recursively updated by a special formula. The iterations stop if the number of iterations reaches a predefined number or the PAPR becomes lower than a desired threshold. In TR technique no side information is transmitted but part of the bandwidth is allocated for the reserved tones.

### 3.6-Active Constellation Expansion
Active Constellation Expansion (ACE) or Active Point Modification (APM) is to dynamically expanding the outer points of the constellation (used in mapping the data symbols) further outside or equivalently increasing the amplitude of these points in a way that does not affect the decision thresholds used to detect the received symbols and at the same time allows manipulating the values of some of the transmitted symbols in order to reduce the peaks in the time domain signal. The problem is to find a vector $C$ whose components represent the magnification factor such that IFFT[$CX$] has a minimized PAPR. **Zhou** and **Jian, 2013,** presented an ACE method based on minimizing quadratic form of $M<N$ variables, the choice of the number of variables $M$ affects performance and complexity. The ACE method does not require sending side information but its drawback beside complexity is the increase of transmitted power.

### 3.7-Tone Injection

In tone injection (TI) Technique, each point of the *M* constellation points is mapped to another set of *K* constellation points and hence the overall constellation is mapped to a new larger *KM*-point constellation that is divided into *M* sub-constellations each represents one symbol. The modulator can use either one of the *K* points to represent each symbol and the choice criteria will be to reduce the PAPR of the transmitted OFDM symbol. **Zhou** and **Jian, 2009,** proposed a multipoint mapping based scheme to eliminate the need for transmitting side information by using a QPSK constellation as information symbols and mapping this constellation to a 16 QAM constellation. The authors presented the work as a PTS scheme, but it actually falls under the TI category. Although this technique does not require transmission of side information, but the constellation expansion of the QPSK to 16 QAM means increase of average transmission power. **Goel *et al*., 2013,** introduced a similar concept except that the mapping is performed from the QPSK constellation to a concentric circles constellation. Goel et al., made a performance evaluation of these to schemes and results show the symbol error rate (SER) of the concentric circles base mapping has a 1 dB advantage over the QPSK to 16QAM mapping.

### 4- PROPOSED SYSTEM

It has been mentioned before, that clipping the OFDM waveform causes undesirable out of band spectral growth and ICI. In this work the clipping is performed in an earlier stage at the output of the IFFT stage where the signal is still in terms of samples, therefore it is referred to as sample clipping. This has the advantage of having no spectral distortion, but it still has the disadvantage of modifying samples in the time domain and this reflects on all the frequency domain samples which are actually the transmitted symbols.

$$e(n) = s(n) - \hat{s}(n) \tag{22}$$

Where, $e(n)$ is the error (noise) term, $s(n)$ is the OFDM symbol given by Eq. (3) and $\hat{s}(n)$ is the clipped OFDM symbol. This means that $e(n)$ is nonzero whenever there is a clipping event and zero when there is no clipping. So, when clipping occurs and $s(n)$ is modified, and it will be reflected on all data symbols $c_k$ (see Eq. (3)). This can be viewed as introducing a sort of impulsive noise on a block of symbols that are the input of the IFFT stage, and this situation can be managed by introducing an error correcting code to the system. Before going into more details, it should be noted that the use of coding in this work is in the general sense and it is not related to the type of coding mentioned earlier that is used to reduced the PAPR. In other words the use of coding here alone does not reduce the PAPR by itself, therefore clipping is still required. The role of the coding is to correct the errors caused by the sample clipping. Another point that is worth mentioning is that introducing a coding scheme into the system does not necessarily mean that we are adding more complexity to the system because almost in every communication system, channel coding is used, so we are only considering the system as a whole instead of focusing on specific part of the system. On the other hand the designer has more freedom to choose the appropriate coding scheme unlike the systems that rely on coding schemes alone to reduce PAPR which are limited and hence may impose certain limitation to the system like the type of modulation, code rate and coding/decoding complexity.

In this work, the convolutional coding is proposed to correct the errors introduced by the sample clipping and since it is expected that the errors due to clipping to be in the form of burst errors,

interleaving is also required and the simplest interleaving technique is used which is the block interleaving. Where the symbols are stored in a rectangular matrix with $N$ row and $L$ columns with each row containing $L$ convolutionally encoded symbols and each column with $N$ symbols to be fed to the IFFT stage, so when clipping is performed at the output of the IFFT stage in case of having a high peak sample, the error is distributed over $N$ different symbols each separated by $L$ symbols, so, the convolutional decoder will not have a burst of clipping errors in its input. The block diagram shown in **Fig. 4** illustrates the components of the proposed system.

## 5- PERFORMANCE EVALUATION

The system was tested by simulation using Matlab R2010a for two types of modulation; the QPSK and 16QAM modulations. These two modulation types were chosen to study the effect of clipping on the constant amplitude modulation (QPSK in this case) and the varying amplitude modulation (16QAM). Additie White Gaussian Noise (AWGN) was introduced as a perturbing factor to the OFDM signal in addition to the clipping error given by Eq. (22). As has been mentioned earlier, the error correcting code used is the convolutional code, the parameters used where coding rate R equals 1/2 and constraint length $K$ (which represents the error correcting capability of the covolutional code) taking the values 3, 4 and 5, with generator polynomials having octal representation [3 5], [13 15] and [23 35] respectively. The circuit diagrams of these encoders are shown in **Fig. 5**. Viterbi algorithm is used as decoding algorithm where the complexity is proportional to $2^K$. The interleaver size is 64X128 and the number of OFDM carriers is $N$=64. The bit error rate (BER) was evaluated by simulation for the different values of $K$. since the clipping will make the OFDM have maximum amplitude equals the value of the sample clipping threshold $T$, then, the PAPR can be evaluates from eq. (5) as

$$PAPR = \frac{T^2}{N} \tag{23}$$

Looking at **Fig. 6** and **Fig. 7**, it can be seen that there is a significant difference in the performance of the system for the QPSK modulation for sample clipping thresholds $T$=2 and $T$=4, which are already very small. Referring to Eq. (12) the PAPR of such signal equals to $N$=64 and from Eq. (23) the PAPR is reduced to 0.0625 and 0.25 respectively. On the other hand, **Fig. 8** and **Fig. 9** show the performance of the system for the 16QAM modulation with square constellation, it has been found that in order to achieve a comparable performance to the QPSK, the threshold of the sample clipping was chosen $T$=10 and $T$=11 which gives PAPR values of 1.56 and 1.89, this is expected because QPSK is a constant amplitude modulation and the demodulation criteria depends on the phase of the received signal not the amplitude, on the other hand, the QAM modulation is an amplitude varying modulation which makes it more sensitive to amplitude clipping. It is clear from these results that there is a significant decrease of the PAPR and if the PAPR is further slightly increased the BER will be reduced much more, so, it is up to the designer to make the proper compromise between the acceptable BER and the desired PAPR.

Further investigation of the graphs in **Fig. 6** to **Fig. 9**, it can be seen that the curves show asymptotic behavior at high values of SNR, remember that the SNR in these graphs are for the AWGN and there is already the clipping-generated noise of Eq. (22), so, when the power of the AWGN is

reduced, the clipping noise will be dominant and cause the graph to reach a certain value of BER because the clipping noise is directly related to the clipping threshold value. The graph shown in **Fig. 10** shows the amount of the SNR when a noise-free OFDM signal is clipped by a given threshold and it clearly shows that the clipping noise decrease (increase of SNR) when the clipping threshold is increased since less clipping events occurs. There are no theoretical formulas for BER performance against clipping-generated noise, but in order to assess the simulation results of **Fig. 6** to **Fig. 9**, the BER performance against AWGN is used as in **Fig. 11**, where the upper bound theoretical values of BER for 1/2 rate convolutionally encoded QPSK and 16QAM signals are plotted against AWGN energy per bit to noise spectral power ($E_b/N_o$), these curves are Matlab generated using BERTool. And the quantity ($E_b/N_o$) is related to SNR by

$$SNR(dB) = E_b / N_o(dB) + 10\log(B) \tag{24}$$

Where $B$ is the amount of information in bits per symbol and it equals to the coding rate times the number of bits per modulation symbol, so for the QPSK B=1/2x2=1 so ($E_b/N_o$)=SNR and for the 16QAM B=1/2x4=2 so the there is a 3 dB difference in this case. The vertical lines shown in the figure reflect the corresponding $E_b/N_o$ for a given clipping threshold and this is obtained from **Fig. 10** and Eq. (24). BER values are obtained from **Fig. 6** to **Fig. 9** where the curves saturate, i.e. where the clipping noise is dominant. It is seen that the QPSK case have BER values below the theoretical cures and there is 3-4 dB advantage, this means that the system has better performance handling clipping noise than AWGN. In the QAM case the BER values are over the curves and there is about 1 dB performance degradation when compared to the AWGN performance and this is because the clipping has direct effect on the symbol amplitude and demodulating QAM signal depends on phase as well as amplitude, therefore the performance is reduced unless higher value of PAPR (or clipping threshold) is allowed.

### REFERENCES

➢ Bhad, S., Gulhane, P., and Hiwale, A.S., 2012, *PAPR Reduction Scheme for OFDM*, Elsevier Procedia Technology Vol. 4 PP. 109-113.

➢ Breiling, M., Müller-Weinfurtner, S. H., and Huber, J. B., 2001, *SLM Peak-Power Reduction without Explicit Side Information*, IEEE Communications Letters, Vol. 5, No. 6, PP. 239-241.

➢ Davis, J. A., and Jedwab, J., 1999, *Peak-to-Mean Power Control in OFDM, Golay Complementary Sequences, and Reed–Muller Codes*, IEEE Transactions on Information Theory, Vol. 45, No. 7, PP. 2397-2417.

➢ Ding, W. and Lin-Bo, X., 2011, *An Improved SLM Algorithm for Reducing PAPR in OFDM System*, IEEE International Conference on  Control, Automation and Systems Engineering (CASE), PP. 1-3.

➢ Goel, A.; Gupta, P., Agrawal, M., 2012, *Concentric Circle Mapping Based PTS for PAPR Reduction in OFDM without Side Information*, Proceedings of 6th IEEE Conference on Wireless Communication and Sensor Networks, Allahabad, India, pp. 201–204.

➢ Goel, A.; Gupta, P., Agrawal, M., 2013, *SER Analysis of PTS Based Techniques for PAPR Reduction in OFDM Systems*, Elsevier Digital Signal Processing Vol. 23 PP. 302–313.

➢ Han, S. H., and Lee, J. H., 2005, *An Overview of Peak-to-Average Power Ratio Reduction Techniques for Multicarrier Transmission*, Wireless Communications, IEEE, Vol. 12, No. 2, PP. 56-65.

➢ Hu, S.; Wu, G., Wen, Q., Xiao, Y., and Li, S., 2010 *Nonlinearity Reduction by Tone Reservation with Null Subcarriers for WiMAX System*, Springer, Wireless Personal Communications Vol. 54 PP. 289-305.

➢ Huang, S. C., Wu, H., Chang, S. Y., and Liu, X.,2010 *Novel Sequence Design for Low-PMEPR and High-Code-Rate OFDM Systems*, IEEE Transactions on Communications, Vol. 58, No. 2, PP. 405-410.

➢ Joshi, A. and Saini, D. S., 2011, *PAPR Analysis of Coded- OFDM System and Mitigating its Effect with Clipping, SLM and PTS*, Proceedings of the 5th International Conference on IT & Multimedia at UNITEN (ICIMU 2011) Malaysia., PP. 118-122.

➢ Lee, H., and Golomb, S. W., 2006, *A New Construction of 64-QAM Golay Complementary Sequences*, IEEE Transactions on Information Theory, Vol. 52, No. 4, PP. 1663-1670.

➢ Lee, B. M., Figueiredo, R., and Kim, Y., 2012, *A Computationally Efficient Tree-PTS Technique for PAPR Reduction of OFDM Signals*, Springer Wireless Personal Communications, Vol. 62, No. 2, PP. 431-442.

➢ Reynaert, P., and Steyaert, M., 2006, *RF Power Amplifiers for Mobile Communications*. Springer ACSP.

➢ Rohling, H., 2011, *OFDM Concepts for Future Communication Systems,* Springer.

➢ Rößing, C. and Tarokh, V., 2001, *A Construction of OFDM 16-QAM Sequences Having Low Peak Powers*, IEEE Transactions on Information Theory, Vol. 47, No. 5, PP. 2091-2094.

➢ Ryan, W. E. and Lin, S., 2009 *Channel Codes*, Cambridge University Press.

➢ Zhou, Y. and Jiang, T., 2013 *Active Point Modification for Sidelobe Suppression with PAPR Constraint in OFDM Systems*, Springer Wireless Networks, Vol. 19, No. 7 PP. 1653-1663,

➢ Zhou, Y. and Jiang, T., 2009 *A Novel Multi-Point Square Mapping Combined with PTS to Reduce PAPR of OFDM signals without Side Information*, IEEE Trans. Broadcast. Vol. 55 PP. 831-835.
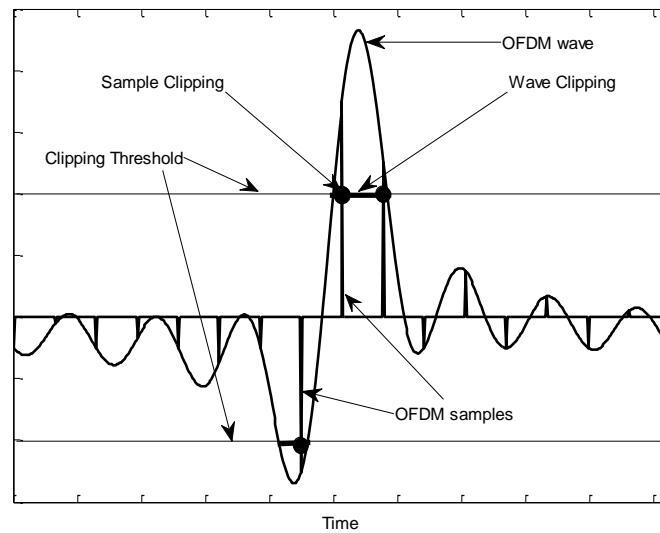
**Figure 1.** An OFDM signal before and after the LPF showing high peaks over the clipping threshold.
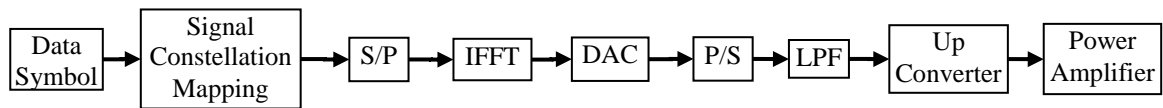


**Figure 2-a.** OFDM transmitter.
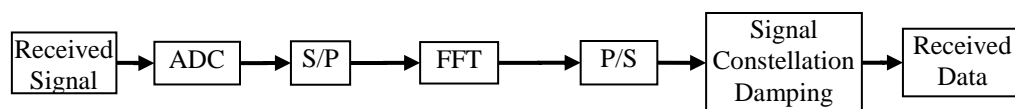


**Figure 2-b.** OFDM receiver.
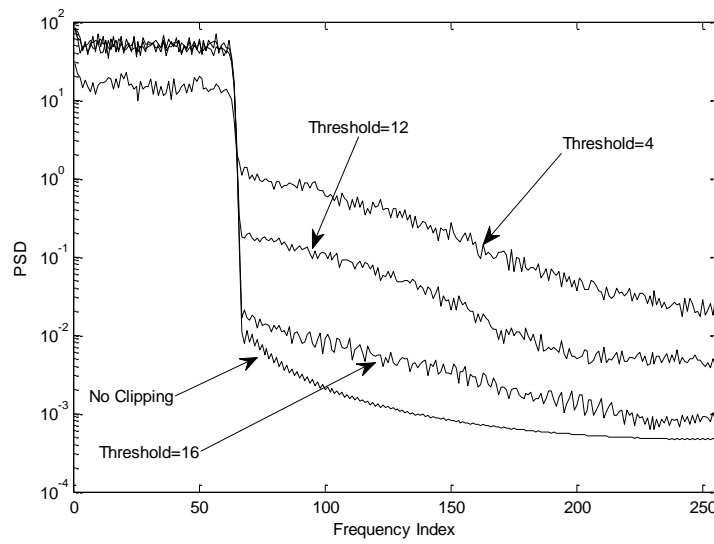
**Figure 3.** The spectrum of OFDM signals with N=64 and different clipping thresholds.
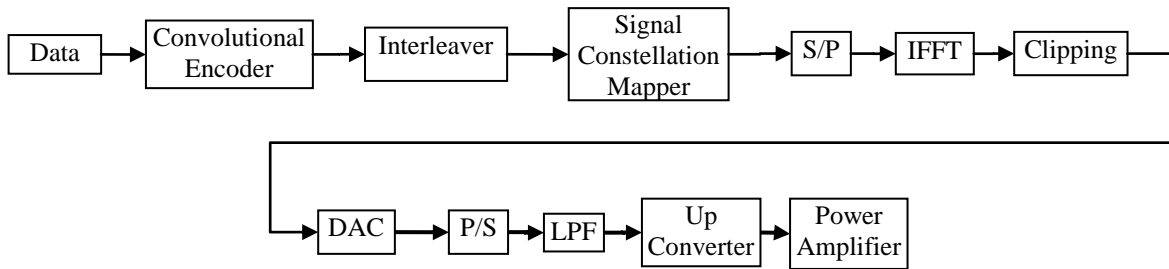


**Figure 4-a.** Proposed OFDM transmitter with clipping and coding.
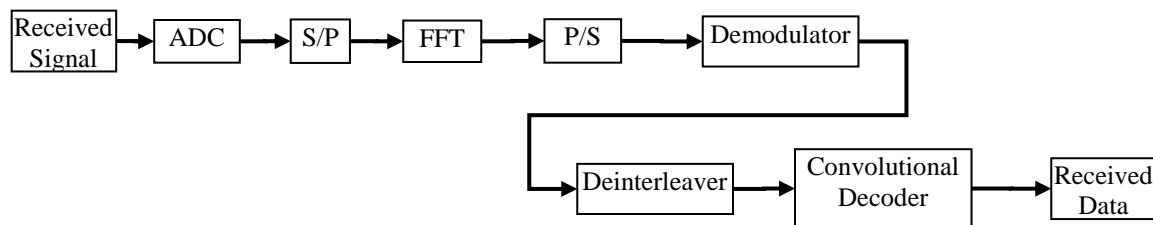


**Figure 4-b.** Proposed OFDM receiver with clipping and coding.

K=3

K=4

K=5
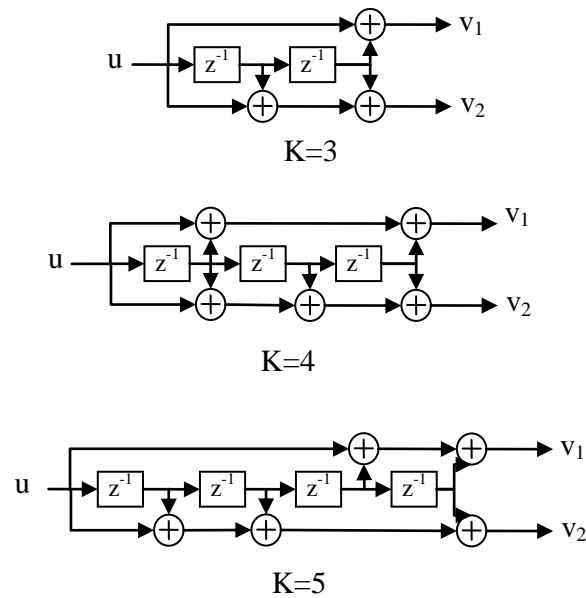
**Figure 5.** The three convolutional encoders used in the proposed transmitter.
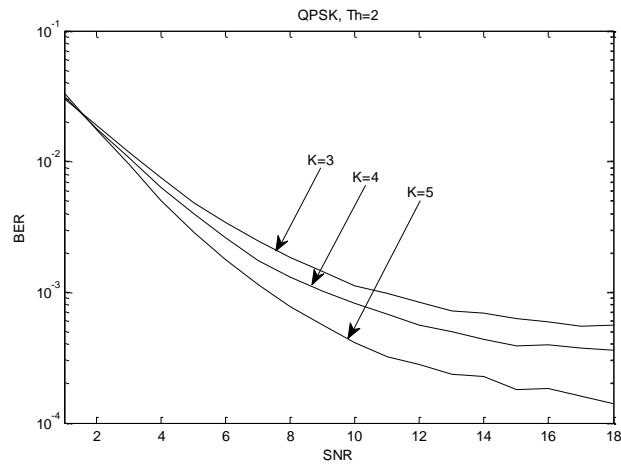


**Figure 6.** BER vs. SNR for QPSK signal and clipping threshold T=2 (PAPR=0.0625).
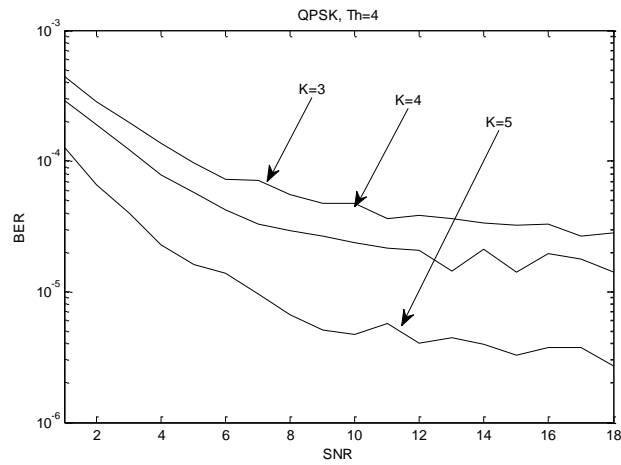
**Figure 7.** BER vs. SNR for QPSK signal and clipping threshold T=4 (PAPR=0.25).
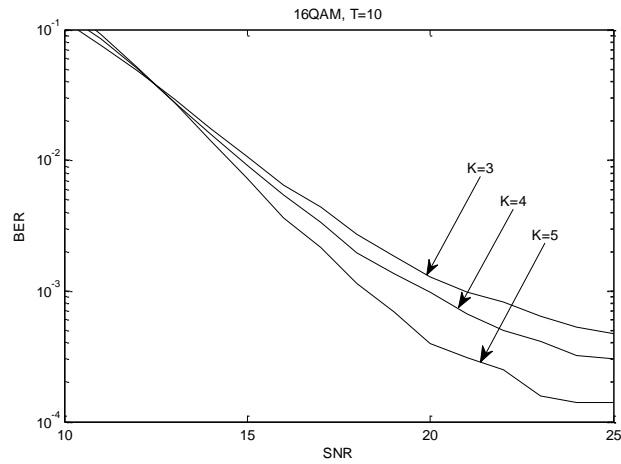


**Figure 8.** BER vs. SNR for 16QAM signal and clipping threshold T=10 (PAPR=1.56).
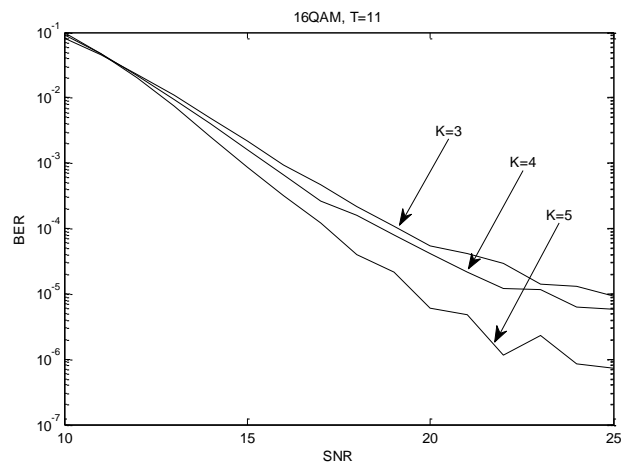


**Figure 9.** BER vs. SNR for 16QAM signal and clipping threshold T=11 (PAPR=1.89).
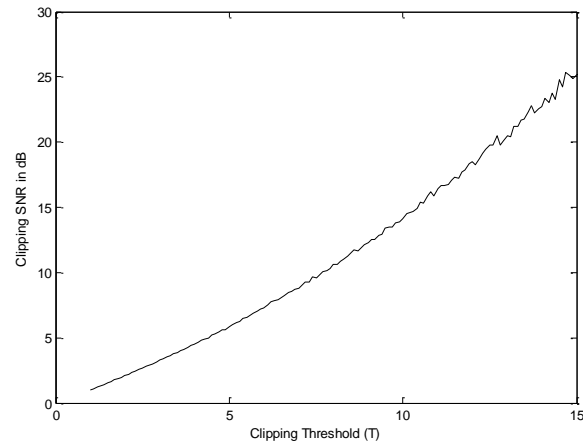
**Figure 10.** Clipping signal-to-noise ration versus clipping threshold.
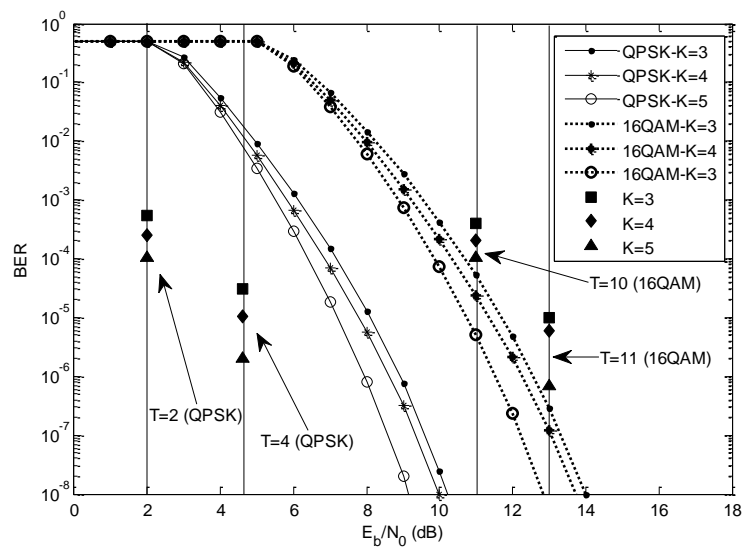


**Figure 11.** Comparison of simulated BER results with theoretical upper bound performance against AWGN.

# Scheduling of Leaching Requirements to Prevent the Secondary Salinisation in the Root Zone

**Amer H. Al-haddad**
Assist. Prof.
Water Resources Eng. Dept.
Ameralhaddad1950@yahoo.com

**Kolood A. Hussien**
M.Sc.
Water Resources Eng. Dept.

## ABSTRACT

Leaching scheduling techniques are one of the suggested solutions for water scarcity problems .The aim of the study is to show the possibility of using leaching scheduling, when applying the irrigation scheduling program for a certain irrigation project, which was prepare by Water Resources Engineering –University of Baghdad with some modifications to generalized it and it make applicable to various climatic zone and different soil types.

The objectives of this research is to build a system that concerns the prediction of the leaching scheduling (depth and date of leaching water), illustrating the main problems (soil salinity, save the amount of leaching requirement, and to maintain crops growth).The other objective is to compare between the calculated amount of leaching water with the amount of water that is suggested by designers. The program includes, the calculating of predicted daily soil salinity ,the depth of leaching water that should be applied to remove the salt from the soil when it reaches a harmful level, and the total annual volume of leaching water.

The results showed, that the use of predicted leaching scheduling with its applicable constrains require high attention when choosing the cropping pattern for each climate zone. Also, it was found that the leaching program is a useful tool for saving irrigation water if cropping pattern has been adapted carefully. This means the leaching water depth should be added only when needed, and may not be necessary with each irrigation event.

**Keywords**: leaching scheduling, irrigation scheduling, maximum root depth, water resources dept. program, water budget, Amara irrigation project.

## جدولة متطلبات الغسيل الإضافية لمنع التملح الثانوي في منطقة الجذور
### الخلاصة

تعرف متطلبات الغسيل بانها الكمية الواجب اضافتها للتربة لغرض الحفاض على مستوى ملحي دون المستوى المؤذي. أن استعمال اسلوب جدولة الغسيل هي أحدى الحلول المقترحة لحل مشكلة شحة المياه. تهدف الدراسة الى معرفة أمكانية أستخدام برنامج جدولة الغسيل من خلال تطبيق برنامج الجدولة الاروائية في مشروع اروائي والذي تم أعداده في قسم هندسة الموارد المائية ـ جامعة بغداد مع أجراء بعض التعديلات عليه لجعله قابل للتطبيق في المناطق المناخية المختلفة ولأنواع مختلفة من الترب.

اهداف البحث هي بناء نظام يهتم بحساب جدولة الغسيل (تاريخ وعمق مياه الغسل)حيث انه يوضح و يناقش المشاكل الرئيسية (ملوحة التربة, وتوفير مياه غسيل والحفاظ على نمو المحاصيل ) ، أما الهدف الأخر للبحث فهو المقارنة مابين النتائج المحسوبة بأستخدام البرنامج مع ما تم أقراره من قبل المصممين ، البرنامج يتضمن حساب الملوحة اليومية ، وعمق الماء الواجب اضافته لأزالة الاملاح من مقد التربة عندما تصل الى مستوى مؤذي للنبات وتشمل الحسابات أيضا حساب حجم مياه الغسيل السنوية المضافة.

أظهرت نتائج البحث أن أستخدام هكذا نوع من جدولة مياه الغسيل المتوقعة وبخصائصه التي تجعله قابل للتطبيق، يتطلب عناية شديدة عند أستخدام نمط توزيع النباتات والمساحات المزروعة بهذه النباتات لكل منطقة مناخية، كما وجد أن البرنامج يمثل أداة مفيدة للحفاظ على المياه أذا ما أحسن أختيار الدورة الزراعية الملائمة. وهذا يعني أن عمق مياه الغسيل بالأمكان اضافته عند الحاجة فقط وليس بالضروري مع كل رية وكنسبة من عمق مياه الري.

الكلمات الرئيسة:جدولة الغسيل, جدولة الري, أقصى عمق جذور, برنامج قسم المواردالمائية, الموازنة المائية, مشروع العمـارة الأروائي.

## 1. INTRODUCTION

Leaching scheduling , means the minimum amount of water that should be added to the irrigation requirements in order to remove the accumulated salt in the root zone due to irrigation. When it reaches a harmful effect on crop growth, the leaching scheduling will be important for saving water. Leaching is the key factor for controlling soluble salts brought by irrigation water.

## 2. LEACHING REQUIREMENTS

The leaching requirements (LR) concept was developed by the U.S. Salinity Laboratory, **Richard, 1954.** It was defined as "the fraction of the irrigation water that must be leached out of the bottom of the root zone in order to prevent average soil salinity from rising above some specific limit, therefore it represents the minimum amount of water that must pass through the root zone to keep salts within an acceptable range.

Leaching requirements depend on the salt concentration in the irrigation water, the amount of water extracted from the soil by the crop (transpiration), and the salt tolerance of the crop, which determines the maximum allowable concentration of the soil solution in the root zone, **Rhoades, and Merrill ,1976**.

The actual leaching requirements can only be determined by monitoring salinity control which is related to field water management. Under some conditions, however, differences in soils, drainage, and water application methods make leaching less than I00% efficient. Cracks, root holes, wormholes and other large pores can transport water quickly through the root zone when these channels are in contact with the irrigation water at or near the surface, **Rhoades, 1990b.Rhoades and Merrill, 1976**, proposed an equation to calculate leaching requirement.

If all the infiltrated water mixes completely with the soil moisture, the relation between the depth of applied water (AW) for consumptive - use and the LR as suggested by **FAO 1985b,** during a cropping season is:

$$AW=ET_c /(1-LR) = Irr.D +Pe \qquad (1)$$

Where :

$ET_c$: consumptive-use (L/T),

Irr.D: net irrigation water depth (L),and

Pe: effective rain-fall (L).

However, under normal conditions, a fraction of the infiltrated irrigation water equivalent to ((1–f) * Irrigation depth), where: (f) is the leaching efficiency coefficient, will percolate directly below the root zone through cracks and macro-pores without mixing with the soil moisture solution. This water does not contribute to the leaching of salts from the root zone.

In practice, the electrical conductivity of drainage water ($EC_{dw}$) value is not readily available, and the U.S. Salinity Laboratory recommends using the average electrical conductivity of the saturation soil solution extract, and the electrical conductivity of irrigation water ($EC_{iw}$)to determine LR. The salt entering into the root zone from irrigation water or capillary rise from ground water remains in the root zone.

The accumulated salt in the root zone is generally leached by applying water in excess of field capacity. Field capacity can be defined as the maximum amount of moisture that can be held against gravity in the soil pores of the root zone. Results from

several laboratory experiments by **Miller, et al., 1965;** and some field trials by **Oster, et al., 1972**, showed that the quantity of salts removed per unit quantity of water leached can be increased appreciably by leaching at soil moisture contents less than saturation, i.e. under unsaturated conditions.

In unsaturated field conditions leaching was obtained by adopting intermittent ponding or by intermittent sprinkling at rates less than the infiltration rate of the soil. The degree of salt removal during leaching is be markedly influenced by the method used. An experiment was carried out at Nahshala Farm, north west of Al-Ain City, U.A.E. during the 1998–2000 growing seasons, using six halophytes (Batis maritima, Distichlis spicata, Juncus roemerianus, Paspalum vaginatum, Salicornia bigelovii and Spartina alterniflora) and two levels of leaching fraction (0·25 and 0·50) under three irrigation salinity levels 10, 20, and 40 (g/l) in a randomized complete block design arranged in split plots. The results indicated that the halophyte species tested can grow with minimum reduction in the growth potential at < 20 (g/l) mean salinity of soil solution. Leaching fraction of 0·25 at the highest salinity of irrigation water 40 (g/l) was inadequate to attain the steady-state salt balance during the growing period, although drainage salinity reached more than 90 (g /l). Furthermore, if the same level of salinity is used for longer periods, soil salinity under this high salt treatment will continue to rise and plant growth may deteriorate. Leaching fraction of 0.50 is preferable if salinity of irrigation water is more than 20(g/l) and dry matter production is considered, although the amount of water used will be excessive, **El-Sayed et al., 2000**.

In the past, the means of estimating LR was based on a set of conditions, referred to as steady-state conditions, which rarely actually exist in real world. The real world is more dynamic and transient-state conditions predominate. The traditional guidelines for the calculation of the crop-specific leaching requirement of irrigated soils have fallen under the microscope of scrutiny and criticism because the commonly used traditional method is believed to over-estimate LR due to the assumption of steady-state flow and disregarding salt precipitation and preferential flow. Over-estimation of LR of detrimentally impacts the environment and reduces water supplies. Steady-state models for calculating LR based on traditional model of the U.S. Salinity Laboratory and water-production-function models were compared to transit-state models. The calculated LR was lower when determined using a transit-state approach than using a steady-state approach. Transit-state conditions and the influence of preferential flow have no significant effect on lowering the value of LR as shown in the study of the Imperial Valley using Colorado River water $EC_{iw}$ 1.23 (ds/m) for irrigation. The LR was 0.08 for a certain crop rotation and certain area, as was calculated by transit- state model, and was found to be the most reasonable estimate for the entire Imperial Valley as compared to LR of 0.13 by using the commonly traditional method.

**Letey et al., 1985**, conducted a reclamation leaching experiment in a drip-irrigated pistachio orchard south of Huron, California, during the winter of 2002-2003. The study was conducted to quantify the leaching water required to remove salts from the effective root zone of trees. This experiment tested a new reclamation leaching technique by using multiple lines of low-flow drip tape to supply water to the area of salinity accumulation along a tree row. This new technique allows water to be supplied where there is salt accumulation along the tree row, instead of supplying water to the entire area of the field. Since reclamation leaching requires a relatively large depth of water, this technique offers potential for significant water savings.

**Bakr, 2011,** calculated monthly, and annually water requirements and calculated the leaching requirements as a percentage from the depth of irrigation water for many projects on Tigris River basin.

To make the right decision, there are some steps that should be followed, namely selecting the cropping pattern, initial salt concentration of soil, salt concentration of irrigation water, leaching efficiency coefficient, and crop characteristics properties. In addition to know growing and harvesting date, root depth, and allowable depletion.

The physical properties of the soil, climate data, availability of water resources, soil water deficit before irrigation, and field water losses should be known as well.

With the aid of the information mentioned above, monthly and annual water requirements for leaching can be calculated, and then the irrigation and leaching scheduling can be adapted. The computer simulation model developed in this research was based on the following constrains:

• The desired salt concentration of soil is 4 (ds/m), at this value the effect of salt on crop growth is negligible,**Richard,1954**, and

• The harmful level of salt concentration index on crop growth is selected as follows: if the expected conductivity of soil saturation extract after irrigation is less than or equal to crop salt tolerance at 50% yield reduction, then leaching water is added to the soil at or before reaching  this value.

Some constrains are required to build the leaching scheduling model and they are as follows:

a. Assuming that the desired salt concentration of soil saturated extract is the initial salt concentration in each reservoir.

b. The soil reservoir is divided into four reservoirs, each one has constant depth of 250 mm, and therefore the soil depth is always one meter. If the depth of root zone is more than one meter, the   remained depth of root zone falls within the drain zone **,Van Der Molen, 1979**, and

c. Two cases are employed, the first case is field water losses cannot be controlled as surface runoff and deep percolation to the drainage zone losses, and the second case is 33% from the field water losses can be controlled and will be considered  as the depth of leaching water            (deep percolation).

## 3.  DESCRIPTION of SELECTED PROJECT AREAS

Five irrigation projects on the Tigris River basin were selected because there are tributaries on the river.

The climate of Iraq is subtropical, continental, summer is long, hot, and dry, and winter is short with mean monthly temperatures above zero, and intensive cyclonic activity in the atmosphere provoking rainfall. The mean annual amount of precipitation in the country tends to decrease from north to south and from east to west. In the summer, no rainfall occurs in the country. Temperature, air humidity, and evaporation increase from north to south.

Iraqi territory was divided into six zones according to the natural humidity, which characterizes identity of crops. Three natural-climatic zones and three subzones were

identified within the territory of the country, **General Scheme of Water Resources and Land Development in Iraq, 1982.**

## 4. CONCEPTUAL FORMULATION

The conceptual concepts were mathematically formulated in order to obtain a workable procedure. Below is a brief description of the mathematical formulation of leaching scheduling procedure as presented by **FAO, 1985**. The first step in leaching scheduling is to determine leaching requirements, and to calculate the leaching requirements by using the salt equilibrium equation, which is based on the application of water balance, salt balance, and leaching coefficient equation.

### 4-1 The Water Balance Equation in the Root Zone

The basis for understanding the impact of irrigation and drainage management on the salt balance is the water balance at the root zone, and can be described by the following equation, FAO**, 1985b**:

$$\text{Irr. } D = R^* + ET_c - Pe \tag{2}$$

Where:
   Irr.D: irrigation depth (L),
    $R^*$: leaching water depth (L), and
    Pe: effective rainfall(L).

### 4-2 The Salt Balance Equation in the Root Zone

In irrigation, salts are added to the root zone because all irrigation waters contain salts. A fraction of the salts is leached below the root zone by deeply percolated water. After a certain period, salt accumulation in the soil will approach an equilibrium or steady-state concentration which depends on the salinity of applied water and leaching requirements, **FAO, 1985.**

The following assumptions were made to formulate the salt balance equation:

• The exchange processes and chemical reactions which take place in the soil are not taken into consideration, and

• The amount of salts supplied by rainfall, fertilizers, and exported by crops is negligible. A zone of shallow groundwater is created with the same average salinity concentration as the percolation water.

The root zone is one meter deep, and the salts are distributed homogenously through it.

The movement of salts starts when the soil moisture content reaches field capacity level.

Under these assumptions, the salinity of the soil water is equal to the salinity of the water percolating below the root zone. The water balance the root zone can be given by the following equation, **FAO, 1985**:

$$\text{Irr. } D * C_{iw} = R^* * C_R \tag{3}$$

Where:
   $C_{iw}$: average salt concentration of irrigation water,( ppm), and
   $C_R$: average salt concentration of leaching water, (ppm).
Other abbreviations are as described earlier.

## 5-LEACHING EFFICIENCY COEFFICIENT

Leaching efficiency coefficient is an essential parameter to be considered in the leaching processes. It indicates the degree of mixing between the applied water and the original soil solution, it could be defined with respect to the water percolating from the bottom of the root zone, or it can be defined as the percentage of water percolating from the original soil water, the remainder of which flows through a bypass consisting of a crack and\or a root hole. This concept of leaching efficiency for vertical water movement was originated carried out during the experimental work carried out in Dujailah Project in Iraq by **Boumans, 1963.** Also, it can be defined as the percentage of irrigation water that mixes with soil water.

The introduction of a leaching efficiency coefficient means that the full amount of water percolated through the soil profile is replaced by the effective amount of water during the leaching process.

In a related work by, **Van Der Molen, 1979**, two different expressions were introduced, each describing a different model of physical leaching process. These two expressions are:

$$f = C_{DP} \backslash C_e \tag{4}$$

$$f = C_{DP} - C_{iw} \backslash C_{fc} - C_{iw} \tag{5}$$

Where:

$C_{DP}$: average salt concentration of the water percolating below the root zone, (ppm)

$C_e$: average salt concentration of the reservoir solution (after leaching) at field capacity,(ppm)

Leaching efficiency coefficient variation with soil depth for many soils in pilot projects in Iraq is presented by **Hussein, 1997**.

To calculate the leaching requirements, the salt equilibrium equation presented by **Richard, 1954,** was used in this study; This equation was obtained from:
- Salt balance equation, Eq.( 2), and
- Leaching efficiency coefficient equation, Eq.( 4).

The salt equilibrium equation therefore is:

$$R^* = ( ETc - Pe ) * [ EC_{iw} / f * ( EC_{fc} - EC_{iw})] \tag{6}$$

Where:

$EC_{fc}$: Electrical conductivity, (ds/cm) ,and :

$$EC_{fc} = EC_\circ * (\theta_{vs} / \theta_{fc}) \tag{7}$$

Where:

$EC_\circ$: Initial electrical conductivity of soil solution at field capacity, ds/m,

$\theta_{fc}$: Soil moisture content of soil at field capacity, fraction of unity, and

$\theta_{vs}$: Soil moisture content of soil at saturation, fraction of unity.

$\theta_{vs} / \theta_{fc}$ For moderate texture soil equal to two as showed by**, Al-Furat Center For Studies and Designs of Irrigation Project, 1992.**

To guarantee that all root zones are leached, the maximum crop root depth was adopted to prevent any crop losses during whole year. The amount of salts that can added during the first irrigation in any month equal to the amount added in the second irrigation ,and for all irrigations during that month .So, the depth of leaching water differs from month to another. The amount of salt added through any irrigation can be calculated from:

$$Z_{ki}= (EC_{iw})_k * NA * RD_j * C \qquad (8)$$

Where:

$Z_{ki}$: amount of salts added on the $k^{th}$ day after irrigation, during the $i^{th}$ month,( grams),

$NA_j$: net area planted with $j^{th}$ crop, hectares,

$RD_j$: root depth at any time of the $j^{th}$ crop, mm,

k: index for time, days,

i: index for time, months, and

C: conversion factor milli equivalent per liter (meq/l) or part per million (ppm), and the unit of electrical conductivity is decisemens per meter (ds/m).

1(ds/m)=640(ppm),or (gm/m$^3$), **Ayers and Westcot, 1985.**

There are three possibilities of supplying irrigation water, which are: If the net depth of irrigation water is equal to the soil water deficit before irrigation (full irrigation), the soil water content after irrigation will reach the field capacity of soil, then:

Irr.D $_{ki}$ = SWDB $_{ki}$

Where:

SWDB $_{ki}$: Soil water deficit on the $k^{th}$ day before irrigation during the $i^{th}$ month, (L).

Second probability**,** if the net depth of irrigation water is less than the soil water deficit before irrigation (partial irrigation).Accordingly there is an additional quantity of water that should be added to raise the water soil content to field capacity level. In this case, and if the salinity reaches a harmful level that will effect growth of crop, the leaching water must be added to remove the salt from the root zone. The additional quantity of water is calculated as extra leaching water depth.

$$(act.R^{*}_{t})_{ki}=ASWD_{ki}+R^{*}_{ki} \qquad (9)$$

$$SWDB_{ki}-Irr.D_{ki}=ASWD_{ki} \qquad (10)$$

Where:

ASWD $_{ki}$: Additional soil water deficit in the $k^{th}$ day during the $i^{th}$ month, which equals to water requirement that raises the soil water content to field capacity level, (L).

Third, the net amount of irrigation water is greater than the soil water deficit before irrigation. According to the contiguity between net irrigation water and soil water deficit, the water losses may be divided into two parts:

**The first** is surface runoff, this amount of water losses cannot be controlled and goes as surface run off, and

**The second** is one third from field water losses which can be controlled and will be used as a depth of leaching water; this part is considered as deep percolation. In this case, the deep percolation must be checked if it is greater than depth of leaching water therefore, there is no need to add water for leaching purposes. If deep percolation is less than the depth of leaching water, leaching water is needed so,

If Irr.D $_{ki}$> SWDB $_{ki}$ , there are two possibility which are:

The first is;

Irr.D $_{ki}$ - SWDB$_{ki}$> R$^{*}_{ki}$  then

(act.R$^{*}_{t}$) $_{ki}$ =0, and the second is;

Irr.Dki - SWDB $_{ki}$< R$^{*}_{ki}$ then:

$$(act.R^{*}_{t})_k = R^{*}_{ki} - [Irr.D_{ki} - SWDB_i] \tag{11}$$

Where:

(act. R$^{*}_{t}$)$_{ki}$: Actual depth of irrigation water on the k$^{th}$ irrigation during the i$^{th}$ month,( L).

## 6- SIMULATION MODEL

The above described mathematical procedure requires tedious calculations if done by hand, so it is translated into a computer simulation. Model inputs, outputs, and flow chart are presented in Fig.1 as a leaching scheduling program.

This model was applied for three different climatic zones with three different cropping patterns and different soil properties.

Spreadsheet Formulas for Microsoft Excel program, version, 2007, was used to program the procedure. The following input data were used to construct the program:

• Number of irrigations around the year together with their dates and depths of irrigation water, and link this work with the main irrigation scheduling program which was built by **Bakr, 2011**, and developed by **Al-Haddad, 1997;** and **Hamad, 1996.**

• The seasonal average of irrigation water salinity in the water source of each project.

• Initial soil salinity, leaching efficiency coefficient, **Hussein, 1997.** , and the salinity at field capacity, as averages. Daily soil water deficit after irrigation around the year, and daily field water losses.

The main outputs of the simulation model are:

The amount of added salinity, salt increase in the soil after each irrigation cycle, and daily, monthly, and annual depths of leaching water,

• Actual daily, monthly, and annual depths of leaching water that should be provided to remove salt from soil reservoir for the two cases: one third of losses is controlled, and the other is uncontrolled, and for different status of soil water content before irrigation,

• Daily percentage of leaching requirements from net irrigation depth,

• Daily, monthly, and annual depths of net irrigation water for each case; volumes of supplied irrigation water to the project, annual amount of saved water by using leaching scheduling, and

• Percentage of drainage water and actual losses of water.

## 7- RESULTS AND DISCUSSION

Amara Irrigation Project in Maysan Government was taken as an example. Currently, this zone has a saline soil to variable degrees; the average salt concentration is 1676.25 (ppm). Additional leaching water requirements in southern zone were taken as 19-19.5% of total irrigation requirement as average,**General Scheme of Water Resource and Land Development of Iraq, 1982.** If the net depth of irrigation water is less than the soil water deficit before irrigation (partial irrigation), additional quantity of water should be added to raise the soil water content to field capacity. In this case and, if the salinity reaches a harmful level, the leaching water must be added to remove salt from the soil.

In all irrigation cycles during autumn and winter seasons, the net depth of irrigation water is greater than the soil water deficit before irrigation (full irrigation), accordingly the contingents between net irrigation depth and soil water deficit will be taken as water losses. In some irrigation applications during summer and spring seasons an additional quantity of water should be added to raise the soil water content to field capacity.

**Table 1**and **Fig.1**, present the difference in applied water distribution between leaching scheduling procedure (calculated) case and designer suggestion (allocated) case. In the first case applied irrigation volumes in scheduled case are less than those allocated to the project, and there is 29.8 %of water lost as drainage water. In these cases assuming that water losses cannot be controlled, 29.8% is lost to the drains, and the real need is 683mm depth of leaching water. **Table 1**, also shows that 1767.64 million $m^3$ of water were saved. In the second case applied irrigation volumes in a scheduled case are less than those allocated to the project and there is 25.5% of water lost as drainage water.

 In these cases assuming that water losses can be controlled and part of water losses (deep percolation) substitute part of leaching, loss of drainage water become 25.5%, and 467.7 mm of leaching water only are needed to leach salts **Table 2**. **Table.1** also shows that 1845.29 million $m^3$ of water are saved.

Introducing leaching scheduling procedures a proper cropping pattern should be used in order to improve water use efficiency, but without crops stress.  Cropping pattern should be chosen carefully. Amara irrigation project with assumed an cropping pattern, five winter-season crops, four summer-season crops, and six perennial crops were planted with cropping intensity equal to 115%. The crops differ in degree of response to salinity; some crops can produce acceptable yields at much greater soil salinity than others. Crops are divided into four relative salinity tolerance rating, sensitive, moderately sensitive, moderately tolerant, and tolerant crops.

The wide range of salt tolerance crops allows using moderately saline water some of them were previously thought to be unusable. Therefore greatly expands the acceptable range of water salinity which is considered suitable for irrigation. In the Amara Irrigation Project, some crops were planted were but with an assumed area, with many trials, the right percentages of plant area which improves water saving without losing crops can be found, in this project it is assumed that no sensitive crops are planted.

Saving crops at 50% yield potential was considered as an index for salinity hazard; in the other words must be added depth of leaching water before the soil salinity become less than or equal to  the threshold value of 50 % yield potential.

The water source of Amara irrigation project is Tigris River in Maysan Government. There were some missing monthly records of salt concentration in irrigation water at Amara during 2000 to 2001were lost, therefore in this study the mean seasonal salt concentration of irrigation water was used which is equal to the mean annual salt concentration, and equal to 1676.25 ppm.

For effective salinity control, adequate drainage to control and stabilize the water table and leaching saline ground water intrusion in the active root zone were considered to be negligible.

**Table 3** and **Fig. 3**, show the differences in applied water distribution between calculated leaching scheduling and designer suggested (allocated). In the first case applied irrigation volumes are less than those allocated, and there is 33.2% of water lost as deep percolation. In this case the water losses cannot be controlled therefore 303 mm of leaching water was needed. The amount of 1891.57 million $m^3$ of irrigation water was saved as shown in **Table 4**. In the second case, applied irrigation water volumes are less than those allocated to the project, and there is 33.2% of water lost as deep percolation. In these cases water losses assume to be controlled, and part of water losses should be substituted, therefore drainage water losses became 30.4%, and 166 mm depth of leaching water is needed to leachout salt. **Table 4** also shows that 1942.26 million $m^3$ of water were saved. Salt concentration of irrigation water at Amara for 2000 to 2010 years point is used. So the mean annual salt concentration for the ten years is 1165.02 ppm as shown in **Table 5**.

## 8- CONCLUSIONS

1. Using the maximum planted crop root depth to leach out salts from the root zone , guarantees preventing crop damage due to salt,

2. The comparison between the monthly applied irrigation volumes using leaching scheduling procedure and the suggested by designers provides flexibility for balancing between monthly applied irrigation volumes; therefore the operation is efficient while the distribution of monthly applied irrigation water suggested by designers has a maximum value at summer season which causes problems in operating irrigation and drainage network,

3. High salinity of irrigation water means high depth of leaching water is needed ,the monthly applied leaching water of the scheduling procedure, and for the two cases are greater than monthly applied leaching water suggested by designers taken into account the crops were not suffer from salinity stress , and

4. The results show that applying leaching scheduling at Amara irrigation project is more acceptable and more economic than using suggestion of designer.

## REFERENCES

➢ Al-Furat Center for Studies Design of Irrigation Project, 1992. *The Soil of West Gharraf Project.*

➢ Ayers, R.S. and Westcot, and D.W. ,1985. *Water Quality for Agriculture.* Irrigation and Drainage Paper 29. Rev. 1. FAO, Rome. 174 p.

➢ Bakr, T. Sh., 2011. *Irrigation Scheduling Effect on Water Requirements.* M. Sc. Dissertation Submitted to the College of Engineering, University of Baghdad.

➢ Boumans ,J.H. 1963.*Some Principles Governing the Drainage and Irrigation of Saline Soil".* Reclamation of Salt Effected Soils in Iraq, pub.II, IRLI , Wageningen, Netherland.

➢ El-Sayed, H., El-Haddad and Maher, M. N. 2000. *Leaching Requirement and Salinity Threshold for the Yield and Agronomic Characteristics of Halophytes under Salt Stress".* Soil Salinity Laboratory, Bacos, Alexandria, Egypt: Plant Production Department, Faculty of Agricultural Sciences, UAE University, Al-Ain, 17555, U.A.E.

➢ Food and Agriculture Organization (FAO). 1985b. *Water Quality for Agriculture".* Irrigation and Drainage Paper, 29. Rev. 1. FAO, Rome. 174 p.

➢ General Scheme of Water Resource and Land Development of Iraq, 1982. *Ministry of Water Wrrigation". Iraq.*

➢ . Hussain, S. M. ,1997, *Leaching Efficiency of Salt Effected Soils in the Mesopotamian Plain.* J. Eng., College of Engineering, Baghdad University, Vol. (4), No. (3), PP. 1-11.

➢ Letey,J.,A., and Knapp,K.C.,1985.*Crop –Water Production Function Model for Saline Irrigation Waters,* Soil Soc. Am. J.49:1005-1009.

➢ Mass, E.V. ,1984. *Salt Tolerance of Plants*. In: The Handbook of Plant Science in Agriculture. B.R. Christie .

➢ Mattax. C. C. and R. L. Dalton, 1990. *Reservoir Simulation* SPE Monograph, vol.13,Society of Petroleum Engineers, Richardson, TX.

➢ Miller, R. J., J.W. Biggar, and D. R.Nielsen, 1965.*Chloride Displacement in Panoche Clay Loam in Relation to Water Movement and Distribution"*. Water Resources Res. 1: 63-73

➢ Oster, J. D., Willardson, L. S. and Hoffman, G. J. ,1972. *Sprinkling and Ponding Techniques for Reclaiming Saline Soils"*. Transactions ASCE, 15: 1115-1117.

➢ Rhoades,J.D.,andMerrill,S.D.,1976. *Assessing the Suitability of Water for Irrigation :Theoretical and empirical Approaches*. In: Prognosis of Salinity and Alkalinity .Soil Bulletin 31,FAO, Rome, pp.69-109.

➢ Rhoades, J.D. ,1990b. *Determining Soil Salinity from Measurements of Electrical Conductivity"*. Commun. Soil Sci. Plant Anal. 21: 1887-1926.

➢ Richard, L. A. (Ed.) et al., 1954. *.Diagnosis and Improvement of Saline and Alkaline Soils*. Ag. Handbook No. 60 U.S.D.A., US Salinity lab, Staff.

➢ Van Der Molen, W. H.,1979. *Salt Balance and Leaching Requirement*. Drainage Principles and Applications, Vol. II, Wageningen, the Netherlands.

Start

INPUT:the seasonal

CALCULATE: $EC_{iw}$ added through each irrigation; $EC_e$

INPUT: the average $EC_\circ$; $EC_{fc}$ ;f

CALCULATE: $EC_{iw}$ added through each irrigation; $EC_e$ accumulative in the soil after each irrigation.

CALCULATE: R * for each soil layers.

No     Check the salinity tolerance if (the salinity tolerance less than assumed % of emergence     Yes

The crops are.

Δ

A

Change the crop

No    DP > \ = R *.    Yes

R * ≠ 0

Calculate R *_{act.}

R * = ˰

Applied R *_{act.}

UTPUT : The amount of depth of leaching water ; depth of net irrigation water ; leaching water requirement as a percent ; saved quantity of water ;actual water losses;% of water losses for selected irrigation project.
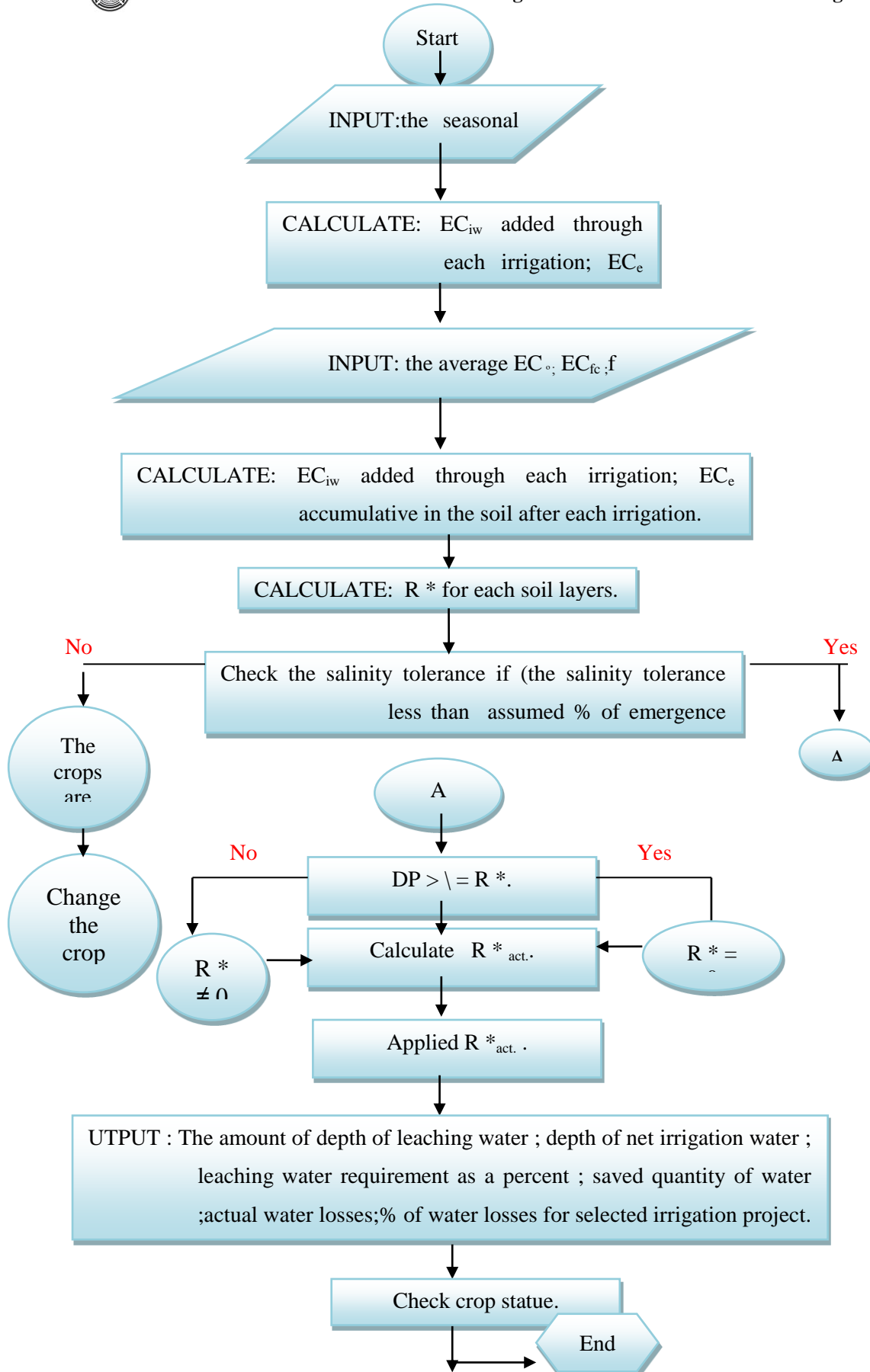
Check crop statue.

End

**Figure 1**. Flow chart illustrates the main steps of the simulation model of the leaching scheduling.

**Table 1.** Monthly and annual irrigation water amounts, Amara Irrigation Project, 2000-2001.

| Month | Calculation results | | Estimated by general scheme (LR =19%) |
|---|---|---|---|
| | **Designed I: net volume of irrigation water, $m^3 x10^6$** | **Designed II: net volume of irrigation water, $m^3 x10^6$** | **NI req. $(m^3)*10^6$** |
| Jan. | 113.29 | 100.42 | 36.96 |
| Feb . | 109.21 | 101.88 | 63.65 |
| Mar . | 120.71 | 116.88 | 105.37 |
| Apr. | 153.49 | 153.18 | 312.37 |
| May . | 146.49 | 136.96 | 455.33 |
| Jun . | 130.71 | 125.16 | 635.12 |
| Jul . | 144.08 | 139.18 | 631.63 |
| Aug . | 147.37 | 140.37 | 571.65 |
| Sep . | 134.37 | 126.15 | 266.49 |
| Oct. | 135.85 | 128.25 | 117.69 |
| Nov . | 66.65 | 64.91 | 62.79 |
| Dec. | 108.85 | 100.42 | 19.98 |
| Sum. | 1511.42 | 1433.76 | 3279.06 |
| | | | |
| Percentage of drainage water | 29.8 | 25.5 | |
| Saved volume of water $10^6$ $m^3$ | 1767.64 | 18545.29 | |
| Percentage of leaching requiremen ts, % | Av. 22.24 | Av. 15.34 | 19.5 |
| Actual water losses, mm | 1111.25 | 895.61 | …… |
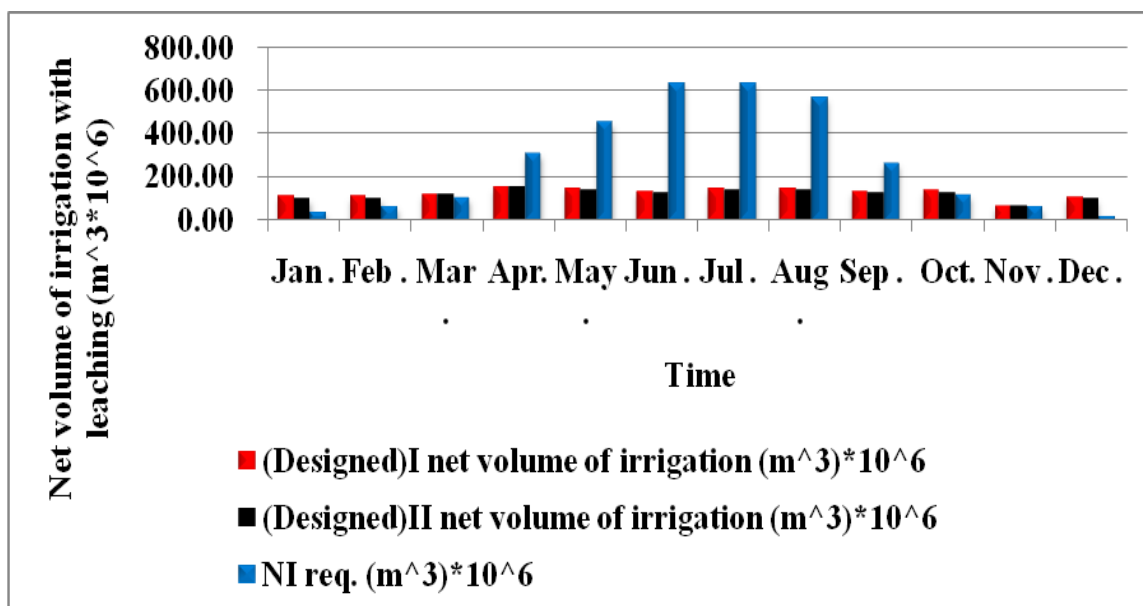
**Figure 2.** Monthly irrigation water amounts; distribution according to leaching scheduling, and designer suggestions if water losses uncontrolled and water losses controlled.

**Table. 2** .Monthly and annual depths of leaching water, Amara Irrigation Project, 2000-2001.

| Month | From calculation | | | From general method (LR = 19.5%) |
|---|---|---|---|---|
| | $R^{*}_t$ (mm) | (act . $R^{*}_t$)I (mm) | act . $R^{*}_t$ ) II (mm) | $R^{*}_t$ (mm) |
| Jan. | 17.49 | 17.49 | 0 | 26.61 |
| Feb . | 27.056 | 27.06 | 17.12 | 23.60 |
| Mar . | 41.77 | 41.776 | 36.69 | 23.12 |
| Apr. | 48.11 | 48.11 | 47.70 | 25.96 |
| May . | 92.85 | 92.85 | 57.78 | 72.02 |
| Jun . | 95.48 | 95.48 | 72.78 | 71.22 |
| Jul . | 102.06 | 102.06 | 81.99 | 80.13 |
| Aug . | 116.75 | 116.75 | 87.94 | 80.64 |
| Sep . | 71.28 | 71.28 | 34.92 | 82.99 |
| Oct. | 44.38 | 44.38 | 18.44 | 66.87 |
| Nov . | 14.6 | 14.6 | 12.29 | 14.65 |
| Dec. | 14.46 | 14.46 | 0.000 | 26.61 |
| Sum | 683.34 | 683.34 | 467.7 | 594.44 |

48

**Table 4**, Monthly and annual irrigation water amounts, Amara Irrigation Project, 2000-2001.

| Month | From calculation | | From general scheme (LR =19.5%) |
|---|---|---|---|
| | (designed)I net volume of irrigation $(m^3)*10^6$ | (designed)II net volume of irrigation $(m^3)*10^6$ | NIreq. $(m^3)*10^6$ |
| Jan. | 106.96 | 100.42 | 36.96 |
| Feb. | 109.46 | 104.34 | 63.65 |
| Mar. | 110.05 | 109.62 | 105.37 |
| Apr. | 133.68 | 131.41 | 312.37 |
| May. | 129.23 | 124.19 | 455.33 |
| Jun | 114.25 | 111.4 | 635.12 |
| Jul. | 129.65 | 126.8 | 631.63 |
| Aug. | 122.27 | 119.37 | 571.65 |
| Sep. | 133.57 | 126.1 | 266.49 |
| Oct. | 128.32 | 122.85 | 117.69 |
| Nov. | 61.71 | 59.24 | 62.79 |
| Dec. | 108.34 | 101.05 | 19.98 |
| Sum. | 1387.48 | 1336.79 | 3279.06 |
| | | | |
| Percentage of drainage water | 33.2 | 30.4 | |
| Saved volume of water $10^6$ m$^3$ | 1891.57 | 1942.26 | |
| Percentage of leaching requirements (%) | Av. 9.95 | Av. 5.47 | 19.5 |
| Actual water losses (mm) | 1111.25 | 977.47 | …… |
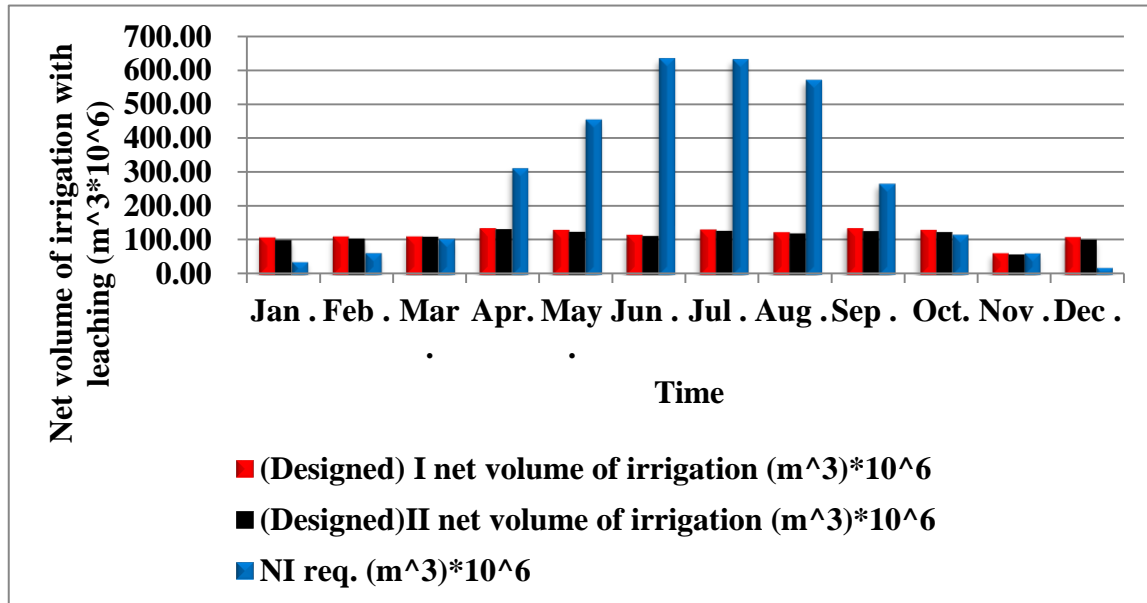
**Figure 5**. Monthly irrigation water amounts; distribution according to leaching scheduling, and to designer suggestions.

**Table 5**, Monthly and annual depths of leaching water, Amara irrigation project, 2000-2010.

| Months | From calculation | | | From general method (LR = 19.5%) |
|---|---|---|---|---|
| | $R^*_t$(mm) | $(act . R^*_t)$I mm | $(act . R^*_t)$II (mm) | $R^*_t$(mm) |
| Jan. | 8.89 | 8.89 | 0 | 26.61 |
| Feb. | 27.39 | 27.39 | 20.45 | 23.60 |
| Mar. | 27.61 | 27.61 | 27.05 | 23.12 |
| Apr. | 18.84 | 21.85 | 18.84 | 25.96 |
| May. | 29.38 | 29.38 | 10.84 | 72.02 |
| Jun. | 28.13 | 28.13 | 16.45 | 71.22 |
| Jul. | 43 | 43 | 31.35 | 80.13 |
| Aug. | 13.39 | 13.39 | 1.43 | 80.64 |
| Sep. | 66.38 | 66.38 | 34.72 | 82.99 |
| Oct. | 18.67 | 18.67 | 0 | 66.87 |
| Nov. | 7.97 | 7.97 | 4.66 | 14.65 |
| Dec. | 10.76 | 10.76 | 0 | 26.61 |
| Sum. | 300.43 | 303.44 | 165.79 | 594.44 |

## ABREVIATIONS

| Symbol | Description | Units |
|---|---|---|
| $act.R^{*}_{t}$ | Actual depth of leaching water. | L |
| $ASWD_{ki}$ | Additional soil water deficit on the $k^{th}$ day during the $i^{th}$ month. | L |
| AW | Available water. | L |
| C | Conversion for units. | … |
| $C_{DP}$ | The average salt concentration of the water percolating below the root zone. | ppm |
| $C_{e}$ | The average salt concentration of the soil saturation extract. | ppm |
| $C_{fc}$ | The average salt concentration of the soil solution at field capacity. | ppm |
| $C_{iw}$ | The average salt concentration of irrigation water. | ppm |
| $C_{R}^{*}$ | The average salt concentration of leaching water. | ppm |
| $EC_{e}$ | Electrical conductivity tolerated by the crop as measured in the soil saturation extract. | ds/m |
| $EC_{fc}$ | Electrical conductivity of soil extract at field capacity. | ds/m |
| $EC_{iw}$ | Electrical conductivity of irrigation water. | ds/m |
| $EC_{\circ}$ | Electrical conductivity of soil before leaching (initial value). | ds/m |
| Etc | Monthly crop evapotranspiration rate. | L/Time |
| f | Leaching efficiency coefficient. | % |
| $f_{c}$ | Specific moisture of soil at field capacity. | |
| I | Index for time. | Month |
| Irr.D | Applied net irrigation water depth infiltrated, which is the total applied irrigation water minus evaporation losses and surface runoff. | L |
| J | Index for crop grown in the project. | … |
| K | Index for time. | Day |
| LR | The leaching requirements. | % |
| $NA_{j}$ | Net area planted with the $j^{th}$ crop. | Don. |
| $P_{e}$ | Effective rain-fall. | L |
| $RD_{j}$ | Root depth at any time of the $j^{th}$ crop. | L |
| $R^{*}$ | Depth of leaching water. | L |
| $R^{*}_{t}$ | Total depth of leaching water. | L |
| SWDB | Soil water deficit before irrigation. | L |
| Z | The amount of salt added after irrigation. | Gram |

# Parametric Study of Active Solar Heating Using a Pebble Bed as a Thermal Collector and Storage Unit

**Saad Mohsen Saleh**
Assistant Professor
College of Engineering-University of Baghdad
E-mail: almashatsaad@yahoo.com

**Mustafa Mahdi Mustafa Alaskari**
Assistant Lecturer
College of Engineering-University of Baghdad
E-mail: mustafa1eng@gmail.com

## ABSTRACT

In this study, pebble bed as an absorber and storage material was placed in a south facing, flat plate air-type solar collector at fixed tilt angle of (45°). The effect of this material and different parameters on collector efficiency has been investigated experimentally and theoretically. Two operation modes were employed to study the performance of the solar air heater. An integrated mode of continuous operation of the system during the period of (11:00 am – 3:00 pm) and non-integrated mode in which the system stored the solar energy through the day then used the stored energy during the period of (3:00 pm – 8:00 pm). The results of parametric study in case of continuous operating showed that the maximum average temperature difference of air between inlet and outlet sections observed on (0.018 kg/s) air mass flow rate were exceeded (17°C) and the maximum outlet temperature that got was exceeded (34°C) for the three months (December, January and February) of experiments. Average efficiency was ranged from 53% to 65%. In the case of storage and then operating, the maximum outlet air temperature was ranged from (27°C) up to (31°C) then decreased with spend of energy to reach (13°C) to (18°C) and the maximum storage energy was (165.14 W) for the porosity of (0.29) , height of (20 cm) and (0.01 kg/s) mass flow rate. The results also, showed that the solar air collector supplied a solar heating fraction (SHF) with an average of (0.65) for a meeting room (3 * 4 * 7 m) located in Baghdad as a case study.

**Keywords:** pebble bed, active solar heating, thermal collector and storage, experimental and theoretical study

## دراسة استدلالية للطاقة الشمسية الفعالة باستخدام فرشة الحصاة كوحدة جمع وخزن للحرارة

**مصطفى مهدي مصطفى العسكري**
مدرس مساعد
كلية الهندسة / جامعة بغداد

**سعد محسن صالح**
استاذ مساعد
كلية الهندسة / جامعة بغداد

## الخلاصة

في هذه الدراسة، وضعت فرشة حصاة باعتبارها مادة امتصاص وتخزين للحرارة باتجاه الجنوب ، وقد تم اجراء دراسة عملية ونظرية لاداء المجمع الشمسي بزاوية مائلة ثابتة (°45) ودراسة تغيير العوامل المختلفة على كفاءة المجمع الشمسي. تم تشغيل المنظومة بطريقتين للتشغيل لتقييم اداء منظومة تجميع الطاقة الشمسية. طريقة متكاملة من التشغيل المستمر للمنظومة الشمسية خلال الفترة  (3:00 pm – 11:00 am) و طريقة غير متكاملة حيث يتم خزن الطاقة الشمسية خلال النهار و تستخدم الطاقة الشمسية المخزونة لاحقا خلال الفترة (8:00 pm – 3:00 pm). أظهرت نتائج الدراسة في حالة التشغيل المستمر أن معدل الحد الأقصى للفرق في درجة حرارة دخول و خروج الهواء من المجمع الشمسي كانت عند معدل تدفق  (0.018 kg/s) والتي تجاوزت (17°C) واعلى درجة حرارة للهواء الخارج من المجمع الشمسي تجاوزت (34°C) لفترة الثلاثة أشهر (ديسمبر، يناير وفبراير) من التجارب. وقد تراوحت متوسط كفاءة المجمع الشمسي من  53% إلى 65%. اما في حالة التخزين والتشغيل، تراوحت درجة الحرارة القصوى لمخرج الهواء من المجمع الشمسي من (27°C) الى (31°C) ثم انخفضت مع

<div dir="rtl">

استهلاك الطاقة ليصل الى مدى تراوح من (C°13) إلى (C°18). وكانت طاقة الخزن القصوى (W 165.14) وذلك عندما كانت المسامية (0.29) و ارتفاع فرشة الحصاة (cm 20) وبمعدل تدفق للهواء (0.01kg/s). أيضا، أظهرت النتائج أن المجمع الشمسي الهوائي يجهز نسبة تدفئة بالطاقة الشمسية (SHF) بمتوسط (0.65) لغرفة الاجتماعات الواقعة في بغداد كحالة دراسية.

**الكلمات الرئيسية:** فرشة الحصاة، التدفئة الشمسية النشطة، التجميع والخزن الحراري، دراسة عملية ونظرية

</div>

## 1. INTRODUCTION

It is becoming increasingly necessary for countries to obtain power from sources other than conventional fossil fuels. This is as a consequence of an increasing population, people becoming more aware of environmental constraints, and the rising cost of conventional fuels. Nuclear and renewable energy sources will have to provide an increasing percentage of total power capacity. Nuclear power is still reliant on limited sources of fuel, and has strong environmental and political implications, limitations by which renewable energy is generally unaffected. It therefore makes sense to consider renewable energy sources as a means of power generation. The largest supply of renewable energy is in the form of solar energy. Several improvements have been suggested in literature to enhance the performance of the system. The use of porous material inside the collector is one method to enhance solar air heater efficiency as suggested by , **Donald** and **John, 1983**. , **Paul** and **Saini, 2003**, **Mittal et al., 2005** and **Ahmed** and **Mohamad, 2007**. Theoretical and experimental study for a solar collector was presented by **Murshid, 2005**. Using porous medium as storage material and heating source, the solar collector was made in case of continuous operating from 9:00 AM to 4:00 PM. The maximum difference between air input temperature and air output temperature from solar collector was reached (15°C) and the maximum efficiency of the solar collector reached up to (50%). Different porous materials have been suggested, such as mild steel particles, **Yeong, 2011**. Fused silica glass, alumina and stainless steel were used by **Mawire, 2009**. **Degirmencioglu, 2006**, investigated the effect of the open-cell polyurethane foam as an absorber material, placed in a south facing, flat plate air-type solar collector at fixed tilt angle on collector efficiency, Collector is tested under the regulations of ASHRAE 93-1986 standard named "Methods of Testing to Determine the Thermal Performance of Solar Collectors". Air passing through the collector has been provided by a fan. Tests are repeated with three air speeds 1.266 m/s, 1.5825 m/s and 1.899 m/s. Maximum average efficiency is calculated on 1.5825 m/s. Maximum average temperature difference of air between inlet and outlet sections observed on 1.266 m/s. Maximum outlet temperature that we get is on the same day with maximum average temperature difference. , **Mohanraj** and **Chandrasekar 2009**, developed and tested performance of an indirect forced convection solar drier integrated with different sensible heat storage maternal. The system consists of a flat plate solar air heater with heat storage unit, a drying chamber and a centrifugal blower. Drying experiments have been performed at an air flow rate of 0.25 kg/s. Drying of chili in a forced convection solar drier reduces the moisture content from around 72.8% (wet basis) to the final moisture content about 9.1% in 24 h. Average drier efficiency was estimated to be about 21%. The specific moisture extraction rate was estimated to be about 0.87 kg/kWh.

In this study, the advantage of using packed beds of pebble to store thermal energy for solar collector has been determined. Effects of various parameters (porosity, height of pebble bed and mass flow rate) on the collector performance had also been investigated.

## 2. MATHEMATICAL MODEL

The packed bed solar air heater model has been considered for this present study is shown in **Fig 1.** The collector consists of a glass cover plate, a blackened absorber plate and a

back plate with blackened pebbles packed in the airflow passage between the absorber and the black colored back plate.

The MATLAB program is used in this work for computer programming. The computation is composed of a main program for one day per month of experiment work. Also it is applicable for each day of the experiment work by changing the variable inputs and the condition of experiment day.

Simplified steps were used to analyze the heat transfer for the air flow across the pebble bed and to calculate the amount of energies and the efficiency. The calculations were based on the following assumptions: (a) study state. (b) one dimensional heat transfer across the glass cover. (c) constant temperature across thickness of glass cover. (d) one dimensional heat transfer across insulation layers. (e) one dimensional heat transfer across the porous media.

## 2.1 Absorption Energy Calculation
The absorption energy could be calculated by the equation below:

$$Q_{ab} = F_t * I_t * A \tag{1}$$

$F_t$ is calculated from Eq. (2) as:

$$F_t = (\alpha_p \tau_g)_e * F_{sh} * F_d \tag{2}$$

## 2.2 Loss Energy Calculation
Losing energy is happening from all sides of the solar collector, in spite of the biggest part of losing is from the absorber surface. However, losing energy from sides and bottom has a clear effect.

The amount of losing energy is given by the following equation:

$$Q_{loss} = U_l * A * (T_p - T_a) \tag{3}$$

Mean plate temperature $(T_p)$ is calculated by **Duffie** and **Beckman, 2008**, as follows:

$$T_p = T_i + \frac{Q_u/A}{F_R U_l} (1 - F_R) \tag{4}$$

The collector overall heat transfer coefficient $(U_l)$ is the sum of top, bottom and edge loss coefficients:

$$U_l = U_t + U_b + U_e \tag{5}$$

The top loss coefficient from the collector plate to the ambient for this single glass cover system is as follows:

$$U_t = [\frac{1}{h_{c,p-g} + h_{r,p-g}} + \frac{1}{h_w + h_{r,g-a}}]^{-1} \tag{6}$$

The wind heat transfer coefficient is calculated as **Duffie** and **Beckman, 2008**.

$$h_w = 5.7 + 3.8\,v \tag{7}$$

The radiation heat transfer coefficient from the glass to the air $(h_{r,g-a})$ is calculated as:

$$h_{r,g-a} = \varepsilon_g \sigma (T_g + T_s)(T_g^2 + T_s^2) \tag{8}$$

The radiation heat transfer coefficient from the plate to the glass cover ($h_{r,p-g}$) is calculated as:

$$h_{r,p-g} = \frac{\sigma(T_p + T_g)(T_p^2 + T_g^2)}{\frac{1}{\varepsilon_p} + \frac{1}{\varepsilon_g} - 1} \tag{9}$$

The convective heat transfer coefficient is calculated as:

$$h_{c,p-g} = \frac{Nu\, K}{D_h} \tag{10}$$

where $D_h = p_t \frac{2Wd}{W+d}$ , ($P_t$= porosity).

Nusselt number $Nu$ is a function of Rayleigh number *Ra* which is given by , **Duffie** and **Beckman, 2008**.

$$Nu = 1 + 1.44 \left[1 - \frac{1708\,(\sin 1.8\beta)^{1.6}}{Ra\cos\beta}\right]\left[1 - \frac{1708}{Ra\cos\beta}\right]^+ + \left[(\frac{Ra\cos\beta}{5830})^{\frac{1}{3}} - 1\right]^+ \tag{11}$$

The heat removal factor $F_R$ is given as:

$$F_R = F''F' \tag{12}$$

Where the collector flow factor F" and the collector efficiency factor F' are calculated as follows:

$$F'' = \frac{\dot{m}_a c_p}{A U_l F'}[1 - \exp(-\frac{A U_l F'}{\dot{m}_a c_p})] \tag{13}$$

$$F' = [1 + \frac{U_l}{h(14)\frac{1}{h} + \frac{1}{h_r})^{-1}}]^{-1}$$

The radiation coefficient between the two air duct surfaces at a mean fluid temperature $T_{mf}$ is:

$$h_r = \frac{4\,\sigma\,T_{mf}^3}{\frac{1}{\varepsilon_p} + \frac{1}{\varepsilon_g} - 1} \tag{15}$$

The heat transfer coefficient inside the duct is:

$$h = Nu1\frac{K}{D_h} \tag{16}$$

Where $Nu1 = 0.0158\,Re^{0.8}$

The useful gain is calculated as follow:

$$Q_u = F_R A[S - U_l(T_i - T_a)] \tag{17}$$

Which is also can be calculated as:

$$Q_u = \dot{m}_a * c_p * (T_o - T_i) \tag{18}$$

"eq. (16) dependent in experimental calculation"

From Eq. (17) & (18), the outlet temperature is:

$$T_o = T_i + Q_u/\dot{m}_a * c_p \tag{19}$$

## 2.3 Thermal Efficiency Calculation

The efficiency of the flat-plate solar collector ($\eta_c$) is defined as the ratio of the rate of useful energy supplied by the collector ($Q_u$) to the rate of incident solar energy in its area.

$$\eta_c = \frac{Q_u}{Q_I} \tag{20}$$

## 2.4 The Performance of a Solar Collector in an Active System

It's a simple procedure which has been devised by **Balcomb** and **McFarland, 1978** and used by the researcher  **Murshid, 2005** for predicting the performance of solar collector in active systems. This calculation can be made based on the values of solar radiation, heating degree days, and the thermal loss and solar gain characteristics of the building. In this study, load collector ratio (LCR) was used as the following steps.

Estimate the building loss coefficient (BLC). This is the sum of the building skin conductance plus infiltration.

$$BLC = (\sum UA_s + INF) * 24 * 3600 \tag{21}$$

The solar heating fraction (SHF) is the fraction of save energy to the net load which is calculated as follows:

$$SHF = Q_{save} / Q_{net} \tag{22}$$

$$Q_{save} = \dot{m}_a * c_p * \sum_1^{24} (T_{ao} - 18)^+ \tag{23}$$

$$Q_{net} = BLC * DD \tag{24}$$

$$DD = \sum_1^{24} (20 - T_a)^+ \tag{25}$$

"The (+) sign in Eqs. (23) and (25) indicate that only the positive value taken into account"

The auxiliary energy ($Q_{aux}$) required keeping the building at (20°C) calculated as follows:

$$Q_{aux} = (1 - SHF) * BLC * DD \tag{26}$$

## 2.4 Energy Balance

Based on the assumptions that have been mentioned and used to solve mathematical equations relating to the performance of solar collector for the collection and storage, we have developed a mathematical model by performing an energy balance on the solar collector.
The equation of thermal energy balance is written as shown in **Fig. 2**

(Energy absorbed by the surface absorber) + (Energy entering the air solar collector) = (Energy leaving the air solar collector) + (Stored Energy) + (Energy lost from the solar collector)

This can be written in the formula as follows:

$$I_t * A + \dot{m}_a * c_p * T_i = \dot{m}_a * c_p * T_o + E_{st} + U_l * A * (T_p - T_a) \tag{27}$$

The above equation can be written as:-

$$Q_{st} = I_t * A - \dot{m}_a * c_p * (T_o - T_i) - U_l * A * (T_p - T_a) \tag{28}$$

## 3. EXPERIMENTAL WORK

Air-type solar collector was used in this project. Basically the experimental setup consists of three main mechanical parts. First and the most important part is the collector itself. Second part is the inlet and outlet channels. Third part is the blower that provides air stream during experiments. Pebble bed with (0.29) and (0.34) porosity placed in the collector flow channel in order to increase heat transfer area.

The solar collector is made locally for the purposes of collect and storage at the same time. It consists of a reservoir of iron with dimensions of (1x0.6x0.25 m) and a thickness of (2 mm) for the purpose of carrying the weight of the porous material used to make the tank in case of consistency and stability. Three brackets of iron mesh were installed to support and facilitate the development of porous media in the collector reservoir, and also to distribute air evenly across the porous media. (1mm) thickness aluminum plate was used as absorber plate and coated with black color to receive maximum amount of solar incident radiation. The solar collector was isolated from all sides and bottom with class wool insulation of (5cm) thickness to reduce the heat losses. A glass cover (4mm) thickness and (1x0.6m) dimensions applied at the surface of the solar collector. It was sealed to prevent leakage of water into the solar collector or heat air loss. The gap between the glass cover and the absorber plate was ranged from (5cm) when the pebble bed depth was (20cm), and it was (10 cm) when the pebble bed depth was (15cm).

The experiments were conducted on the days of December, January and February in Baghdad. The collector was located with 45 angle towards the south (For winter load, the tilt should be (latitude + 10) degrees and for year round use, the tilt = latitude, [12]). **Fig. (1)** shows the general aspect of experimental setup. The experiments were carried out at the same time periods between (11:00 to 15:00) of the days (In the case of continuous operation) and between (15:00 to 20:00) of the days (In the case of storage and operation) for (0.01 kg/s) & (0.018 kg/s) of mass flow rates. The air flow through the collector was supplied by an electric blower and adjusted via a regulator integrated with the blower. The velocity of the air was measured by an anemometer sensor. The incident solar radiation on collectors' inclined upper surface was measured up to date by (Datalogging Solar Power Meter TES-1333R). Type K thermocouples were placed at inlet, outlet flow channels, back plate, pebble bed, absorber plate, glazing cover of the collector and a free one to measure ambient temperature.

## 4. RESULTS AND DISSCUSION

**Fig. 3** shows the variation of the intensity of solar radiation with time for the days (21 Dec., 5 Jan. and 10 Feb.). As shown in this figure, the intensity of solar radiation increases steadily with time and attained peak values at the mid-day then decrease steadily with time as the sun goes down in the late afternoon. It observed that the maximum solar intensity reaches to (764.5 W/m$^2$) in (21 Dec) and it is reached to (1005 W/m$^2$) in (5 Jan) while it is (900.3 W/m$^2$) in (10 Dec).

In the case of continuous operating for the solar collector the solar collector has been run with electric blower which is working from 11:00 am to 3:00 pm. The temperature was meas-

ured at different sections, air inlet, air outlet, back plate, pebble bed, absorber plate, glazing cover of the collector and the ambient. According to these measurements, the efficiency, the useful, storage and loss energy were calculated. **Fig. 4** shows the effect of height of the pebble bed on average temperature (by using thermocouples distributed at three equal distance) of porous media with time for mass flow rate of (0.01 kg/s) for days in Dec., Jan. and Feb. The temperatures of porous media increase gradually from (11:00 am) and reach the maximum value at (3:00 pm) which exceed (30°C) with height of (15 cm) of pebble bed. In one hand variation of temperature of the porous media with time because the intensity of solar radiation increase gradually and through this period the temperature of absorber plate increase and this is lead to increase of the temperature of porous media. In another hand it can be observed that the maximum temperature of pebble bed is at (15 cm) because it heated faster than (20 cm) pebble bed height.

**Fig. 5** shows the variation of inlet air temperature to the collector and the experimental and theoretical outlet air temperature with time for (0.018 kg/s) mass flow rate for the days of (21 Dec., 5 Jan. and 10 Feb.). **Fig. 5a** shows a convergence between the experimental and theoretical outlet air temperature and matching point at 12:30 pm. The maximum outlet air temperature from the solar air collector was (35.5°C experimentally and 33.07°C theoretically). The maximum temperature difference between inlet and outlet air from the solar collector was (17.9°C). The convergence with less error was found in **Fig. 5b** and the matching was achieved from (1:00 to 2:00 pm). The maximum outlet air temperature from the solar air collector was (34.6°C experimentally and 33.03°C theoretically) and the maximum temperature difference between inlet and outlet air from the solar collector was (20°C). The same behavior was shown in Fig. (5c) with matching points at (1:00 and 1:30 pm) respectively. The maximum outlet air temperature from the solar air collector was (34.3°C experimentally and 32.9°C theoretically) and the maximum temperature difference between inlet and outlet air from the solar collector was (18.2°C). The differences between the experimental and theoretical values in the previous figures because of the different in the theoretical values of useful energy which are actively involved in the Eq. (19), and that because the theoretical calculation of solar intensity which effect on useful energy are different from the experimental values of solar intensity. The average of the maximum outlet air temperature from the solar air collector was (34.8°C) and the average of the maximum temperature difference between inlet and outlet air from the solar collector was (18.7°C).

**Fig. 6** shows the variation of thermal efficiency with solar radiation for mass flow rate of (0.01 and 0.018 kg/s) respectively, pebble bed height of (15 cm) and (0.34) porosity for the days of (22 Jan. and 2 Feb.). The efficiency increases with an increase in the solar radiation. This is due to the increase of temperature difference which is directly proportion to the efficiency. But it can be seen that even when the solar radiation decrease after (1:30 pm), the efficiency continue to rise. This is also because increase of temperature difference and this is a positive point for use the porous media that help to store heat even when the sun goes down in the late afternoon.

The effect of temperature rise on the efficiency of the solar collector for mass flow rate of (0.01 and 0.018 kg/s), pebble bed height of (15 cm) and (0.34) porosity for the days of (22 Jan. and 2 Feb.) is shown **Fig. 7.** The thermal efficiency increases with the increase in the temperature rise because of the direct proportion of efficiency with the temperature rise that has direct proportion to the useful gain and that approved by applying Eq. (20).
The effect of mass flow rate of air on the variation of inlet and outlet air temperature difference with time is shown in **Fig. 8** for different height and porosity of the pebble bed. It has been observed that the temperature difference increases with increase in mass flow up to (26%). The figure also shows that the temperature difference has been reached the maximum value between (1:30 to 2:00 pm) then the curve goes down for the days of experimental work. This is because

of the behavior of solar radiation shown in **Fig. 4**. Temperature difference is directly proportion to solar radiation.

There is a significant effect of mass flow rate on efficiency. It is evident from **Fig. 9**, that for higher mass flow rate, efficiency is much higher with a rate ranging from (48%) to (54%). This behavior has been obtained experimentally and it can be approved theoretically from Eq. (20).

**Fig. 10** shows the effect of porosity of pebble bed on the variation of air temperature difference between inlet and outlet of the solar collector with time, which is higher for low porosity. It has been observed that the values in the two porosity experiment are quite close, but deviation occur with time progress. It can be concluded that there is an increment ranging from (4%) to (20%) showing the effect of porosity on the temperature difference.

There was no significant effect of porosity on efficiency with higher mass flow rate. This is shown in **Fig. 11** It has been seen randomly behavior of the curves in the previous figure because of the effect of the experimental amount of solar radiation which is involve in Eq. (20), and that because the different weather in which the experiments process.

**Fig. 12** shows the effect of height of pebble bed on the variation of temperature difference with time. It has been shown that the pebble bed with (15cm) height has the higher temperature difference with a rate ranging from (5%) to (29%) in Dec. and Jan. for (0.018 kg/s) air mass flow rate and ranging from (10%) to (38%) in Feb. for (0.01 kg/s) air mass flow rate. The solar radiation takes less time to reach pebble bed with (15cm) than the pebble bed with (20cm), so the lower pebble bed will get more heat and thus the higher temperature difference.

**Fig. 13** shows the variation of solar heating fraction for a different height of the pebble bed. This comparison shows that for (h=15 cm) in the months of December and January, the (SHF) was higher than that for (20 cm) with a fraction reached to (57 %). While in February, the behavior was inversed because of the different in (SHF) values which are depend on the amount of solar intensity measured experimentally. The variation of auxiliary energy that we need to add it for the days of (27 Dec., 5 Jan., and 10 Feb.) and the days of (10 Dec., 10 Jan., and 23 Feb) was shown in **Fig. 14** It was observed that in (5 Jan) it is need higher auxiliary energy reached to (21, 093 kJ) while in (17 Feb.) less energy must be adding. The maximum auxiliary energy (2,276 kJ) in (23 Feb.) and it is need (2,795 kJ) in (10 Jan) these amounts depended on the (SHF) values, where the higher value (SHF) there is less need for the auxiliary energy.

## 5. CONCLUSIONS

The main conclusions from the present work may be stated as follows:

- The increment of efficiency due to pebble placing can be observed easily in spite of decreasing the solar radiation.
- The solar collector supply hot air up to (29 C°) with average temperature difference of (14 C°),
- The efficiency of the solar collector increases with the increment of air velocity with a rate ranging from (48%) to (54%).
- Decreasing the pebble bed height, increasing the efficiency with a rate of (4% to 30%) and the increment of the temperature difference ranging from (10%) to (38%) for a given mass flow rate.
- The variation of air temperature difference between inlet and outlet of the solar collector with time was higher for low porosity with an increment ranging from (4%) to (20%).
- The solar collector supplied a solar heating fraction (SHF) with an average of (0.65).

## REFERENCES

➢ Ashish K., 2009, *Mathematical Modeling of Solar Air heater with Different Geometries*, M.Sc. thesis, Thapar University.

➢ Bashria, A., Yousef, A. and Adam, N. M, 2007, *Analysis of single and Double Passes V-Grooves Solar Collector with and without Porous Media*. International Journal of Energy and Environment,vol.2,No.1,PP.109-114.

➢ Beasley, D.E. and Clark J.A., 1983, *Investigation of Rock Bed Solar Collector Cum Storage System*, International Journal of Heat and Mass transfer, vol.27, No.9, PP.1659-1669.

➢ Bennamoun, L. and Belhamri, A., 2008, *Study of Heat and Mass Transfer in Porous Media*, Tech Science Press, vol.4, No.4, PP. 221-230.

➢ Cheung, A. C.; Chiang, C. W.; Chen, M. S., 1979, *Heat Transfer in a Porous Medium Flat Plate Solar Collector*, Proceedings of the Multi-Phase Flow and Heat Transfer Symposium-Workshop, PP.16-18.

➢ Choudhury C., Chauhan P. M. and Garg H. P., 2008, *Economic Design of a Rock Bed Storage Device for Storing Solar Thermal*, Center for Energy Studies, Indian Institute of Technology.

➢ Degirmencioglu, C., 2006, *The Use of Open Cell Polyurethane Foams in Air-Type Solar Collectors as the Heat Absorbing Element*, M.Sc. Thesis, The Graduate School of Engineering and Sciences of İzmir Institute of Technology.

➢ Garg, Bandyo and Sharma, 1981, *Investigation of Rock Bed Solar Collector Cum storage system*, Center of energy studies, Indian Technology.

➢ Irfan Kurtbas and Emre Turgut, 2006, *Experimental Investigation of Solar Air Heater with Free and Fixed Fins*, International Journal of Science & Technology, vol. 1, No.1, PP.75-82.

➢ Kenneth Guy Allen, 2010, *Performance Characteristics of Packed Bed Thermal Energy Storage for Solar Thermal Power Plants*, M.Sc. Thesis, University of Stellenbosch.

➢ Klein, S. A., Beckman, W. A. and Duffie, J. A., 1975, *Design Procedure for Solar Air Heating System*, International Solar Energy Society, Los Angeles.

➢ Mawire A., 2009, *Simulated Performance of Storage Materials for Pebble Bed Thermal Energy Storage (TES) Systems*, Journal of Applied Energy.

➢ Mittal, M.K., Varshney, L., 2005, *Optimal Thermo Hydraulic Performance of a Wire Mesh Packed Solar Air Heater*, Solar Energy, vol.80, PP.1112-1120.

➢ Mohandraj M. And Chandrasekar P., 2009, *Performance of a Forced Convection Solar Drier Integrated With Gravel as Heat Storage Material for Chili Drying*, Journal of Engineering Science and Technology, vol. 4, No. 3, PP.305 – 314.

➢ Murshid A. M., 2005, *Performance Study of Using the Active Solar Energy for Heating by Using Porous Media*, M.Sc. Thesis, University of Tikrit.

➢ Navarrete, J.J., Cervantes J.G., 2008, *Energy Analysis of a Rock Bed Thermal Storage System*, International Journal of Energy, vol.5, No.1, PP.18-30.

➢ Paul B. and Saini J. S., 2003, *Thermohydraulic Performance of Pebble Bed Solar air Heaters*. Proceedings of the International Conference on Mechanical Engineering.

➢ Qenawy, A. M. and Mohamad, A. A., 2007, *Analysis of High Efficiency Solar Air Heater for Cold Climates*, 2nd Canadian Solar Buildings Conference Calgary, vol.10, No.14.

➢ Yeong, W., Lai, Y. and Foo J., 2011, *Improvement of a Solar Heating Panel's Thermal Efficiency*, vol.4, No.1, PP.44-55.

## 7. NOMENCLATURE

A =  area of solar collector, $m^2$.
As = area of skin condition, $m^2$.
BLC = building loss coefficient, J/DD.
Cp = specific heat of air, J/kg.°C.
Fd = dust coefficient, dimensionless.
Fsh = shading coefficient, dimensionless.
Ft = effective transmittance-absorption factor, dimensionless.
FR = heat removal factor, dimensionless.
F' = collector efficiency factor, dimensionless.
F" = collector flow factor, dimensionless.
Dh = hydraulic diameter, m.
DD = degree-Day, °C.
H = coefficient of heat transfer, $W/m^2.K$.
It = total incident radiation, $W/m^2$.
INF = infiltration, W/°C.
K = thermal conductivity, W/m.K.
L = length of bed, m.
m.a = mass flow rate of air, kg/s.
Nu = nusselt number, dimensionless.
Pt = porosity, dimensionless.
Q = energy, W.
Ra = rayleigh number, dimensionless.
Re = reynolds number, dimensionless.
S = absorbed solar radiation, $W/m^2$.
SHF = solar heating fraction, dimensionless.
T = temperature, °C.

Ub = back loss coefficient, $W/m^2.K$.
Ue = edge loss coefficient, $W/m^2.K$.
Ul = overall loss coefficient, $W/m^2.K$.
Ut = top loss coefficient, $W/m^2.K$.

**GREEK SYMBOLS**
α = absorptance of surface for solar radiation, dimensionless.
β = tilt angle, degree.
τ = glass transmittance, dimensionless.
Δ = difference, dimensionless.
η = efficiency, dimensionless.
$ε_g$ = penetration of glass cover, dimensionless.
σ = bultzmann constant, dimensionless.
$ε_p$ = emittance of surface, dimensionless.

**SUBSCRIPTS**
a = ambient, dimensionless.
b = bottom, dimensionless.
c = convection, dimensionless.
e = edge, dimensionless.
f = fluid, dimensionless.
g = glass, dimensionless.
i = inlet, dimensionless.
m = mean, dimensionless.
o = outlet, dimensionless.
p = plate, dimensionless.
r = radiation, dimensionless.
u = useful, dimensionless.
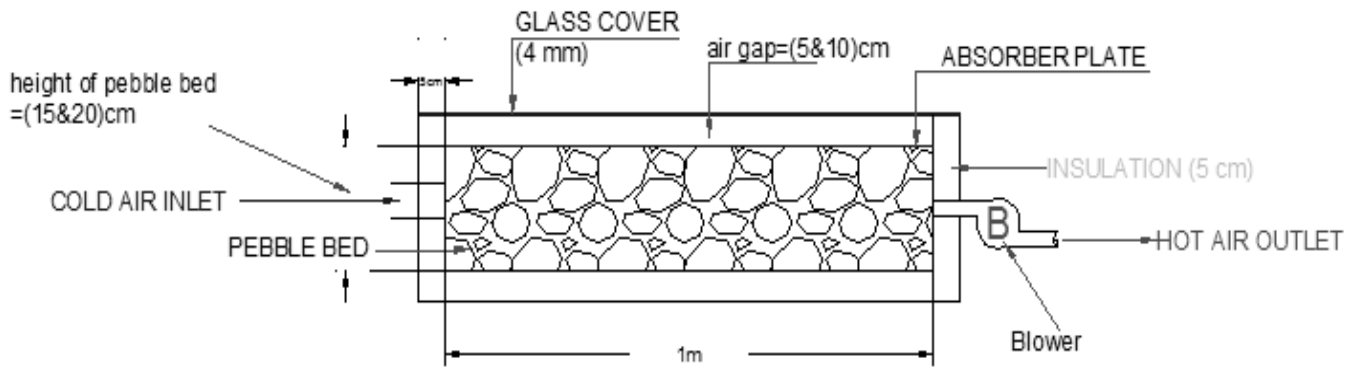
**Figure 1.** Cross section of the solar air heater.
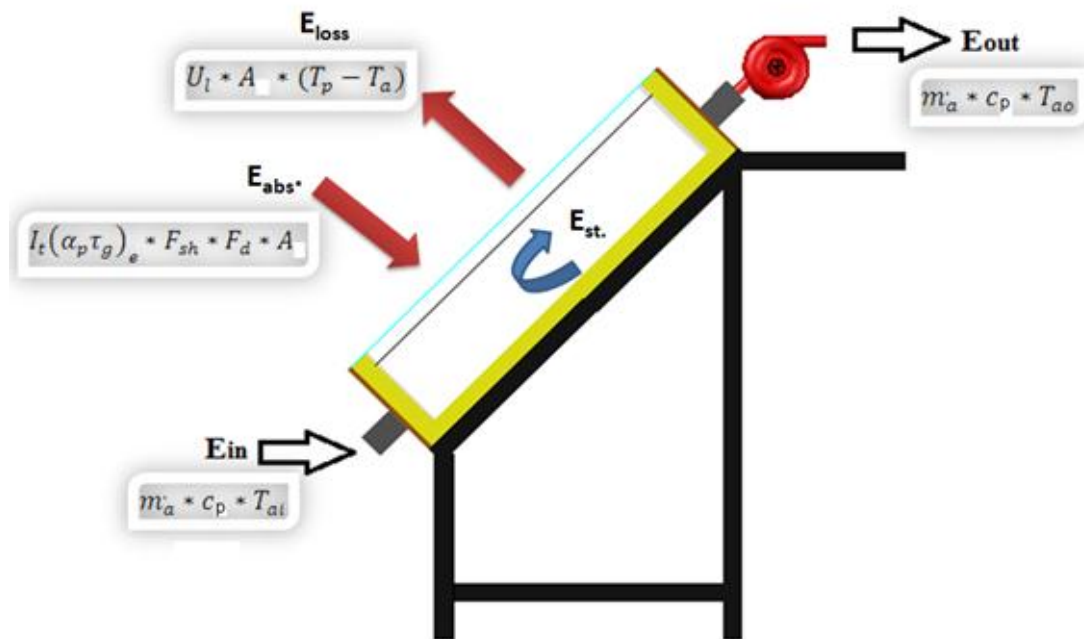


**Figure 2.** Energy balance on the solar collector.

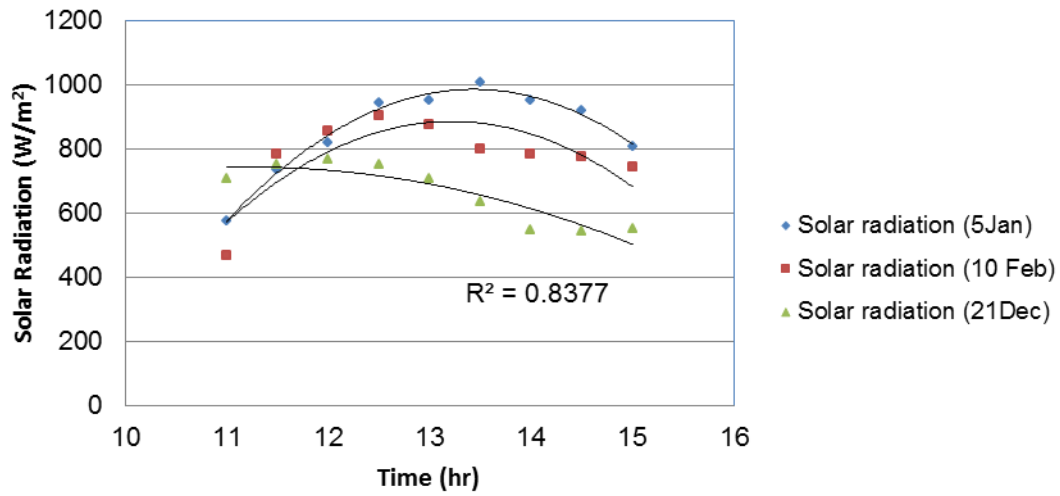**Parameters: (h=height of pebble bed, m'=air mass flow rate, p=porosity)**



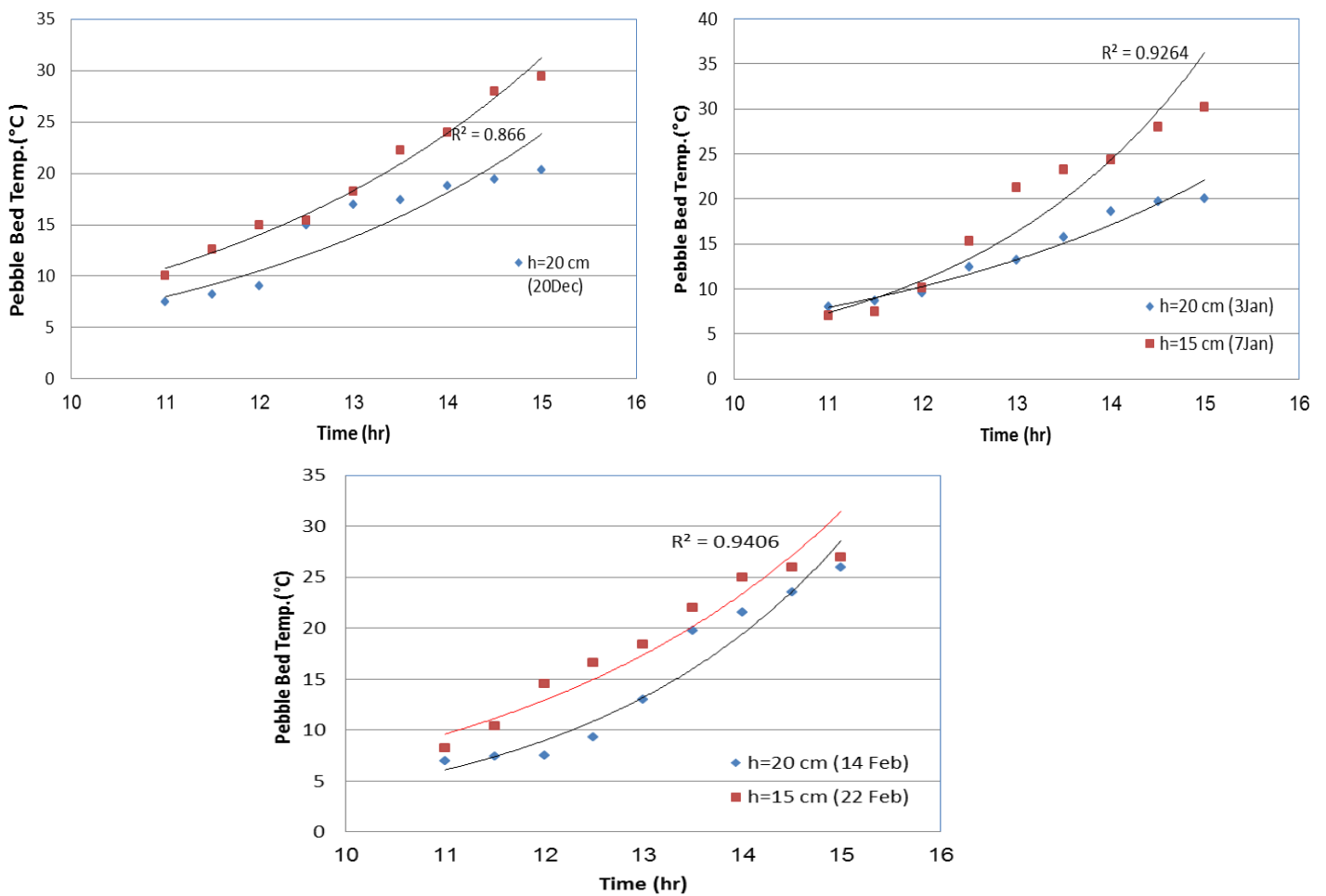**Figure 3.** Variation of Solar radiation with time (h=20 cm, m'=0.018 kg/s , p=0.29).



**Figure 4**. Variation of temperature of porous media with time for different pebbles bed heights (m'=0.01 kg/s, p=0.29).
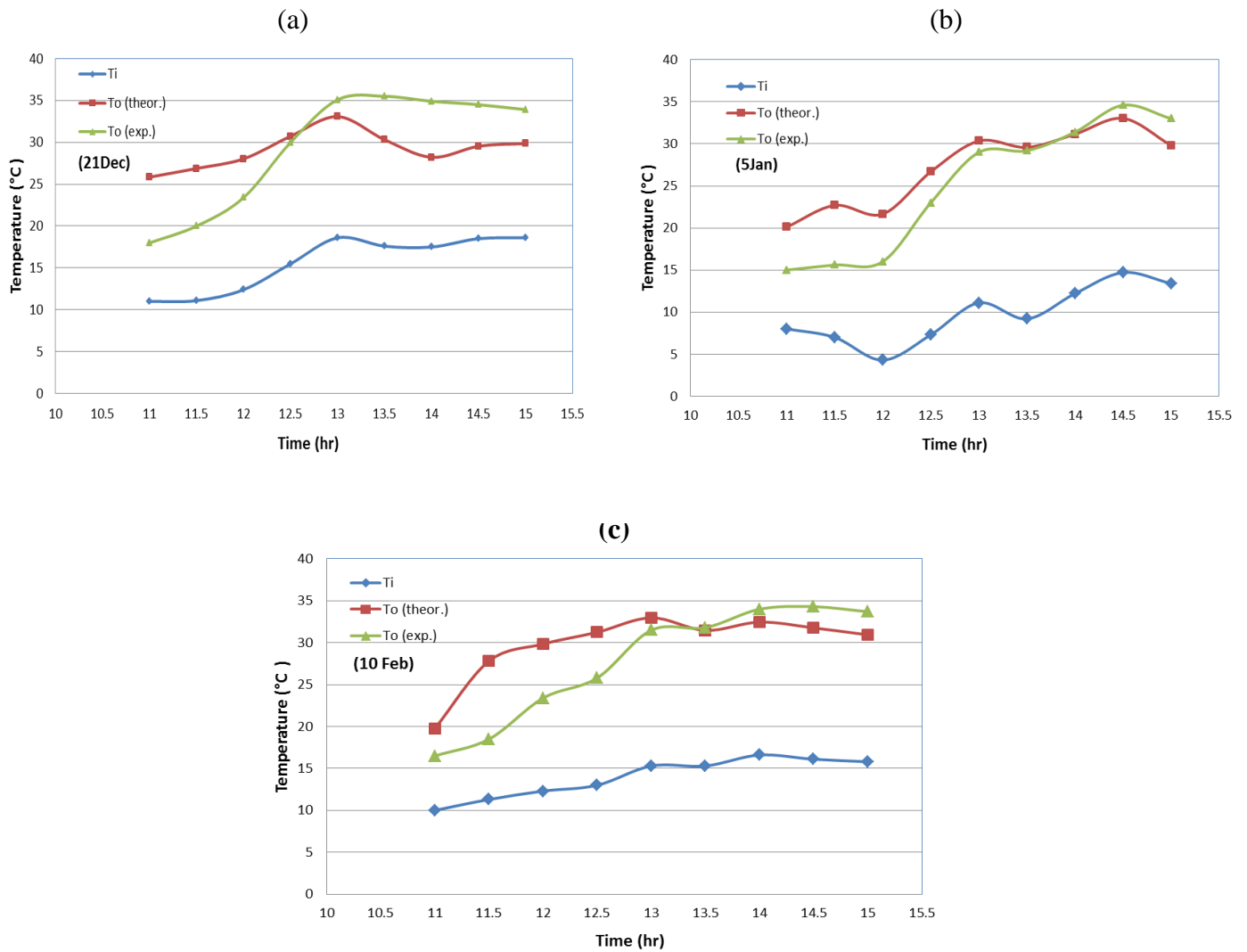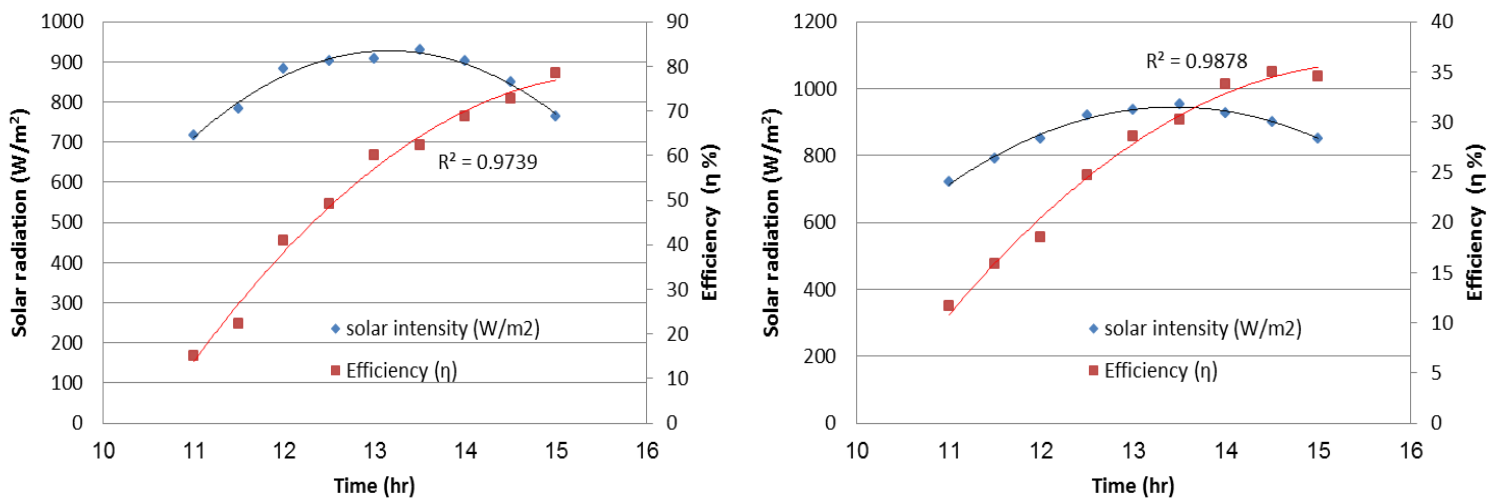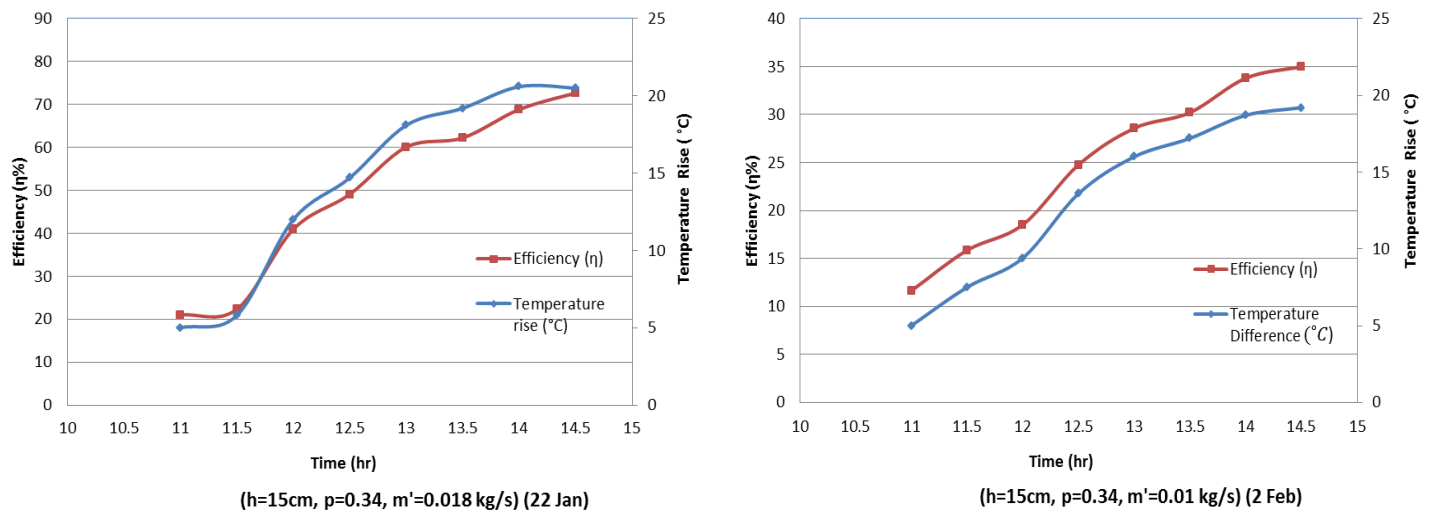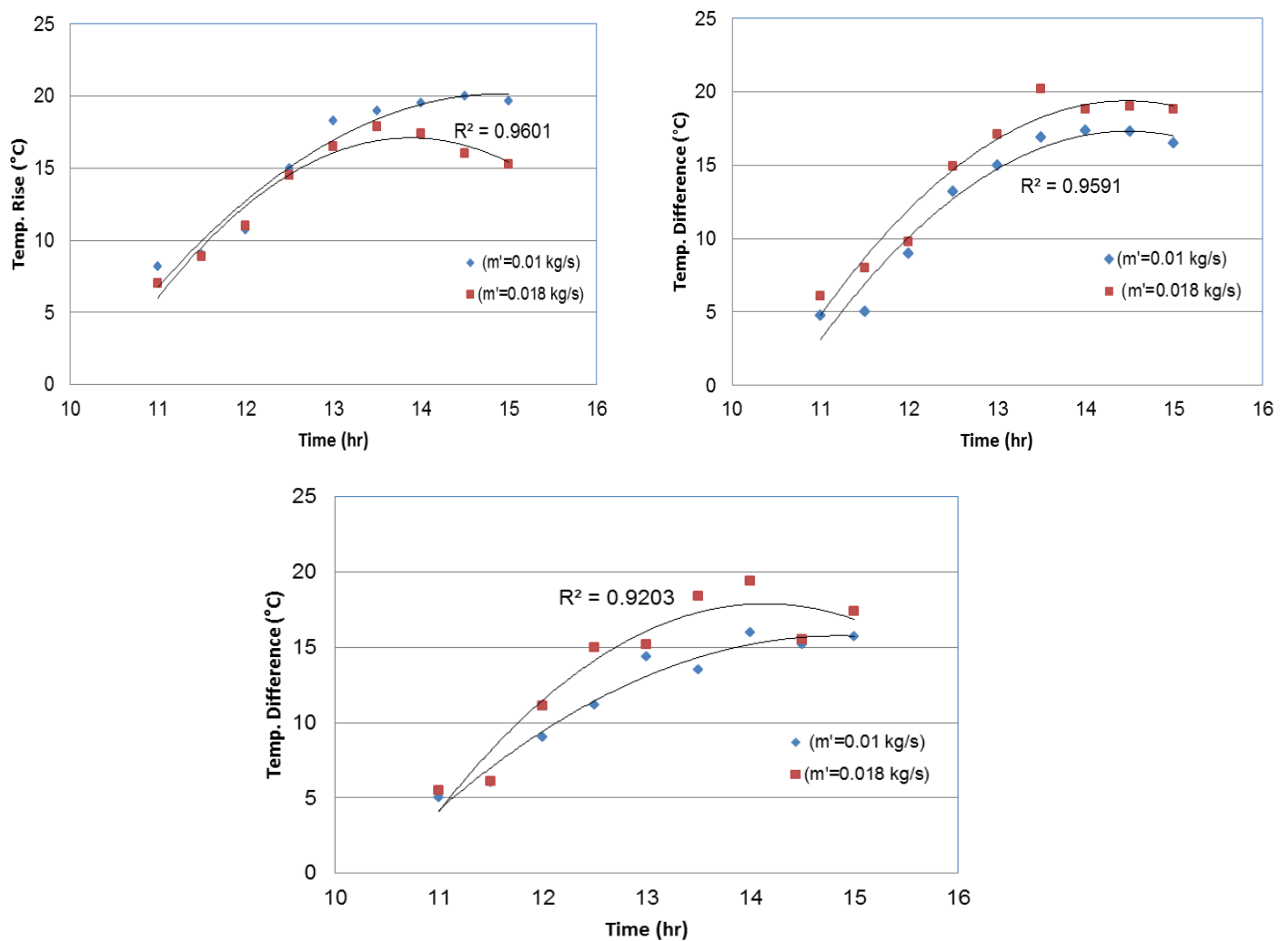
(a)

(b)



(c)



**Figure 5.** Variation of inlet and outlet temperatures with time (h=20 cm, m'=0.018 kg/s , p=0.34).

**Figure 6.** Effect of solar radiation on efficiency with time.



(h=15cm, p=0.34, m'=0.018 kg/s) (22 Jan)

(h=15cm, p=0.34, m'=0.01 kg/s) (2 Feb)

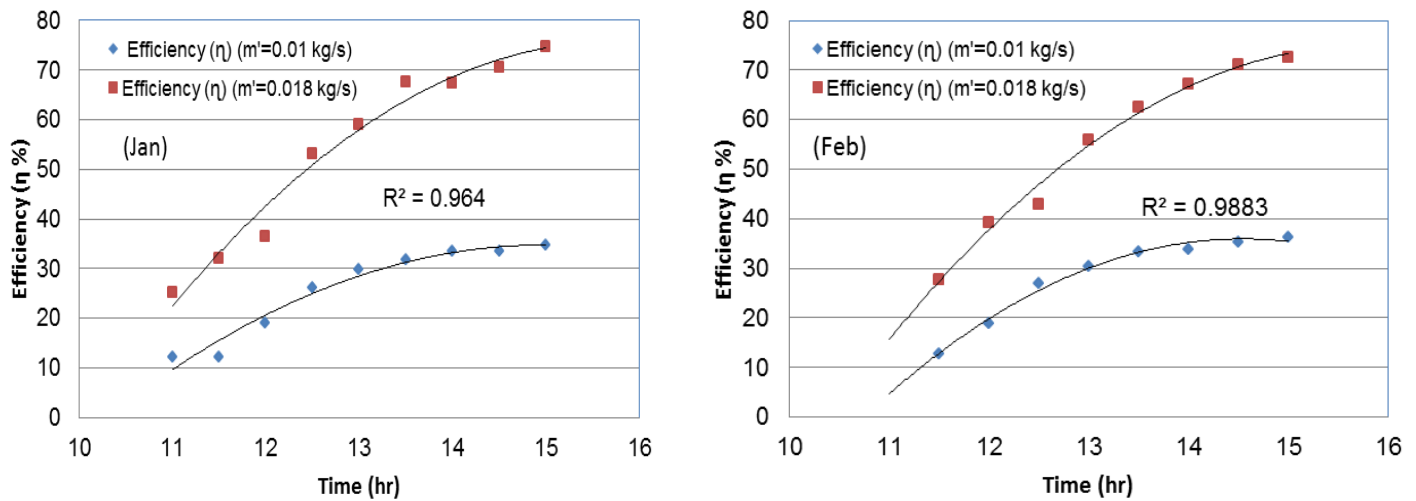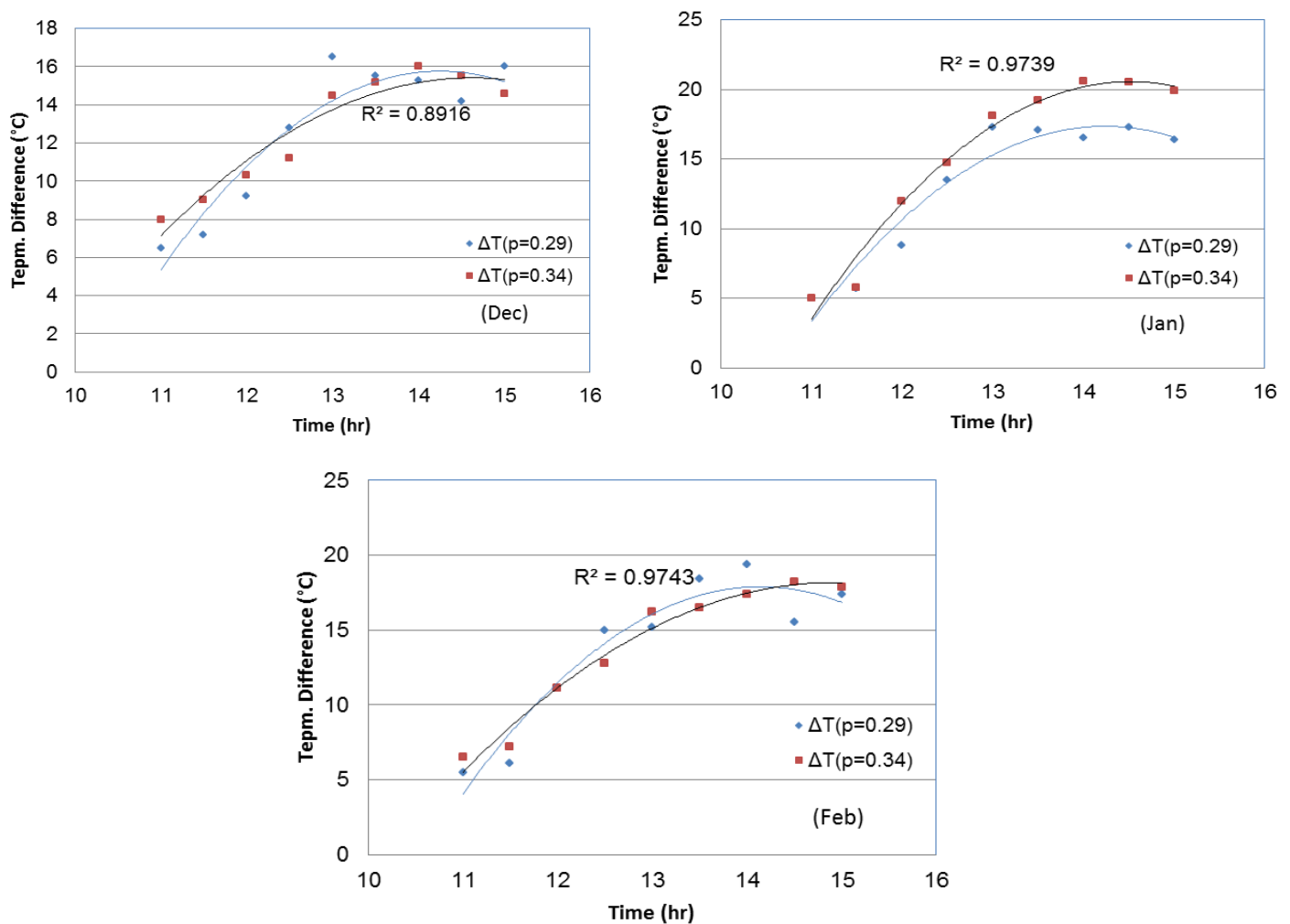**Figure 7.** Effect of temperature rise on efficiency with time.

**Figure 8.** Effect of mass flow rate on variation of temperature rise with time.



**Figure 9.** Effect of mass flow rate on variation of efficiency with time.

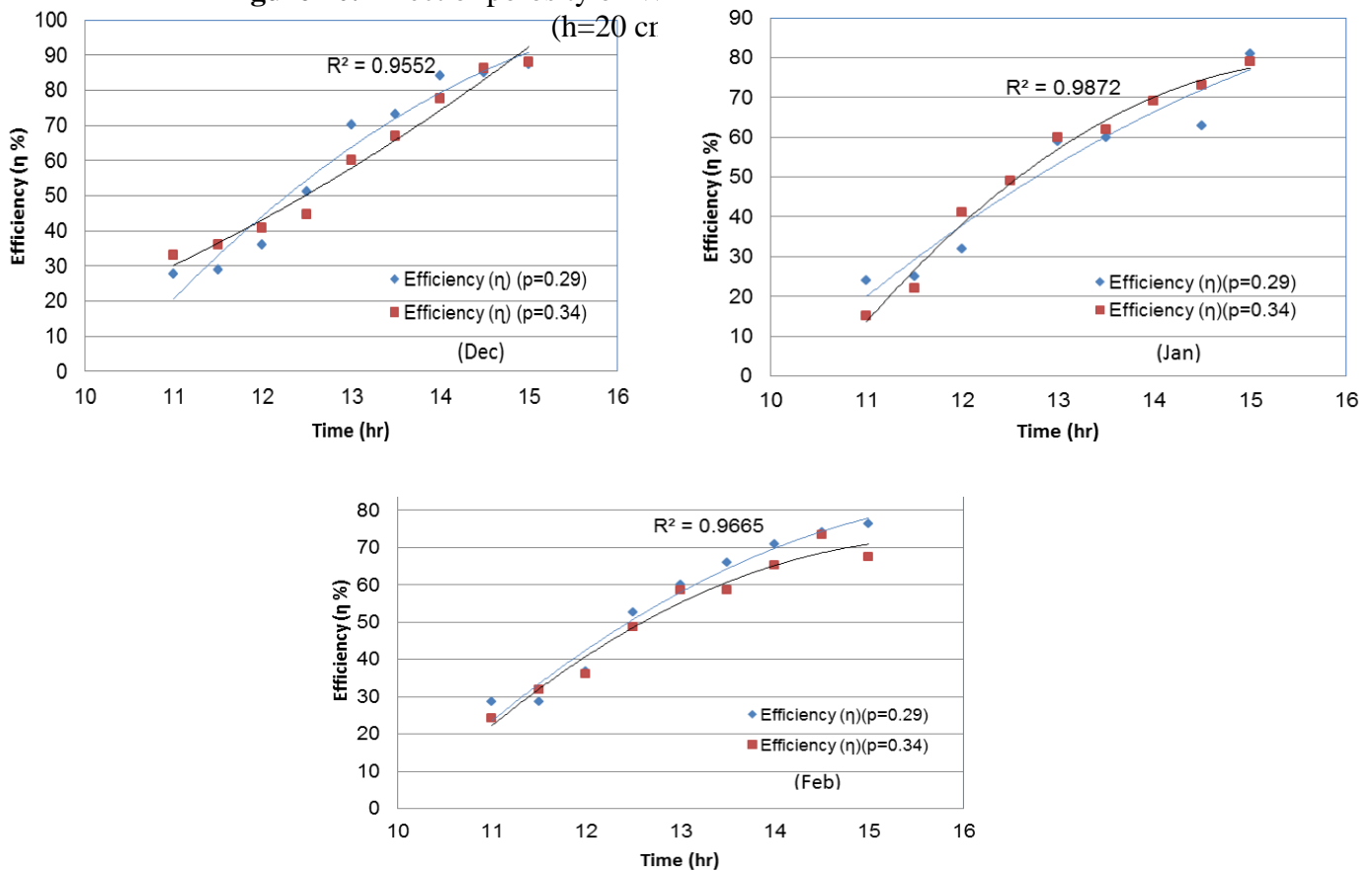**Figure 10.** Effect of porosity on variation of efficiency with time
(h=20 cm



**Figure 11.** Effect of porosity on variation of efficiency with time (h=15 cm, m'=0.018 kg/s).
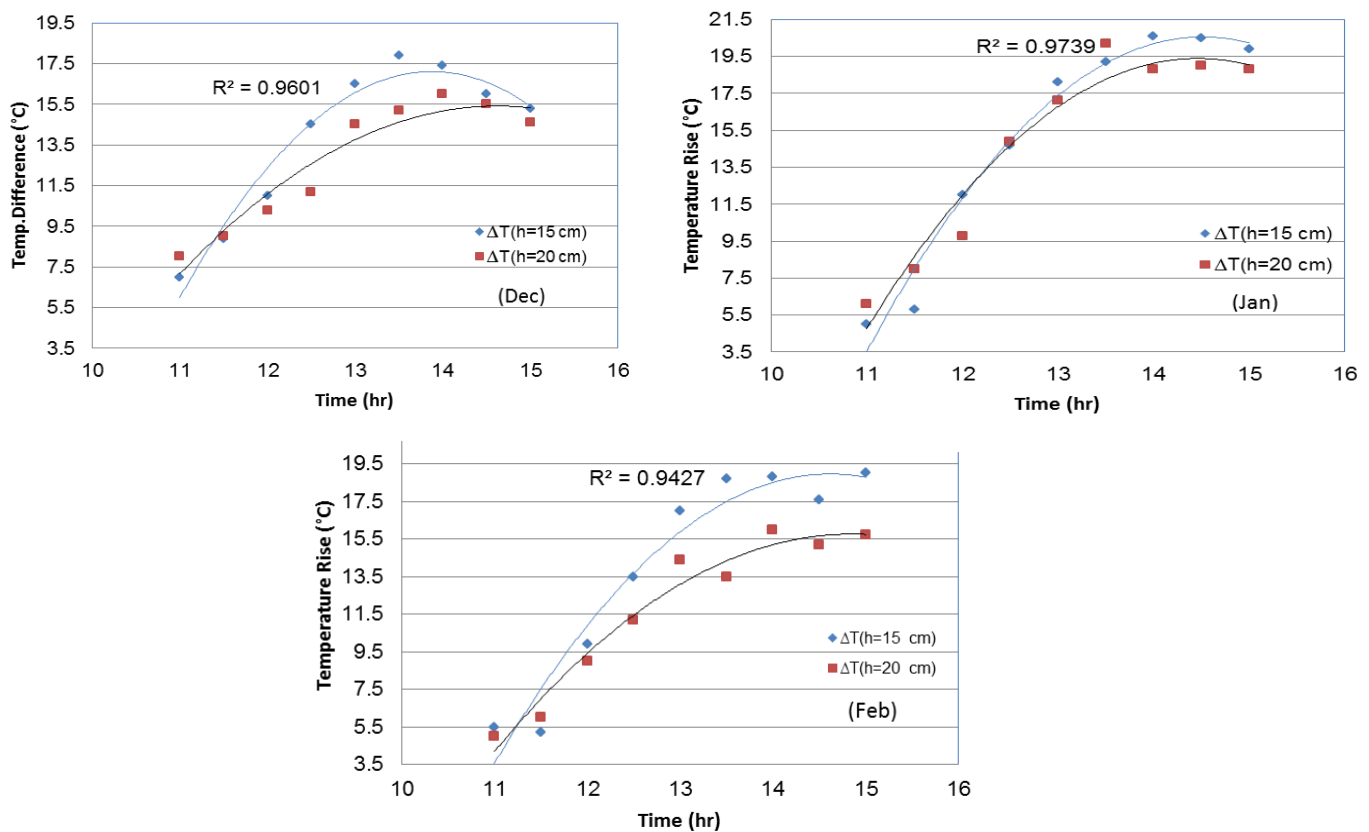
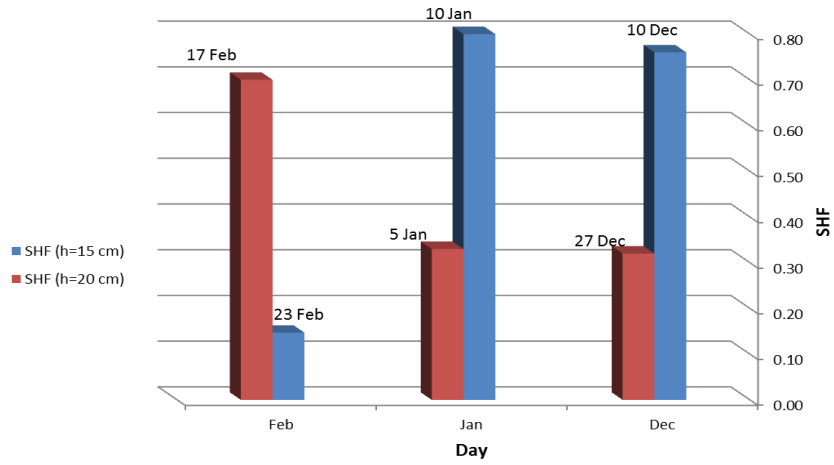**Figure 12.** Effect of height on variation of temperature difference with time.



**Figure 13.** Variation of solar heating fraction for different height of pebble bed
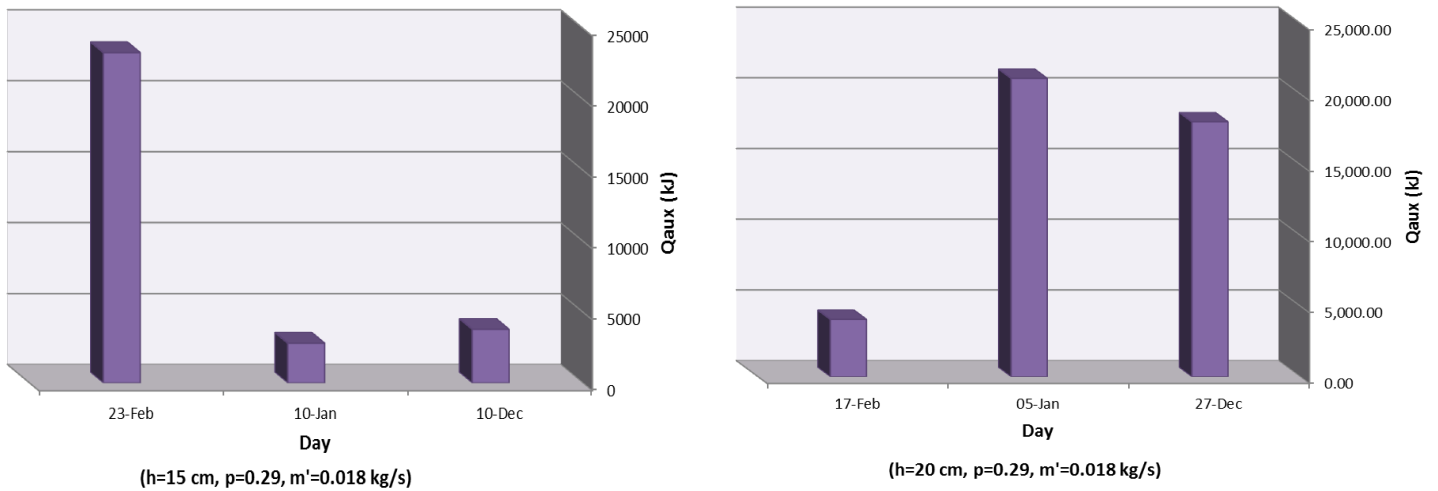(p=0.29, m'=0.018 kg/s).



**Figure 14.** Variation of the auxiliary energy.

# Buckling Analysis of Stiffened and Unstiffened Laminated Composite Plates

**Dr. Adnan Naji Jameel**
Professor
University of Baghdad
College of Engineering
Mechanical Engineering Dep.
adnanaji2004@yahoo.com

**Dr. louay Sabah yousuf**
Assistant Professor
University of Baghdad
College of Engineering
Mechanical Engineering Dep.
louaysabah79@yahoo.com

**Eng.Ahmed Mahdi Salih**
Researcher
University of Baghdad
College of Engineering
Mechanical Engineering Dep.
flightstar8888@yahoo.com

## ABSTRACT

The present study focused mainly on the analysis of stiffened and unstiffened composite laminated plates subjected to buckling load. Analytical, numerical and experimental analysis for different cases has been considered. The experimental investigation is to manufacture the laminates and to find mechanical properties of glass-polyester such as longitudinal, transverse young modulus, shear modulus. The compressive test was carried to find the critical buckling load of plate. The design parameters of the laminates such as aspect ratio, thickness ratio, boundary conditions and number of stiffeners were investigated using high order shear deformation theory (HOST) and Finite element coded by ANSYS .The main conclusion was the buckling load could increase and decrease depending on the boundary conditions, thickness ratio, and, the aspect ratio and number of stiffeners of the plate.

**Keywords:** composite laminated plate, glass-polyester, bucking load, high order shear deformation, stiffened and unstiffened plate.

<div dir="rtl">

## تحليل الصفائح المركبة المقواة والغير مقواة تحت تأثير حمل الانبعاج

**المهندس احمد مهدي صالح**
باحث
جامعة بغداد \ كلية الهندسة

**د. لؤي صباح يوسف**
أستاذ مساعد
جامعة بغداد \ كلية الهندسة

**د. عدنان ناجي جميل**
أستاذ
جامعة بغداد \ كلية الهندسة

### الخلاصة

هذه الدراسة ركزت بشكل رئيسي على تحليل الصفائح المركبة المقواة والغير مقواة المعرضة لحمل الانبعاج.وتم التحليل النظري،التحليل العددي والعملي لمختلف الحالات.في الجانب العملي تم تصنيع الصفائح المركبة المصنوعة من الالياف الزجاجية والبوليستر لايجاد الخواص الميكانيكية مثل معامل يونك الطولي والعرضي ومعامل القص.تم عمل اختبار الانضغاط للعثور على القيمة الحرجة لحمل الانبعاج للصفيحة. كما تم بحث عناصر تصميم شرائح مثل نسبةالعرض إلى الارتفاع،ونسبة سماكة وشروط الحدية وعدد المقويات باستخدام النظرية تشوه القص الدرجة العالية و طريقة العناصر المحددة المبرمجة باستخدام برنامج ANSYS.وكان الاستنتاج الرئيسي ان قيمة حمل الانبعاج يمكن ان يقل او يزيد تبعا لشروط الحدية،ونسبة سماكة،ونسبةالعرض إلى الارتفاع لوحة وعدد المقويات للبيليتة.

**الكلمــات الرئيسـية:** صـفائح مركبـة,أليـاف زجاجيـة , حمـل الانبعـاج , نظريـة تشـوه القـص الدرجة العاليـة للصـفائح الطباقية,الصفائح المقواة وغير المقواة.

</div>

## 1.  INTRODUCTION
### 1.1 General

During the last decades, needs for *composite materials* which contain two or more types of materials mixed together homogenously have appeared.

Composite materials have many advantages such as high strength with low weight compared with traditional engineering materials; furthermore, their properties can be controlled during mixing of their components to meet the suitable design requirements.

When a flat plate is subjected to low in-plane compressive loads, it remains flat and is in equilibrium condition. As the magnitude of the in-plane load increases, however, the equilibrium configuration of the plate is eventually changed to a non-flat configuration and the plate becomes unstable and begins to deflect to the middle portion. **, Reddy J.N. 2004.**

Many researches had studied buckling analysis of stiffened and unstiffened plate.

**Guedes Soares C.** and **Gordo J. M.1997,** performed of three methods to design stiffened panels under predominantly in plane uniaxial compressive loading is compared by referring to numerical and experimental results.

**Satish Kumar Y.V.,  Madhujit Mukhopadhyay  1999,** presented the basic plate element is a combination of Allman's plane stress triangular element and a Discrete Kirchhoff-Mindlin plate bending element. The element includes transverse shear effects. The model accommodates any number of arbitrarily oriented stiffeners within the plate element and eliminates constraints on the mesh division of the plate.

**Rikards  R. etal 2001,** concentrated on the development of triangular finite element for buckling and vibration analysis of laminated composite stiffened shells. For the laminated shell, an equivalent layer shell theory is employed. The first-order shear deformation theory including extension of the normal line is used. In order to take into account a non-homogeneous distribution of the transverse shear stresses a correction of transverse shear stiffness is employed. Results of vibration and buckling analysis of stiffened plates and shells are discussed.

 **Samuel Kidane2002,** investigated buckling loads of stiffened composite cylinders under uniaxial loading condition by using analytical and experimental approaches. The stiffness contributions of the stiffeners are computed by analyzing the moment and force effect of the stiffener on a unit cell. Then the equivalent stiffness of the stiffener/shell panel is computed by superimposing the stiffness contribution of the stiffeners and the shell. Once the equivalent stiffness parameters are determined for the whole panel, the buckling load is calculated using the energy method.

**Aseel Jasim Mohammed Al-Hassani 2005,** investigated the vibration   characteristic of composite plates with and without holes ,manufactures  of fiber glass+ polyester  in the presence of steel layers reinforcement , stiffeners subjected to various load conditions and constraints (simply supported and clamped).

An experimental programmed was also conducted in order to obtain the material properties of the used plates and study the plate behavior under static load and measuring the strain and deflection from which the structures are obtained and compared with the numerical results.

**Akl W. etal 2008,** selected the orientation angles of stiffeners arranged in the form of isogrid configuration over a flat plate to optimize the static and dynamic characteristics of these plates/stiffeners assemblies. The static characteristics are optimized by maximizing the critical buckling loads of the isogrid plate, while the dynamic characteristics are optimized by maximizing multiple natural frequencies of the stiffened plate.

**Tran Ich Thinh and Tran Huu Quoc2010,** studied free vibration and bending failure of laminated stiffened glass fiber/polyester composite plates with laminated open section (rectangular or T-shaped) and closed section (hat shaped) of stiffeners by finite element method and experiment. The results calculated by computational model for above plates under different boundary conditions are in good agreement with experiments. The failure problems of these stiffened glass fiber/polyester composite plates are also investigated.

**Hasanain Ibrahim Nsaif 2011,** investigated Buckling analysis of composite laminates for critical thermal and mechanical loads. The analytical investigation involved certain mathematical preliminaries, a study of equations of orthotropic elasticity for classical laminated plate theory (CLPT), higher order shear deformation plate theory (HSDT), and numerical analysis (Finite element method).

The present work is focused on how to derive the analytical solution of critical bucking load for stiffened and unstiffened composite laminated plates by high order shear deformation theory by applied different type of boundary condition on the symmetric cross-ply composite laminated plates using Levy solution .Mechanical properties, buckling load for composite plate made from (glass-polyester) with fiber volume fraction (0.3) are determined experimentally.

Also Finite element coded by ANSYS12.1used to find critical buckling load of stiffened and unstiffened composite laminate plate.

## 2. ANALYTICAL SOLUTION (HIGHER ORDER SHEAR DEFORMATION PLATE THEORY)
### 2.1. Unstiffened Laminated Plate
### 2.1.1 Displacement

High order shear deformation plate theory (HSDT) based on assuming the straight line perpendicular to the mid surface before deformation become curve line after deformation, **Reddy, J.N. 2004**.

$$u(x,y,z,t) = u_o(x,y,t) + z\emptyset_x(x,y,t) - \frac{4}{3h^2}z^3\left(\emptyset_x + \frac{\partial w_0}{\partial x}\right) \tag{1. a}$$

$$v(x,y,z,t) = v_o(x,y,t) + z\emptyset_y(x,y,t) - \frac{4}{3h^2}z^3\left(\emptyset_y + \frac{\partial w_0}{\partial y}\right) \tag{1. b}$$

$$w(x,y,z,t) = w_o(x,y,t) \tag{1. c}$$

### 2.1.2 Stress and strain

The total strains can be written as follows

$$\begin{Bmatrix} \varepsilon_{xx} \\ \varepsilon_{yy} \\ \gamma_{xy} \end{Bmatrix} = \begin{Bmatrix} \varepsilon_{xx}^{(0)} \\ \varepsilon_{yy}^{(0)} \\ \gamma_{xy}^{(0)} \end{Bmatrix} + z\begin{Bmatrix} \varepsilon_{xx}^{(1)} \\ \varepsilon_{yy}^{(1)} \\ \gamma_{xy}^{(1)} \end{Bmatrix} + z^3\begin{Bmatrix} \varepsilon_{xx}^{(3)} \\ \varepsilon_{yy}^{(3)} \\ \gamma_{xy}^{(3)} \end{Bmatrix} \tag{2.a}$$

$$\begin{Bmatrix} \gamma_{yz} \\ \gamma_{xz} \end{Bmatrix} = \begin{Bmatrix} \gamma_{yz}^{(0)} \\ \gamma_{xz}^{(0)} \end{Bmatrix} + z\begin{Bmatrix} \gamma_{yz}^{(1)} \\ \gamma_{xz}^{(1)} \end{Bmatrix} + z^2\begin{Bmatrix} \gamma_{yz}^{(2)} \\ \gamma_{xz}^{(2)} \end{Bmatrix} \tag{2.b}$$

The transformed stress-strain relations of an orthotropic lamina in a plane state of stress are; for $\bar{Q}_{ij}$ see ,**Reddy J.N. 2004**.

$$\begin{Bmatrix} \sigma_{xx} \\ \sigma_{yy} \\ \sigma_{xy} \end{Bmatrix}_k = \begin{bmatrix} \bar{Q}_{11} & \bar{Q}_{12} & \bar{Q}_{16} \\ \bar{Q}_{12} & \bar{Q}_{22} & \bar{Q}_{26} \\ \bar{Q}_{16} & \bar{Q}_{26} & \bar{Q}_{66} \end{bmatrix}_k \begin{Bmatrix} \varepsilon_{xx} \\ \varepsilon_{yy} \\ \gamma_{xy} \end{Bmatrix} \qquad \textbf{(3.a)}$$

$$\begin{Bmatrix} \sigma_{yz} \\ \sigma_{xz} \end{Bmatrix}_k = \begin{bmatrix} \bar{Q}_{44} & \bar{Q}_{45} \\ \bar{Q}_{45} & \bar{Q}_{55} \end{bmatrix} \begin{Bmatrix} \gamma_{yz} \\ \gamma_{xz} \end{Bmatrix} \qquad \textbf{(3.b)}$$

The result stress Nxx, Nyy and Nxy, Mxx,Myy and Mxy , shear force Qxz, Qyz, Rxz, Ryz , and the higher order stress resultants Pxx, Pyy and Pxy  acting on a laminate are obtained by integration of the stress in each layer or lamina through the laminate thickness. Knowing the stress in terms of the displacement, the stress resultants Nxx, Nyy, Nxy, Mxx, Myy, Mxy, Qxz, Qyz, Pxx, Pyy, Pxy, Rx and Ry can be obtained .

The inplane force resultants are defined as

$$\begin{Bmatrix} N_{xx} \\ N_{yy} \\ N_{xy} \end{Bmatrix} = \sum_{r=1}^{N} \int_{z_k}^{z_{k+1}} \begin{Bmatrix} \sigma_{xx} \\ \sigma_{yy} \\ \sigma_{xy} \end{Bmatrix}_k dz \qquad \textbf{(4.a)}$$

Where $\sigma_x$ , $\sigma_y$ and $\sigma_{xy}$ are normal and shear stress.

$$\begin{Bmatrix} N_{xx} \\ N_{yy} \\ N_{xy} \end{Bmatrix} = \begin{bmatrix} A_{11} & A_{12} & A_{16} \\ A_{12} & A_{22} & A_{26} \\ A_{16} & A_{26} & A_{66} \end{bmatrix} \begin{Bmatrix} \varepsilon_{xx}^0 \\ \varepsilon_{yy}^0 \\ \gamma_{xy}^0 \end{Bmatrix} + \begin{bmatrix} B_{11} & B_{12} & B_{16} \\ B_{12} & B_{22} & B_{26} \\ B_{16} & B_{26} & B_{66} \end{bmatrix} \begin{Bmatrix} \varepsilon_{xx}^1 \\ \varepsilon_{yy}^1 \\ \gamma_{xy}^1 \end{Bmatrix} - c_1 \begin{bmatrix} E_{11} & E_{12} & E_{16} \\ E_{12} & E_{22} & E_{26} \\ E_{16} & E_{26} & E_{66} \end{bmatrix} \begin{Bmatrix} \varepsilon_{xx}^{(3)} \\ \varepsilon_{yy}^{(3)} \\ \gamma_{xy}^{(3)} \end{Bmatrix} \qquad \textbf{(4.b)}$$

$$\begin{Bmatrix} M_{xx} \\ M_{yy} \\ M_{xy} \end{Bmatrix} = \sum_{r=1}^{N} \int_{z_k}^{z_{k+1}} \begin{Bmatrix} \sigma_{xx} \\ \sigma_{yy} \\ \sigma_{xy} \end{Bmatrix}_k z \, dz \qquad \textbf{(5.a)}$$

$$\begin{Bmatrix} M_{xx} \\ M_{yy} \\ M_{xy} \end{Bmatrix} = \begin{bmatrix} B_{11} & B_{12} & B_{16} \\ B_{12} & B_{22} & B_{26} \\ B_{16} & B_{26} & B_{66} \end{bmatrix} \begin{Bmatrix} \varepsilon_{xx}^0 \\ \varepsilon_{yy}^0 \\ \gamma_{xy}^0 \end{Bmatrix} + \begin{bmatrix} D_{11} & D_{12} & D_{16} \\ D_{12} & D_{22} & D_{26} \\ D_{16} & D_{26} & D_{66} \end{bmatrix} \begin{Bmatrix} \varepsilon_{xx}^1 \\ \varepsilon_{yy}^1 \\ \gamma_{xy}^1 \end{Bmatrix} - c_1 \begin{bmatrix} F_{11} & F_{12} & F_{16} \\ F_{12} & F_{22} & F_{26} \\ F_{16} & F_{26} & F_{66} \end{bmatrix} \begin{Bmatrix} \varepsilon_{xx}^{(3)} \\ \varepsilon_{yy}^{(3)} \\ \gamma_{xy}^{(3)} \end{Bmatrix} \qquad \textbf{(5.b)}$$

$$\begin{Bmatrix} P_{xx} \\ P_{yy} \\ P_{xy} \end{Bmatrix} = \sum_{k=1}^{N} \int_{z_k}^{z_{k+1}} \begin{Bmatrix} \sigma_x \\ \sigma_y \\ \sigma_{xy} \end{Bmatrix}_k z^3 \, dz \qquad \textbf{(6.a)}$$

$$\begin{Bmatrix} P_{xx} \\ P_{yy} \\ P_{xy} \end{Bmatrix} = \begin{bmatrix} E_{11} & E_{12} & E_{16} \\ E_{12} & E_{22} & E_{26} \\ E_{16} & E_{26} & E_{66} \end{bmatrix} \begin{Bmatrix} \varepsilon_{xx}^0 \\ \varepsilon_{yy}^0 \\ \gamma_{xy}^0 \end{Bmatrix} + \begin{bmatrix} F_{11} & F_{12} & F_{16} \\ F_{12} & F_{22} & F_{26} \\ F_{16} & F_{26} & F_{66} \end{bmatrix} \begin{Bmatrix} \varepsilon_{xx}^1 \\ \varepsilon_{yy}^1 \\ \gamma_{xy}^1 \end{Bmatrix} - c_1 \begin{bmatrix} H_{11} & H_{12} & H_{16} \\ H_{12} & H_{22} & H_{26} \\ H_{16} & H_{26} & H_{66} \end{bmatrix} \begin{Bmatrix} \varepsilon_{xx}^{(3)} \\ \varepsilon_{yy}^{(3)} \\ \gamma_{xy}^{(3)} \end{Bmatrix} \qquad \textbf{(6.b)}$$

$$\begin{Bmatrix} Q_{yz} \\ Q_{xz} \end{Bmatrix} = \int_{-h/2}^{h/2} \begin{Bmatrix} \sigma_{yz} \\ \sigma_{xz} \end{Bmatrix}_k dz \tag{7.a}$$

$$\begin{Bmatrix} Q_{yz} \\ Q_{xz} \end{Bmatrix} = \begin{bmatrix} A_{44} & A_{45} \\ A_{45} & A_{55} \end{bmatrix} \begin{Bmatrix} \gamma_{yz}^{(0)} \\ \gamma_{xz}^{(0)} \end{Bmatrix} - c_2 \begin{bmatrix} D_{44} & D_{45} \\ D_{45} & D_{55} \end{bmatrix} \begin{Bmatrix} \gamma_{yz}^{(2)} \\ \gamma_{xz}^{(2)} \end{Bmatrix} \tag{7.b}$$

$$\begin{Bmatrix} R_{yz} \\ R_{xz} \end{Bmatrix} = \int_{-h/2}^{h/2} \begin{Bmatrix} \sigma_{yz} \\ \sigma_{xz} \end{Bmatrix}_k z^2 \, dz \tag{8.a}$$

$$\begin{Bmatrix} R_{yz} \\ R_{xz} \end{Bmatrix} = \begin{bmatrix} D_{44} & D_{45} \\ D_{45} & D_{55} \end{bmatrix} \begin{Bmatrix} \gamma_{yz}^{(0)} \\ \gamma_{xz}^{(0)} \end{Bmatrix} - c_2 \begin{bmatrix} F_{44} & F_{45} \\ F_{45} & F_{55} \end{bmatrix} \begin{Bmatrix} \gamma_{yz}^{(2)} \\ \gamma_{xz}^{(2)} \end{Bmatrix} \tag{8.b}$$

*Where*

$$A_{ij}, B_{ij}, D_{ij}, E_{ij}, F_{ij}, H_{ij} = \sum_{k=1}^{N} \int_{z_k}^{z_{k+1}} \bar{Q}_{ij}^{(k)} (1, z, z^2, z^3, z^4, z^6) \, dz \tag{9}$$

**2.1.3** Equation of motion

The Euler-Lagrange equations are obtained by setting the coefficient of $\delta u_0$, $\delta v_0$, $\delta w_0$, $\delta\emptyset_x$, $\delta\emptyset_y$ to zero separately

$$\frac{\partial N_{xx}}{\partial x} + \frac{\partial N_{xy}}{\partial y} = 0 \tag{10.a}$$

$$\frac{\partial N_{xy}}{\partial x} + \frac{\partial N_{yy}}{\partial y} = 0 \tag{10.b}$$

$$\frac{\partial Q_x}{\partial x} - c_2 \frac{\partial R_x}{\partial x} + \frac{\partial Q_y}{\partial y} - c_2 \frac{\partial R_y}{\partial y} + c_1 \left( \frac{\partial^2 P_{xx}}{\partial x^2} + 2 \frac{\partial^2 P_{xy}}{\partial x \partial y} + \frac{\partial^2 P_{yy}}{\partial y^2} \right) + \widehat{N}_{xx} \frac{\partial^2 w}{\partial x^2} + \widehat{N}_{yy} \frac{\partial^2 w}{\partial y^2} + 2\widehat{N}_{xy} \frac{\partial^2 w}{\partial x \partial y} = 0 \tag{10.c}$$

$$\frac{\partial M_{xx}}{\partial x} - c_1 \frac{\partial P_{xx}}{\partial x} + \frac{\partial M_{xy}}{\partial y} - c_1 \frac{\partial P_{xy}}{\partial y} - Q_x + c_2 R_x = 0 \tag{10.d}$$

$$\frac{\partial M_{xy}}{\partial x} - c_1 \frac{\partial P_{xy}}{\partial x} + \frac{\partial M_{yy}}{\partial y} - c_1 \frac{\partial P_{yy}}{\partial y} - Q_y + c_2 R_y = 0 \tag{10.e}$$

These equations of motion (10a-e) can be expressed in terms of displacements ($\delta u_0$, $\delta v_0$, $\delta w_0$, $\delta\emptyset_x$, $\delta\emptyset_y$)by substituting the forces results from eqs. (4,5,6,7,8) into eq. (10.a) to (10.e) and get partial differential equations, then the analytical solution done by levy method as derived in[9].

## 2.2 Stiffened Laminated Plate
**2.2.**1 Stress and strain

The displacements field of laminated plate are as given in Eqs (1(a-c)). The distribution of the normal strains over the depth of the stiffened plate is shown in **Fig. (1),** [10]
Then, the stress strain relations for laminated plate are as in Eqs. (3,a-b) and the stress strain relations for stiffeners can be defined as:

$$\sigma_{xx})st = E_x^{st}.\mathcal{E}_{xx}., \qquad \sigma_{yy})st = E_y^{st}.\mathcal{E}_{yy}$$
$$,\tau_{xy}) st = 0, \qquad \tau_{yz}) st = G_y^{st}.\gamma_{yz},$$
$$\tau_{xz}) st = G_x^{st}.\gamma_{xz} \tag{11}$$

Where, $G_x^{st}$ and $G_y^{st}$ are shear modules of elasticity of stiffeners in x and y directions , respectively. The force and moment relation for stiffened plate are:

$$\begin{bmatrix} N \\ M \\ P \end{bmatrix} = \begin{bmatrix} N \\ M \\ P \end{bmatrix}_{unst} + \begin{bmatrix} N \\ M \\ P \end{bmatrix}_{st} ,$$

$$And, \quad \begin{bmatrix} Q \\ R \end{bmatrix} = \begin{bmatrix} Q \\ R \end{bmatrix}_{unst} + \begin{bmatrix} Q \\ R \end{bmatrix}_{st} \tag{12}$$

Where, $\begin{bmatrix} N \\ M \\ P \end{bmatrix}_{unst}$ and $\begin{bmatrix} Q \\ R \end{bmatrix}_{unst}$ are force and moment relations for laminated plate as in

Eqs. (4, 5, 6, 7, 8(a-b)).

And $\begin{bmatrix} N \\ M \\ P \end{bmatrix}_{st}$ and $\begin{bmatrix} Q \\ R \end{bmatrix}_{st}$ are forces and moment relations for stiffeners can be defined as:

$$N_{xx})st. = \int_{Zi-1)x^{st}}^{Zi)x^{st}} \sigma_x)st . \frac{tx}{bx} . dZ$$

$$N_{yy})st. = \int_{Zi-1)y^{st}}^{Zi)y^{st}} \sigma_y)st. \frac{ty}{by} . dZ, N_{xy})st = 0$$

$$M_{xx})st. = \int_{Zi-1)x^{st}}^{Zi)x^{st}} \sigma_x)st . \frac{tx}{bx} . Z. dZ$$

$$M_{yy})st. = \int_{Zi-1)y^{st}}^{Zi)y^{st}} \sigma_y)st. \frac{ty}{by} . Z. dZ, M_{xy})st = 0$$

$$P_x)st. = \int_{Zi-1)x^{st}}^{Zi)x^{st}} \sigma_x)st . \frac{tx}{bx} . Z^3 . dZ \tag{13}$$

$$P_y)st. = \int_{Zi-1)y^{st}}^{Zi)y^{st}} \sigma_y)st. \frac{ty}{by} . Z^3 . dZ,$$

$$P_{xy})st = 0$$

Where,

$Zi)x^{st} , Zi-1)x^{st} , Zi)y^{st} ,$
$Zi-1)y^{st} , t_x , b_x , t_y , b_y$ as shown in **Fig.2** or, Eq. (13) can be written as:

$$\begin{bmatrix} N_{xx} \\ N_{yy} \\ M_{xx} \\ M_{yy} \\ P_x \\ P_y \end{bmatrix}_{st} = \begin{bmatrix} A_{11}^{st} & 0 \\ 0 & A_{22}^{st} \\ B_{11}^{st} & 0 \\ 0 & B_{22}^{st} \\ E_{11}^{st} & 0 \\ 0 & E_{22}^{st} \end{bmatrix} \begin{bmatrix} \varepsilon_{xx} \\ \varepsilon_{yy} \end{bmatrix} \tag{14}$$

Where,

$$(A_{11}^{st}, B_{22}^{st}, D_{11}^{st}, E_{11}^{st}) = \int_{Zi-1)x^{st}}^{Zi)x^{st}} \frac{tx}{bx} . Ex^{st}. (1, Z, Z^2, Z^3). dZ \tag{15a}$$

$$(A_{11}^{st}, B_{22}^{st}, D_{11}^{st}, E_{11}^{st}) = \int_{Zi-1)y^{st}}^{Zi)y^{st}} \frac{ty}{by} . Ey^{st}. (1, Z, Z^2, Z^3). dZ \tag{15b}$$

And, $\begin{bmatrix} Q \\ R \end{bmatrix}_{st}$ can be defined as in equations:

$$
\left.\begin{aligned}
Q_{yz})st &= \int_{Zi-1)y^{st}}^{Zi)y^{st}} \gamma_{yz} . Gy^{st} . \frac{ty}{by} . dZ \\
Q_{xz})st &= \int_{Zi-1)x^{st}}^{Zi)x^{st}} \gamma_{xz} . Gx^{st} . \frac{tx}{bx} . dZ \\
R_{yz})st &= \int_{Zi-1)y^{st}}^{Zi)y^{st}} \gamma_{yz} . Gy^{st} . \frac{ty}{by} . Z^2 . dZ \\
R_{xz})st &= \int_{Zi-1)x^{st}}^{Zi)x^{st}} \gamma_{xz} . Gx^{st} . \frac{tx}{bx} . Z^2 . dZ
\end{aligned}\right\}
$$

(16a)

Or, equation (16a) can be written as:

$$
\begin{bmatrix} Q_{yz} \\ Q_{xz} \\ R_{yz} \\ R_{xz} \end{bmatrix} st =
\begin{bmatrix} A_{44}^{st} & 0 \\ 0 & A_{55}^{st} \\ D_{44}^{st} & 0 \\ 0 & D_{55}^{st} \end{bmatrix}
\begin{bmatrix} \gamma_{yz} \\ \gamma_{xz} \end{bmatrix}
$$

(16b)

Where,

$$
A_{44}^{st} = \int_{Zi-1)y^{st}}^{Zi)y^{st}} Gy^{st} . \frac{ty}{by} . dZ,
$$

$$
A_{55}^{st} = \int_{Zi-1)x^{st}}^{Zi)x^{st}} Gx^{st} . \frac{tx}{bx} . dZ
$$

$$
D_{44}^{st} = \int_{Zi-1)y^{st}}^{Zi)y^{st}} Gy^{st} . \frac{ty}{by} . Z^2 . dZ
$$

$$
D_{55}^{st} = \int_{Zi-1)x^{st}}^{Zi)x^{st}} Gx^{st} . \frac{tx}{bx} . Z^2 . dZ
$$

**2.2.2** Equations of motion
The refined analysis of such a plate, the governing differential equations are expressed in terms of the displacements, u, v, and w of the middle surface of the plate in the directions x, y, and z, respectively. The displacements at any point are related to those at the middle surface.

### 3. NUMERICAL ANALYSIS
### 3.1 Element Selection and Modeling
An element called shell281 as shown in **Fig. 3.** Is selected for unstiffened plate which is suitable for analyzing thin to moderately thick shell structures. The element has eight nodes with six degrees of freedom at each node: translations in the x, y, and z axes, and rotations about the x, y, and z axes. It may be used for layered applications for modeling composite shells. It includes the effects of transverse shear deformation.

Finite element method has been employed to analyze natural frequency and dynamic response. The model was developed in ANSYS 12.1using the 121 quadrate elements (i.e. there are 11 elements in the axial direction and 11 along the width) which means (4416 DOF). Convergence study is the reason for choosing the particular mesh used in this study. The global x coordinate is directed along the width of the plate, while the global y coordinate is directed along the length and

the global z direction corresponds to the thickness direction and taken to be the outward normal of the plate surface. for stiffened plate, the element used is solid-shell 190. SOLSH190 is used for simulating shell structures with a wide range of thickness (from thin to moderately thick) and for stiffened plate. The element possesses the continuum solid element topology and features eight-node connectivity with three degrees of freedom at each node: translations in the nodal x, y, and z directions. And adding degree of freedom rotation on x ,y and z for the present solution by command adding degree of freedom.  Thus, connecting SOLSH190 with other continuum elements requires no extra efforts. A degenerate prism option is available, but should only be used as filler elements in mesh generation. The element has plasticity, creep, large deflection, and large strain capabilities. SOLSH190 can use for layered applications such as modeling laminated shells or sandwich construction. . Accuracy in modeling composite shells is governed by the first-order shear-deformation theory (also known as Mindlin-Reissner shell theory).

### 3.2 Verification Case Studies

In the present study, Series of preselected cases are modeled to verify the accuracy of the method of analysis. The results are compared to analytical solution (Levy) and numerical solution (Finite element method).see **Table 1** and **Table 2** for unstiffened plate, and **Table 3** for stiffened plate. From these results, it is obvious that the methods of solution gives better results for both analytical and numerical solution.

### 4. EXPERIMENTAL WORK

In the present work, three- purposes were investigated. First, to outline the general steps to design and fabricate the rectangular test models from fiber (E-glass) and polyester resin to form laminate composite materials. Second, the manufactured models are then used to evaluate the mechanical properties $(E_1, E_2, G_{12})$ of unidirectional composite material. Third, compressive test to find buckling load of cross ply laminate plate.

### 4.1 Tensile Test

Each laminate was oriented in longitudinal, transverse and $45^{\circ}$ angle relative to designated $0^{\circ}$ direction to determine the engineering parameters $E_1$, $E_2$, $G_{12}$. Tensile test specimen includes standard geometry according to ASTM (D3039/D03039M); and the mechanical properties for glass-polyester which obtained from tensile test as shown in **Table 4.**

### 4.2 Buckling Test

In this study, buckling load of laminated plate (stiffened and un-stiffened) determined analytically, numerically and experimentally. The laminated plate length was 200 mm. the width and thickness of it are 100 mm and 4 mm respectively.

For stiffened plate the same dimensions of the un-stiffened plate except with the use of (stiffeners with width of 6mm, two specimen one of them with one stiffener and the other with two). With stiffeners depth 4mm, length of 200mm and the lamination angle for all stiffeners was 0° . The mechanical properties for glass-polyester are obtained from tensile test as shown in **Table 4.**

The specimen was loaded in axial compression (vertical direction) using tensile test machine of 200 KN capacity as shown in **Fig. 4**. the specimen was simply supported by two ends and kept free at the other two ends. The specimen was loaded slowly until buckling. The experimental set up has shown in **Figs. 5a-c)** for three cases. (Un-stiffened and stiffened with one stiffener and with two stiffeners)

Simply supported boundary conditions were simulated along the top and bottom edges. For axial loading, the test specimen was placed between two extremely stiff machine heads of which the lower one was fixed during the test, whereas the upper head was moved downwards by servo hydraulic cylinder. The laminated plate was loaded at constant cross-head speed of 5 mm/min.

The buckling load is determined from the load-displacement curve. The vertical displacement is plotted on the x-axis in (mm) and the load was plotted on the y-axis in (KN).

## 5. RESULTS AND DISCUSSION
### 5.1 Experimental R%esults
The critical buckling load is shown in **Tables 5 and 6** for un-stiffened and stiffened plate respectively. Maximum error between analytical and experimental is (3.925%) in case 0/90/90/0 un-stiffened plate and maximum error between numerical and experimental is 8.27% for the same case. For stiffened plate (pate with one stiffener) maximum error between analytical and experimental is (1.762%) in case 0/90/0 stiffened plate and maximum error between numerical and experimental is7.72% for the same case. For stiffened plate (pate with two stiffeners) maximum error between analytical and experimental is (2.608%) in case 0/90 stiffened plate and maximum error between numerical and experimental is5.47% for the same case.

### 5.2 Theoretical Results Contain (analytical and numerical (ANSYS))
In this section the effect of different parameter on critical buckling load are discussed such as boundary conditions aspect ratio, thickness ratio, number of stiffeners and stiffener depth ratio for cross ply composite laminate plate. This result found by analytical method using HSDT with Levy method and numerically using ANSYS 12.1 program.

### 5.2.1 Boundary conditions
From the results listed in **Table 7** it can be observed that the boundary conditions always affect on the buckling load. It′s worth mentioning that the critical buckling load in SCSC and SSSC for cross ply and CSCS are higher than other cases because of B.C′S. effect.

### 5.2.2 Aspect ratio
For unstiffened plate, **Fig. 6** shows that in SSSF and SFSF the buckling load decreases when a/b increases with high percentage reaches to 72.51% and 74.45% in SSSF and SFSF respectively. On the other hand in SCSC the buckling load decreases with small percentage reaches to 11.569% when a/b varies from 0.5 to 1.5, Then, it′s increases when a/b varies from 1.5 to 2. The maximum buckling load in SCSC is at a/b=0.5. While the minimum is at a/b=1.5.

**Fig.7** shows that in un stiffened plate and plate with one stiffener the buckling load decreases when a/b increase with high percentage reaches to 67.383% and 57.878% in un stiffened plate and plate with one stiffener respectively. On the other hand in plate with two stiffeners the buckling load decreases with percentage reaches to 12.204%, It′s worth mentioning the buckling load in plate with two stiffeners is higher than other cases because of the number of stiffener effect with percentages (78.4% with plate with one stiffener and 88.19% with plate without stiffener when a/b=1).

### 5.2.3 Thickness ratio

In **Fig. 8,** for unstiffened plate the buckling loads increase when thickness ratio increases. It can be observed that the buckling load is increased with high percentage when b/h varies from 10 to 20. Then, this percentage gets smaller when b/h varies from 20 to 50; it is worth mentioning that the increasing in buckling load in case $(0/90/0)_S$ is more than other case where this increase reaches to10.81%.

### 5.2.4 Effect Number of Stiffeners:

From **Fig. 9,** it can be obtained that the buckling load increases with high percentage when the number of stiffeners increases because of the resistance of stiffener against load that causes buckling. Then, it is shown that in, SSSS, SFSF, the buckling load increases when number of stiffeners increases with percentage reaches to 57.988% and 81.619% respectively,increasing in buckling load in case SCSC is more than other case, it reaches to 59.94%.

### 5.2.5 Effect of stiffener depth ratio for stiffened plates:

It is shown from **Fig. 10,** the buckling loads decreases and increases with different percentage when d/h varies from 2 to 8 in all cases. It can be observed that the buckling load is decreased when d/h varies from2 to 4. Then, it is increased when d/h varies from 4 to 8; it is worth mentioning that the increasing in buckling load in case of plate with two stiffeners is more than other case where this increase reaches to17.733 %.Because of the number of stiffener and its resistance against load that causes buckling.

### 6. CONCLUSIONS

This study considers the buckling analysis of cross-ply composite laminate plate with various B.C's. From the present study, the following conclusions can be made:

1- The boundary conditions affect

 On the critical buckling load the maximum critical buckling load occurs at clamped boundary condition of plate. while the B.C's change from SSSS to SSCC ,the percentage of increasing the buckling load is (48.86%) for anti-symmetric cross under uniaxial load and the percentage of increasing buckling load when changing B.C's from SSFF to SSCC is (79.5%) for symmetric cross ply under uniaxial load.

2- The uniaxial buckling load decreases when a/b increase with high percentage reaches to 72.51% and 74.45% in SSSF and SFSF un-stiffened plate respectively. On the other hand in SCSC the buckling load decreases with small percentage reaches to 11.569% when a/b varies from 0.5 to 1.5, Then, it′s increases when a/b varies from 1.5 to 2. For un-stiffened plate under biaxial SFSS and SFSF, the buckling load decreases with high percentage when a/b increase reaches to 75.133% and77.129% in SFSS and SFSF respectively.

3- In unstiffened plate and plate with one stiffener the buckling load decreases when a/b increases with high percentage reaches to 67.383% and 57.878% in un stiffened plate and plate with one stiffener respectively.

4- The buckling loads increases when thickness ratio increases for un-stiffened plate under uniaxial or biaxial load. It can be observed that the buckling load is increase with high percentage when b/h varies from 10 to 20. Then, this percentage gets smaller when b/h varies from 20 to 50.

5- it can be obtained that the uniaxial buckling load increases with high percentage when the number of stiffeners increased , in SSSS, SFSF, the buckling load increase when number of

stiffeners increase with percentage reaches to 57.988%   and   81.619 % respectively , increasing in buckling load in case SCSC is more than other case, it reaches to 59.94%.Then, for biaxial load  SSSS, SCSC, the buckling load increase when number of stiffeners increase with small percentage reaches to 18.76 % and 18.91% in SSSS, SCSC, respectively , increasing in buckling load in case SCSC is more than other case, it reaches to 18.91%.

6- The buckling loads decreases and increases with different percentage when d/h varies from 2 to 8 in all cases for uniaxial load. It can be observed that the buckling load is decreased when d/h varies from2 to 4. Then, it is increase when d/h varies from 4 to 8; it is worth mentioning that the increasing in buckling load in case plate with two stiffeners is more than other case where this increase reaches to 17.733 %..

## REFERENCES

➢ C. Guedes Soares and J.M.Gordo, 1997, *Design Methods for Stiffened Plates under Predominantly Uniaxial Compression,*Elsevier Science Limited, PII: S0951-8339(97)00002-6.

➢ Y.V.SatishKumar,Madhujit Mukhopadhyay, 1999, *A New Finite Element for Buckling Analysis of Laminated Stiffened Plates* Composite Structures, 46 (1999) 321-331.

➢ R.Rikards, A. Chate, O. Ozolinsh, 2001, *Analysis* for *Buckling And Vibrations Of Composite Stiffened Shells And Plates,* Composite Structures 51 (2001) 361-370.

➢ Samuel Kidane, 2002, *Buckling Analysis of Grid Stiffened Composite Structures.* M.Sc. thesis. Louisiana State University and Agricultural and Mechanical College.

➢ Aseel Jasim Mohammed Al-Hassani ,2005 *Instructional Model for Dynamic Analysis  of Composite Plates  Structure ,* PhD. Thesis Submitted to the University of Technology .

➢ W.Akl, A. El-Sabbagh, and A .Baz **,** 2008 *Optimization of The Static and Dynamic Characteristics of Plates with Isogrid Stiffeners, F*inite Elements in Analysis and Design 44 (2008) 513 – 523.

➢ Tran IchThinh, and Tran HuuQuoc, 2010, *Finite Element Modeling and Experimental Study on Bending and Vibration of Laminated Stiffened Glass Fiber/Polyester Composite Plates,* Computational Materials Science 49 (2010) S383–S389.

➢ Hasanain Ibrahim Nsaif**,** 2011 **,** *Buckling Analysis of Composite Plates under Thermal and Mechanical Loading*, M.sc, Thesis, University of Baghdad (2011)

➢ Reddy J.N. 2004 , *Mechanics of Laminated Composite Plates and Shells: Theory and Analysis*. 2ed; CRC Press 2004.

➢ M. S. Troitsky, D.Sc. 1976 , *Stiffened Plates Bending, Stability and Vibrations,* Elsevier Scientific Publishing Company (1976).

➢ Theory, analysis, and element manuals ANSYS 12.1 Program.

➢ Mei-Wen Guo, Issam E. Harik, Wei-XinRen, 2002, *Buckling Behavior of Stiffened Laminated Plates,* International Journal of Solids and Structures 39 (2002) 3039–3055.
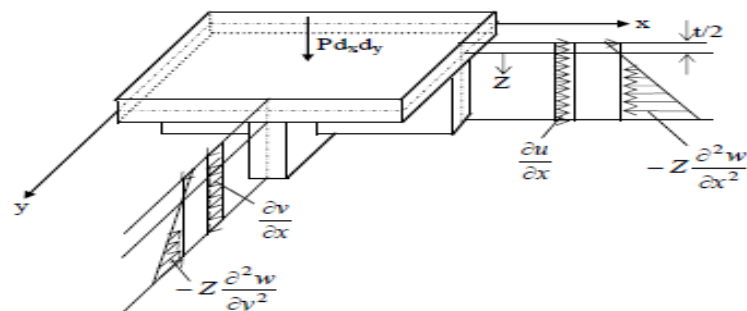
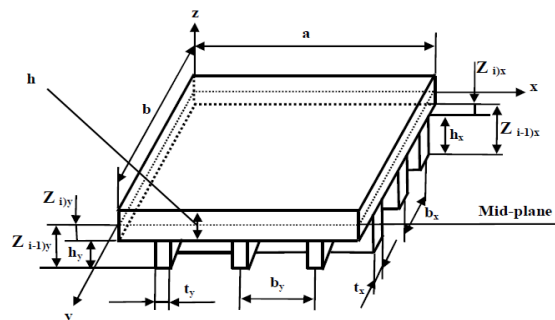**Figure 1:** Distribution of normal strains for stiffened plates.



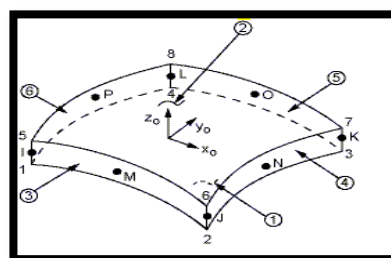**Figure 2:** Dimensions and directions of stiffened laminated plates.



**Figure 3:** Shell281 Geometry [11]

**Table 1.** Dimensionless uniaxial buckling load $\overline{N}{=}N_{cr}\frac{a^2}{E_2h^3}$ of anti-symmetric cross ply laminates.

| B.C'S | [9] Levy method | Present Levy method | (Discrepancy %) | E1/E2=40 G12=G13=0.6 E2 G23=0.5 E2 $\nu$12=0.25 a=b h=1 N=10 |
|-------|------|---------|-----------------|---|
| S-F-S-F | 6.78 | 6.796 | (0.235%) | |
| S-F-S-S | 7.05 | 7.417 | (4.94%) | |
| S-F-S-C | 8.221 | 8.276 | (0.664%) | |
| S-S-S-S | 12.109 | 12.722 | (4.818%) | |
| S-S-S-C | 12.607 | 12.86 | (1.96%) | |
| S-C-S-C | 13.254 | 13.41 | (1.12%) | |

**Table (2)** Dimensionless uniaxial buckling load $\overline{N}{=}N_{cr}\frac{a^2}{E_2h^3}$ of anti-symmetric cross ply laminates$[0°/90°/90°/0°]$  b/h = 10, $G_{12}{=}G_{13}{=}0.6E_2, G_{23}{=}0.5E_2$ , $\nu_{12}{=}0.25$ , a=b , h=1.

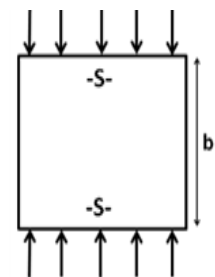| E1/E2 | [9] | ansys | discrepancy% |
|-------|-----|-------|--------------|
| 3 | 5.114 | 5.2556 | 2.77% |
| 10 | 9.777 | 9.6985 | 0.80% |
| 20 | 15.298 | 15.027 | 1.77% |
| 30 | 19.957 | 19.405 | 2.76% |
| 40 | 23.34 | 23.068 | 1.17% |

**Table 3.** Dimensionless uniaxial buckling load $(\lambda)$ of anti-symmetric cross-ply laminated stiffened plate.$E_1 = 60.7GPa$ ,$E_2 = 24.8GPa, G_{12} = G_{31} = G_{23} = 12GPa$ ,$v_{12} = 0.23$ ,$\lambda = \frac{12N_{cr}a^2h(1-v^2)}{E_1h^3}$, h=1,  h/a=0.01, a=100, Stiffener Depth ratio (d/h) =4

| a/b | Ref.[4] | Present F.E.M (**Discrepancy** %) | Present Levy Method (**Discrepancy** %) |
|-----|---------|-----------------|---------------------|
| 0.5 | 54 | 52.84 (2.148%) | 53.126 (1.61%) |
| 1 | 75 | 74.66936 (0.44%) | 72.865 (2.84%) |
| 1.5 | 89 | 85.952 (3.048%) | 87.357 (1.86%) |
| 2 | 139 | 142.773 (2.7%) | 140.236 (0.88%) |

**Table 4.** Experimental mechanical properties of fiber glass-Polyester and young modulus for polyester.

| Mechanical properties | Glass-polyester |
|---|---|
| $E_1$ (Mpa) | 24800 |
| $E_2$ (Mpa) | 4485 |
| $G_{12}$ (Mpa) | 1466 |
| $V_f$ | 0.3 |



**Figure 4.** Buckling test machine.



**Figure 5a.** Buckling test of S-F-S-F laminates without stiffener.

**Figure 5b.** Buckling test of S-F-S-F laminates with one stiffener.



**Figure 5 c.** Buckling test of S-F-S-F laminates with two stiffeners

**Table 5.** Dimensionless buckling load [ $\bar{N} = N_{yy}^0 * b^2/E_2 * h^3$ ]  of SFSF laminates for un stiffened plate.

| Laminated plate | Levy (Error %) | ANSYS (Error %) | Experimental |
|---|---|---|---|
| 0/90 | 1.753 (3.57%) | 1.712 (5.83%) | 1.818 |
| 0/90/0 | 0.981 (1.3%) | 0.972 (2.2213%) | 0.994 |
| 0/90/0/90 | 2.487 (1.87%) | 2.439 (3.77%) | 2.5346 |
| 0/90/90/0 | 1.346 (3.925%) | 1.285 (8.27%) | 1.401 |

**Table 6.** Dimensionless buckling load [ $\bar{N} = N_{yy}^0 * b^2 / E_2 * h^2$ ] of SFSF laminates for stiffened plate

| Number of stiffeners | Laminated plate | Levy (Error %) | ANSYS (Error %) | Experimental |
|---|---|---|---|---|
| One stiffener | 0/90 | 11.923 (1.217%) | 11.645 (3.52%) | 12.07 |
| | 0/90/0 | 13.04 (1.762%) | 12.249 (7.72%) | 13.274 |
| | 0/90/0/90 | 29.53 (1.369%) | 28.944 (3.326%) | 29.94 |
| | 0/90/90/0 | 29.856 (1.747%) | 29.26 (5.21%) | 30.387 |
| Two stiffeners | 0/90 | 13.738 (2.608%) | 13.334 (5.47%) | 14.106 |
| | 0/90/0 | 15.127 (2.065%) | 14.665 (5.05%) | 15.446 |
| | 0/90/0/90 | 33.691 (1.044%) | 33.337 (2.084%) | 34.046 |
| | 0/90/90/0 | 43.752 (1.38%) | 43.603 (1.719%) | 44.366 |

**Table 7.** Effect of boundary condition on buckling load under uniaxial loading (0/90/90/0) with or without stiffeners.

| Boundary condition | Unstiffened plate | | Plate with Single stiffener | | Plate with two stiffeners | |
|---|---|---|---|---|---|---|
| | Levy | ANSYS Error% | Levy | ANSYS Error% | Levy | ANSYS Error% |
| S-C-S-C | 50.45 | 52.33 3.59% | 245.23 | 247.5 0.91% | 260.18 | 264.25 1.54 % |
| S-C-S-S | 38.25 | 39.98 4.33% | 242.53 | 245.1 1.07% | 276.24 | 279.74 1.25 % |
| S-S-S-S | 25.97 | 28.47 8.78% | 218.24 | 220.6 1.09% | 225.79 | 228.33 1.11% |
| S-F-S-C | 11.56 | 12.29 5.91% | 97.142 | 100.8 3.69% | 126.34 | 131.25 3.73 % |
| S-F-S-S | 2.45 | 2.59 5.4 % | 114.97 | 118.2 2.76% | 130.25 | 133.55 2.47% |
| S-F-S-F | 1.25 | 1.28 2.34% | 7.28 | 7.43 2.01% | 13.176 | 14.544 9.40% |
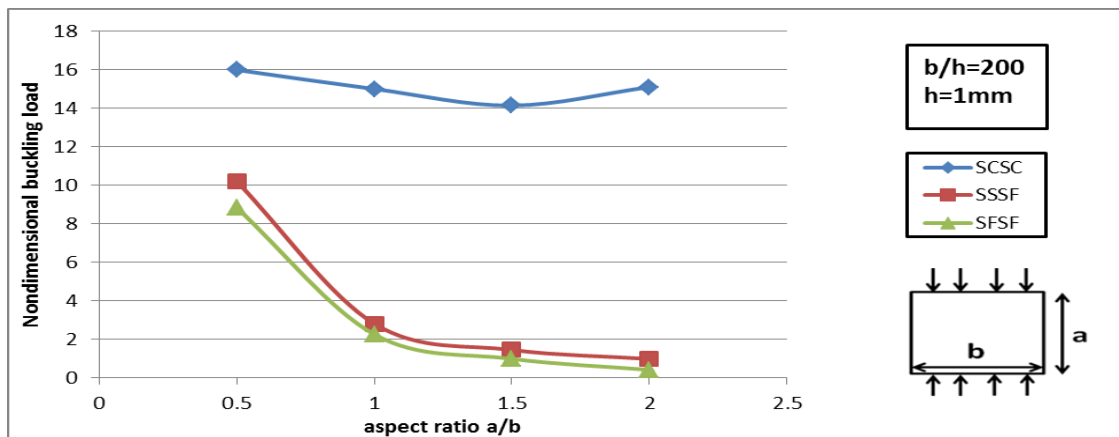
**Figure 6.** Non-dimensional buckling load($\lambda$) versus aspect ratio (a/b) of anti-symmetric cross-ply (0/90/0/90) laminates under uniaxial compressive buckling load.
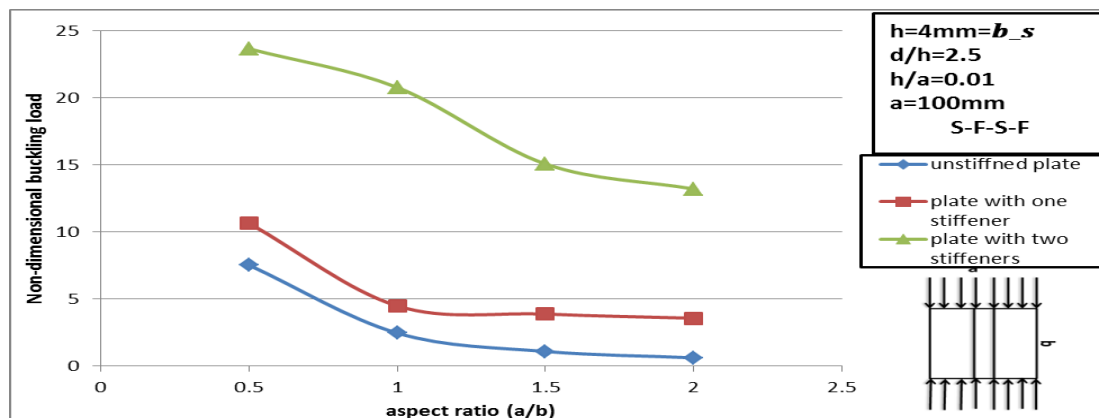


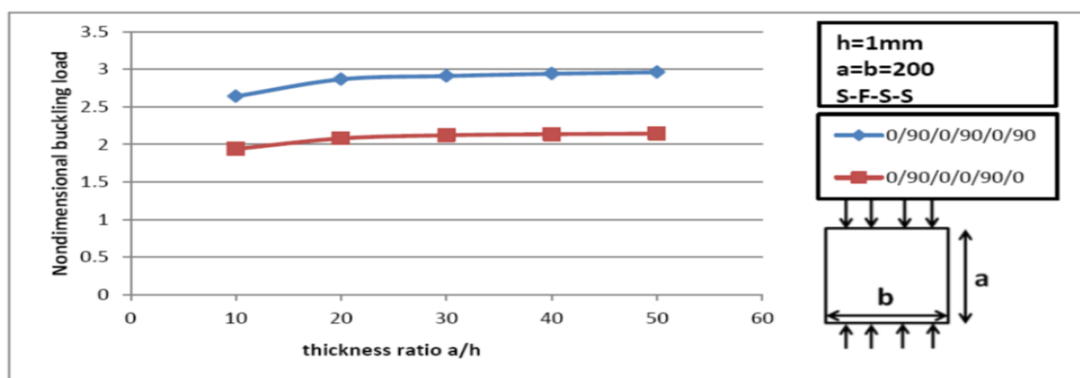**Figure 7 .** Dimensionless uniaxial buckling load versus aspect ratio for stiffened and un stiffened plates.



**Figure 8.** Non-dimensional buckling load($\lambda$) versus thickness ratio, (a/h).
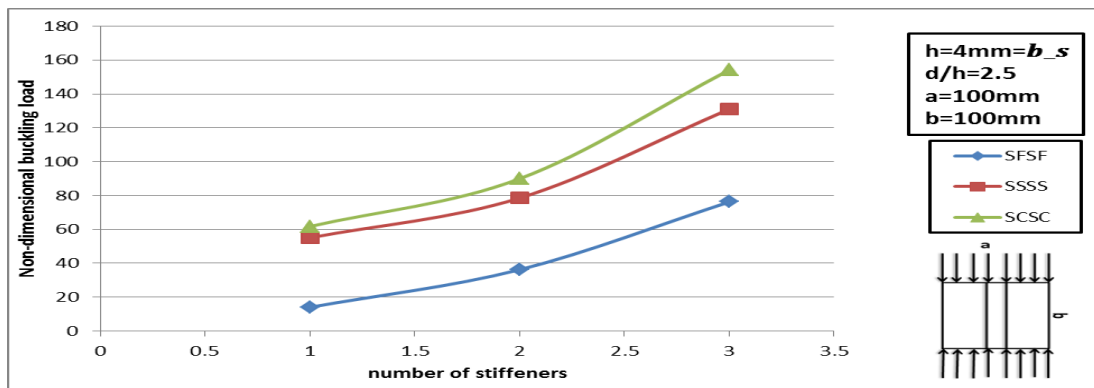
**Figure 9.** Dimensionless uniaxial buckling load versus No. of stiffeners of stiffened laminated plate.
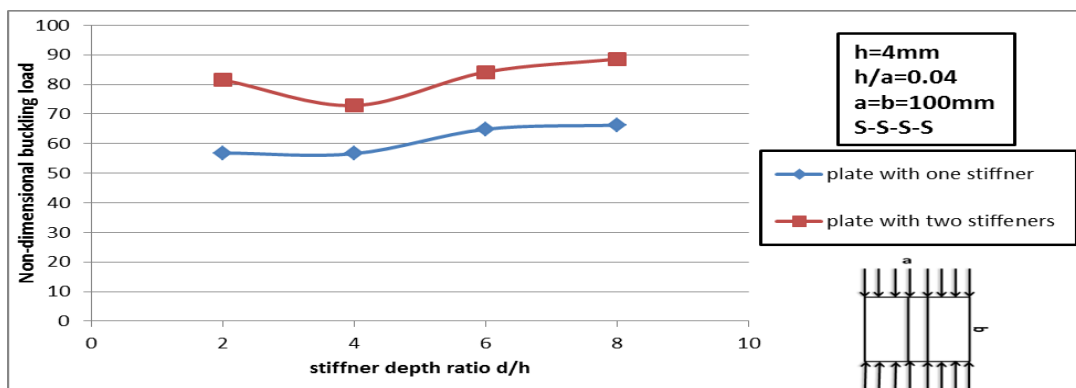


**Figure 10.** Dimensionless uniaxial buckling load versus stiffener depth ratio for stiffened plates.
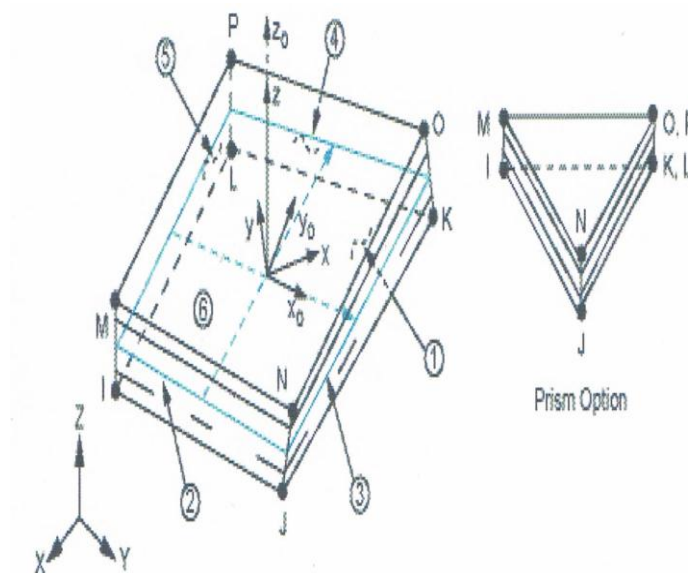


**Figure 11.** SOLSH190 Geometry [11].

# Numerical Simulation of The Influence of Geometric Parameter on The Flow Behavior in a Solar Chimney Power Plant system

**Prof. Dr. Arkan khilkhal Husain**   **Asst.Prof.Dr Waheeds Shate Mohammad**   **Lecturer. Abbas JassimJubear**

Mechanical Engineering Dep.          Mechanical Engineering Dep          Mechanical Engineering Dep.

University of Technology          University of Technology          University of Wassit

Email: alaalwn@yahoo.com          Email: alaalwn@yahoo.com          Email:Abbaskut72@yahoo.com.au

## ABSTRACT

$\mathbf{N}$umerical simulations have been carried out on the solar chimney power plant systems. This paper gives the flow field analysis for a solar chimney power generation project located in Baghdad. The continuity, Naver-stockes, energy and radiation transfer equations have been solved and carried out by Fluent software. The governing equations are solved for incompressible, 3-D, steady state, turbulent is approximated by a standard $\mathbf{k} - \mathbf{\epsilon}$ model with Boussiuesq approximation  to study and evaluate the performance of solar chimney power plant in Baghdad city of Iraq. The different geometric parameters of project are assumed such as collector diameter and chimney height at different working conditions of solar radiation intensity (300,450,600,750 and 900 W/m$^2$) to gain the optimal designed structure. The results show that the change of collector diameter and chimney height has considerable effects on the performance of the system. The velocity increase when the collector diameter  and chimney height increase and reach to the maximize  value at H=D 12 m and when solar intensity (900 W/m$^2$). The study shows that Iraqi weather are suitable for this system.

**Keywords:** Solar chimney; Solar energy; Collector; Natural convection.

<div dir="rtl">

## نمذجة رقمية لتاثير المعاملات الهندسية على سلوك الجريان في منظومة مدخنة شمسية لتوليد القدرة

**م. عباس جاسم جبير**          **أ.م.د. وحيد شاتي محمد**          **أ. د.اركان خلخال حسين**

قسم هندسة الميكانيك/جامعة واسط          قسم هندسة الميكانيك/الجامعة التكنولوجية          قسم هندسة الميكانيك/الجامعة التكنولوجية

### الخلاصة

تم اجراء محاكات عددية على نظام محطة المدخنة الشمسية للطاقة.تبين هذه الدراسة تحليل لحقل الجريان  لمشروع محطة المدخنة الشمسية للطاقة في بغداد. تم حل معادلات الاستمرارية,Naveries-Stokes, الطاقة والاشعاع الشمسي باستخدام برنامج (Fluent(14.في هذه الدراسة تم حساب اداء المدخنة الشمسية من خلال حل المعادلات الحاكمة خلال جريان لاانظغاطي ,ثلاثي الابعاد,مستقر واضطرابي حيث تم الاستعانة بالموديل الاضطرابي (k-ε) في اجواء بغداد-العراق.خلال هذه الدراسة تم فرض عدد من المتغيرات الهندسية المختلفة مثل قطر المجمع الشمسي و ارتفاع المدخنة الشمسية وذلك عند ضروف اختبار مختلفة من شدة الاشعاع الشمسي (300,450,600,750,900) واط/م$^2$ وذلك لغرض التوصل الى افضل تصميم. من ابرز النتائج التي تم التوصل اليها , ان قطر المجمع وارتفاع المدخنة له تاثير كبير على متغيرات اداء النظام. تزداد السرعة داخل المدخنة الشمسية بزيادة قطر المجمع وارتفاع المدخنة وتصل الى اقصى قيمه لها عندما كان قطر المجمع وارتفع المدخنة ( 12 م ) وعند شدة اشعاع شمسي (900 واط/م$^2$ ). ان اجواء العراق تعتبر ملائمة لهذا النوع من الانظمة.

**الكلمات الرئيسيه**: مدخنه شمسيه, الطاقه الشمسيه, مجمع, الحمل الحر

</div>

## 1.  INTRODUCTION

A solar chimney power plant, SCPP is a solar thermal power plant that uses greenhouse principle (solar air collector) and buoyancy effect created by a chimney to generate a solar induced convective flow which drives pressure staged turbogenerator(s) to generate electricity, A traditional solar chimney power plant consists of a circular transparent canopy or roof raised a certain height above the ground, with a chimney/tower at its center as shown in **Fig. 1**. The chimney at the center houses one or more turbogenerator(s) located at its base. Ambient air from the surrounding enters the system along the circumference of the collector roof and the ground. Radiation from the sun penetrates the collector roof and strikes the ground surface and the heated ground in turns heats the adjacent air from the ambient temperature to warm air temperature at the collector outlet. The Warm air underneath the collector moves toward and up into the central chimney as a result of buoyancy and pressure difference between the ambient air and the warm air inside the plant. The kinetic energy in the warm air is converted to electrical energy using turbogenerator (s), **Aja, and Hussain, 2011.** Detailed theoretical preliminary research and a wide range of wind tunnel experiments led to the establishment of an experimental plant with a peak output of 50 kW on a site made in Manzanares (about 150 km south of Madrid) in 1981/82. The experimental plant in Manzanares operated for about 15,000 hours from 1982 onwards. In Australia a 200MW solar tower project is currently being developed, **Schlaich, et al., 2005,Bergermann, and Partenr, 2002, and www.wikipedia.org. Maia et al, 2009,** presented a theoretical analysis of a turbulent flow inside a solar chimney. They showed that the most important physical elements in a solar chimney system are the tower dimensions as they cause the most significant variation in the flow behavior. An increase in the height and diameter of the tower produces the rise in the mass flow rate and decrement in the flow temperature. **Bernardes et al. 2009.** developed a validated mathematical model to estimate the temperature and power output of solar chimneys. The maximum power can be reached when the factor pressure drop at the turbine is equal to approximately 0.97 from the total potential pressure. The other parameters were also involved in the study such as; distance between absorber and ground, double cover area, water-storage system area and thickness. The results showed that their effect was insignificant since the energy output was the same. Similarly, **Backström et al., 2006**. found that maximum fluid power was available at a much lower flow rate and much higher turbine pressure drop than the constant pressure potential assumption given. **Koonsrisuk & Chitsomboon, 2009.** studied the ventilation efficiency of solar chimney by comparing between five of the mathematical simulations and five of CFD simulations both from the previous researches. Moreover, **Maia et al., 2009.** presented a validated numerical simulation showed that the height and diameter of the tower were the most significant physical variables for solar chimney design. The maximum chimney height for convection avoiding negative buoyancy at the latter chimney and the optimal chimney height for maximum power output were presented and analyzed by, **Zhou et al., 2009.** using a theoretical model validated with the measurements of the prototype in Manzanares. The results showed that maximum height gradually increased with the lapse rate increasing and go to infinity at a value of around 0.0098 K/ m. **Walter, and Sergio,1984.** described the design, construction and testing the variation in the geometry of the chimney for solar dryer system, the results indicated that a slight geometry modification of the chimney (convert cone keeping height constant) will increase air velocity by a factor of 2- 3 with respect to a chimney of cylindrical shape. **Bernardes et al., 2003.** developed a model to estimate the power output of solar chimneys and to examine the effect of  various ambient conditions and structural dimensions of the power output. **Zhou et al., 2007.** built a pilot experimental solar chimney thermal power generating equipment in China. They carried out a simulation study to investigate the power generating system performance

based on a developed mathematical model. **Ming Tingzhen et al., 2006.** advanced a model to evaluate the performance of a solar chimney power plant system, in which the effects of various parameters(chimney and collector) on the relative static pressure, driving force, power output and efficiency have been further investigated. **Tingzhena et al., 2008.** presented a numerical simulation of the solar chimney power plant systems coupled with turbine. **Mathur et al., 2006.** presented experimental investigations on solar chimney for room ventilation and **Bassiouny, and Koura, 2008.** presented an analytical and numerical study of solar chimney used for room natural ventilation.

In the present study we modeled a 3-D solar chimney power plant which includes the parts of the ground, collector, and chimney together. The flow details production of plants with different dimensions and different solar intensities are presented.

## 2. NUMERICAL IMPLEMENTATIONS

Advanced solver technology provides fast, accurate CFD results, flexible moving and deforming meshes, and superior parallel scalability. Computational Fluid Dynamics (CFD) procedures solve all the interacting governing equations in a coupled manner, albeit in a finite framework. With a careful use of CFD, its results could be used to validate those of the theoretical models, at least qualitatively.

### 2-1 Modelling in GAMBIT

For the simulation part, the model is designed by using GAMBIT 2.4.6 for this configuration. This software is provided with the advanced geometry and meshing tools. The functions of GAMBIT are design the three dimensional (3-D), setup the boundary condition for each edge and faces ,and provide the meshing analysis for each configuration.

The solar chimney power plant  was modeled with the following dimensions, Circular absorber ground with the different diameter of  (6,8,10 and 12 m), inclined collector angle ($\theta = 0°$), different chimney height (6,8,10 and 12 m), chimney diameter 0.3 m and the gap between the absorber  and the transparent cover (glass) is 0.1m as shown in **Fig.2**.

The numerical examination of the flow behavior of air under the steady state condition was studied at both the inlet and the chimney base where the turbine is expected to be staged. The fluid flow calculation was simulated using FLUENT software. The buoyancy driven flow in the system was assumed to be turbulent based on previous studies. Set up the boundary condition is to define the situation occur at the surface condition in term of friction. Meanwhile, defining the meshing is vital in order to discrete each part to certain section for more accuracy FLUENT's analysis. It is important to define model, meshing, and boundary conditions before running into FLUENT.

Proper boundary conditions are needed for a successful computational work. After creating a geometry which have one volume defined the specify boundary types of solar collector, solar chimney and the base such as the wall , while the entry and exit zones type is Inlet and Outlet-Pressure. Now The assembly is meshed using tetrahedral elements of T-grid scheme type, **Jinhua, et al., 2007.** Gambit scheme with spacing interval size (0.0275) is chosen as shown in **Fig. 3**, the Gambit grid generator with approximately (2-4.5) million computational cells for different cases. No-slip condition for velocity and temperature on the walls.

### 2-2 Simulation with FLUENT

FLUENT solves the governing integral equations for the conservation of mass, momentum, energy, and other scalers, such as turbulence.There are two processors used to solve the flow and heat transfer equations. The first preprocessor is the program structure which

creates the geometry and grid by using GAMBIT. The second post processor is solving Navier-Stokes equations which include continuity, momentum and energy.

The set of conservation equations used by CFD are:

Mass conversion equation

$$\frac{\partial \rho}{\partial t} + \frac{\partial}{\partial x_i}(\rho u_i) = 0 \tag{1}$$

Momentum.

In x-direction

$$\rho[U\frac{\partial U}{\partial x} + V\frac{\partial U}{\partial y} + W\frac{\partial U}{\partial z}] - \frac{\partial p}{\partial x} + \frac{\partial}{\partial x}[\mu\frac{\partial U}{\partial x} - \overline{\rho u'u'}][\frac{\partial}{\partial y}[\mu\frac{\partial U}{\partial y} - \overline{\rho u'v'}] + \frac{\partial}{\partial z}[\mu\frac{\partial U}{\partial z} - \overline{\rho u'w'}]S_U \tag{2}$$

In y-direction

$$\rho\left[U\frac{\partial V}{\partial x} + V\frac{\partial V}{\partial y} + W\frac{\partial V}{\partial z}\right] = -\frac{\partial p}{\partial y} + \frac{\partial}{\partial x}[\mu\frac{\partial V}{\partial x} - \overline{\rho u'v'}] + [\frac{\partial}{\partial y}[\mu\frac{\partial V}{\partial y} - \overline{\rho v'v'}] + \frac{\partial}{\partial z}[\mu\frac{\partial V}{\partial z} - \overline{\rho v'w'}] +$$
$$S_V \tag{3}$$

In z-direction

$$\rho[U\frac{\partial W}{\partial x} + V\frac{\partial W}{\partial y} + W\frac{\partial W}{\partial z}] - \frac{\partial p}{\partial z} + \frac{\partial}{\partial x}[\mu\frac{\partial W}{\partial x} - \overline{\rho u'w'}] + [\frac{\partial}{\partial y}[\mu\frac{\partial W}{\partial y} - \overline{\rho v'w'}] + \frac{\partial}{\partial z}[\mu\frac{\partial W}{\partial z} -$$
$$\overline{\rho w'w'}] + S_W \tag{4}$$

Energy.

$$\rho[U\frac{\partial T}{\partial x} + V\frac{\partial T}{\partial y} + W\frac{\partial T}{\partial z}] = \frac{\partial}{\partial x}[\frac{\mu}{\sigma_T}\frac{\partial T}{\partial x} - \overline{\rho u't'}] + [\frac{\partial}{\partial y}[\frac{\mu}{\sigma_T}\frac{\partial V}{\partial y} - \overline{\rho v't'}] + \frac{\partial}{\partial z}[\frac{\mu}{\sigma_T}\frac{\partial V}{\partial z} - \overline{\rho w'tw'}] \tag{5}$$

The viscous medium is also taken. the analysis is carried using turbulent flow and then the standard k-epsilon is considered and take  standard wall functions near wall functions, **Launder, and Spalding, 1972.** The Boussinesq approximation is used to estimate the effect of density variation with temperature.Selecting a radiation model enables radiation heat transfer. Discrete Ordinates (DO) was selected under this model and then selected DO Irradiation under the solar load model .Define the solar parameters, Enter values for the X, Y, and Z components of the Sun Direction Vector.

In the current study used different direct solar irradiation (300 ,450 ,600 ,750 ,900 W/m$^2$) data were obtained from Ministry of Transportation-Iraqi Meteorological Organization And Seismology of  Baghdad  city of 8-8-2008 in the following times (7:30 , 8:15 , 9 ,10 A.M. and 12:30 P.M.) and the sun direction vector obtained from, **John, 1980.**

Boundary conditions specify the flow and thermal variables on the boundaries of the physical model. They are, therefore, a critical component of the FLUENT simulations and it is

important that they are specified appropriately. The boundary conditions applied in this research are those shown in **Table 1., Ming, et al., 2006.** Initially the first order upwind scheme was used to get a napproximate solution. This solution is then used as the initial conditions for the second order up wind solver.

## 3- SIMULATION RESULTS

In order to validate the results of the numerical part of the present work, a comparison with the numerical study of, **Rafah, 2007.** was carried out. It can be seen from **Fig. 4,** and **5** the absorbing ground temperature and exit velocity when using asphalt aggregates as an absorption background, with (0.1m) periphery of collector at radiation intensities of (310,415,505 $W/m^2$). A good agreement with the numerical results is achieved.

### 3-1 Variation of the Solar Intensity and Sunlight Direction

The results of the temperature distribution and velocity vectors of solar insolation (300,450,600,750,900 $W/m^2$) at times of (7:15,8:15,9,10 AM and 12:30 PM) with D=12m and H =10m regarding the solar chimney passage are presented in **Figs. 6. to 11.** The increase in air velocity is very small up to about half the radius of the collector. The very steep increase is obtained in the inner half of the collector. This trend is noticed in all solar intensities and sunlight direction as shown in **Figs. 6.** and **7** The reason is the combined effect of flow area reduction and the amount of the heat transfer from the ground to the working fluid, which increases the kinetic energy of the flow particles. To compare the velocities of the air at the solar collector passage for different solar intensity times (7:30,8:15,9,10 AM and 12:30 PM) generally, it could be seen that the maximum velocity occurs in the (900$W/m^2$ ) solar radiation intensity at (12:30 PM) and the minimum velocity in the morning with (300$W/m^2$ ) solar intensity at (7:15AM). The numerical solution has shown that the velocity in the center of the chimney is higher than near the wall. This is logical and in agreement with measurements of real fluid in rounded passages.

The variations in the air temperature through the collector passage, i.e. in the radial direction are found to be very gradually as shown in **Figs. 8.** and **9** for different solar insolations. The temperature near the ground is high compared with other regions. Consequently, the density near the walls is lower. Generally, along the collector passage, the temperature is increased but the density and pressure decreased. It is clear from the figures that the air enters the collector at ambient temperature and is heated as it moves toward the chimney. The temperature gradient present in the air is steeper near the collector inlet as the boundary layer is thinner in this zone than in regions closer to the chimney.

The development of flow in the chimney can be seen through the enlargement regions shown in **Figs. 10.** and **11**. The flow in the lower and middle regions is developing non uniform flow, but in the top region is uniform fully developed flow (turbulent flow). The velocity increases when the chimney height and collector diameter increase.

To compare the temperatures of air at the ground, collector diameter at different solar intensity and sunlight direction, it can be seen that the maximum temperature occurs in insolation of (900$W/m^2$) at (12:30 Am) because the solar radiation intensity is very high compared to other times, as shown in **Figs. 12.** and **13**. Figures also show a strong temperature drop at the collector center when the solar intensity is (600,750, and 900 $W/m^2$ because the velocity in this point is very low, which is a stagnation point.

The velocity profiles from ground to top chimney for different solar intensities, shown in **Figs. 14.** and **15**. The numerical results indicate that air velocity shows a large increase near surface of the ground about (0.3m to 0.4m) chimney height and then the increase of air velocity reduced, and the maximum velocity occur near the top of the chimney. Furthermore, the turbine may be positioned at a higher position when the velocity is large to improve power output.

## 3-2 Collector Diameter Variation

The maximum air temperature differences between inlet and absorbing ground occurred at the larger diameter due to the collector area exposed to the incident radiation with different solar intensities (300-900W/m$^2$), as in **Fig. 16.** The increase of the collector diameter means, the area of the absorbing ground is increased and the air temperature in the system is increased too, which result in the decrease in air density. Thereby, the  static pressure in the system increased and the driving force increased accordingly. **Fig. 17**. shows the computed updraft velocities at the end section of the  chimney for all  test cases, as a function of solar intensity. All distributions display the expected increasing trend with the insolation. The rates of an increase of the velocities appear to be slightly lower as the insolation increases. Furthermore the increase in collector diameter causes an increase in temperature so the velocity will be increased too.

## 3-3 Chimney Height Variation

The simulations were carried out for chimney heights of (6m, 8m,10m, and 12m). The results show that an increase in the height of the chimney causes an increase in the pressure drop along the chimney, causing greater mass flow rates and higher flow velocity. As observed, larger mass flows and velocities cause a reduction in local temperature values as shown in  **Figs. 18.** and **19**. It is clear from **Figs. 20.** and **21**, that as chimney height increased then buoyancy force will increase so one can anticipate increase  the air velocity with increasing  chimney height.

## 3-4 Temperature Distrbution at a Different Height Above the Ground

The distribution of air temperature at different heights above ground level are shown in **Figs. 22.** and **23.** The variations of air temperature within the collector near the ground (h=0m), at height (h=0. 05m) above the ground level, and at the inner glass collector surface (h=0. 1m). Air temperatures decrease with an increase in height above ground level, which is induced by the greenhouse effect. Solar radiation firstly heat the absorber bed, which heat the cool air nearly. Cool air  obtains heat mainly by free convection and radiation. The temperature of the ground is higher in the region due to the storage heat in the bed, while the inner glass has a minimum temperature because the glass acts as a bed conducting material on hard and passes most of the radiation.

## 4- CONCLUSION

A theoretical analysis of the turbulent flow inside a solar chimney was presented. Flow was modeled through the numerical solution of the conservation equations of mass, energy, and momentum, as well as the turbulent variables transport equations. The model includes a flow detail inside a collector and chimney. Numerical simulations were conducted in order to evaluate the performance of solar chimney power plants with different dimensions. This observation would be useful in the preliminary plant design. The results show:

1.  The numerical results and figure of this study have a good agreement with the numerical results of, Rafah, 2007. at the same conditions.
1.  The maximum air temperature was 80.29C°, at (D=12m and H=6m).

2. Maximum outlet air velocity was 4.91 m/s, at (D=12m and H=12 m).
3. Both, maximum air temperature and exit air velocity were at solar radiation intensity; 900 W/m$^2$.
4. Almost, increasing in collector diameter leads to increased air temperature and velocity.
5. The increasing in chimney height leads to decreasing of air temperature but increasing in velocity.
6. Under the Iraqi weather radiation conditions, large scale solar chimney in Iraq is recommended for a power plant.

**REFERENCES**

Aja, O.C., and Hussain, H., 2011, *Review on the Enhancement Techniques and Introduction of an Alternate Enhancement Technique of Solar Chinmey Power Plant*,  Journal of Applied Sciences, ISSN 1812-5654/DOI: 10,3929.

Backström, T. W., and Fluri, T. P.,2006, *Maximum fluid power condition in solar chimney power plants – an analytical approach*, Int. J Solar Energy, Vol.80, PP.1417-1423

Bassiouny R., and Koura NSA., 2008,  *An analytical and numerical study of solar chimney use for room natural ventilation*, Energ Buildings Vol.40, PP.865–873.

Bergermann, S., and Partner, 2002, *The Solar Chimney", Structural Consulting Engineers*.

Bernardes, M. A., Dos, S., Backström, T. W., and Kröger, D. G.,2009, *Analysis of some available heat transfer coefficients applicable to solar chimney power plant collectors. Int. J Solar Energy*, Vol.83, PP. 264–275.

Bernardes MA dos S., and Weinrebe G., 2003, *Thermal and technical analyses of solar chimneys. Sol Energy*, Vol.75, PP.511–524.

Jianhua F., Louise J.and Simon F.,2007,  *Flow Distribution in a Solar Collector Panel with Horizontally Inclined Absorber Strips*, http://www.sciencedirect.com, Solar Energy, Vol. 81, PP. (1501–1511),2007.

John A. D.,1980, *Solar Engineering of Thermal Processes*, Book, John Wiley and SONS , INC.,Second Edition.

Koonsrisuk, A., and Chitsomboon, T.,2009, *Accuracy of theoretical models in the prediction of solar chimney performance*, Solar Energy,    Vol.38, PP. 1764-1771.

Launder, B. E. and Spalding, D. B.,1972,  *Lectures in Mathematical Models of Turbulence*, Academic Press, London, England.

Maia, C. B., Ferreira, A. G., Valle, R. M., and Cortez, M. F. B., 2009, *Theoretical evaluation of the influence of geometric parameters and materials on the behavior of the airflow in a solar chimney, Computer & Fluid*, Vol.38, PP. 625–636.

Mathur J., Bansal NK., Mathur S., and Jain M., 2006, *Anupma. Experimental investigations on sol chimney for room ventilation,* Sol Energy, Vol.80, PP.927–935.

Ming Tingzhen, Liu Wein Y.Z. and Xu Guoliang, 2006, *Analytical and numerical investigation of the solar chimney power plant systems*, International Journal of Energy Research, Vol. 30, PP.861–873.

Ming T., Liu W., and Xu G., 2006, *Analytical and Numerical Investigation of the Solar Chimney Power Plant Systems*, International Journal of Energy Research, Vol. 30, Issue 11, PP. ( 861–873).

Rafah A. N., 2007, *Numerical Prediction of a Solar Chimney Performance Using CFD Technique*, Ph.D. Thesis Submitted to Electromechanical Engineering Department University of Technology Baghdad.

Schlaich, J., Bergermann, R., Schiel,W., and Weinrebe, G., 2005, *Design of Commercial Solar Updraft Tower Systems – Utilization of Solar Induced Convective Flows for Power Generation*.

Tingzhena M., Weia L., Guolinga X., Yanbina X., Xuhua G., and Yuanb P., 2008, *Numerical simulation of the solar chimney power plant systems coupled with turbine* , Renew Energy Vol.33, PP.897–905.

Walter Z., and Sergio A., 1984, *Design Construction and testing of a Chimney that Reduces Dangerous Temperature in a radiative Convective Solar Dryer*, Solar Energy, Vol. 32, NO.5.
4- www.wikipedia.org

Zhou X, Yang J, Xiao Bo, and Hou G. ,2007, *Simulation of a pilot solar chimney thermal power generating equipment,* Renew Energy, Vol.32, No.10, PP.1637–1644.

Zhou X., Yang, J., Xiao, B., Hou, G. and Xing, F.,2009. *Analysis of chimney height for solar chimney power plant,* Applied Thermal Engineering,Vol.29, PP.178–185.

## SYMBOLS AND ACRONYMS

| Symbol | Description | Unit |
|---|---|---|
| D | Diameter of absorbing ground | m |
| g | Gravitational acceleration | $m/s^2$ |
| H | Chimney height | m |
| h | Heat transfer coefficient | $W/m^2k$ |
| I | Solar radiation | $W/m^2$ |
| K | Turbulent kinetic energy | $m^2/s^2$ |
| p | Pressure | Pa |
| $S_\phi$ | General source term | |
| T | Temperature | C° |

| t | Time | s |
|---|---|---|
| $u'$ , $v'$ | Fluctuation of mean velocities | m/s |
| U,V, W | Time-average velocity | m/s |
| u, v,w | Velocity components (x,y&z) direction | m/s |
| Δ | Differentive | |
| α | Absorbtance | |
| ∂ | Partial derivative | |
| ε | Rate of dissipation of kinetic energy | $m^2/s^2$ |
| θ | Angle | degree |
| ρ | Fluid density | kg/m3 |
| μ | Dynamic viscosity | $N.s/m^2$ |
| $\mathbf{\mu_t}$ | Turbulent viscosity | N.s/m2 |
| π | Pi | |
| o | Ambient | |
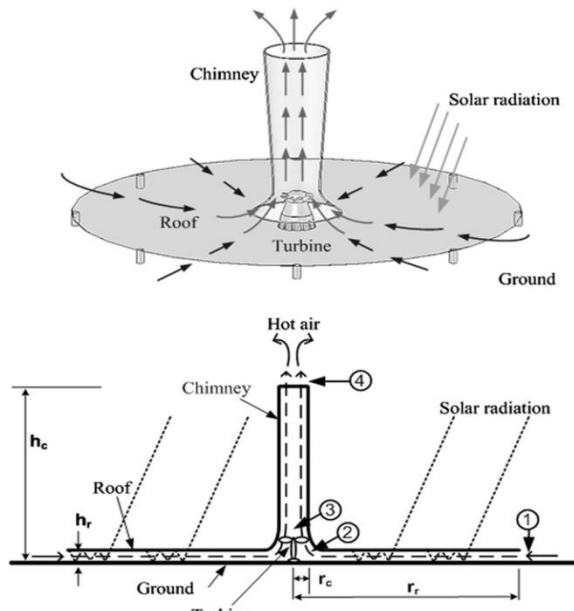
**Figure 1.** Schematic layout of the conventional solar chimney power plant.



**Figure 2.** Physical prototype

**Table 1.** Boundary conditions in detail.

| Boundary | Type | Boundary condition |
|---|---|---|
| **Inlet** | Pressure - inlet | $\Delta P=0$ ; T= $T_{ambient}$; |
| **Exit** | Pressure -out let | $\Delta P=0$; $T = T_{ambient} - 0.0065*\square chimney\ height$ |
| **Ground (asphalt)** | Wall | Thermal condition: Mixed  h=8 W/m$^2$K;T=$T_{ambint}$ |
| **Chimney Wall** | Wall | Constant heat flux:  q=0 |
| **Glass(semi-transparent)** | Wall | Thermal condition:  Radiation(Thicness= 0.004mm |



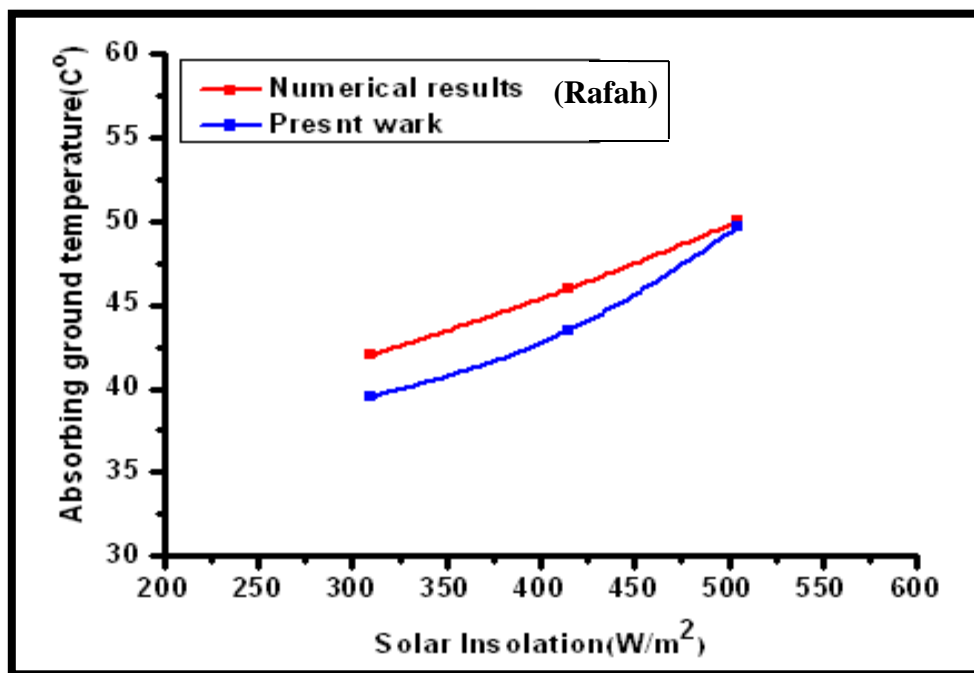**Figure 3.** Computational grad.

**Figure 4.** Variation in absorbing ground temperature with solar insolation comparing, with an numerical study.
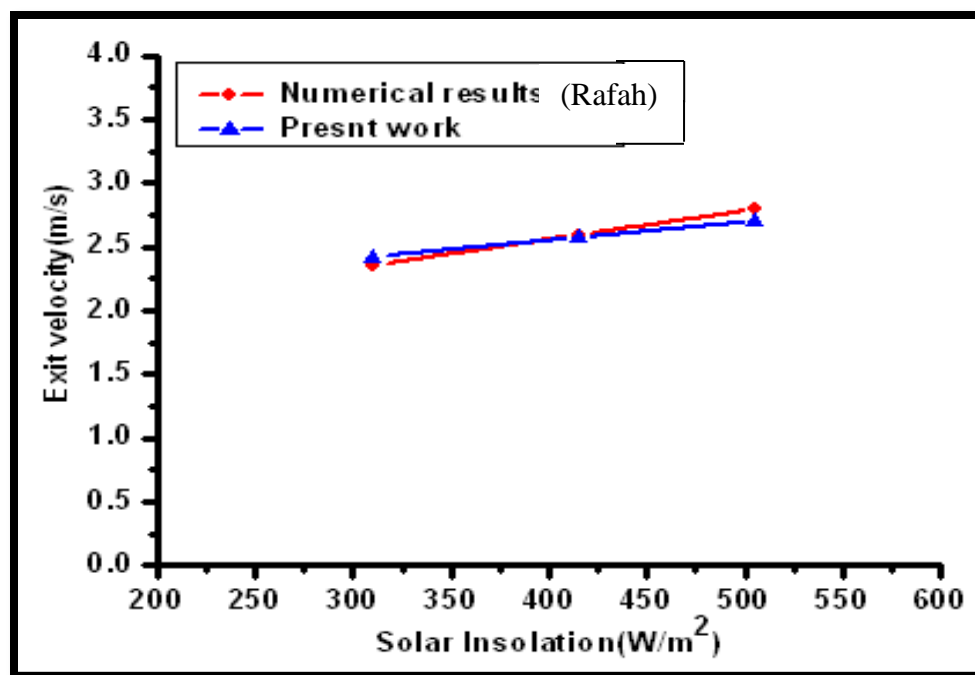


**Figure 5.** Variation in exit air velocity with solar insolation comparing, with an numerical study.
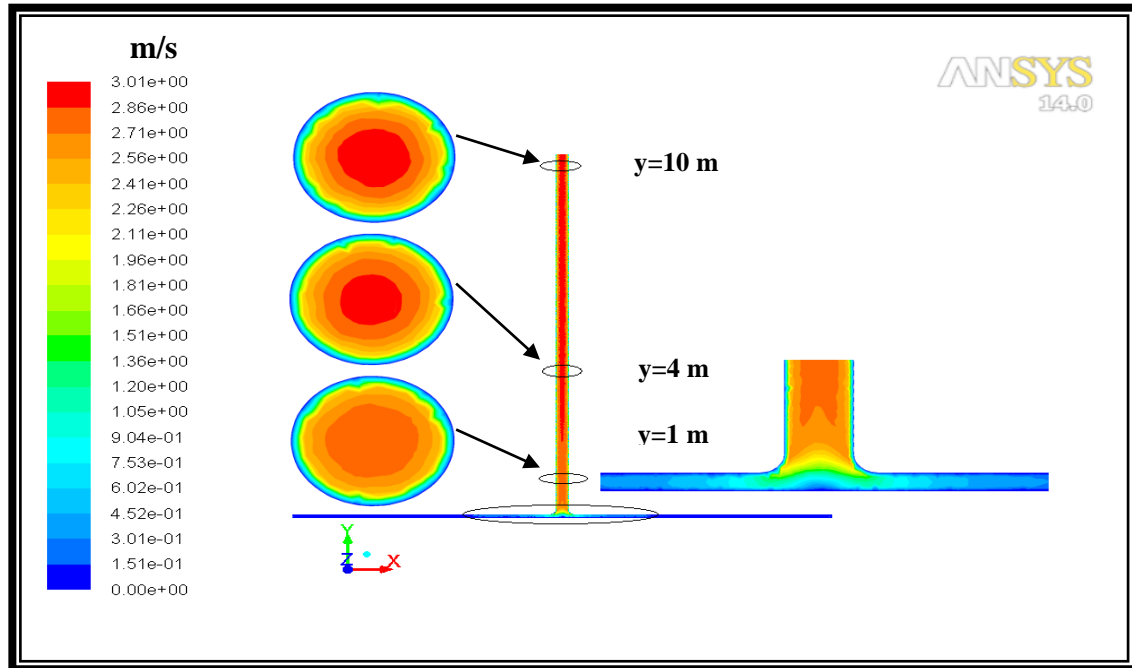
**Figure 6.** Velocity distribution contours of the solar chimney with solar insolation (300 W/m$^2$) for D=12m, H=10m.
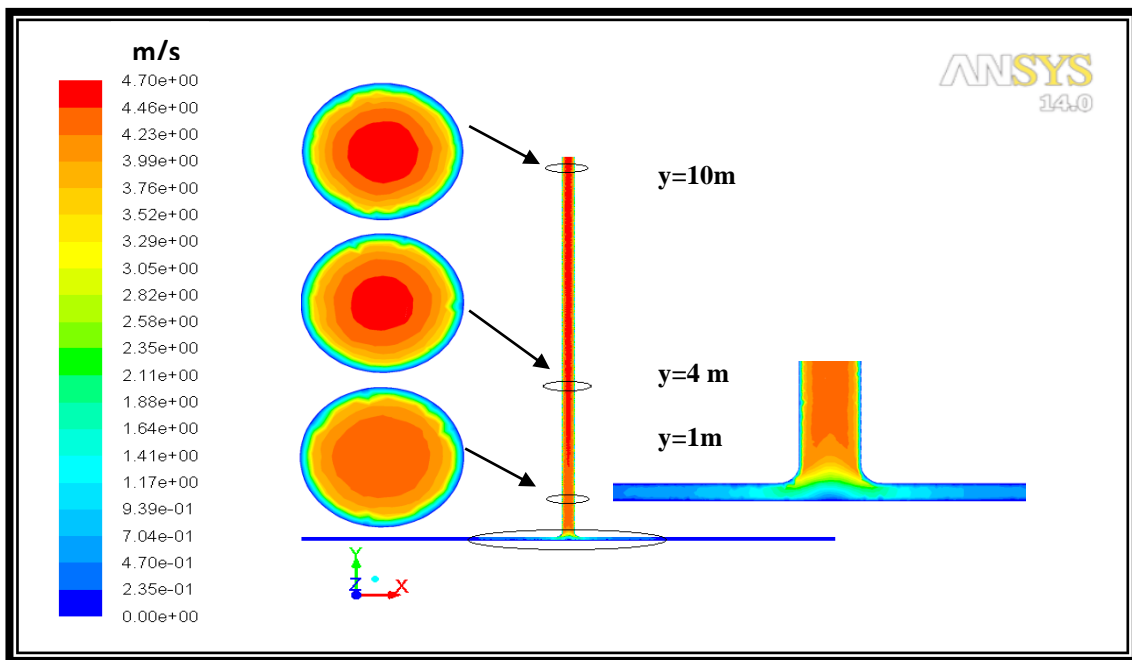


**Figure 7.** Velocity distribution contours of the solar chimney with solar insolation (900 W/m$^2$) for D=12m, H=10m.

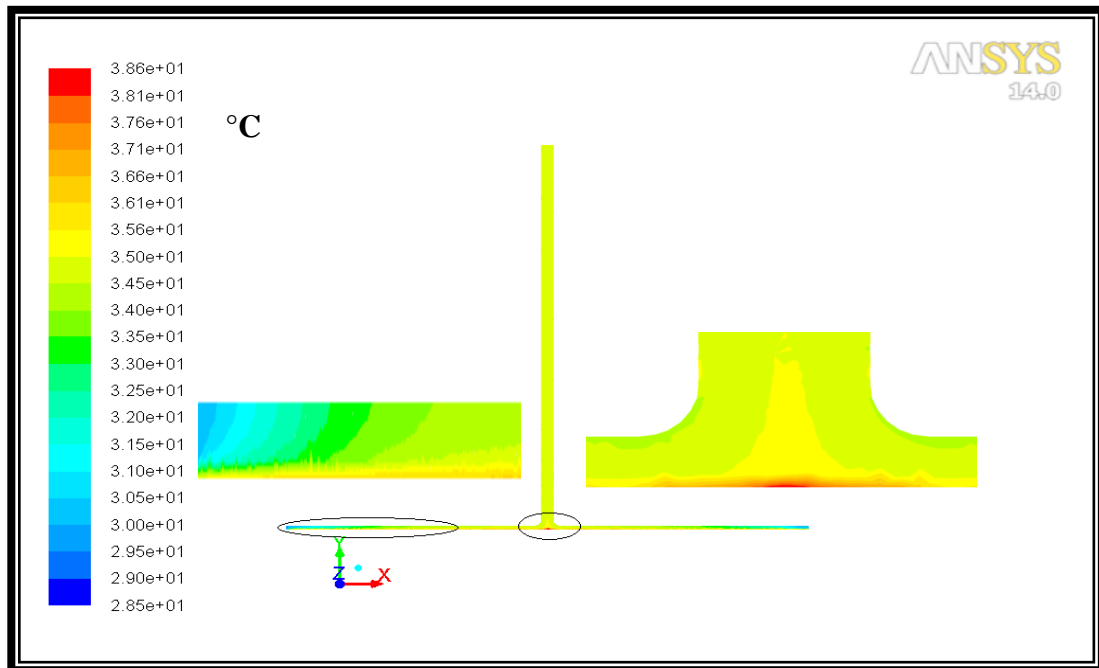**Figure 8.** Temperature distribution  contours of  the solar chimney with solar insolation (300 W/m$^2$) for D=12m, H=10m.



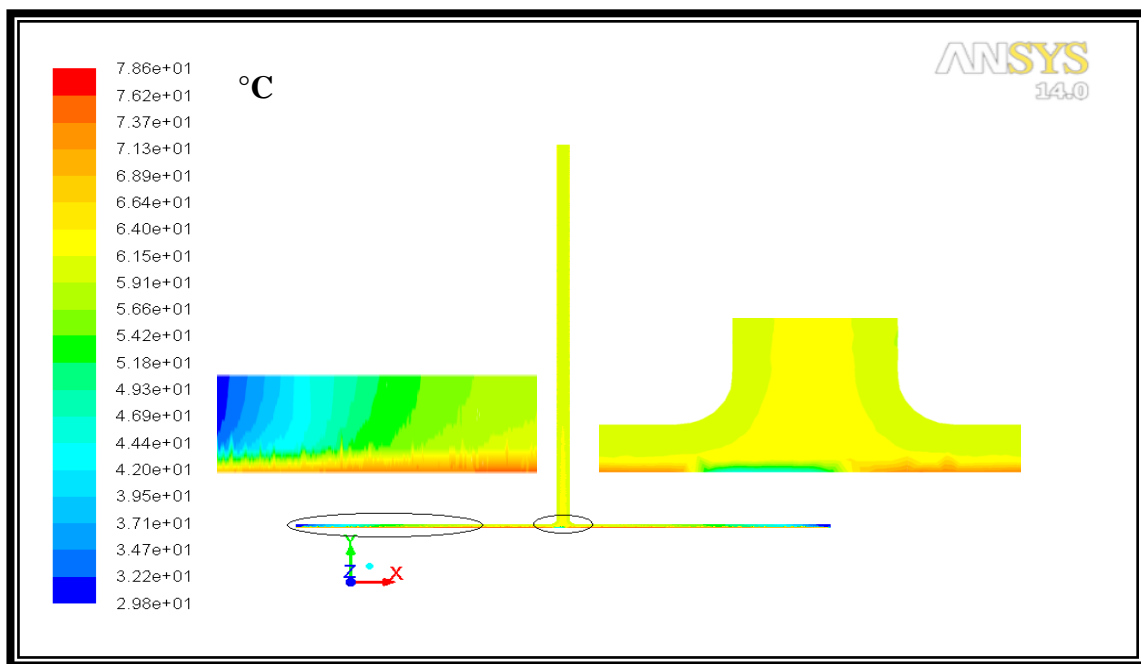**Figure 9.** Temperature distribution  contours of  the solar chimney with solar insolation (900 W/m$^2$) for D=12m, H=10m.
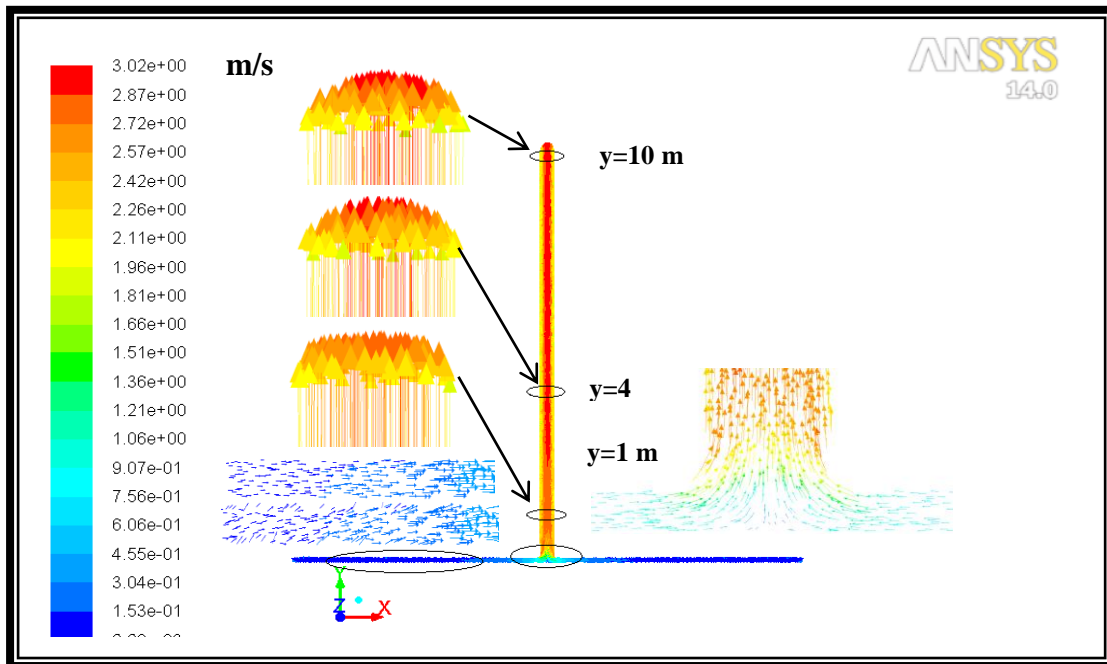
**Figure 10.** Flow felid of air in solar chimney with solar insolation (300 W/m$^2$) for D=12m, H=10m.
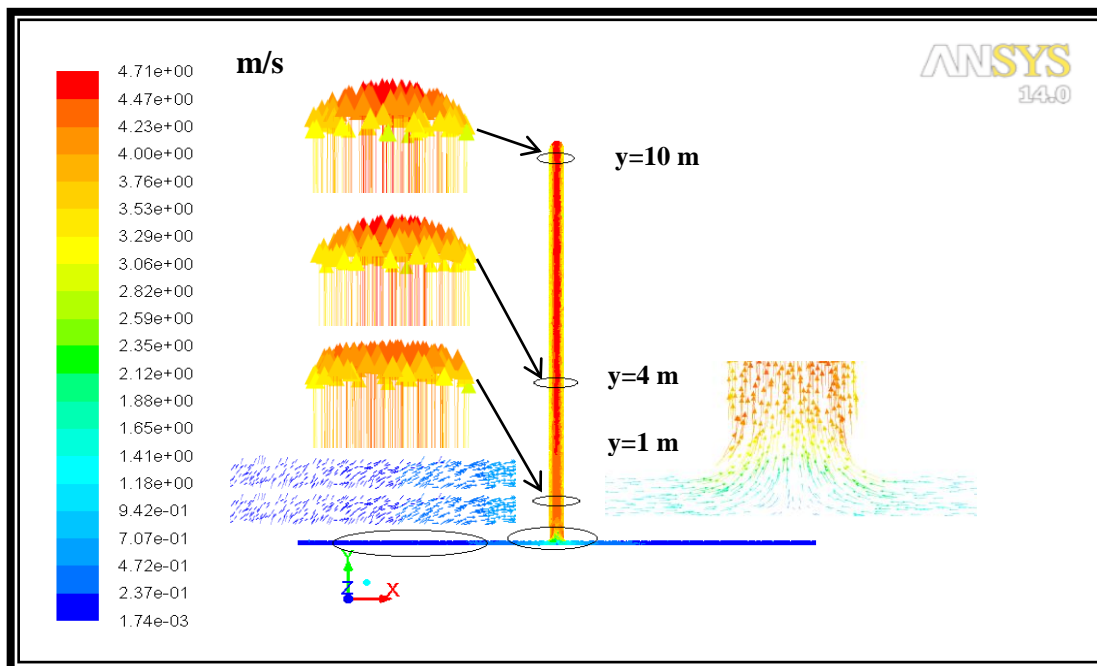


**Figure 11.** Flow felid of air in solar chimney with solar insolation (900 W/m$^2$) for D=12m, H=10m.
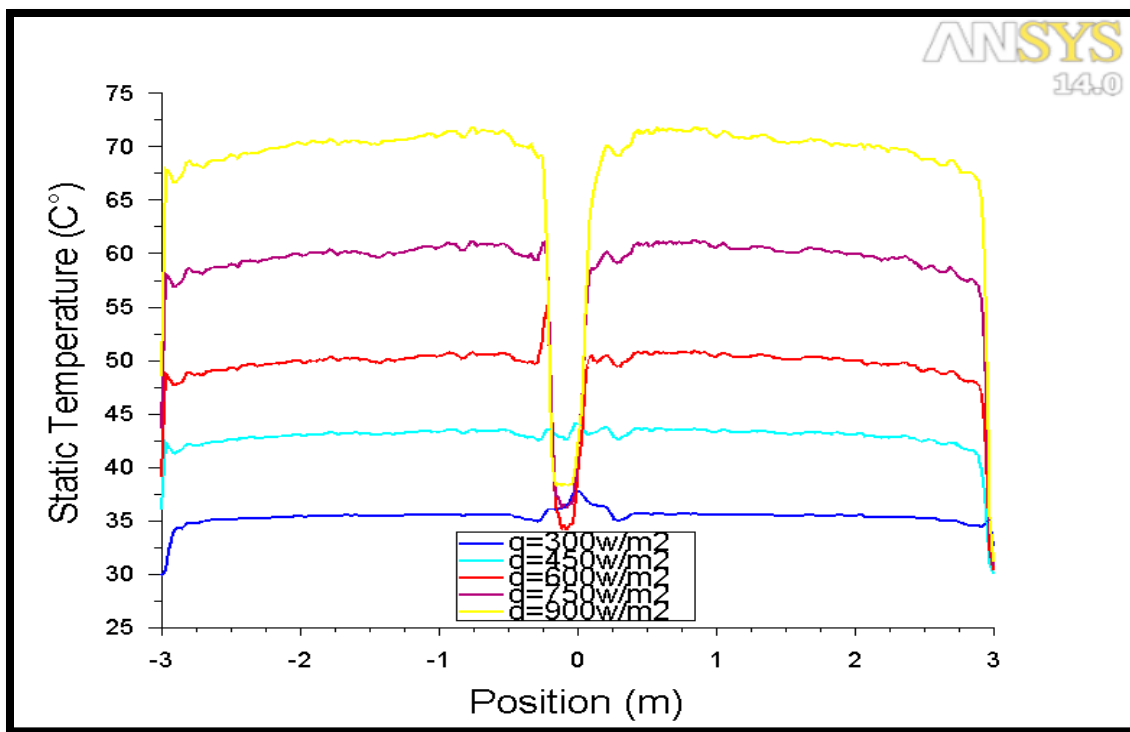
**Figure 12.** Ground  temperature variation  from solar collector diameter at different solar insolation for D =6m, H =6m.
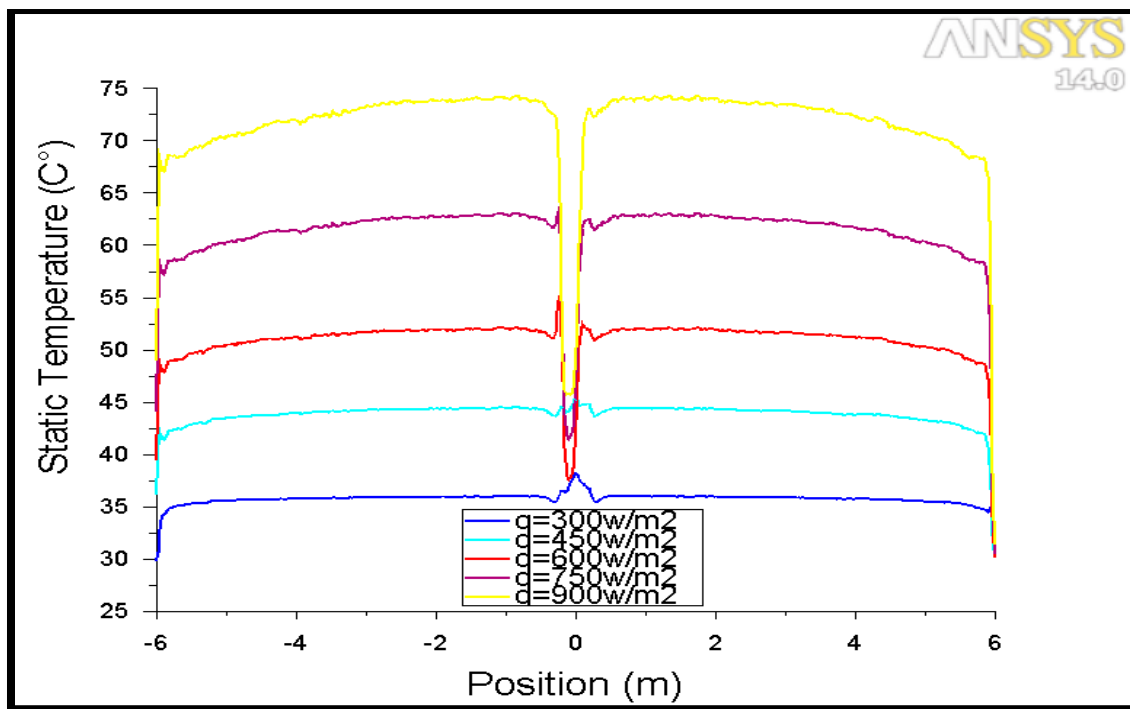


**Figure 13.** Ground  temperature variation  from solar collector diameter at different solar insolation for D =12m, H =12m.
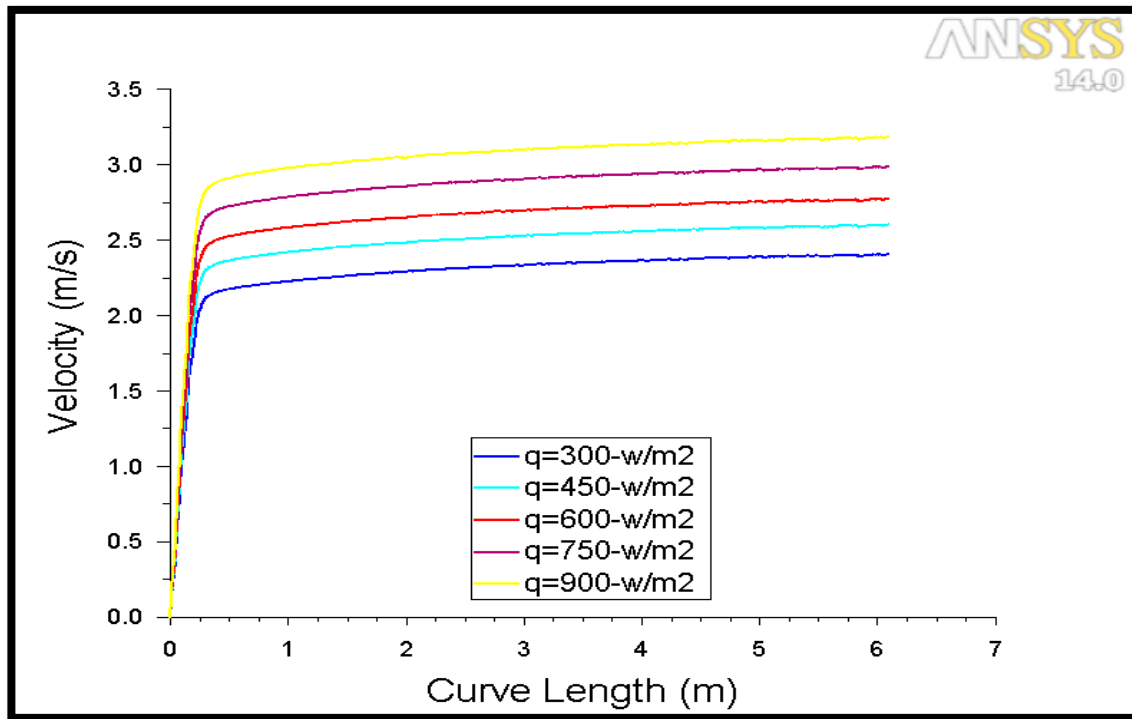
**Figure 14.** Air velocity variation from center collector exit to chimney exit at different solar insolation for D =6m, H =6m.
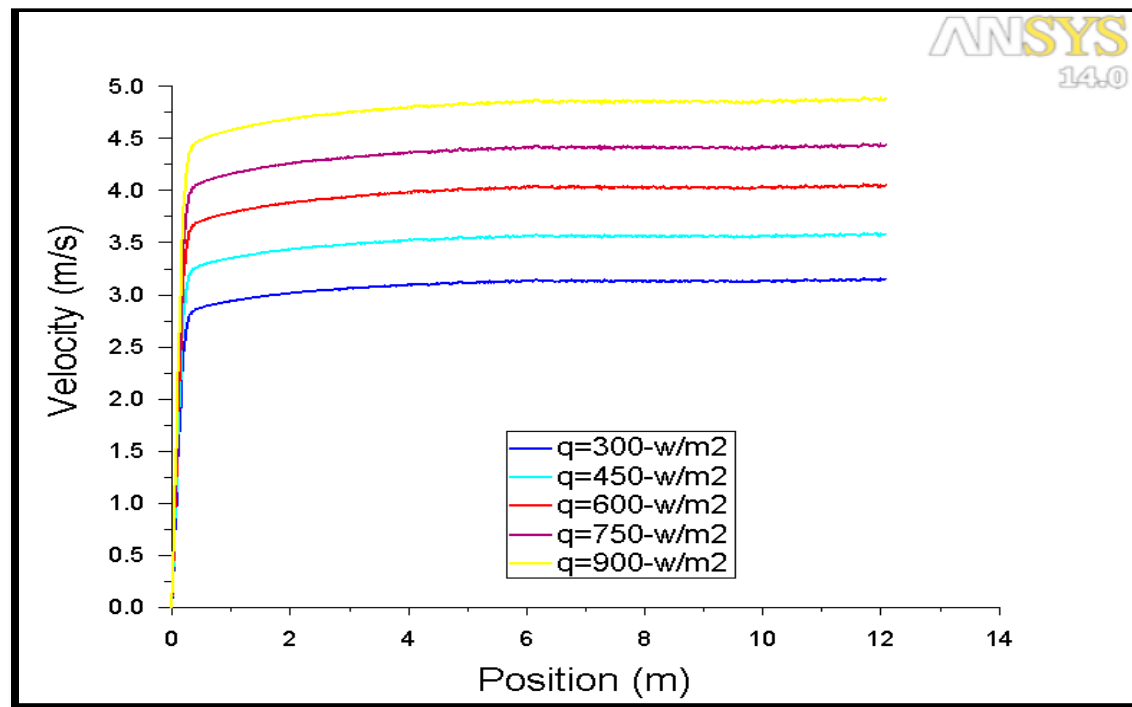


**Figure 15.** Air velocity variation from center collector exit to chimney exit at different solar insolation for D =12m, H =12m.
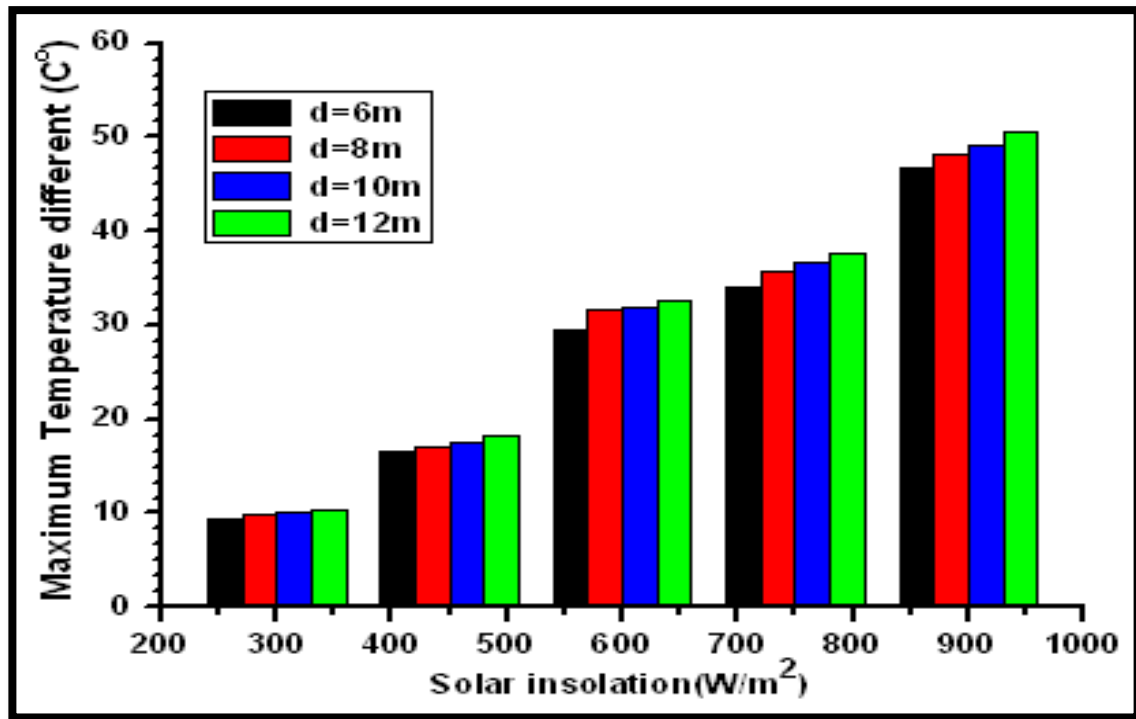
**Figure 16.** The effect of collector diameter on maximum temperature different at different solar insolation for H =6m.
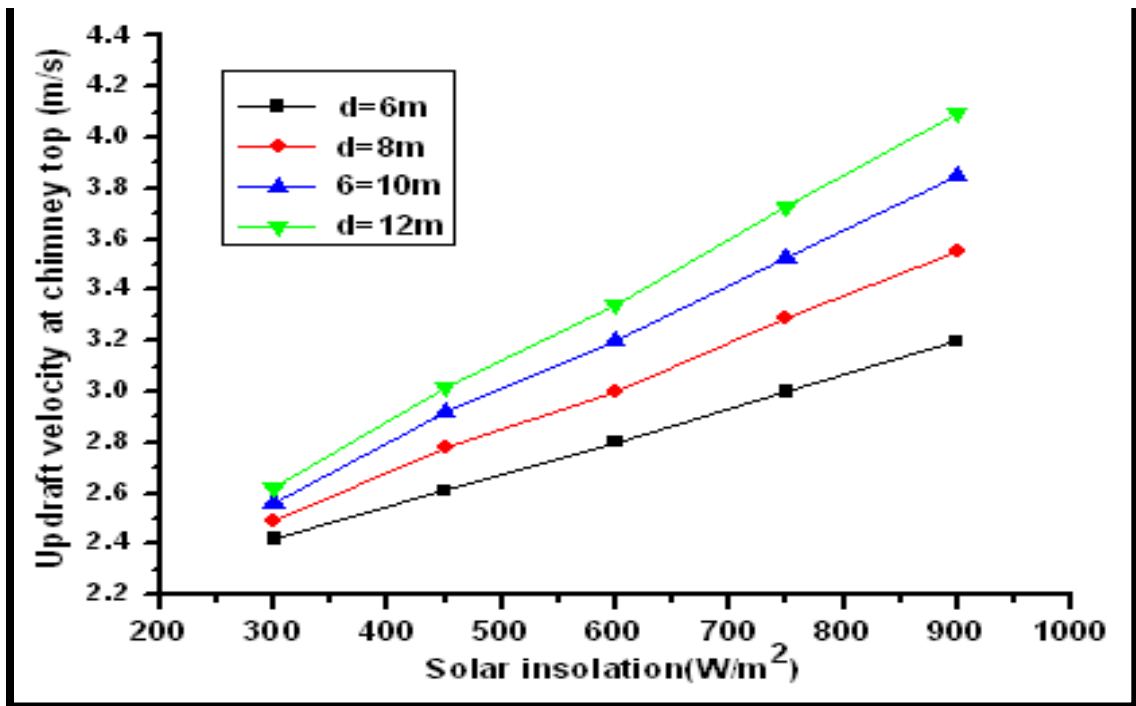


**Figure 17.** The effect of collector diameter on updraft velocity at chimney top at different solar insolation for H =6m.
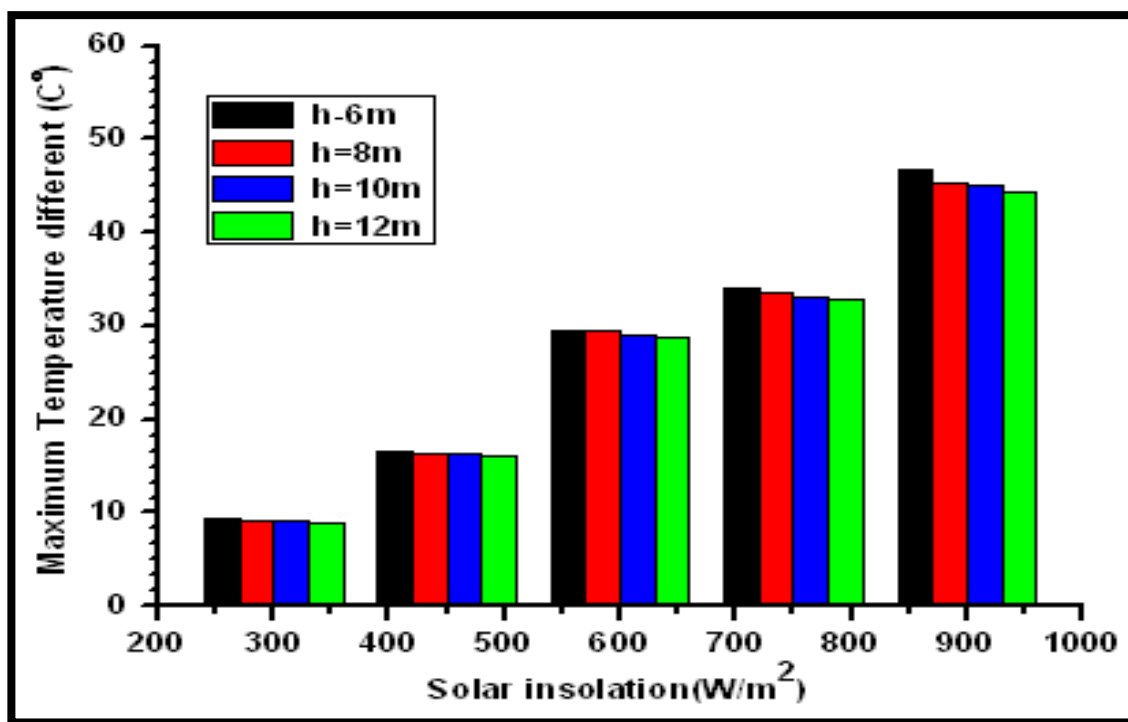
**Figure 18.** The effect of chimney height on maximum temperature different at different solar insolation for D =6m.
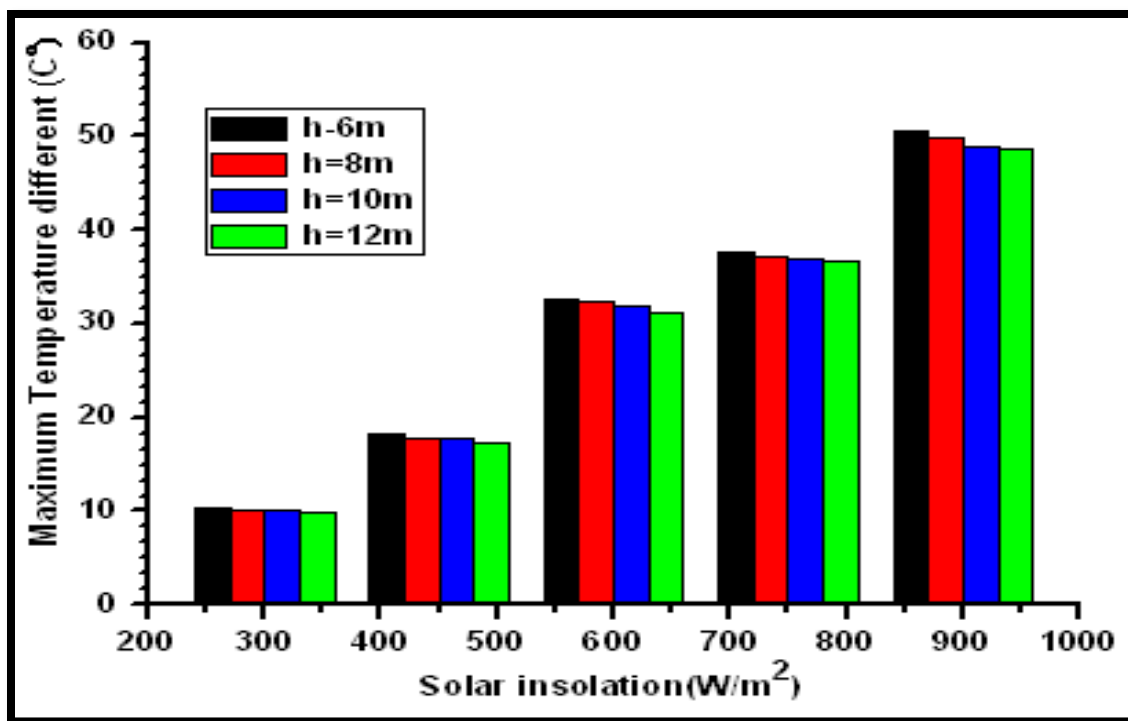


**Figure 19.** The effect of chimney height on maximum temperature different at different solar insolation for D =12m.
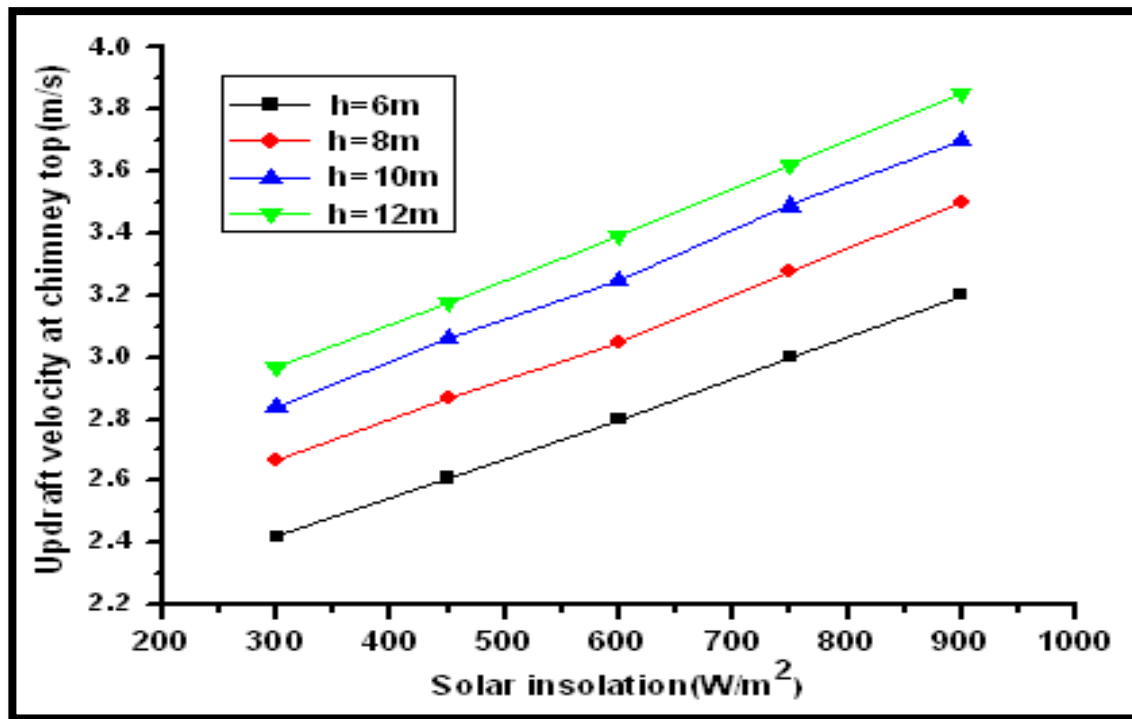
**Figure 20.** The effect of chimney height on updraft velocity at chimney top at different solar insolation for D =6m.
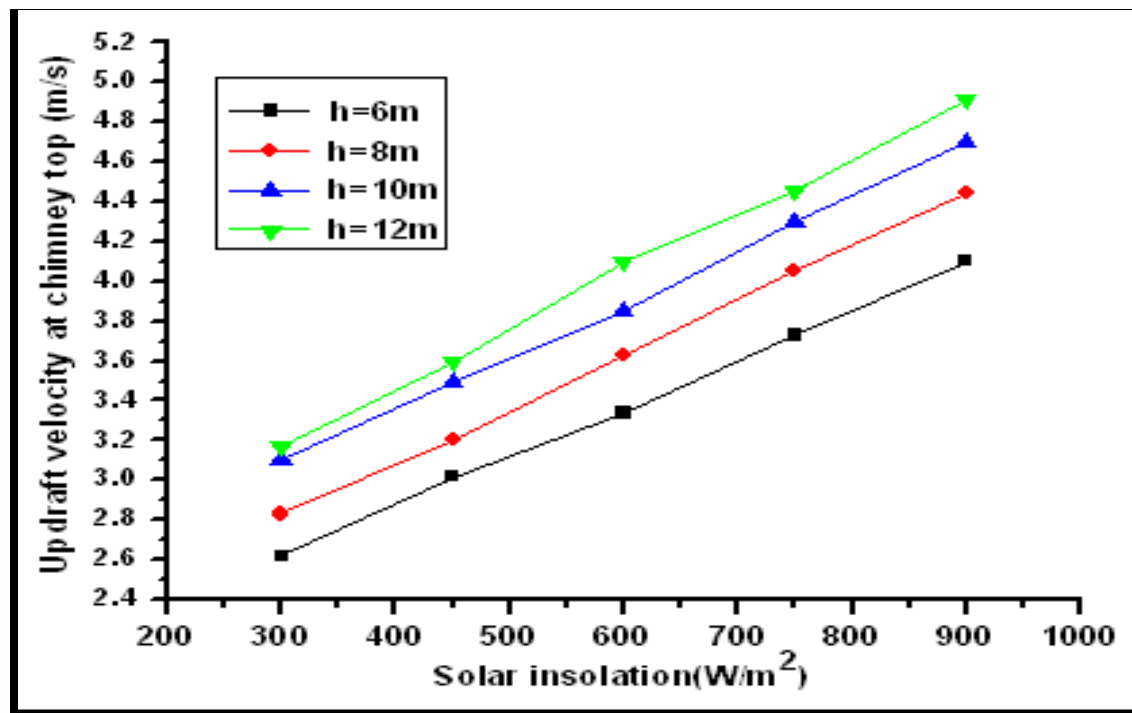


**Figure 21.** The effect of chimney height on updraft velocity at chimney top at different solar insolation for D =12m.
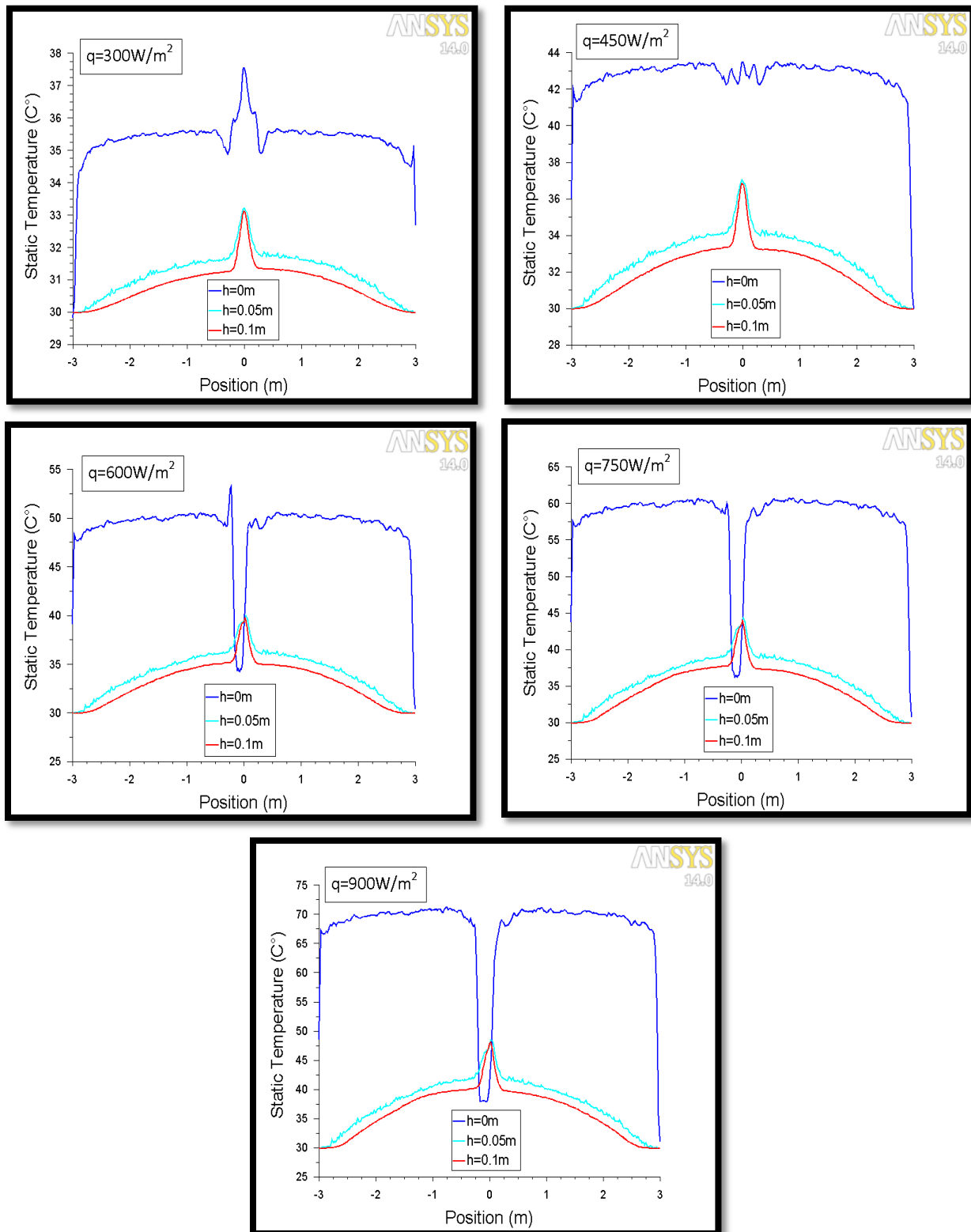
**Figure 22.** Air temperature at different heights above the ground level in the solar collector and at different solar insolation for D =6m, H =12m.
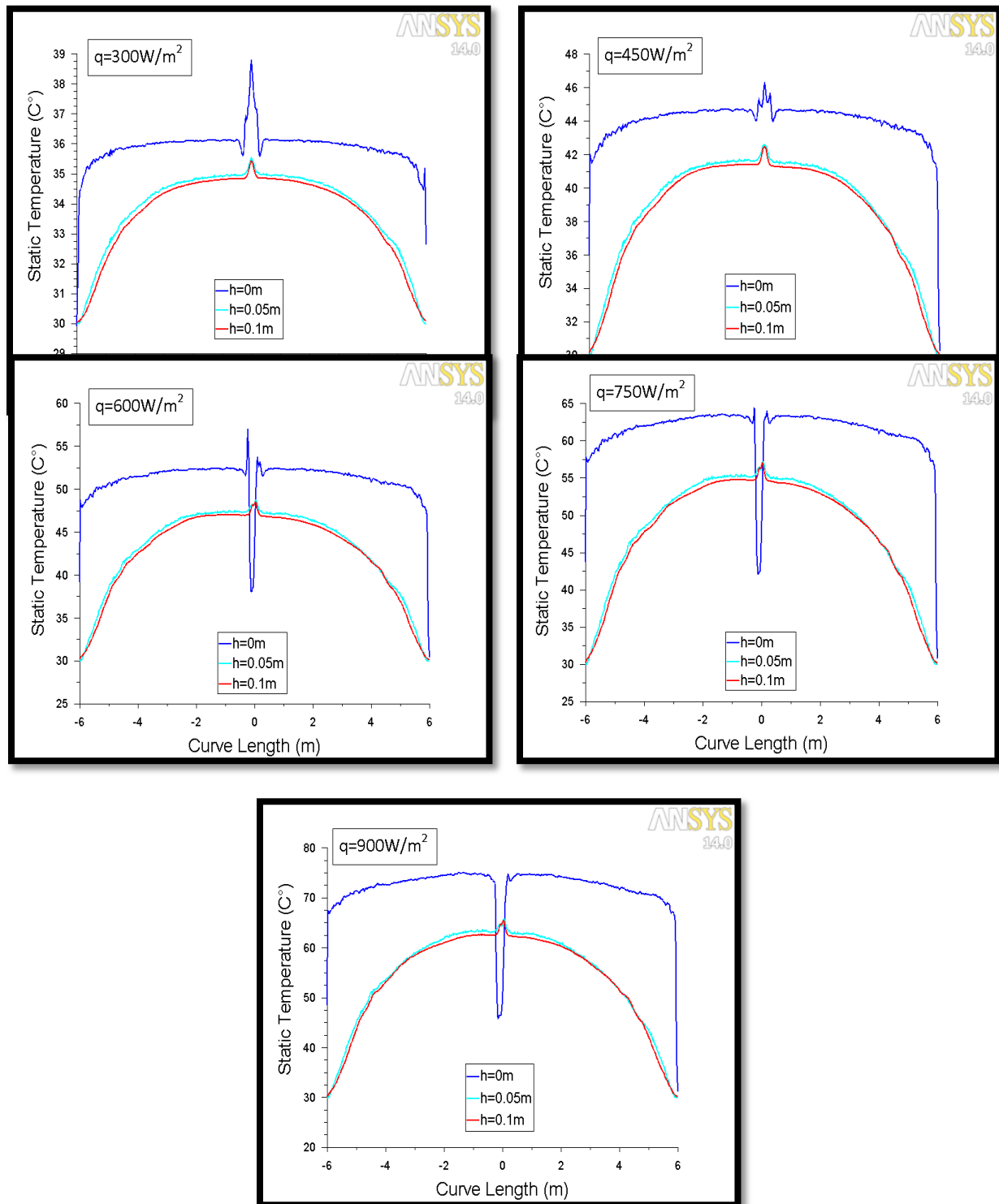
**Figure 23.** Air temperature at different heights above the ground level in the solar collector and at different solar insolation for D =12m, H =6m.

# Bioremediation of Soil Contaminated with 2,4-D Herbicide Using Bioslurry Reactor

**Asst. Prof. Dr. Yasmen A.  Mustafa**
Dept.of Env. Eng.
Baghdad University
yasmen.mustafa@gmail.com

**Ins.Dr. Hayder M.Abdul- Hameed**
Dept.of Env. Eng.
Baghdad University
hayderalmunshi@yahoo.com

**Zainab Abdul Razak**
Dept.of Env. Eng.
Al-Mustansiriyah University
zainababdulrazak@yahoo.com

## ABSTRACT

**E**x-situ bioremediation of 2,4-D herbicide-contaminated soil was studied using a slurry bioreactor operate at aerobic conditions. The performance of the slurry bioreactor was tested for three types of soil (sand, sandy loam and clay) contaminated with different concentration of 2,4-D, 200,300and500mg/kg soil. Sewage sludge was used as an inexpensive source of microorganisms which is available in large quantities in wastewater treatment plants. The results show that all biodegradation experiments demonstrated a significant decreases in 2,4-D concentration in the tested soils. The degradation efficiency in the slurry bioreactor decreases as the initial concentration of 2,4-D in the soils increases.A 100 % removal was achieved at initial concentration of 200mg 2,4-D/kg of sandy soil after 12 days and 92 % at 500mg 2,4-D/kg sandy soil after 14 days.Clay soil represented minimum removal efficiency among the three soils, 82 % at initial concentration of 200mg 2,4-D/kg clay soil after 12 days and 72 % for 500mg 2,4-D/kg clay soil after 14 days.

Abiotic conditions were performed to investigate the desorption efficiency of the contaminant from soil to liquid phase through the three soils. In abiotic reactor the results showed that the rate of desorption for sand and sandy loam soils were nearly the same, it varied between0.102-0.135 $day^{-1}$ at different initial concentration of 2,4-D. While for clay soil the desorption rate varied between 0.042- 0.031 $day^{-1}$ at different initial concentration of 2,4-D.  The decrease in desorption rate in clay soil refers to the characteristic of clay soil, (fine texture, high organic matter and high cation exchange capacity compared with the other soils) that may retain the 2,4-D in the organic matter and the clay minerals.

**Keywords:2,4-D removal;soil contamination; biodegradation process; sewage sludge.**

## المعالجة البيولوجية للتربة الملوثة بمبيد الاعشاب D-2,4 باستخدام المفاعل البيولوجي

أ.م.د.ياسمين عبد العزيز مصطفى     م.د حيدر محمد عبد الحميد     م. زينب عبد الرزا ق
قسم الهندسة البيئية /جامعة بغداد     قسم الهندسة البيئية /جامعة بغداد     قسم الهندسة البيئية /الجامعة المستنصرية

### الخلاصة

تمت دراسة المعالجة البيولوجية للتربة الملوثة بمبيد الاعشاب D-2,4  في مفاعل بيولوجي يعمل تحت الظروف الهوائية. اجريت دراسة اداء المفاعل البيولوجي لثلاثة أنواع من التربة (رملية وزراعية وطينية) ملوثة بتراكيز  مختلفة من ال D-2,4 200 و300 و500ملغم/كغم من التربة. استخدمت حمأة الصرف الصحي كمصدررخيص الثمن لتجهيز المفاعل بالكائنات الحية الدقيقة والذي تتوفر  بكميات كبيرة  في محطات معالجة مياه الصرف الصحي.

بينت النتائج العملية أن جميع التجارب للمفاعل البيولوجي أدت الى انخفاض ملحوض في تراكيزال D-2,4في التربة. ان كفاءة التحلل البايولوجي في المفاعل البيولوجي تناقصت مع ازدياد التركيز الابتدائي لل D-2,4 في التربة واعطت إزالة 100٪ عند تركيز 200ملغم / كغم من التربة الرملية بعد 12 يوما و 92٪ إزالة عند تركيز 500ملغم / كغم من التربة الرملية بعد 14 يوما.

اظهرت التربة الطينية اقل كفاءة أزالة بين انواع الترب الثلاثة  حيث ان نسبة الازالة بلغت 82٪ عند تركيز 200ملغم / كغم من التربة الطينية بعد 12 يوما و 72٪ عند تركيز 500ملغم / كغم من التربة الطينية بعد 14 يوم. استخدم المفاعل عند الظروف اللاحيوية (اي بدون اضافة الاحياء المجهرية) وذلك للتحقق من كفاءة انتقال الملوثات من التربة  بانواعها الثلاث إلى السائل الموجود في المفاعل. حيث بينت النتائج ان معدل انتقال المبيد من التربة الرملية والزراعية الى السائل كانت متقاربة وبلغ معدل الانتقال بين (0.102-0.135day$^{-1}$) لتراكيز مختلفة من ال D-2,4في التربة.بينما بالنسبة للتربة الطينية كانمعدل انتقال المبيد من التربة الى السائل بين ( 0.042-0.031day$^{-1}$ )لتراكيز مختلفة من ال D-2,4في التربة الطينية. ان انخفاض معدل انتقال المبيد من التربة الطينية الى السائل في المفاعل البيولوجي سببه طبيعة التربة الطينية والتي تمثل نعومة حجم الدقائق والمحتوى العالي من المواد العضوية وزيادة السعة التبادلية الكاتيونية مقارنة مع الترب الأخرى.

**الكلمات الرئيسية: ازالة D-2,4 ، تلوث التربه، عملية التحلل البايلوجي، الحماه المنشطه.**

## 1. INTRODUCTION

A pesticide is generally a chemical or biological agent (such as virus, bacterium, antimicrobial- or disinfectant) that through its effect deters, incapacitates, kills or otherwise discourages pests. Target pests can include insects, plant pathogens, weeds, mollusks, birds, mammals, fish, nematodes (round worms) and microbes , that destroy property, cause nuisance, spread disease or are vectors for disease. Pesticides can be classified by target organism, (e.g. herbicides, insecticides, fungicides, rodenticides, and pediculicides), chemical structure (e.g. organic, inorganic, synthetic, or biological (biopesticide), and physical state (e.g. gaseous(fumigant)). Biopesticides include microbial pesticides and biochemical pesticides, **Tiryaki,**and **Temur,2010**.

Herbicides are widely used to control unwanted plant species that are competing for light, water, and nutrients with the wanted plant species. Whenever herbicides are applied, they are transported to areas distant from the original site of application, ends up to rivers and streams. 2,4-Dichlorophenoxyacetic acid (2,4-D) is a common system herbicide used in the control of broadleaf weeds. It is the most widely used herbicide in the world, and the third most commonly used in North America**, USEPA, 2007**.

2,4-D is a synthetic auxin (plant hormone), and as such it is often used in laboratories for plant research and as a supplement in plant cell culture media. It is a major ingredient in Agent Orange(one of the herbicides and defoliants used by the U.S. military as part of its chemical warfare program , during the Vietnam War. 2,4-D is the active ingredient in several formulations of herbicides recommended for the control of broadleaf weeds, cereal crops such as wheat, corn, oats, and barley, and the cane crops. It is also widely use to control dandelions and other broadleaf weeds in lawns, rangeland, and pastures. Other uses include the control of aquatic weeds, some woody vegetation, and site preparation and conifer release in forests, **USEPA, 2007**.

2,4-D is classified by both ANVISA (Brazilian National Agency for Sanitarian Vigilance) and WHO (World Health Organization) as a hormonal herbicide of level II toxicity. After its application in field, the excess of the herbicide is easily transferred to the groundwater, due to its high solubility in water. Even after a long period of disuse, considerable amounts of either 2,4-D or its main product of degradation, 2,4-dichloro-phenol (2,4-DCF), might be found in surface waters, and groundwater as well, **Amarante, et al., 2003.**

Ingestion of high doses of 2,4-D have shown a moderate acute toxicity to lower mammals and humans (gastrointestinal irritation, spasms to the miocardio, depression of the central nervous system, and damage to liver and kidney, **Kwangjick, et al., 2001**. Studies on the environmental effects of 2,4-D indicate that this herbicide may be toxic to aquatic invertebrates, phytoplankton, and fish, although the extent and degree of toxicity and damage vary among the species ,**Villalobos, et al., 1996;Cheney, et al., 1997.** 2,4-D present in soil water, as well as adsorbed on the colloidal hydroxides of  Fe and Al and the organic matter of soils and sediments , may pose a potential risk to the aquifers and the trophic chain, **Dejonghe, et al., 2000**.

The remediation methods currently available for the treatment of pesticide contaminated soil are, low temperature thermal desorption, incineration, bioremediation and phytoremediation.

Bioremediation is the most attractive method for environmental protection due to its cost effectiveness and is unique by offering the potential for complete destruction. Bioremediation is a process that uses microorganisms or their enzymes to promotedegradation and/or removal of contaminants from the environment, **Dobson,**and **Burgess, 2007**. The use of microbial metabolic

ability for degradation /removal of environmental pollutants provide an economic and safe alternative compared to other physicochemical methodologies. However,although highly diverse and specialized microbial communities present in the environmentdo efficiently remove many pollutants, this process is usually quite slow, which leads to a tendency for pollutants to accumulate in the environment and this accumulation canpotentially be hazardous. Different strategies can be employed of improving the process of bioremediation, depending of the state of the contaminatedenvironment. One of these strategies, biostimulation, involves promoting the growth ofmicroorganisms at the contaminated site by introducing nutrients, surfactants and oxygen and as a consequence, the rate ofbiodegradation/ bioremediation can be increased. Another strategy,bioaugmentation orbioaddition, is the addition of microbial populations, indigenous, alien or genetically modified organisms (GMO), in places where there is an insufficiency of indigenousmicroorganisms, **Vidali, 2001; Silva, et al., 2004;Li,** and **Li,2011**. Bioremediation is a versatile process that can be appliedin-situ, at the contaminated site, or ex-situ, involving removal of contaminated material to betreated elsewhere. In-situ bioremediation technologies are more economical and releasefewer pollutants into the environment; however, they may require longer treatmenttime frames than the ex-situ techniques, **Tabak, et al., 2005.** Treatment in a slurry bioreactor is considered to be one of the fastest ex-situ bioremediation methods. Soil slurry bioreactors consist of a mixture of soil in water in various ratios and greatly enhance rates over solid treatment systems by maximizing the contact between micro-organisms, contaminants, nutrients, and oxygen. In slurry bioreactors, the increase in soil moisture results in a larger amount of solubilized contaminant, therefore increasing bioavailability, **Weber,**and **Kim, 2005.**

Currently, there is wide variety of microorganisms (bacteria, fungi, yeasts and algae) that are being studied for use in bioremediation processes, **Bogacka, 2011; Ali, 2011**. Sewage sludge is a biomass waste generated from the regular biological activities of municipal wastewater treatment plants, it contains bacteria, fungi, yeast and protozoa. Rather than disposing the sludge, this waste material seems to be a promising way of turning it into a useful resource. Sewage sludge is also generally rich in nitrogen, which is essential for the growth of microorganisms. Furthermore, it has a high microbial diversity. The microorganisms overgrown in such wastewater systems can be utilized for treatment different types of contaminants including herbicides, **Bogacka,2011.**

The aim of this research is to treat three types of contaminated soils, sand, sandy loam and clay with 2,4-D herbicide, using sewage sludge as an inexpensive, heterogeneous source of microorganisms, in ex-situ bioremediation process. The effect of using different concentrations of 2,4-D (200, 300 and 500mg/kg soil) on the bioremediation process was studied.

## 2. MATERIALS AND METHODS
### 2.1 Materials
2,4-D ( $C_8H_6Cl_2O_3$) was selected as a model herbicide in this study because of its unique behavior in soil. This chemical is both very degradable and vulnerable to leaching. 2,4-D used in this study was purchased from Fluka. Its purity is 95% and its solubility in water is 900mg/L at $20^oC$. Other chemicals are: methanol ($CH_2CL_2$) of 99.9% purity was provided by Biosolve Chemicals; acetone ($CH_3COH_3$) of purity > 99.8% was obtained from Fluka; acetonitrile ($CH_3CN$) of 99.5% purity was obtained from BDH Chemicals Limited and Phosphoric acid of 85 % purity from SDF chemical limited .

## 2.2 Nutrients

Modified McKinney's medium was used for the bacterial growth. The composition of the minerals in one liter of growth media is shown in **Table 1** and the composition of trace elements is shown in **Table 2**. The medium was prepared by dissolving the inorganic chemicals in one liter of reverse osmosis water that resulted in a buffered solution of pH 6.5-6.7 which was then sterilized at 121°C.

## 2.3 Soil

Three types of soils were used in the present work: sand, clay and sandy loam. Sand and clay soil samples were obtained from the Ministry of Industry and Minerals (Iraq general establishment for geological survey and mineral investigations), while the third type of soil (sandy loam) was collected from agricultural soils in Baghdad City which was sieved to 2mm. The physical and chemical properties of the three soils are given in **Table 3**.The analysis was performed in the Ministry of Industry and Minerals (Iraq general establishment for geological survey and mineral investigations).

## 2.4 Preparation of 2,4-D Spiked Soil

To prepare the 2,4-D contaminated soil, a stock of 50, 30, 20 mg of 2,4-D was dissolved in 100 mL acetone . In a stainless steel container, a clean, air dried-soil was placed and sprayed with appropriate volume of this stock to give the desired contaminated soil. Mechanical mixing for 1 hour was applied to assure homogenization. The 2,4-D contaminated soil then dried for 24 hour at $35^o$C in order to evaporate the acetone, then stored in an air-tight stainless steel jar in a ventilated hood in the dark. Each batch of 2,4-D spiked soil was used within 2 weeks.

## 2.5 Microorganisms

Sewage sludge was used in the present study as 2,4-D degrading microorganisms. The sewage sludge was collected from the sludge drying bed in Al-Rustamiyah Sewage Treatment Plant, the old project in Baghdad city. A specified volume of sewage sludge providing at least $10^7$cells/mL was used in the experiments. The average mixed liquor volatile suspended solid of the sludge was measured according to , **Clesceri,et al., 1999** to be 5000 mg/L.
The number of bacteria in the sludge was estimated using the standard plate count which reflects the number of viable bacteria and assumes that the bacteria grow into single colonies.

## 2.6 Experimental Procedure

Sewage sludge of 20mL plus 60ml of nutrients were placed in three conical flasks (each of 250mL volume).Then 20mg of contaminated soil with concentration of 200, 300 and 500mg 2,4-D/kg of sandy soil were added in each flask. The flasks equipped on rotary shaker (from Heidolph, Germany), which operated at 200 rpm for 14 days. The required dissolved oxygen (2.5mg/L) was supplied by continuous mixing. The temperature was maintained at $25^o$C by inserting the rotary shaker inside the incubator. 2, 4-D concentration in both liquid and soil phases also the bacterial growth in liquid phase were measured in regular interval (mainly every 2 days), by removing 5mLsample from the aqueous phase by a clean syringe and1gm of settled soil phase using a spatula. The same procedure was followed for sandy loam and clay soils. For control reactor the same procedure was followed but without using sewage sludge (i.e. 80mL of nutrients were placed in the conical flasks).

**2.7 Extraction of 2,4-D from Soil Slurry**

   Air dried soil sample (0.25gm) at room temperature was extracted with 30mL of a mixture of acetonitrile-water-acetic acid 60:39:1, **Garibay, et al., 2005.** The suspension was vortexed, at maximum speed for 10 min. The solvent extract was recovered by centrifugation at 4000 rpm for 15 min to separate the liquid from the soil, the procedure was repeated twice before analysis by HPLC. The liquid was filtered through filter paper (grade No.1, Whatman, England) and then passed through 0.45 μm PTFE syringe filter before analysis by HPLC.

**2.8 Analysis**

   High performance liquid chromatography (HPLC), type Varian 9065, Netherlands, was used to identify the concentration of 2,4-D in the samples , at Environmental Engineering Department laboratories of Al-Mustansiriyah University. Analyses were carried out with the following conditions:  wavelength of 282 nm, 1.5 mL/min flow rate and elution with an  acetonitrile + aqueous phosphoric acid (1.0M, pH=3) solution (first using 60+40 solution by volume for 10 min and then 65+35 solution for 20 min).The HPLC was equipped with C18 column (250 mm long, 4 mm ID). The peak of 2,4-D was detected after 2.7 min .

**3. RESULTS AND DISCUSSION**

**3.1 2,4-D Partitioning between Soil and Liquid Phase in Abiotic Control Reactor**

   Abiotic control reactor represents a reactor with no microorganisms. The behavior of 2,4-D partitioning between soil and liquid in abiotic control reactor for three types of soil (sand, sandy loam and clay) were investigated in the present experiments. For each type of soil three different initial concentrations of 2,4-D (200, 300 and 500 mg/kg  soil) were tested, **Figs.1-3**.

After startup of the reactor 2,4-D was desorbed from the soil to the liquid phase. It approached a steady state condition after nearly 12 days for sand and sandy loam soil. For clay soil the steady state appearedafter 12-14 days. **Fig. 1** shows that at initial 2,4-Dconcentration of  200 mg/kg soil, the release of  2,4-D from the soil to the liquid  phase reaches  97% , 95% and 72%  for sand, sandy loam and clay soil respectively.  **Fig. 2** shows that at initial concentration of 300mg 2,4-D/kg soil, the release of 2,4-D from the soil to the liquid  phase reaches 86% , 89% and 72% for sand , sandy loam and clay soil respectively. While from **Fig. 3**  at initial concentration  of 500mg 2,4-D/kg  soil ,the release of  2,4-D from the soil to liquid  phase reaches 89%, 88% and58% for sand, sandy loam and clay soil respectively. These results were tabulated in **Table 4**. The results show that the release efficiency decreased with the increase of 2,4-D initial concentration. A high initial concentration of 2,4-D enhance the sorption  into the soil. This observation was coinciding, **Boivin, et al., 2005**. Also a distinct decrease in the release efficiency was observed for clay soil, reaching 58% compared with 89% for sandy soil at initial concentration of 500mg 2,4-D/kg soil. This    attribute to the fine texture of clay soil , high content of  organic  matter  (1.967 %)  and  high  value  of  cation  exchange  capacity (68.34meq/100mg),  which enhance the sorption of 2,4-D in to the soil . **Bolan**and **Baskaran, 1996** in their study for adsorption/ desorption behavior and degradation of 2,4-D, examine 10 soils from New Zealand that have different organic matter and clay content .They observed that the extent of adsorption increased with the increase in soil organic compounds.

   At early period of time desorption of pesticides follows first-order reaction kinetics, Eq.(1):

$$S_t = S_0 exp[-k_0 t] \tag{1}$$

where $S_0$ and $S_t$ are the amount of 2,4-D (mg/kg) in the soil phase at time zero and t , t the desorption period (day), and $k_0$ is the rate of desorption (day$^{-1}$). A linear relationship with R$^2$ of more than 0.90% was obtained as illustrated in **Fig.4**.

It can be observed that the rate of desorption $k_0$ for sand and sandy loam soils were nearly the same, it varies between 0.102-0.135 day$^{-1}$ at different initial concentration of 2,4-D. While for clay soil the desorption rate $k_0$ varies between 0.031- 0.042 day$^{-1}$ at different initial concentration of 2,4-D. The decrease in desorption rate refers to the characteristic of clay soil, (fine texture, high organic matter and high cation exchange capacity) that may retain the 2,4-D in the organic matter and the clay minerals, as confirmed by **Bolan,**and **Baskaran, 1996; Smith, et al., 1992.**

**3.2 2,4-D Partitioning Between Soil and Liquid Phase in Biological Active Reactor**

The effect of microbial activity, bioaugmentation (adding of sewage sludge) and biostimulation (adding of nutrient) together on 2,4-D degradation using slurry bioreactor were investigated in these experiments.

2,4-D partitioning between soil and liquid phase for sand ,sandy loam and clay at different initial concentrations 200, 300 and 500 mg/kg soil are plotted in **Figs. 5-7**.

In all experiments the 2,4-D concentration in liquid phase increased initially reaching maximum concentration and then rapid degradation of 2,4-D was observed. The reason for this is that the desorption rate of 2,4-D is higher than the biodegradation rate during the first period of experiments. In the soil phase a continuous decrease in 2,4-D concentration continued until the end of the experiments. This result indicates that the desorbed 2,4-D in the liquid phase was subjected to continuous biological degradation therefore desorption was enhanced due to the partitioning effect.

**Fig.5** represents the partitioning between solid and liquid phases for 200mg 2,4-D/kg soil in the biological active reactor, for the three different soils. From this figure, the maximum concentration of 2,4-D in liquid phase can be observed to be 2.2, 6.8 and 1.4mg/L after two days of the reactor operation for sand , sandy loam and clay respectively.

For 2,4-D initial concentration of 300mg/kg soil as represented by**Fig.6**, the maximum concentration was achieved in liquid phase equal to 13.9 and 37mg/L after two days for sand and sandy loam soil and 30.2 mg/L after six days for clay soil.

For 500mg 2,4-D/kg soil, **Fig.7**, the maximumconcentration in liquid phase was obtained to be 19, 12.4 and 18.9 mg/L after two days for sand ,sandy loam and clay soil respectively.

From the above results it can be concluded that 2,4-D in liquid phase increased until almost two days of the reactor operation reaching a maximum concentration and then decreased at different rates indicating that 2,4-D was subjected to continues biological degradation.

At early period of time the degradation of pesticides also follows first-order reaction kinetics, Eq.(2):

$$C_t = C_0 exp[-k_1 t] \tag{2}$$

where $C_0$ and $C_t$ are the amount of 2,4-D (mg/kg) in the soil phase at time zero and t ,t the degradation period (days), and $k_1$ is the rate constant of degradation (day$^{-1}$).

A linear relationship with R$^2$ of more than 0.93 was obtained as illustrated in **Fig.8**, revealing that the rate of degradation is directly proportional to the concentration of 2,4-D in the soil phase. The rate of degradation of organic pesticide has often been observed to follow first order reaction kinetics, **Cycon, et al., 2011; Plangklang,** and **Reungsang, 2010**.

$k_1$for each type of soil with different concentrations of initial 2,4-D were tabulated in **Table 5**. From **Table 5** and **Fig.8**, it can be observed that the rate of degradation  $k_1$ decreased with the increase of initial concentration of  2,4-D.

**Macur,**and **Wheeler, 2007** studed the impact of 2,4-D application on soil microbial community structure. They showed that at high 2,4-D concentration (100 and 500mg/kg soil) a significant reduce in the diversity of 2,4-D degradation of bacterial strains was observed. They also illustrated that clay soil has minimum degradation rate among the three soils (sand, sandy loam, clay).

Considering the 2,4-D removal efficiency for the three soils in the present experiments as it is plotted in **Fig. 9** and listed in **Table 5**, the removal efficiency decreases as the initial concentration of 2,4-D in the soils increases.  A 100 % removal at initial concentration of 200mg 2,4-D/kg soil after 12 days for sandy soil was acheived and this percent decreases to 92% at 500mg 2,4-D/kg soil after 14 days .

**Fournier, et al., 1981** found that the degradation rate of 2,4-D is highly dependent on the initial concentration (the higher the degradation, the lower  the initial concentration).

Clay soil represent the less removal efficiency among the three soils , 82% for  200mg 2,4-D/kg soil after 12 days and  72% for  500mg 2,4-D/kg soil after 14 days . Clay soil characteristics enhance the sorption capacity and limits the release of 2,4-D to the liquid phase in which biological degradation is performed .

**Nikakhtari, et al., 2009** mentioned that the biodegradation rate in the bioslurry reactor with clay is slower than with sandy loam and sandy soil.

### 3.3 CFU Variation

CFU (Colony Forming Unit) was investigated in the present experiments as an important parameter indicating the microbial activity. **Figs. 10-12** show the biomass growth with 2,4-D degradation in the liquid phase during the bioreactor operation. Different initial concentration of 2,4-D (200, 300, 500 mg/kg) in sand ,sandy loam and clay soils were studied.

Initial microbial cell numbers of the sewage sludge which was utilized in the biodegradation operation were about $200\times10^7$ CFU/mL.

A lag phase of almost 2 days was observed through all the experiments. The lag phase is related to the time required to develop a population of microorganisms that could effectively degrade the 2,4-D. The lag phase is a period of adaption of cells to a new environment. Microorganisms reorganize their molecular constituents when they transfer to a new medium. Depending on the composition of nutrients new enzymes are synthesized, the synthesis of some other enzymes is repressed, and the internal machinery of cells is adapted to the new environmental conditions. During this phase, cell mass may increase a little, without an increase in cell number density, **Yu,**and **Ruihong, 2006**.

After the lag phase a period of an active growth was observed. The microorganisms multiply rapidly and enter the exponential growth phase. The maximum CFU/mL observed in the present experiments was in the range of $700\times10^7$- $1200\times10^7$ CFU/mL which achieved after almost six days of operation as shown in the **Figs. 10-12**. After the exponential growth, a stationery phase then a decline in microbial growth was observed, due to the nutrient (2,4-D) depletion.

It can be noticed that the maximum release of 2,4-D from the soil to the liquid phase happened during the lag phase period. The results show that when the 2,4-D concentration increased the biodegradation retarded due to inhibition created by the substrate and the toxicity of high 2,4-D concentration.

### 3.4 pH Variation

The pH variation in the liquid phase during the abiotic and biotic bioreactor operation was measured to track the microbial activity. **Fig. 13** shows the variation in pH for sand, sandy loam and clay for 200, 300 and 500 mg 2,4-D/kg soil. It can be noticed that the pH variation in the reactor with biological activity (biotic) was more obvious compared to the control reactor (abiotic). The variation could result from the products obtained from the biodegradation activity. The decrease in pH in the biological active reactors may be due to the formation of $CO_2$ from mineralization of the metabolic intermediates formed, **Mohan, et al., 2008**.

## 4. CONCLUSIONS

The main conclusions that can be drawn from the experimental work of this research are as follows:

• The rate of desorption in the abiotic reactor for sand and sandy loam soils were nearly the same, it varies between (0.102-0.135 day$^{-1}$) at different initial concentration of 2,4-D. While for clay soil the desorption rate varies between (0.031-0.042 day$^{-1}$) at different initial concentration of 2,4-D.

• In all biological active reactor experiments the 2,4-D concentration in the liquid phase increased initially reaching a maximum level and then rapid degradation of 2,4-D was observed. The maximum release of 2,4-D from the soil to the liquid phase happened during the lag phase period of microbial growth.

• The degradation of 2,4-D in the bioreactor follows first-order reaction kinetics. A linear relationship between $\ln(C_t/C_0)$ vs. t with correlation coefficient $R^2$ of more than 0.93 was obtained revealing that the rate of degradation was directly proportional to concentration of 2,4-D in the soil phase.

• The removal efficiency of 2,4-D in the bioslurry reactor decreases as the initial concentration of 2,4-D in the soils increases, it
reached 100% at initial concentration of 200mg 2,4-D/kg sandy soil after 12 days and decreased to 92% at 500 mg 2,4-D/kg sandy soil after 14 days .

• Clay soil represent the less removal efficiency in the bioslurry reactor among the three soils , 82% for 200mg 2,4-D/kg clay soil after 12 days and 72% for 500 mg 2,4-D/kg clay soil after 14 days .

• The pH variation in biological active reactor was more obvious compared to the control reactor (abiotic) in all experiments.

**REFERENCES**

Ali, A. H.,2011, *Performance of Adsorption / Biosorption for Removal of Organic and Inorganic Pollutant*, PhD thesis, University of Baghdad, Environmental Engineering Department College of Engineering.

Amarante, J. O.P.,Brito,N.M.,Santos,T.C.R.,Nunes,G.S., and Ribeiro,M.L., 2003, *Determination of 2,4- Dichlorophenoxyacetic Acid and its Major Transformation Product in Soil Samples by Liquid Chromatographic Analysis,* Talanta, Vol.60 ,PP.115-121.

Bogacka, E. K., 2011, *Surface Properties of Yeast Cells During Heavy Metal Biosorption,*Cent. Eur. J. Chem., Vol. , No.2, PP. 348-351.

Boivin, A., Amellal, S., Schiavon, M., and Van Genuchten, M.T., 2005,*2,4-Dichlorophenox-yacetic acid (2,4-D) Sorption and Degradation Dynamics in Three Agricultural Soils*, Environ. Pollut. , Vol. 138, PP. 92–99.

Bolan, N.S., and Baskaran, S.,1996,*Biodegradation of 2,4-D Herbicide as Affected by its adsorption-Desorption Behavior and Microbial Activity of Soils*,Aust. J. Soil Res.,Vol. 34 , PP. 1041-1053 .

Clesceri, L.S., Creenberg A.E., and Eaton D. A.,1999, *Standard  Method for the Examination of Water and Wastewater* ,20th edition , 2540G.

Cheney, M., Fiorillo R, Criddle R., 1997, *Herbicide and Estrogen Effects on the Metabolic Activity of Elliptio Complanata Measured by Calorespirometry*,Comp Biochem Physiol,Vol. 118C, PP. 159–64, 1997.

Cycon´, M., Wo´jcik, M., and Piotrowskaseget, Z.,2011,*Biodegradation Kinetics of the Benzimidazole Fungicide Thiophanate-Methyl by Bacteria Isolated from Loamy Sand Soil* ,Biodegradation, Vol. 22 , PP. 573–583.

Dejonghe, W., Goris, J., El-Fantroussi, S., Hofte, M., DeVos P., and Verstraete W., 2000, *Effect of Dissemination of 2,4-Dichlorophenoxyacetic Acid (2,4-D) Degradation Plasmids on 2,4-D Degradation and on Bacterial Community Structure in Two Different Soil Horizons*, Appl. Environ. Microbiol. ,Vol. 66, No. 8 , PP. 3297–304.

Dobson, R.S., and Burgess, J.E., 2007,*Biological Treatment of Precious Metal Refinery Wastewater*,*A Review,* Miner. Eng. Vol. 20,PP. 519-532.

Fournier, J.C., Codaccioni, P., Soulas, G.,1981, *Soil Adaptation to 2,4-D Degradation in Relation to the ApplicationRates and the Metabolic Behavior of the Degrading Microflora*, Chemosphere,Vol.10 (8) , PP. 77–84.

Garibay-Orijel, C., Rı´os-Leal, E., Garcı´a-Mena, J., and Poggi-Varaldo,  HM. ,2005,*2,4,6-Trichlorophenol and Phenol Removal in Methanogenic and Partially-Aerated Methanogenic Conditions in a Fluidized Bed Bioreacto*r, Chem. Technol. and Biotechnol., Vol. 80, No. 10, PP. 7-1180.

Kwangjick, L., Johnson V. J., Barry, R., and Blakley, B. R.,2001,*The Effect of Exposure to a Commercial 2,4-D Formulation During Gestation on the Immune Response in CD Mice*, Toxicology,Vol. 165, No. 1, PP. 39-49.

Li, Y. and Li, B.,2011,*Study on Fungi-Bacteria Consortium Bioremediation of Petroleum Contaminated Mangrove Sediments Amended with Mixed Biosurfactants*,Adv.Mat. Res., Vol. 183-185, PP. 1163-1167.

Macur, R.E., and Wheeler, J.T., 2007, *Impacts of 2,4-D Application on Soil Microbial Community Structure and on Populations Associated with 2,4-D Degradation*, Microbiol. Res.,Vol. 162 (1) , PP. 37-45.

Mohan,S. V., Prasanna, D., Purushotham, B., Reddy, P.N., and     Sarma, 2008, *Ex Situ Bioremediation of Pyrene Contaminated Soil in Bioslurry Phase Reactor Operated in periodic Discontinuous Batch Mode: Influence of Bioaugmentation*, International Biodeterioration  and Biodegradation, Vol. 62 , PP. 162-169.

Nikakhtari, H., Kumar, P., Nemati, M.,and Hill, G.A., 2009,  *Biodegradation of Diesel Oil in a Baffled Roller bioreactor*, J. Chem. Technol., Biotechnol. ,Vol . 84, PP. 525–532.

Plangklang ,P., and Reungsang A., 2010,*Bioaugmentation of Carbofuran by Burkholderia Cepacia PCL3 in a Bioslurry Phase Sequencing Batch Reactor*,Process Biochemistry ,Vol.45, PP.230–238.

US Environmental Protection Agency (EPA) Information on US Pesticide Usage, from 2007.

Silva, E., Fialho, AM., Sá-Correia, I., Burns, RG., and Shaw, L. J.,2004, *Combined Bioaugmentation and Biostimulation to Cleanup Soil Contamined with High Concentrations of Atrazine*, Environ. Sci. Technol., Vol. 15-38, No. 2, PP. 632-637.

Smith, S.C., Ainsworth, C.C., Traina, S., and Hicks, R.J., 1992,*The Effect of sorption on the biodegradation of Quinoline*, S. S. S.A., Vol. 56 , PP. 737-746.

Tabak, HH., Lens, P., Hullebusch, EDV., and Dejonghe, W., 2005,*Bioremediation of Soil and Sediments Polluted with Metals and Radionuclides. Microbiolal Processes and Mechanisms Affecting bioremediation of Metal Contamination and Influencing Meal Toxici*ty, Rev. Environ. Sci. Biotechnol., Vol. 4, PP. 115-156.

Tiryaki, O., and Temur, C., 2010, *TheFate of Pesticide in the Environment*, J. Biol. Environ. Sci., Vol. 4 (10) , PP. 29-38.

Yu, and Ruihong, 2006, *Bioremediation of Polycyclic Aromatic  Hydrocarbon (PAH) - Contaminated Soils in a Roller Baffled  Bioreactor*, M.Sc.Thesis, Univ. of Saskatchewan Schafer,coll. of Chemical Engineering.

Vidali, M., 2001,*Bioremediation,Overview*, Pure Appl. Chem.,  Vol. 73, No. 7, PP. 1163- 1172.

Villalobos, AR., Dunnick, CA., and Pritchard, JB.,1996, *Mechanism Mediating Basolateral Transport of 2,4-Dichlorophenoxyacetic Acid in Rat Kidney*,J. Pharmacol. Exp. Ther.,PP. 278:582–9.

Weber, Jr. and Kim, H.S., 2005, *Optimizing Contaminant Desorption and Bioavailability in Dense Slurry Systems. Rheology, Mechanical Mixing, and PAH Desorptio*n, Environ. Sci. Technol., Vol. 39 (7),PP.  2267– 2273.
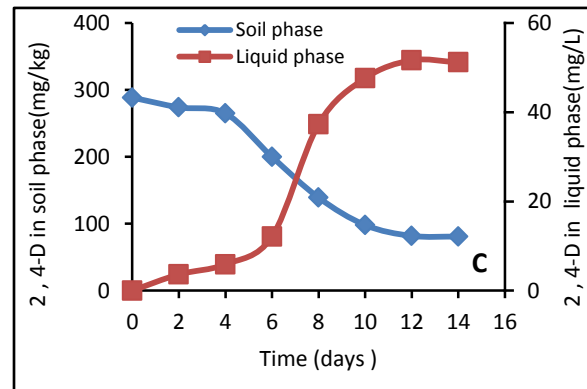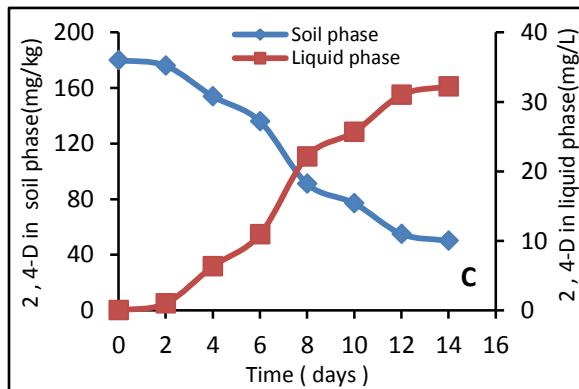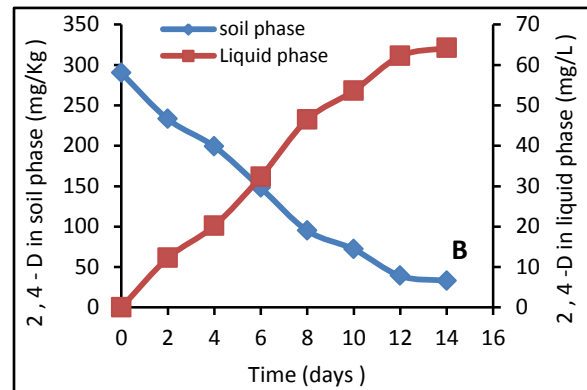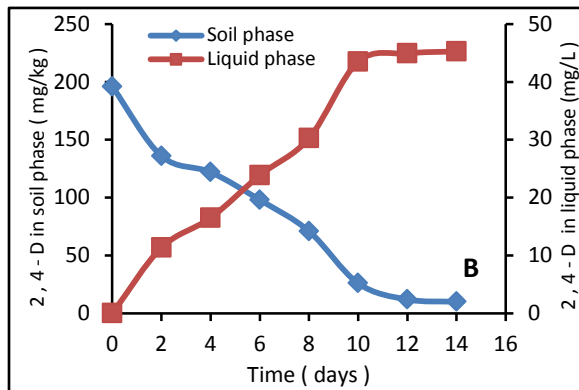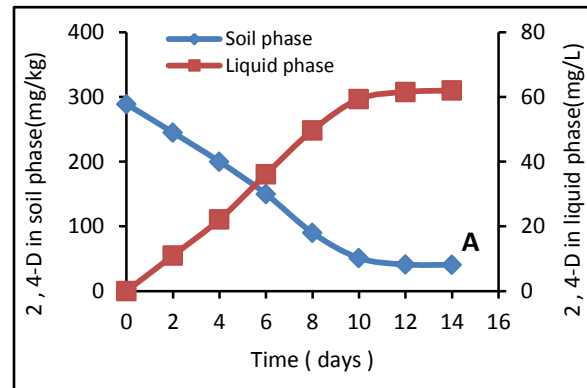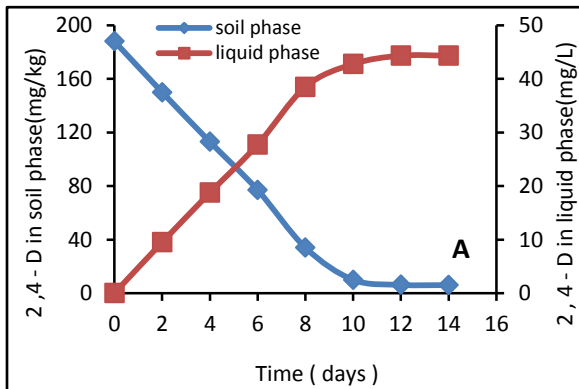
**Figure 1.** Partitioning between soil and liquid phase  in abiotic control reactor using three typesof soil (A) sand,(B) sandyloam, (C) clay. 2,4-Dconcentration  = 200mg/kg soil.

**Figure 2.** Partitioning between soil and liquid in abiotic control reactor using three typesof soil (A) sand,(B) sandyloam, (C) clay. 2,4-Dconcentration = 300mg/kg soil.
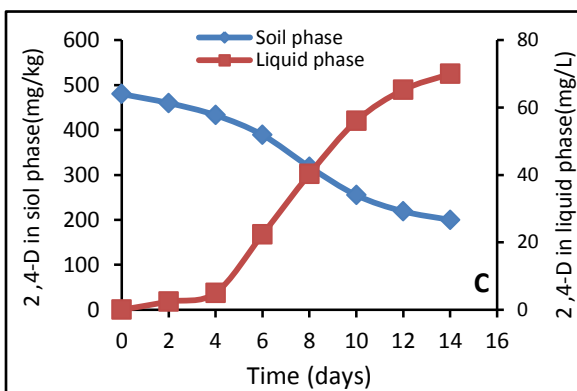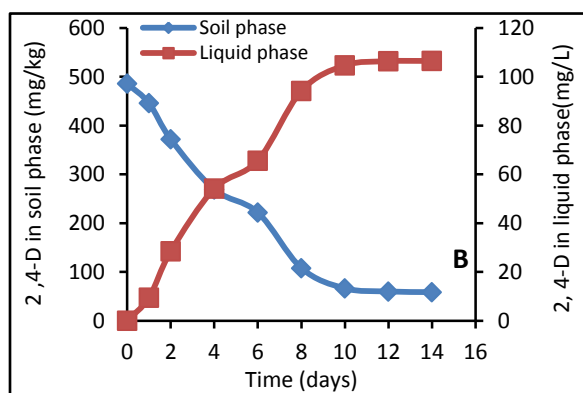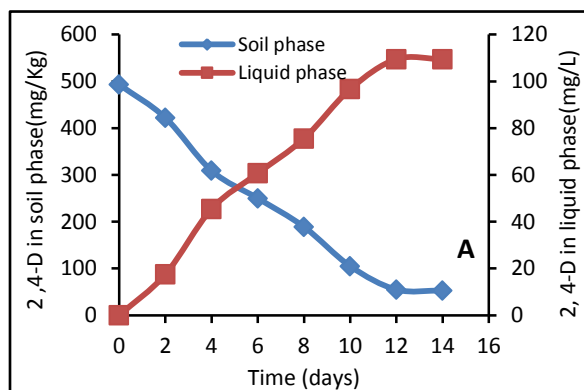
**Figure 3.** Partitioning between soil and liquid phase  in abiotic control reactor using three typesof soil (A)  sand,(B)sandyloam, (C) clay. 2,4-Dconcentration  = 500mg/kg soil.
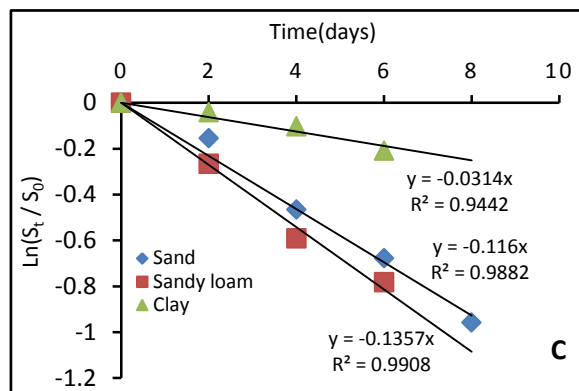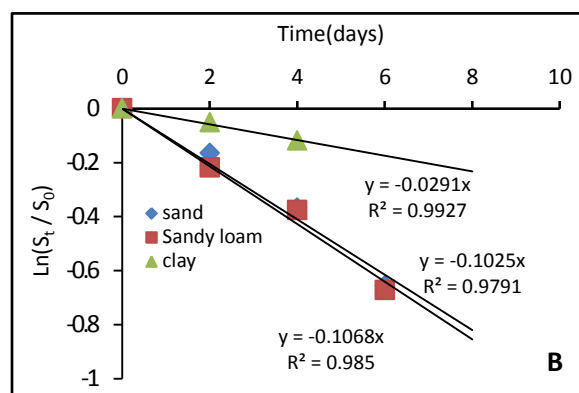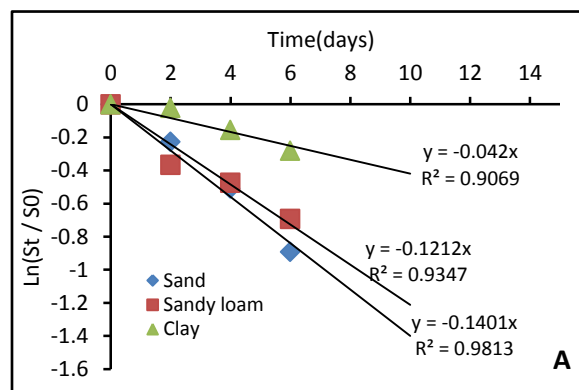
**Figure 4.** First order  rate constant  for 2,4-D in abiotic  control  reactor  at  different  initial concentrations,(A)200mg/kgsoil,(B)300mg/kg soil, (C)500mg/kg soil.
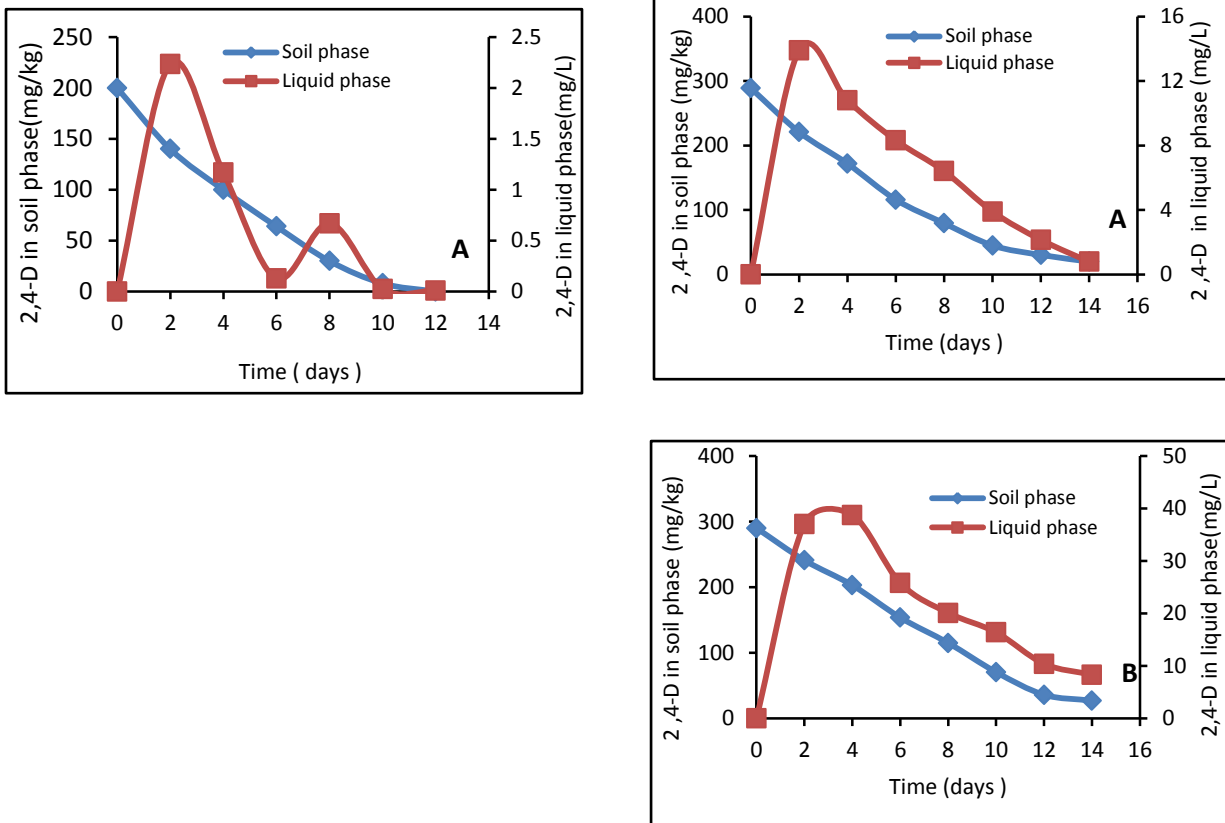
**Figure 5.** Partitioning between soil and liquid
 phase  in bioslurry reactor using three  types
of soil (A) sand,(B )sandyloam, (C) clay.
2,4-Dconcentration  = 200mg/kg soil.
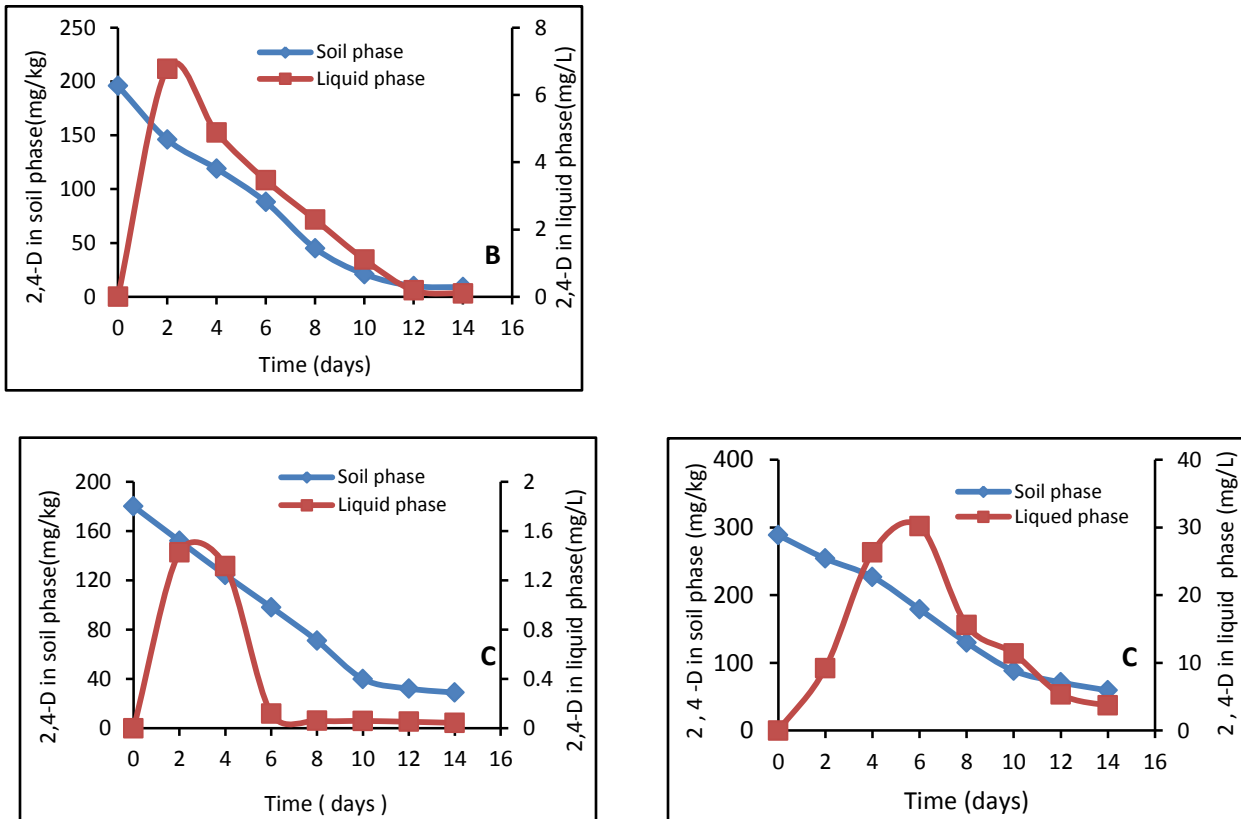
**Figure 6.** Partitioning between soil and liquid
phase in bioslurry reactor using three types
of soil (A) sand,(B)sandyloam, (C) clay.
2,4-Dconcentration = 300mg/kg soil.
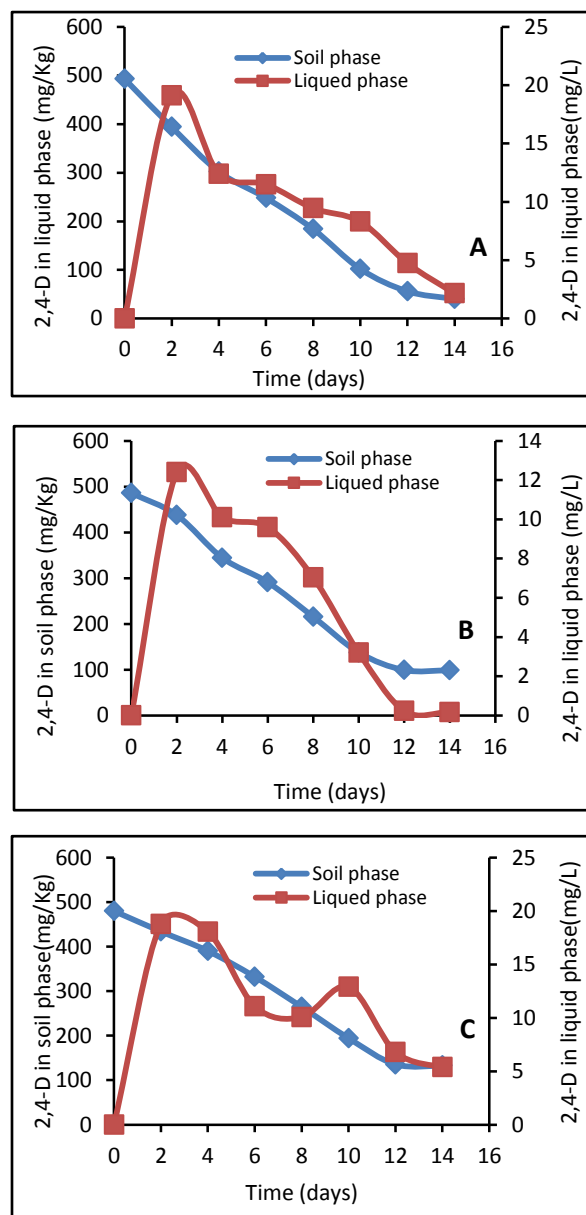
**Figure 7.** Partitioning between soil and liquid phase  in bioslurry reactor using three  types of soil, (A) sand,(B)sandyloam, (C) clay. 2,4-Dconcentration  = 500mg/kg soil.
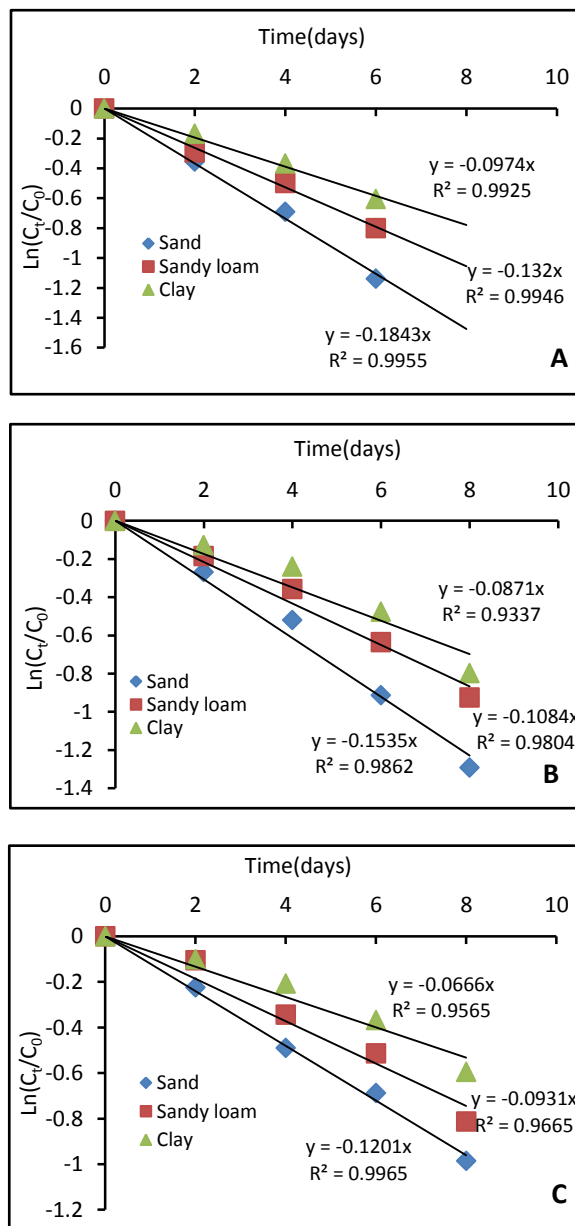


**Figure 8.** First order  rate constant for 2,4-D in  bioslurry  reactor     at  different  initial concentrations,(A)200mg/kgsoil,(B)300mg/ kg soil,(C)500mg/kg soil.

123
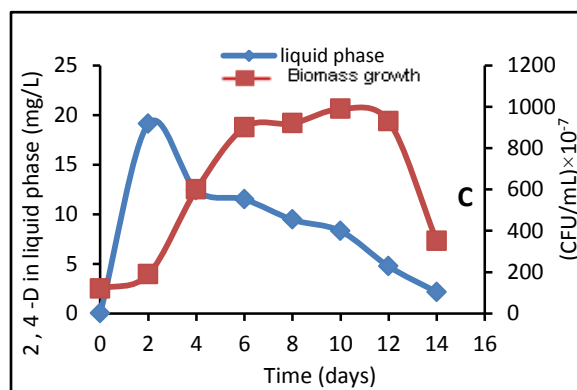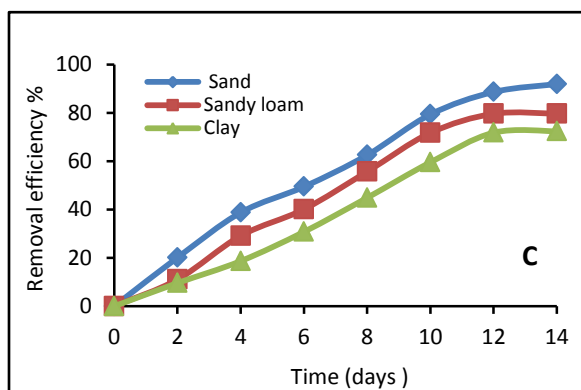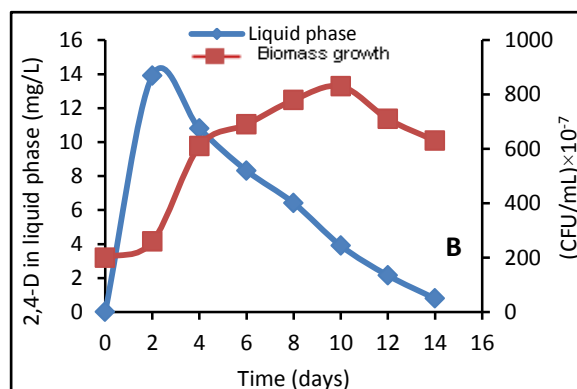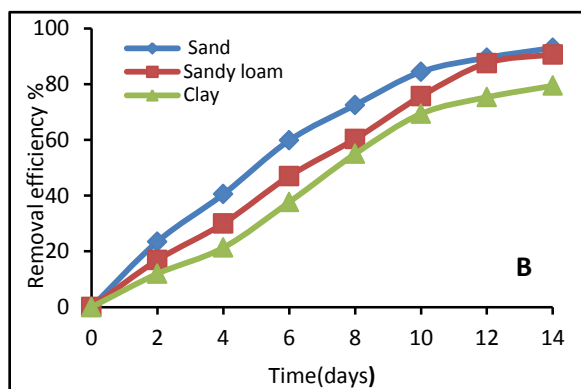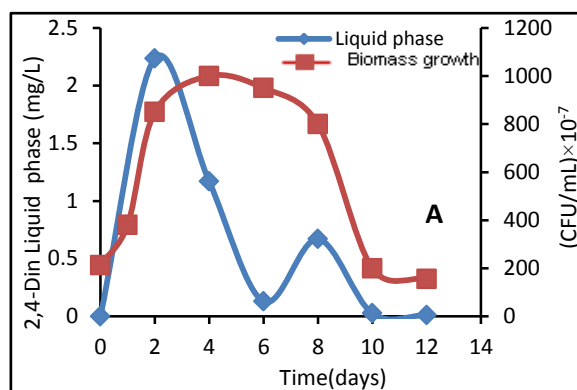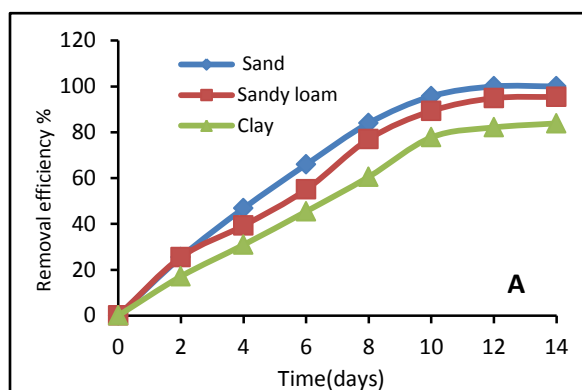
**Figure9.** Removal efficiency for bioslurry reactor using three types of soil at (A)200 mg 2,4-D/kg soil, (B) 300mg2,4-D/kg soil , (C) 500mg2,4-D/kg soil .

**Figure10.** Biomass growth and 2,4-D degradation in liquid phase, during bioslurry reactor operation for sandy soil. 2,4-D concentration (A) 200mg, (B) 300mg, (C) 500 mg/kg soil.
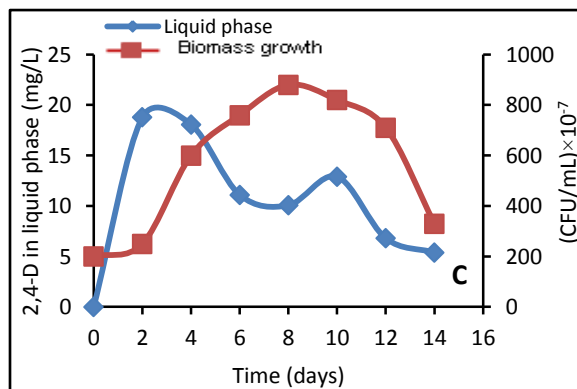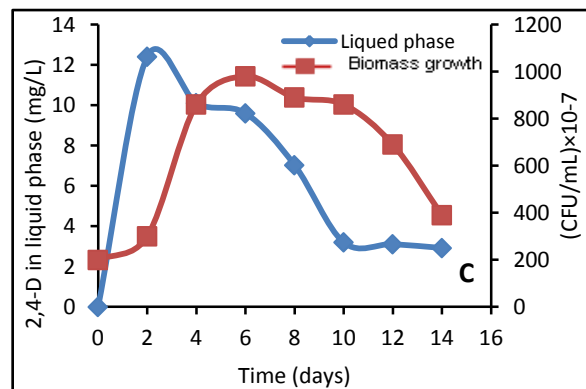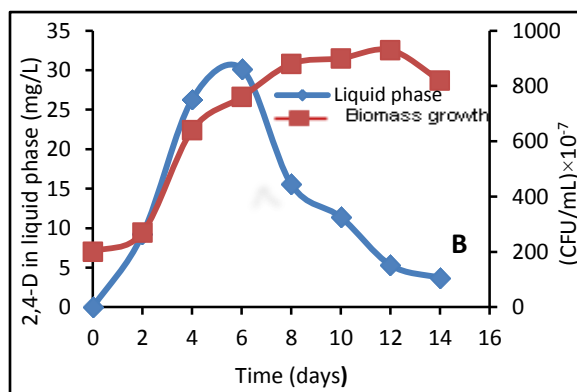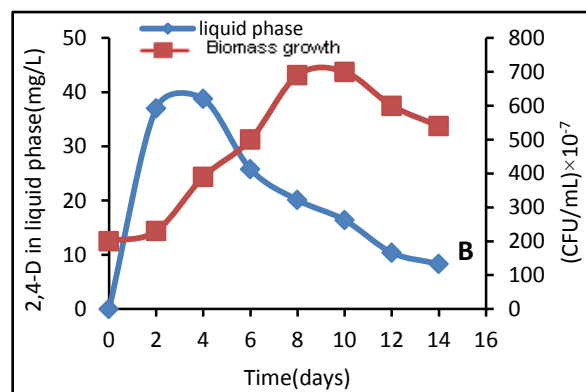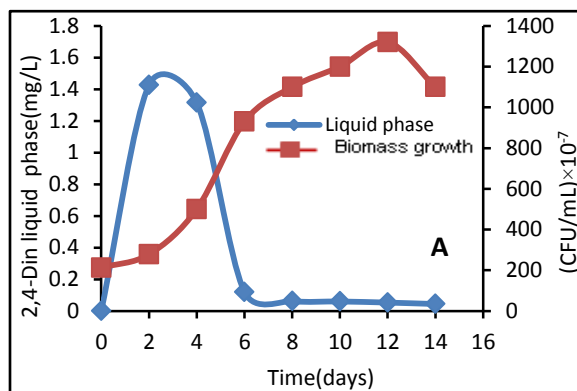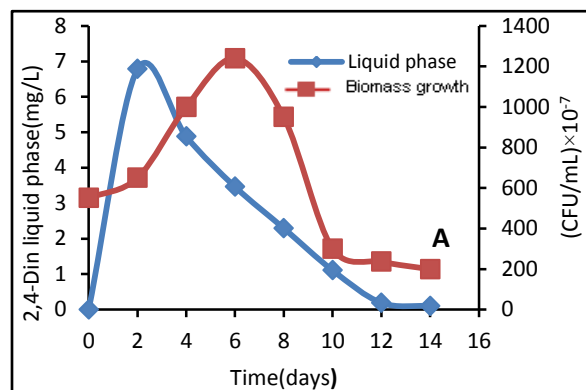
**Figure11.** Biomass growth and 2,4-D degradation in liquid phase, during bioslurry reactor operation for sandylaom soil. 2,4-D concentration (A) 200mg, (B) 300mg, (C) 500 mg/kg soil.

**Figure12.** Biomass growth and 2,4-D degradation in liquid phase, during bioslurry reactor operation for clay soil. 2,4-D concentration (A)200mg,(B) 300mg, (C) 500 mg/kg soil.
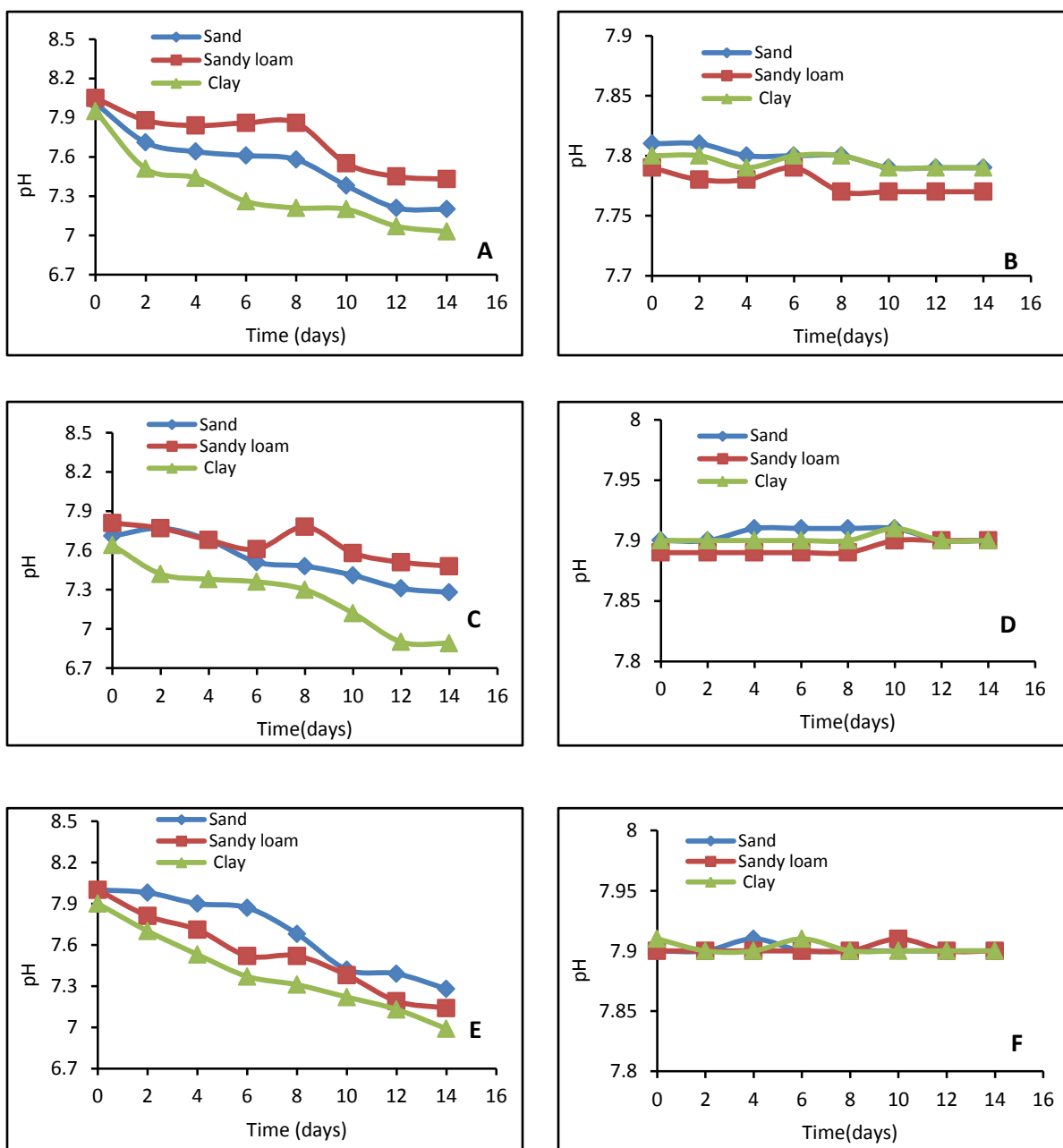
**Figure 13.** Variation of pH during biotic and abiotic reactor, (A)200, (C)300, (E) 500 mg 2,4-D/kg soil, for biotic reactor,(B)200, (D)300, (F)500 mg 2,4-D/kg soil for abiotic reactor.

**Table1.** Modified McKinney's medium in 1 liter of reverse osmosis water.

| Substance | Mass or Volume |
|---|---|
| $KH_2PO_4$ | 420 mg |
| $K_2HPO_4$ | 375 mg |
| $(NH_4)_2SO_4$ | 237 mg |
| NaCl | 30 mg |
| $CaCl_2$ | 30 mg |
| $MgSO_4$ | 30 mg |
| $Fe(NH_4)_2SO_4$ | 10 mg |
| Trace element | 1mL |

**Table 2.** Trace elements composition in l liter of reverse osmosis water.

| Substance | Mass(mg) |
|---|---|
| $H_3BO_3$ | 300 |
| $CoCl_3$ | 200 |
| $ZnSO_4.7H_2O$ | 100 |
| $MnCl_2$ | 30 |
| $Na_2MoO_4$ | 30 |
| $NiCl_2$ | 20 |
| $CuCl_2$ | 10 |

**Table 3.** Characteristics of the three soils.

| Soil type | Soil texture | | Soil pH | OMC % | CEC (meq/100mg) |
|---|---|---|---|---|---|
| Sand | Sand | 98.93% | 8.75 | 0.027 | 0.071 |
| | Silt | 1.07% | | | |
| | Clay | ----- | | | |
| Sandy loam | Sand | 88.03% | 8.61 | 0.28 | 1.42 |
| | Silt | 11.97% | | | |
| | Clay | ----- | | | |
| Clay | Sand | 2.3% | 8.05 | 1.967 | 68.34 |
| | Silt | ------ | | | |
| | Clay | 97.7% | | | |

OMC: Organic matter content

CEC: Cation exchange capacity

**Table 4.** Release efficiency and rate of release of 2,4-D from the three soils withdifferent concentration.

| Initial 2, 4-D conc. (mg/kg) | Sand | | | | Sandy loam | | | | Clay | | | |
|---|---|---|---|---|---|---|---|---|---|---|---|---|
| | $k_0$ (day$^{-1}$) | $R^2$ | Residue (mg/kg) | Release (%) | $k_0$ (day$^{-1}$) | $R^2$ | Residue (mg/kg) | Release (%) | $k_0$ (day$^{-1}$) | $R^2$ | Residue (mg/kg) | Release (%) |
| 200 | 0.140 | 0.98 | 6 | 97 | 0.121 | 0.93 | 10 | 95 | 0.042 | 0.91 | 50 | 72 |
| 300 | 0.102 | 0.98 | 40.5 | 86 | 0.106 | 0.99 | 33 | 89 | 0.029 | 0.99 | 80.8 | 72 |
| 500 | 0.116 | 0.99 | 53 | 89 | 0.135 | 0.99 | 58.7 | 88 | 0.031 | 0.94 | 200 | 58 |

**Table5.** Removal efficiency of 2,4-D and rate of degradation in theshake flask bioreactor.

| Experiment Time (days) | Initial 2, 4-D conc. (mg/kg) | Sand | | | Sandy loam | | | Clay | | |
|---|---|---|---|---|---|---|---|---|---|---|
| | | $k_1$ (day$^{-1}$) | $R^2$ | Removal efficiency % | $k_1$ (day$^{-1}$) | $R^2$ | Removal efficiency % | $k_1$ (day$^{-1}$) | $R^2$ | Removal efficiency % |
| 12 | 200 | 0.184 | 0.996 | 100 | 0.132 | 0.995 | 95 | 0.097 | 0.993 | 82 |
| 14 | 300 | 0.153 | 0.986 | 93 | 0.108 | 0.9804 | 91 | 0.087 | 0.934 | 80 |
| 14 | 500 | 0.120 | 0.997 | 92 | 0.0931 | 0.967 | 80 | 0.067 | 0.957 | 72 |

# Two-Phase Partitioning Bioreactor for the Treatment of Crude Oil-Contaminated Aqueous Solution

**Zainab Ziad Ismail**
Assistant professor
College of Engineering-University of Baghdad
Email: zismail@gmail.com

**Ibtihaj Abdlwahab Abdulrazzak**
Senior Engineer
Ministry of Environment
Email: ibt_mam@yahoo.com

## ABSTRACT

A new application of a combined solvent extraction and two-phase biodegradation processes using two-liquid phase partitioning bioreactor (TLPPB) technique was proposed and developed to enhance the cleanup of high concentration of crude oil from aqueous phase using acclimated mixed culture in an anaerobic environment. Silicone oil was used as the organic extractive phase for being a water-immiscible, biocompatible and non-biodegradable. Acclimation, cell growth of mixed cultures, and biodegradation of crude oil in aqueous samples were experimentally studied at $30\pm2$ºC. Anaerobic biodegradation of crude oil was examined at four different initial concentrations of crude oil including 500, 1000, 2000, and 5000 mg/L. Complete removal of crude oil was achieved biphasic bioreactor after 3 weeks compared to 73-82% in the monophasic bioreactor for the same time period.

**Keywords:** bioreactor, crude oil, biodegradation, biphasic reactor, anaerobic biotreatment

## المفاعل البيولوجي ثنائي الطور لمعالجة المياه الملوثة بالنفط الخام

ابتهاج عبد الوهاب عبد الرزاق                    زينب زياد اسماعيل
مهندس أقدم                                      استاذ مساعد
وزارة البيئة                                    كلية الهندسة-جامعة بغداد

## الخلاصة

تم في هذه الدراسة ولأول مرة معالجة المياه الملوثة بالنفط الخام باستخدام تقنية جديدة تتضمن عمليتين مشتركة في آن واحد وهي الاستخلاص باستخدام مذيب عضوي والتحلل الاحيائي بوجود المعالجة البيولوجية باستخدام المفاعل البيولوجي ثنائي الطور (TLPPB). يتكون هذا المفاعل (TLPPB) من طورين سائلين احدهما مائي والاخر عضوي (Silicon oil) لمعالجة التراكيز العالية من النفط الخام. ان اختيار استخدام زيت السليكون كمذيب عضوي في (TLPPB) تم على اساس كونه غير قابل للامتزاج بالمياه، لا يؤثر على فعالية ونشاط الاحياء المجهرية , وغير قابل للتحلل. تم اجراء عملية تأقلم وتنمية للخلايا البكتيرية ليتم بواسطتها التحلل الاحيائي للنفط الخام في درجة حرارة 30 ± 2º درجة مئوية. تمت مقارنة التحلل اللاهوائي للنفط الخام في مفاعل ثنائي الطور مع مفاعل البيولوجي احادي الطور لتراكيز مختلفة من النفط الخام تتضمن 500، 1000، 2000، و 5000 ملغم / لتر ، وقد تم تحقيق ازالة تامة للنفط الخام في وسط الماء ـ ثنائي الطور في خلال 3 أسابيع, مقارنة مع نسبة ازالة 73-82% في المفاعل أحادي الطور.

**الكلمات الدالة:** المفاعل الاحيائي، النفط الخام، التحلل الاحيائي، مفاعل ثنائي الطور ، المعالجة الاحيائية اللاهوائية

# 1. INTRODUCTION

Two-phase partitioning bioreactors (TPPB) concept is based on the use of a water immiscible and biocompatible organic solvent that is allowed to float on the surface of a cell-containing aqueous phase. The solvent is used to dissolve large concentrations of pollutants (as substrates) which are readily achievable because most organic contaminants are very hydrophobic, and then partition into the aqueous phase at low levels, **Hernandez et al., 2011**. However, although very high amounts of toxic organic substrates can be added to a bioreactor, the cells experience only very low (sub-inhibitory) concentrations. Moreover, as the cells consume some of the substrate, disequilibrium is created, which causes more of the hydrophobic contaminants to be partitioned into the aqueous phase as the system tries to maintain thermodynamic equilibrium. Thus, not only do appropriate amounts of contaminants get delivered to the cells but also substrate delivery is ongoing until the organic phase becomes completely depleted and the rate is determined by the metabolic activity of the microorganisms, **Yeom,** and **Daugulis, 2001**.The system is well suited for biodegradation of hazardous pollutants, **Janusz** and **Malinowski, 2001**. The two-phase partitioning bioreactor concept appears to have a great potential in enhancing the productivity of many bioprocesses. The proper selection of an organic solvent is the key to successful application of this approach in industrial practice. The integration of fermentation and a primary product separation step has a positive impact on the productivity of many fermentation processes. The controlled substrate delivery from the organic to the aqueous phase opens a new area of application of this strategy to biodegradation of pollutants, **Janusz** and **Malinowski, 2001.** Several studies have been reported concerning the application of TPPB technique for the degradation of toxic organics including phenanthrene and pyrene in the presence of silicon oil as the second phase. Complete phenanthrene biodegradation was achieved within 3 days. Its concentration in the monophasic reactors dropped by 93% within 4 days, but the removal rate remains at that rate till the end of the experiment. Pyrene removal occurred to a limited extent only in the presence of phenanthrene, **Guieysse et al., 2001. Janikowski et al., 2002** used a two-phase partitioning bioreactor (TPPB) utilizing the bacterium *Sphingomonas aromaticivorans* B0695 to degrade 4 low molecular weight polycyclic aromatic hydrocarbons (PAHs). The TPPB achieved complete biodegradation of naphthalene, phenanthrene, acenaphthene and anthracene at a volumetric consumption rate of 90mg/L.h in approximately 30 h. **Tomei et al., 2007**, investigated the performance of two phase liquid-solid systems applied to the removal of 4-nitrophenol, Hytrel 8206 copolymer was utilized in batch kinetic test, this polymer was also employed as the partitioning phase in a lab scale sequencing batch reactor. The completely removal reached after 26 h. **Zilouei et al., 2008**, developed an organic-aqueous two-liquid-phase partitioning system to degrade high concentrations of pentachlorophenol. At the initial biomass concentrations of 7, 25, and 58 mg/l, the volumetric removal rates of PCP obtained were 25.7±0.5, 32.1±0.1, and 39.3 ± 2.9 mg /l.h, respectively. **Zhao et al., 2009**, determined the potential of a two-phase partitioning bioreactor (TPPB) for enhancing the treatment of phenol at high initial concentrations, The maximum volumetric consumption rate of phenol decreased in the order: immobilized microorganisms with organic modified montmorillonite OMMT-PSF capsules in a TPPB (342.4 mg/l.h) > immobilized microorganisms without OMMT-PSF capsules (300 mg/l.h) > free microorganisms with OMMT-PSF capsules in a TPPB (208.4 mg/l.h) > free microorganisms without OMMT-PSF capsules (125.8 mg/l.h). Tomei et al. (2011) compared the performance of a TPPB, relative to single phase operation, in which a small volume (5%, v/v) of the beads polymer Hytrel 8206 was used to treat aqueous mixtures of 2,4-dimethylphenol and 4-nitrophenol, Hytrel 8206 was selected from a range of polymers that were tested for their partition coefficient for the target molecules, with the more hydrophobic compound (2,4-dimethylphenol) having a higher

partition coefficient value of 201 compared to 4-nitrophenol partition coefficient of 143. **Ramos et al., 2012**, proposed a two phase partitioning bioreactor to carry out the degradation of the poorly soluble compound anthracene by laccase from *Trametes versicolor*. The organic phase consisted of silicone oil saturated with anthracene. The surfactant, Triton X-100 was added to the aqueous phase at concentration above the critical micelle concentration to enhance anthracene solubility. **Munoz et al., 2013**, investigated an innovative operation mode in a two liquid phase bioreactor (TLPB) for the treatment of volatile organic compounds (VOC), a removal efficiency of 80% was recorded for 26 days. None of the previously mentioned studies concerned of the crude oil biodegradation in a Two-Phase Partitioning Bioreactor (TPPB). Exploring and investigating new environmentally friendly approaches for oil removal from aquatic environment became mandatory due to the wide occurrence of accidental oil spills on local, regional, and global scales. Based on this fact, this study was devoted to evaluate the performance and efficiency of TPPB for crude oil biodegradation.

This study aimed to evaluate the performance of a bench-scale two-phase partitioning bioreactor (TPPB) for the degradation of crude oil in aqueous phase compared to the performance of conventional monophasic bioreactor.

## 2. MATERIALS AND METHODS
### 2.1 Microorganisms, nutrient, and MSM
A mixed culture was freshly collected from the aeration tanks in Al-Rustamia Sewage Treatment Plant, Baghdad. The stock culture was stored at $4^{o}C$. The nutrient media (NM) contained 15000 mg/L meat papain peptone, and 15000 mg/L Tryptone. The composition of mineral salt media (MSM) in (mg/L) were, $(NH_4)_2SO_4$ (100), $KH_2PO_4$ (350), $K_2HPO_4$ (775), $MgSO_4$ .$7H_2O$ (100), $CaCl_2$ (40), $FeSO_4.7H_2O$ (1), $MnSO_4.H_2O$ (1), $NaMoO_4$ (0.21), and Sodium Chloride (5000). The MSM was prepared at pH 6.8, which was accurately controlled by daily measurement. Sulfuric acid (0.1M) and potassium hydroxide (0.1M) were used for pH adjustment. The prepared MSM was sterilized in an autoclave at $121^{o}C$ for 30 min, **Ted** and **Christine, 2010.**

### 2.2 Crude oil samples
Crude oil samples were obtained from midland refineries company /Al-Dora Refinery. The properties of the crude oil are given in **Table 1**.

### 2.3 Organic solvent
The organic phase used in this study was silicone oil (polydimethylsiloxane) of purity 100%, purchased from Gainland Chemical Company (GCC).

### 2.4 Analysis
The chemical oxygen demand (COD) concentrations in aqueous samples were measured using the COD analyzer Type: Lovibond, RD 125. Oil content analysis was carried out using the oil content analyzer Type: HORIBA OCMA-350, based on infrared analysis. It includes a single-beam, fixed wavelength, non-dispersive infrared filter-based spectrophotometer. Infrared radiation from a tungsten lamp is transmitted through a cylindrical, quartz cuvette containing a sample extract. The radiation which passed through the extract enters a detector containing a filter that isolates analytical wavelengths.

## 2.5 Biomass measurements

Engineers have traditionally used volatile suspended solids (VSS) as an indication of biomass concentration. The VSS parameter has the advantage of fitting directly into mass balance equations, **(Degenaar et al., 2000).** Volatile suspended solids were determined according to the procedure reported in the Standard Methods **(APHA, 1998).** Additional approach known as (Standard Plate Count) was used in this study to quantitatively measure the bacteria growth **(Ted & Christine, 2010)**. The major part of the procedure deals with a series of successive dilutions of the original culture in sterilized bottles using sterilized water. Thereafter, the diluted culture is poured into Petri dishes along with the nutrient agar, and then number of colonies is counted after incubation. The production of biogas was considered in this study as an additional approach to examine the growth and activity of microorganisms.

## 2.6 Enrichment of microorganisms

The freshly collected activated sludge samples were centrifuged at 3000 rpm for 10 min to separate the biomass from liquid phase. Thereafter, the culture suspension was reactivated and enriched at $30\pm2^{o}C$ in 250 ml mineral salt media (MSM), into which 20 mg/L of crude oil was added to 10 mL of mixed culture suspension in a 500 mL - Erlenmeyer flask to be adapted for 24h. Prior to starting the adaptation process, the flasks were flushed with nitrogen to achieve anaerobic environment, and then agitated by an orbital shaker at 100 rpm to enrich the culture seeds.

## 2.7 Sequential cultivation process

The growing cells were collected after centrifugation of the enriched suspension at 3000 rpm for 10 min. The collected activated cells were re-suspended and re-inoculated into fresh culture media in 500-ml Erlenmeyer flasks with the addition of 80 mg/L crude oil. After inoculation, the flasks were flushed with $N_2$, capped and placed in an orbital shaker controlled at 100 rpm and $30\pm2^{o}C$. This cultivation cycle were sequentially repeated for 20 cycles with increased initial concentrations of crude oil up to 5000 mg/L. For each cultivation cycle, the initial and final concentration of cell, were determined.

## 2.8 Two-Phase Partitioning Bioreactors

Eight bench scale two phase portioning bioreactors (TPPB) were prepared and setup with four different initial concentrations of crude oil including 500, 1000, 2000, and 5000 mg/L using alternatively mineral salt media (MSM) and distilled water (DW). Silicon oil was used as the organic liquid phase. In order to examine the efficiency of TPPB towards the conventional bioreactor, additional eight bioreactors were identically set up without using the silicon oil as the mono-phasic bio reactors. Also, a set of four reactors were set up to examine the effect of abiotic processes including sorption, volatilization, and chemical degradation. Accordingly, a total of 16 bench reactors were prepared as given in **Table 2** which summarizes the experimental set up and data related to the amounts and types of the reactors contents, respectively. All experiments were conducted in duplicate in 250-mL Erlenmeyer flasks. The flasks were closed with butyl septa, tightly sealed with parafilm and incubated on a rotary shaker at 120 rpm and $30 \pm 2$ºC. All flasks were flushed with nitrogen to maintain anaerobic environment.

## 3. RESULTS AND DISCUSSION

### 3.1 Enrichment and acclimation of cultures

As mentioned in section 2.5, results of the acclimation process are presented by 3 different approaches as follows:

1- Characterization of the dominant cultures

Results of this method indicated the presence of several types of microorganisms, in particular *E.Coli, Pseudomonas seroginosa*, and *Bacillus subtilis* which represent the dominant and the most widely available types of organisms in activated sludge composition. However, **Table 3** illustrates the dominant types of species and their numbers before and after the acclimation process.

2- Visual characterization of biomass granules

Results of SEM technique are given in **Fig. 1a &b** before and at the end of the acclimation period, respectively. The bacterial colonization and dense growth at the end of acclimation process are well characterized as shown in **Fig. 1b** indicating the dense growth of microorganisms.

3- Measurements of produced biogas

As a result of the anaerobic biodegradation process, the biogas mainly represented by $CH_4$ was released as the end product of this anaerobic bioprocess. Accordingly, the released amounts of $CH_4$ could be another potential approach for indicating the startup progress and the end of anaerobic biodegradation process of crude oil during the acclimation period. **Fig. 2** presents the amounts of released biogas during the acclimation process using 20, 80, 280, 400, and 500 mg/L crude oil. **Fig. 3** illustrates the bioreactors before and after acclimation period.

### 3.2 Significance of TPPB application

The sets of experiments were alternatively conducted with distilled water (DW) and mineral salt media (MSM) to examine the effectiveness of each system for the anaerobic biodegradation of crude oil, also to investigate the potential of biphasic bioreactors compared to monophasic bioreactors. Results revealed that higher removal efficiency was achieved up to 100% in the DW-biphasic bioreactor after less than 3 weeks. However, lower efficiencies of crude oil removal were observed in the MSM-monophasic, MSM-biphasic, and DW-monophasic bioreactors indicating the effectiveness of the DW-biphasic bioreactor system compared to the other reactors. Table 4, illustrates the removal efficiencies (ranging from 73% to 100%) of the four bio-systems at different initial concentrations of crude oil. **Figs. 4 to 7** illustrate the profiles of crude oil removals with time in the bioreactors. However, results revealed complete removal of crude oil in the DW-biphasic bioreactors at different initial concentration of crude oil**.** The effect of silicone oil existence as the immiscible organic phase in the bioreactor was well observed in controlling the dispersion and transfer of crude oil into the aqueous phase to feed the biomass. Silicone oil exhibited as a sponge adsorbed the high initial concentration of crude oil, and then gradually desorbs batch doses of oil as a substrate for the starving microorganisms to prevent the substrate shock loading which may cause consortiums toxicity and death.

However, the relatively lower efficiency of MSM-biphasic bioreactor compared to the DW-biphasic bioreactor could be attributed to the availability of regular substrate (MSM) to the microorganisms making them less longing for unconventional type of substrates (crude oil).

## 4. CONCLUSION

The main conclusions that can be drawn from this research are represented by a successful bacterial acclimation process which was accomplished to tolerate the high concentrations of crude oil as the sole toxic organic pollutant in the aqueous solution samples. Also, results

demonstrated that the removal efficiency of crude oil at 500, 1000, 2000, and 5000 mg/L initial concentrations in DW-biphasic bioreactor was 100% after 3 weeks, compared to 73-86% in the MSM-monophasic, MSM-biphasic, and DW-monophasic bioreactors for the same time period.

## REFERENCES

- APHA, *Standard methods for examination of water and wastewater*, 20th ed. American Public Health Association, Washington, DC, 1998.

- Degenaar A.P., Mudaly D.D., Manganyi A., and Bux F., 2000, *An Evaluation of Volatile Suspended Solids as a True Measure of Metabolic Activity in Activated Sludge*, Centre for Water and Wastewater Research, Technikon Natal, South Africa.

- Guieysse, B., Cirne, M., and Mattiasson, B., 2001, *Microbial Degradation of Phenanthrene and Pyrene in a Two-Liquid Phase-Partitioning Bioreactor*, Journal of Application Microbiology Biotechnology, Vol. 56, PP. 796-802.

- Hernandez, M., Quijano, G., Thalasso, F., Daugulis, A.J., Villaverde, S., and Munoz, R., 2011, *A Comparative Study of Solid and Liquid Nonaqueous Phases for the Biodegradation of Hexane in Two Phase Partitioning Bioreactors,* Biotechnology Bioengineering, Vol. 106, PP. 731-740.

- Janikowski, T.B, Velicogna, D., Punt, M., and Daugulis, A.J., 2002, *Use of a Two-Phase Partitioning Bioreactor for Degrading Polycyclic Aromatic Hydrocarbons by a Sphingomonas Species*, Application of Microbial Biotechnology, Vol. 59, PP. 368–376.

- Janusz, J. and Malinowski, A., 2001, *Two-Phase Partitioning Bioreactors in Fermentation Technology*, Biotechnology Advanced, Vol. 19, PP. 525-538.

- Munoz, R., Eleonora, I.H., Ganb, H., Hernandeza, M., and Quijanoa, G., 2013, *Hexane Biodegradation in Two Liquid Phase Bioreactors: High Performance Operation Based on the Use of Hydrophobic Biomass*, Biochemical Engineering Journal, Vol. 70, PP. 9-16.

- Ramos, A.A., Eibes, G., Moreira, M.T., Feijoo, G., and Lema, J.M., 2012, *Mass Transfer Enhancement by the Addition of Surfactant in a Two Phase Partitioning Bioreactor for the Degradation of Anthracene by Laccase*. Jornal of Chemical Engineering Transactions, Vol. 27, PP. 187-192.

- Ted, R. J., and Christine, L., 2010, *Dilution Cultivation of Bacteria*, Laboratory Experiments in Microbiology, ninth edition, Benjamin Cummings in the U.S.

- Tomei, C.M, Cristina, A.M., Vincenzo, P., Sara, R., and Daugulis, A.J., 2007, *Solid-Liquid Two Phase Partitioning Bioreactors as a Tool for Xenobiotic Biodegradation,* Environmental Pollution, Vol. 16, PP. 355-374.

- Tomei,C.M, Sara, R., Domenica, M.A., Cristina, A.M., and Daugulis, A.J., 2011, *Treatment of Substituted Phenol Mixtures in Single Phase and Two-Phase Solid–Liquid Partitioning Bioreactors,* Journal of Hazardous Materials, Vol. 191, PP. 190–195.

- Yeom, S.H. and Daugulis, A.J., 2001, *Development of a Novel Bioreactor System for the Treatment of Gaseous Benzene*, Biotechnology and Bioengineering. Vol. 72, PP. 156–165.

- Zhao, G., Zhou, L., Liu, X., and Ren, X., 2009, *Enhancement of Phenol Degradation Using Immobilized Microorganisms and Organic Modified Montmorillonite in a Two-Phase Partitioning Bioreactor*, Journal of Hazardous Materials, Vol. 169, PP. 402–410.

- Zilouei, H., Guieysse, B., and Mattiasson, B., 2008, *Two-Phase Partitioning Bioreactor for the Biodegradation of High Concentrations of Pentachlorophenol Using Sphingobium Chlorophenolicum DSM 8671*. Chemosphere, 27, PP. 1788-1794.

**NOMENCLATURE**
COD = chemical oxygen demand, mg/L.
DW = distilled water.
MSM = mineral salt media.
NM = nutrient media.
OMMT = organic modified montmorillonite.
TLPPB = two-liquid phase partitioning bioreactor.
TPPB = two-phase partitioning bioreactor.
VOC = volatile organic compounds.
VSS = volatile suspended solids.

**Table 1** Properties of the crude oil.

| Constituent | Value | Unit |
|---|---|---|
| Density | 0.8745 | gm/ml |
| Viscosity | 55.0 | cp |
| API gravity | 30.3 | - |
| Pour point | -30 | $^oC$ |
| Water content | Nil | %wt |
| Salt content | 10 | Ptb[*] |
| Sulphur | 3.1 | %wt |
| Wax | 1.2 | %wt |
| Asphaltene | 2.6 | %wt |

* Pounds per thousand barrel

135

**Table 2** Types and classification of the bench scale bioreactor.

| Reactor | Contents | | | | | Liquid phases |
|---|---|---|---|---|---|---|
| | MSM (mL) | DI (mL) | Crude oil conc. (mg/L) | Culture (mL) | Silicone oil (mL) | |
| **Anaerobic biodegradation processes** | | | | | | |
| BR1 | 450 | - | 500 | 15 | - | Single |
| BR2 | 300 | - | 500 | 10 | 150 | Two |
| BR3 | - | 450 | 500 | 15 | - | Single |
| BR4 | - | 300 | 500 | 10 | 150 | Two |
| BR5 | 450 | - | 1000 | 15 | - | Single |
| BR6 | 300 | - | 1000 | 10 | 150 | Two |
| BR7 | - | 450 | 1000 | 15 | - | Single |
| BR8 | - | 300 | 1000 | 10 | 150 | Two |
| BR9 | 450 | - | 2000 | 15 | - | Single |
| BR10 | 300 | - | 2000 | 10 | 150 | Two |
| BR11 | - | 450 | 2000 | 15 | - | Single |
| BR12 | - | 300 | 2000 | 10 | 150 | Two |
| BR13 | 450 | - | 5000 | 15 | - | Single |
| BR14 | 300 | - | 5000 | 10 | 150 | Two |
| BR15 | - | 450 | 5000 | 15 | - | Single |
| BR16 | - | 300 | 5000 | 10 | 150 | Two |
| **Control reactors for examination of abiotic processes effects** | | | | | | |
| R1 | - | 450 | 1000 | - | - | Single |
| R2 | - | 300 | 1000 | - | 150 | Two |
| R3 | - | 450 | 5000 | - | - | Single |
| R4 | - | 300 | 5000 | - | 150 | Two |

**\*MSM, mineral salt media**
 **\*\*DW, distilled water**

**Table 3** Types of organisms in the mixed culture samples

| Microorganisms | Aeromonas hydrophilla (colonies/mL) | |
|---|---|---|
| | before acclimation | after acclimation |
| Pseudomonas aeroginosa | $2.0 \times 10^3$ | Heavy growth |
| Fecal Coliform | $1.6 \times 10^3$ | $3.7 \times 10^5$ |
| E.Coli | $6.5 \times 10^7$ | Heavy growth |
| Bacillus  subtilis | $8.5 \times 10^4$ | $6.2 \times 10^7$ |
| Total Coliform | $1.2 \times 10^3$ | $3.0 \times 10^6$ |
| T.P.C. | $9.8 \times 10^7$ | Heavy growth |

| Table 4 The removal efficiencies of the tested systems..**Types of reactor** | **Average initial concentration mg/L** | **Removal efficiency % after 3 weeks** |
|---|---|---|
| | **Crude oil** | **Crude oil** |
| MSM-monophasic | 511 | 79% |
| MSM-biphasic | 517 | 86% |
| DW-monophasic | 520 | 82% |
| DW-biphasic | 521 | 100% |
| MSM-monophasic | 1017 | 78% |
| MSM-biphasic | 1093 | 85% |
| DW-monophasic | 1100 | 81% |
| DW-biphasic | 1112 | 100% |
| MSM-monophasic | 2080 | 76% |
| MSM-biphasic | 2093 | 84% |
| DW-monophasic | 2112 | 80% |
| DW-biphasic | 2120 | 100% |
| MSM-monophasic | 5088 | 73% |
| MSM-biphasic | 5100 | 80% |
| DW-monophasic | 5090 | 80% |
| DW-biphasic | 5120 | 100% |



SEM MAG: 1.01 kx    SEM HV: 16.00 kV    |||||||||    VEGA\\ TESCAN
Name: 1              WD: 10.88 mm        50 µm
Date(m/d/y): 04/07/13                    Performance in nanospace

**(a)**

137
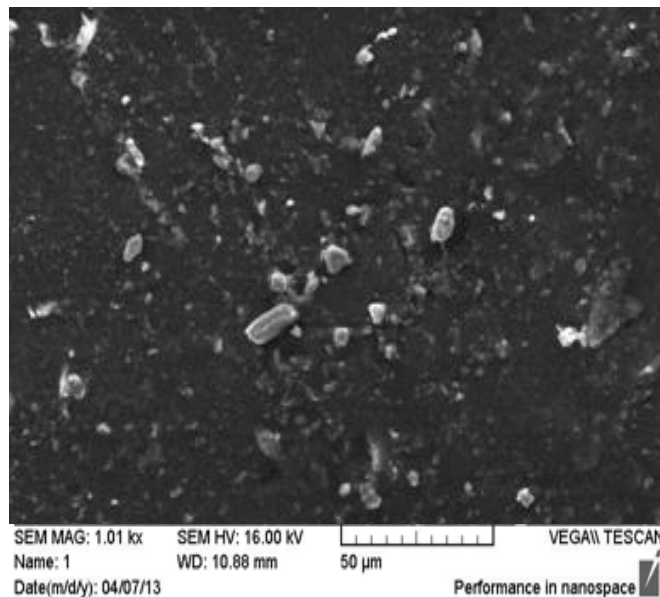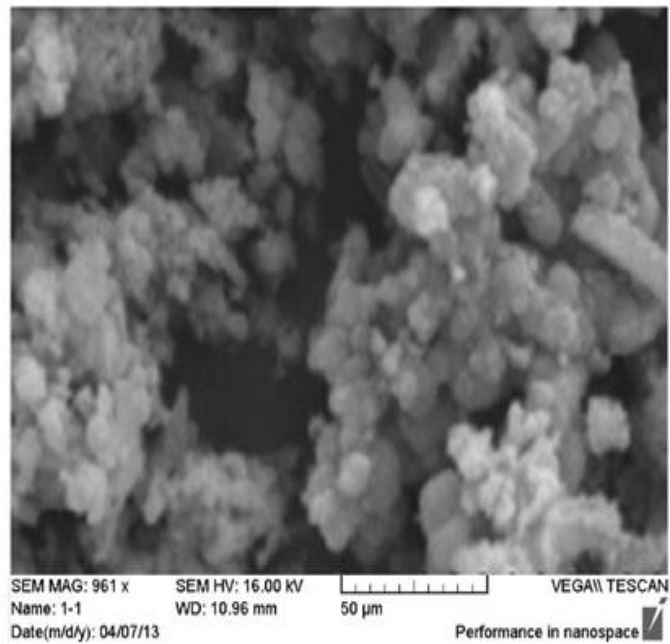
**(b)**

**Figure. 1** SEM images for the mixed culture; (a) before, (b) after acclimation process.
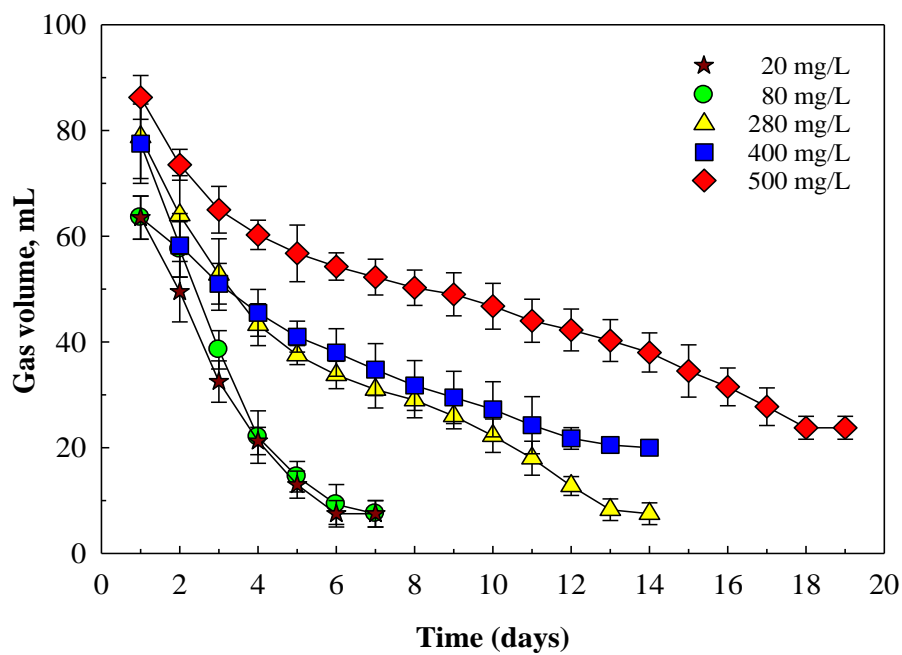


**Figure. 2** Biogas production profiles for the enrichment process at different initial concentrations of crude oil.

138

(a)                                                    (b)
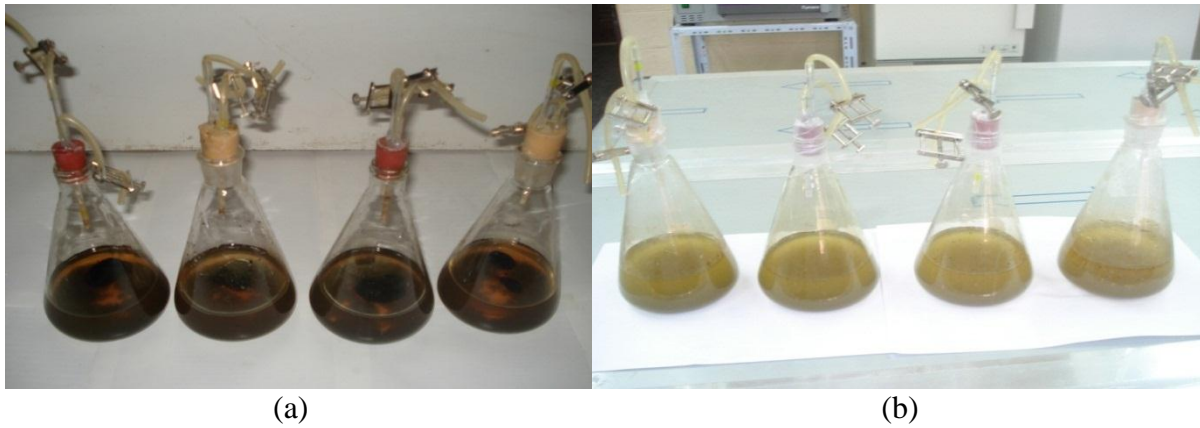
**Figure. 3** The enrichment process; (a) before acclimation, (b) after acclimation.
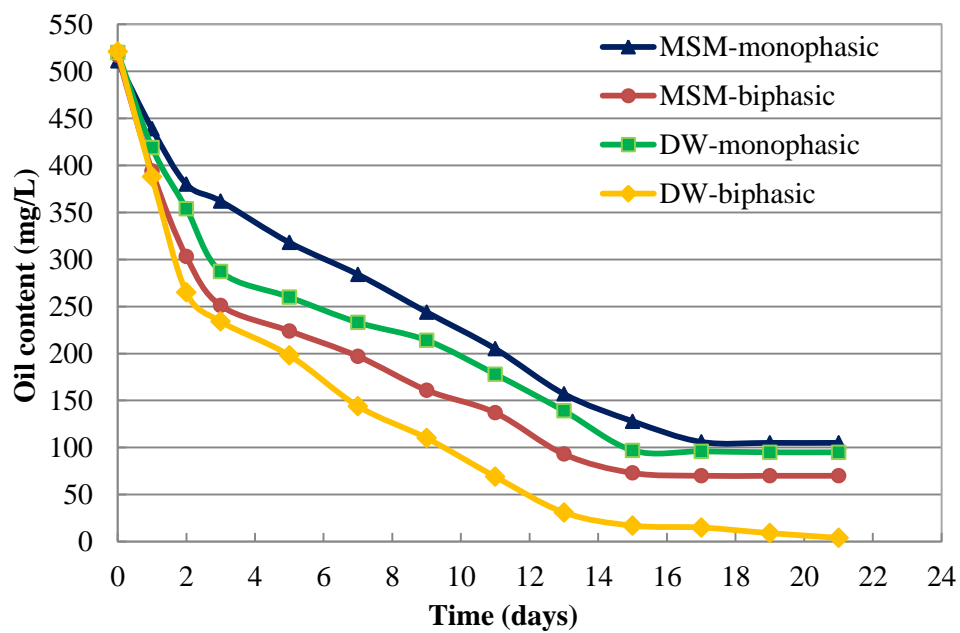


**Figure. 4** Oil content gradient in the 4 bioreactors at 500 mg/L concentration of crude oil.
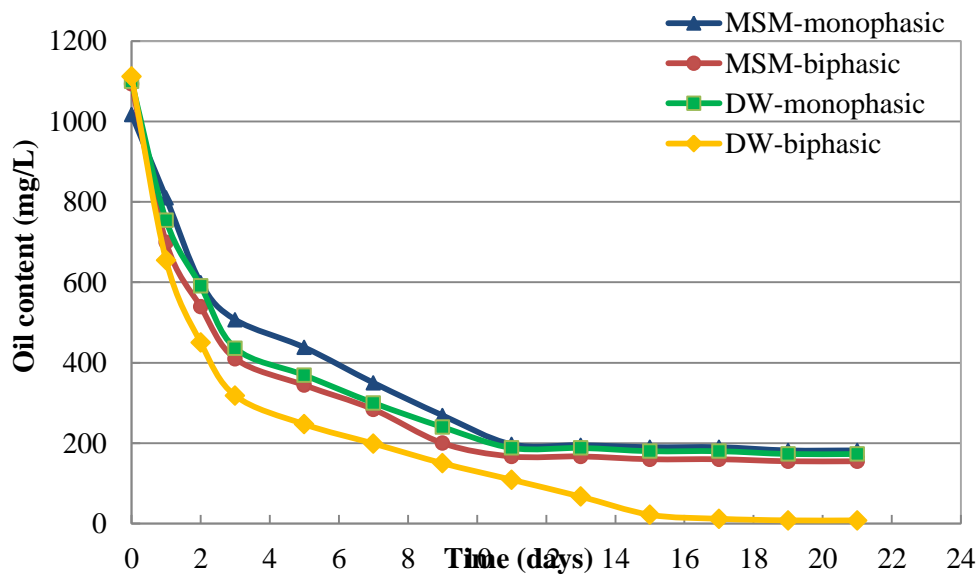
**Figure. 5** Oil content gradient in the 4 bioreactors at 1000 mg/L concentration of crude oil.
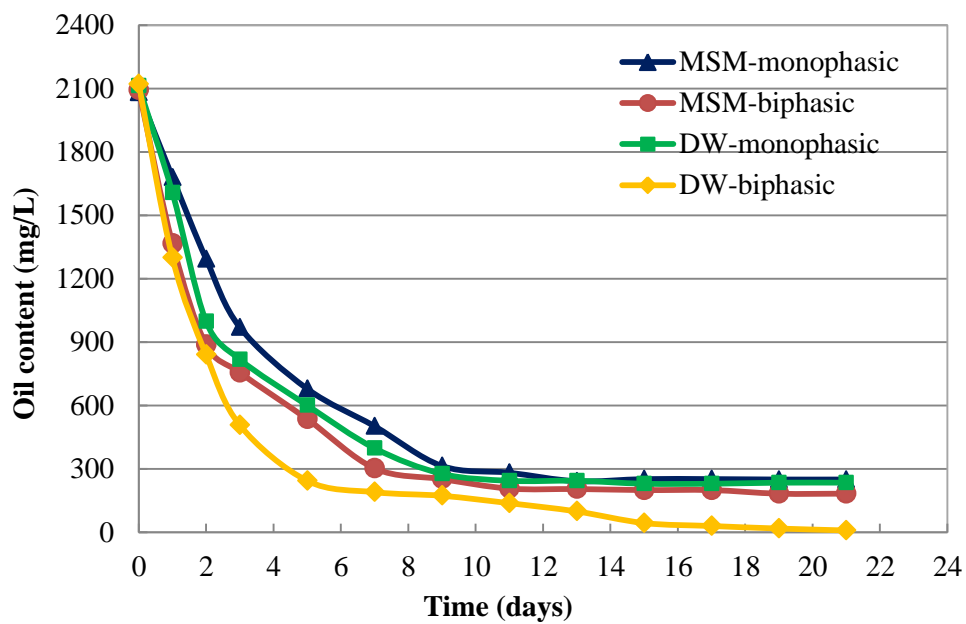


**Figure. 6** Oil content gradient in the 4 bioreactors at 2000 mg/L concentration of crude oil.
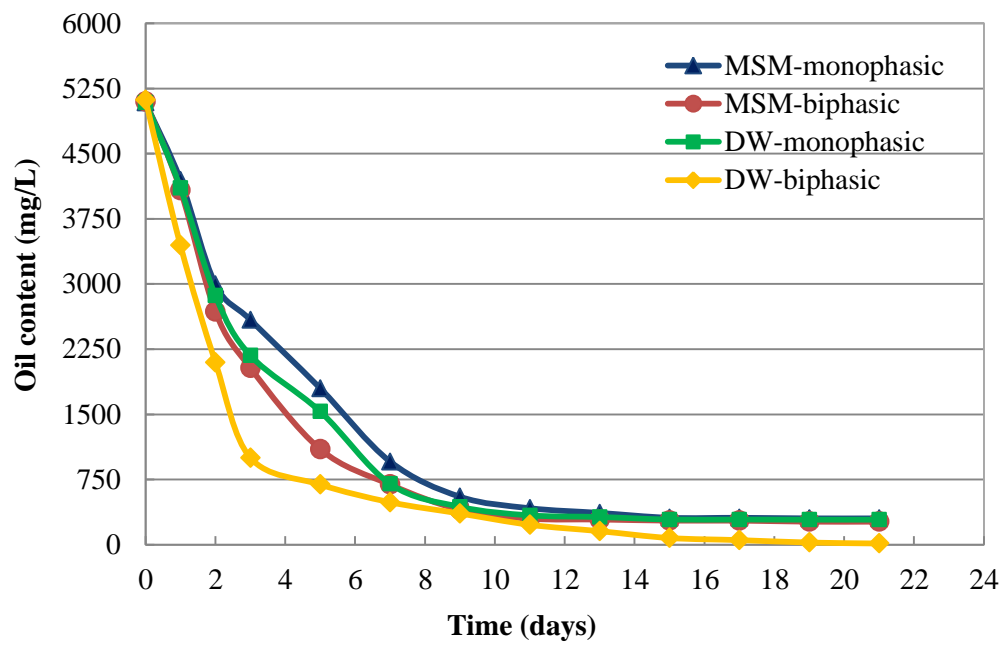
**Figure. 7** Oil content gradient in the 4 bioreactors at mg/L initial concentration of crude oil.

# New Approach in Detection MAC Spoofing in a WiFi LAN

**Asst. Prof. Hamid Mohamed Ali**
Department of Computer Engineering
College of Engineering
Baghdad University
Email: habdul_hussain@yahoo.com

**M.Sc. Student Ammna Mohamed Abbas**
Department of Computer Engineering
College of Engineering
Baghdad University
Email: ammna_maa@yahoo.com

## ABSTRACT

**M**edium Access Control (MAC) spoofing attacks relate to an attacker altering the manufacturer assigned MAC address to any other value. MAC spoofing attacks in Wireless Fidelity (WiFi) network are simple because of the ease of access to the tools of the MAC fraud on the Internet like MAC Makeup, and in addition to that the MAC address can be changed manually without software. MAC spoofing attacks are considered one of the most intensive attacks in the WiFi network; as result for that, many MAC spoofing detection systems were built, each of which comes with its strength and weak points. This paper logically identifies and recognizes the weak points and masquerading paths that penetrate the up-to-date existing detection systems. Then the most effective features of the existing detection systems are extracted, modified and combined together to develop more powerful detection system called Sequence Number with Rate and Signal Strength detection method (SN-R-SS).

SN-R-SS consists from three phases. First phase is Window Sequence Numbers; to detect suspicious spoofed frames in the network. Second phase is Transmission Rate Analysis; to reduce the amount of the suspicious spoofed frames that are generated from the first phase. Finally, the third phase is Received Signal Strength; this phase is decisive phase because it decides whether the suspicious spoofed frames are spoofed or not. Commview for WiFi network monitor and analyzer is used to capturing frames from the radio channals. Matlab software has been used to implement various computational and mathematical relations in SN-R-SS. This detection method does not work in a real time because it needs a lot of computation.

**Keywords:** Sequence Number with Rate and Signal Strength detection method, detection, frame, spoof.

<div dir="rtl">

## طريقة جديدة في اكتشاف تزوير المتحكم بالوصول للوسط في شبكة الواي فاي المحلية

**أ.م. حامد محمد علي**
قسم هندسة الحاسبات
كلية الهندسة/جامعة بغداد

**طالبة ماجستير آمنة محمد عباس**
قسم هندسة الحاسبات
كلية الهندسة/جامعة بغداد

### الخلاصة

الهجمات عن طريق تزوير المتحكم بالوصول الى الوسط تشمل تغيير المهاجم العنوان المصنعي للمتحكم بالوصول الى الوسط الى اي قيمة اخرى. هجمات التزوير للمتحكم بالوصول الى الوسط  في شبكات الواي فاي بسيطة بسبب سهولة الوصول الى الادوات التي تزور المتحكم بالوصول الى الوسط  على الانترنتوبالاضافة الى ذلك نستطيع تبديل عنوان المتحكم بالوصول الى الوسط  يدويا بدون ادوات. هجمات تزوير المتحكم بالوصول الى الوسط  تعتبر من اخطر الهجمات في الشبكات الواي فاي؛ ونتيجة لذلك, عدة انظمة لاكتشاف التزوير بنيت, جميعها لها نقاط قوة ونقاط ضعف. هذه المقالة تعرف وتميز نقاط الضعف

</div>

ومسارات الاختراق لانظمة الاكتشاف الموجودة. بعد ذلك يتم استخلاص المميزات المؤثرة لانظمة الاكتشاف الموجودة, تعديلها ودمجها مع بعض لتطوير نظام الاكتشاف اكثر قوة.

طريقة الاكتشاف رقم التسلسل مع السرعة وقوة الاشارة يتضمن ثلاثة اطوار. الطور الاول هو نافذة تسلسل الارقام: هذا الطور يكشف عن الرسائل المشكوك بتزويرها في الشبكة. الطور الثاني هو تحليل سرعة الارسال. هذا الطور يقلل من عدد الرسائل المشكوك بها في الشبكة. الطور الاخير هو قوة الاشارة المستلمة: هذا الطور هو طور القرار وذلك لانه من خلاله يتم الكشف ما اذا كانت الرسالة المشكوك بها مزورة ام لا. تم استخدام برنامج ماتلاب لتطبيق العلاقات الرياضيةوالحسابية الموجودة في طريقة الاكتشاف رقم التسلسل مع السرعة وقوة الاشارة.هذه الطريقة لاتعمل في الزمن الحقيقي لانها تحتاج الى حسابات كثيرة.

**الكلمات الرئيسية :**طريقة الاكتشاف, رقم التسلسل مع السرعة وقوة الاشارة, إكتشاف, إطار, خداع.

## 1.  INTRODUCTION

Existing Institute of Electrical and Electronics Engineers(IEEE) 802.11 security techniques, such as Wired Equivalent Privacy (WEP), Wi-Fi Protected Access (WPA), or IEEE 802.11i (WPA2), can only protect data frames **Bansal, R., etal., 2008**.

Detection of adversary presence avoids the launching of other wireless attacks **Goel, S., etal., 2009**. Guo and Chiueh **Guo, F., etal., 2006** proposed spoof detection scheme based on the SN field in IEEE 802.11 MAC header. The difference modulus 4096 between consecutive frames SN transmitted by a STA is calculated. This detection system generated many false positive and false negative alarms **Li, Q., etal., December 2007**.This method results in large amounts of false positives on wireless networks which experience even small amounts of frame loss **Madory,D., June 2006**, and caused in large amount of false positive in case both of the victim and attacker have QoS propriety in Wireless Local Area Network (WLAN) card, or one of them has this propriety **Chandrasekaran, G., etal., 2009**. Douglas Madory **Madory,D., June 2006** proposed detection system based on the same field of MAC header that is SN field. Instead of raising alarm simply on the basis of SN gap, Douglas Madory considers the transmission rate of the frames transmitted by a STA. By using this method the false alarm that was raised due to natural loss of frames will not be generated. The transmission rate is calculated by taking difference modulo 4096 of the SN of consecutive frames and dividing it by the difference of their arriving time. This method generates large amount of false positive alarms caused by the existence of Quality of Service (QoS) propriety **Chandrasekaran, G., etal., 2009**. Qing and W. Trappe **Li, Q., etal., December 2007** defined a relation to detect spoofing using the linear behavior of SN. Rather than operating strictly on two consecutive frames, the detection scheme operates on a window of frames coming from a specific STA. This method also results in large amounts of false positives on wireless networks which experience even small amounts of frame loss **Chandrasekaran, G., etal., 2009**. Also this method caused in large amount of false positive in case both of the victim and attacker have QoS propriety in WLAN card,  or one of them has this propriety **Chandrasekaran, G., etal., 2009**. Yong Sheng and et al. **Sheng, Y., etal., April 2008** proposed an approach based on Gaussian mixture models, building received signal strength (RSS) profiles for spoofing detection. They proposed to use Gaussian Mixture Modeling (GMM) for RSS profiling.  This approach cannot detect attackers who spoof the MAC addresses of mobile STAs. Shikha Goel and Sudesh Kumar **Goel, S., etal., 2009** proposed algorithm analyze the possible reasons for generating false positive and false negative in Forge Resistance Relationship (FRR) spoof detection method and proposed an improved method Forge Resistance Relationship Rate Analysis (FRR-RA) with reduced false alarms. This method caused in large amount of false positive in case both of the victim and attacker have QoS propriety in WLAN card, or one of them has this propriety **Chandrasekaran, G., etal., 2009**.T. Saelim, C. Sriklauy and P. Chumchu **Chumchu, P., etal., 2011** proposed new MAC Address Spoofing Detection Algorithm using Physical Layer Convergence Protocol (PLCP) Header. In this algorithm they are utilizing PLCP header of IEEE 802.11 frames to differentiate an attacker STA from a victim STA. PLCP header of IEEE 802.11 frames maybe changed for each frame. It depends on transmission rate adaptation algorithm which is designed by vendors of wireless interfaces driver. The rate adaptation of an attacker STA and a victim STA is different depending on adaptive algorithm and

143

environments; therefore it is much harder to spoof PLCP header. This algorithm performs by setting a number of monitoring STAs. Then STAs whose MAC addresses are the monitored MAC address will reply the special frame. If the monitoring STAs receive more than one response frames, they decide that spoofing occurs. The drawback of this approach is the attackers could avoid this detection algorithm by stopping to reply any frames. This is could be modified drivers of wireless adaptors. The rest of the paper is organized as follows; Section 2 describes variations of MAC spoofing attacks. Section 3 describes SN-R-SS method. Section 4 describes the evaluation. Finally, section 5 concludes the paper and gives further work.

## 2. MAC SPOOFING ATTACKS

The theory of the MAC spoofing attack is that the attacker masquerades as a legitimate client. Thereby the attacker gains access to the network. As the name implies the masquerading is done by spoofing the MAC address of the legitimate client. This information can easily be obtained through eavesdropping.

There exist several variations of this attack. They differ in the way the victim is treated, whether the attacker tries to avoid detection, and as a result the complexity of performing the attack. In the remaining of this section five different versions will be briefly explained without going into the practical details of performing each of the attacks.

**MAC freeloader attack:** This is the simplest variation of the attack. It does not require much skill, and it does not try to avoid any form of detection. The attack consists of spoofing the MAC address of a legitimate client and nothing more. In this case both the attacker and victim will be connected to the network at the same time, and as a result both STAs will receive each other's traffic. It is pointed out in [20] that this behavior should cause problems in the Transmission Control Protocol (TCP) layer. More specifically it should result in a termination of the ongoing TCP connections, thus making it very difficult for the attacker to use TCP.

**QoS optimized MAC freeloader attack:** In the QoS optimized version the attacker tries to avoid detection based on simple SN analysis. This is done by changing IEEE 802.11 QoS priorities to some priority not currently in use by the legitimate client. Each QoS class has its own sequence counter. By using a previous unused class the attacker will obtain his own counter and fool some systems based on plain SN analysis.

**Wait-for-availability attack:** This attack is very similar to the freeloader attack, but there is one important difference. In this case the attacker waits until there is no longer any traffic going to or from the victim's STA. Then, assuming the victim has left; the attacker spoofs the address and tries to connect. This is the most relevant version of the MAC spoofing attack as it is easy to perform and very hard to detect with existing methods based on two STAs transmitting at the same time.

**Session hijacking deauthenticates attack:** In this variation the attacker first spoofs the AP's MAC address in order to send fake deauthenticate messages to the victim. The victim's STA believes that the deauthenticate is legit, and as a result it terminates its association with the AP. The attacker can then spoof the victims MAC and have the session for himself. To prevent the victim from reconnecting the deauthenticate procedure will have to be repeated frequently.

**Session hijacking channel switch attack:** A recent variation of the session hijacking, called channel switch attack is described in [21]. In this version the attacker does not send fake deauthenticate messages; instead he sends a channel switch announcement element. A correctly crafted element would result in the victim changing channel (to an invalid one) immediately, and stay on that channel for up to 255 beacon intervals before switching back. The authors report that a denial of service (DoS) effect of up to one minute can be achieved with a single message **Idland, C., June 2011**.

## 3. SEQUENCE NUMBER WITH RATE AND SIGNAL STRENGTH DETECTION METHOD (SN-R-SS)

### 3.1 Window of Sequence Numbers Phase

This phase is used to analyze and inspect out of order frames for the intention of detecting spoofing activity. The proposed detection scheme should operate on a window of frames which are coming from a specific MAC address MAC(i). Suppose that an observation w(k) to be a collection of n states corresponding to the kth frame from MAC(i). For example, one choice for w(k) might be to take w(k)={S(k), S(k-1)}, which is simply two consecutive frame states. The window w(k)={S(k), S(k-1),….., S(k-n-1)}, where n consider as window size consisting of n consecutive SN of frames S(k) **Li, Q., etal., December 2007**. This phase consists of two stages:

**First stage** of this phase is carried out by checking for the presence of two frames with same SN in the window of certain STA MAC address [16]. The purpose of this stage is to discover the phenomenon of a retransmitted frame due lost Acknowdgement (ACK). This phenomenon occurs when the ACK frame sent by the receiver STA is lost and is not received by the sender STA. If the window contains two frames with same SN, then the contents of the two frames are compared. The second arrival frame is considered a retransmitted frame and thus has to have the same content as the first arrival frame. This means that the frame is not spoofed and cannot possibly do any harm as it is just a duplicate and it is dropped by the monitor STA from the window. Otherwise, if the contents of the two frames, with same SN, have not the same contents, then this window is marked as containing suspicious spoofed frame and is passed to the third phase for further analysis.

**Second stage** of this phase adopts the Window of SNs techniques. By using a window of frames, rather than only two consecutive frames, different degrees of detection accuracy can be used to enhance the detection system. The detection accuracy can be adjusted to increase or decrease the false positive and negative alarms generated by the detection system. In this stage, the detector calculates the n-1 SN differences {d1, d2, d3,…., dn-1}, where dn=[SN(k-n+1) - SN(k-n)] (mod 4096). The detector determines the occurrence of spoofed frames if Max (di) > T. Where 'i' varies from 1 to n and 'T' correspond to a threshold that governs the probability of false alarms and missed detection. Threshold value 'T' usually taken to be '3' on considering frame loss, where frames are sent by the sender STA and are not received by the receiver STA. Usually the frame SN is incremented by one for each consecutive frame. The lost frame would cause the frames not to be received sequentially. A threshold value is used to reflect approximately the maximum number of acceptable loss of consecutive frames in IEEE 802.11 based wireless network **Goel, S., etal., 2009**. The threshold value can be adjusted according to the level of security required in a network. With the decrease in threshold value the number of false positive alarms will increase but there will be a decrease in false negatives. When the frame SN differences are greater than that threshold, then it is an indication of suspicious spoofed frame which is the purpose of the next phase.

### 3.2 Transmission Rate Analysis Phase

This phase adopts the Transmission Rate Analysis method to inspect the window of suspicious spoofed frame passed from previous phase. Transmission Rate Analysis considers the time difference between consecutive frames and permit for naturally occurring loss frames while still detecting invalid SNs. To avoid false positive situation due to heavy frame loss, the window of suspicious frames of the previous phase is passed to this phase. This phase works on the basis of measuring the transmission rate of each STA in the WLAN. To detect the spoofing in the window, Transmission Rate Analysis on the suspicious frame with its previous and next frame is performed. Transmission rate considers possibility of frame loss and do not raise false positive alarm for it. Transmission rate is calculated by taking difference modulo 4096 of SNs from consecutive frames and dividing by the difference of their respective arrival time. The function can be defined as **Goel, S., etal., 2009**:

Transmission Rate= ((S (i)-S (i-1)) mod 4096) / (T (i)-T (i-1))           (1)

Where S (i) and S (i-1) is the SN and T(i) and T(i-1) are the arrival time of ith and (i-1)th frame respectively. By using this method, gaps from natural frame loss do not cause false alarms because they will not yield an abnormally large difference in transmission rate. It is necessary to show the relationship between the frame SN and its arrival time. For example, assume, the frame sequence numbers: { 1, 2, 3, 5, 6, 7}, are sent one millisecond apart, then the transmission rate between the first two frames would be (2-1) frames/0.001 second or 1000 frames/seconds as frame of SN 2 is arrived one millisecond after the arrival of frame of SN 1.

The rate between the third and fourth frames would be (5-3)/0.001 or 1000 frames/second as frame 5 arrived two millisecond later than frame 3 due lost frame 4. The rate between the four and fifth frames would be (6-5)/0.001 or 1000 frames/second.

### 3.3 Received Signal Strength Phase

This phase adopts RSS approach to inspect suspicious spoofed frames passed from previous phase. RSS is the signal strength of a received frame measured at the receiver's antenna. RSS is correlated to the transmission power. A wireless STA does not often changes its transmission power, so distribution pattern of a STA mostly remain same. Also the attacker has no idea what RSS looks like from the receiver perspective. Thus, a drastic change in RSS value of received frames from same MAC address indicates spoofing. Hence, two STAs at different places have two separate and distinct signal signatures (mean and variance of signal strength values).

In this phase, the monitor STA is placed in a monitor mode, while in monitor mode it can determine the RSS for all frames being transmitted within the range of the receiver. The monitor STA will compute mean value and variance value of captured RSS sample for each MAC address of the wireless STAs. Practical work shows, for stationary wireless STAs, the RSS does not deviate more than 5dBm, taking in account that the other affecting factors, like obstacles, temperature degree. are fixed. Hence, the RSS can be modeled as normal distribution with mean and variance values calculated as follows **Konings, B., etal., 2009**:

$$\text{Mean} = \sum_{i=1}^{n} \sum_{j=1}^{m} RSS(i,j) * P(i,j) \tag{2}$$

$$\text{Variance} = \sum_{i=1}^{n} \sum_{j=1}^{m} RSS^2(i,j) * P(i,j) - \text{Mean} \tag{3}$$

Where (j) is the numbers of frames for specific MAC address (i), (P) is the probability of the occurrence of specific RSS.

The false positive alarms, generated by previous phases, which is due to the wireless cards that have QoS extensions, where assumptions about monotonic of SNs in frames originating from a STA do not typically hold. In this phase, in addition to detecting spoofed frames in WLAN STAs that are not equipped with QoS interface, the QoS specification is one of the main metrics used to detect spoofing. Therefore, this phase will make extra test on the windows of suspicious frames and use the RSS as a final solution for detecting MAC spoofing. The steps performed by this phase are summarized as follows:

• For the suspicious window that contains duplicate frames of unequal contents, the type field of the frame is examined, a management frame indicates spoofed frame. A data frame leads to examine the subtype field of the duplicate frames, matched priority of the two frames indicates spoofed frame. Unmatched priority of the two suspicious frames leads to examining the RSS of the two frames. If the value of the RSS of the two frames in the range of the variance value, then there is no indication of spoofing. Otherwise, any RSS value deviated from the mean with a value greater than the variance then it is indication of spoofing.

• A challenge for the Transmission Rate Analysis, of the second phase technique is the handling the phenomenon of retransmitted frames due to the frame loss. This phenomenon occurs when a frame is sent and is not received by the receiver STA. In IEEE 802.11, every data frame transmitted is assumed lost if, in response, an acknowledgement frame is not received. When this loss is detected, a frame is

retransmitted with the same SN as was previously sent. In order to solve this problem, in this phase, the monitor STA checks the Retry bit of suspicious frames marked from the previous phase. The following steps are performed:

1.     In case, the Retry bit is equal to one (which means a retransmitted frame), the RSS of the suspicious frame is examined. If the value of the RSS is the range of the variance value, then there is no indication of spoofing. Otherwise, the frame is spoofed.

2.     IF the Retry bit is equal to zero, the monitor STA checks the type of the suspicious spoofed frame, a management frame indicates spoofing. Because management frame is associated with a single MAC sequence counter, it must be in linear progression. A data frame leads to examine the subtype field of the previous and next frames, matched priority of the two frames indicates spoofed frame. Unmatched Frame priority leads to examine the RSS of the suspicious frame. The RSS indicates either spoofing or not which depends on RSS deviation from the mean.

## 4. SIMULATION RESULTS

This section evaluates the performance of the SN-R-SS detection method by comparing it with two other well-known different methods; FRR and FRR-RA methods. FRR and FRR-RA methods are implemented separately in this work, and then the results obtained from these methods are used to evaluate the SN-R-SS detection method for MAC spoof detection. An attack view has one genuine STA, one attacker STA which spoofs the MAC address of the genuine STA; both of them are able to be connected to the internet as shown in **Fig. 1**. The distance between an attacker STA and Access Point (AP) is 7 meter, between a genuine STA and Ap is 3 meter, and between an attacker and genuine STAs is 10 meter. The practical works is conducted by changing the MAC address of the attacker STA to the address of the victim STA. Then around 80 frames are extracted from the file, produced in the capturing stage, to evaluate the performance of the SN-R-SS detection method compared to the FRR and FRR-RA detection methods. The window size for the implementation of the three methods mentioned above is taken to be ten.

Description and evaluation the performance of the system with two types of wireless IEEE 802.11 attacker models are studied. The two types of wireless IEEE 802.11 are:

- STAs without QoS property.
- STAs with QoS property.



**Figure 1.** an Attacker model.

## 4.1 STAs without QoS Property

In this case, victim STA and attacker STA do not have QoS Property. Figures (2, 3, and 4) illustrate the results performance of applying FRR, FRR-RA and the SN-R-SS detection methods, respectively. The raising edge lines of the three Figures indicate spoofing or false positive alarms. When there are no spoofed frames and no false positive alarms, the Figures show only straight line (the x-axis) shown in the Figures. The false negative alarms are not shown in the figures because they are passed through the detection system as they were genuine frames.

In terms of false positive alarms and spoof detection, it is observed from the figures that both the SN-R-SS detection method and FRR-RA methods give better performance than FRR method since FRR method generates large number of false positive alarms than the others. Also the SN-R-SS detection method gives better performance than FRR-RA method since FFR-RA generates larger number of false positives than the SN-R-SS detection method.

**Fig. 2** shows the result performance which is obtained from FRR method. The FRR method produces 82.5% spoofing and false positive. The spoof and false positive alarms signs, shown in the figure, is very high compared to other methods.  Actually, FRR method generates many false positive alarms mostly due to the following reasons:
- Frame loss.
- Out of order frames.
- One of duplicate frames is spoofed.
- Retransmitted frame due to the loss of an ACK frame.



**Figure 2.** FRR method.

The results which are obtained from the FRR-RA method are shown in **Fig. 3.** The FRR-RA method produces 28.75% spoofing and false positive. The spoof and false positive alarms signs are less than the spoof and false positive alarms signs shown in **Fig. 2** of FRR method. This method decreases the false positive alarms which occur in FRR method because:

- It treats and overcomes the states of the frame loss.

- This method treats the spoofing in duplicate frames which are not treated in the FRR method.

But also this method suffers from generating false positive alarms for the following states:

- Out of order frames.

- Retransmitted frame due to the loss of an ACK frame
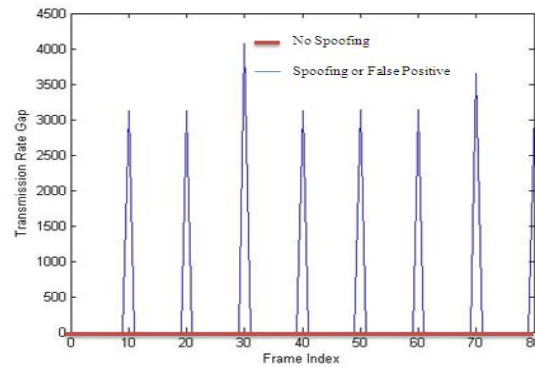
**Figure 3.** FRR-RA method.

Fig. 4 shows the results which are obtained from SN-R-SS detection method. The SN-R-SS detection method produces 25% spoofing and false positive. This Figure shows a better performance results than FRR-RA method. As shown in the Figure, the spoof and false positive signs are less than the spoof and false positive alarms signs shown in **Fig. 3**. This is because the SN-R-SS detection method can solve all of the following problems that are encountered in FRR and FRR-RA:

- Frame loss.

- Out of order frames.

- One of duplicate frames is spoofed.

- Retransmitted frames due to the loss of an ACK frame.
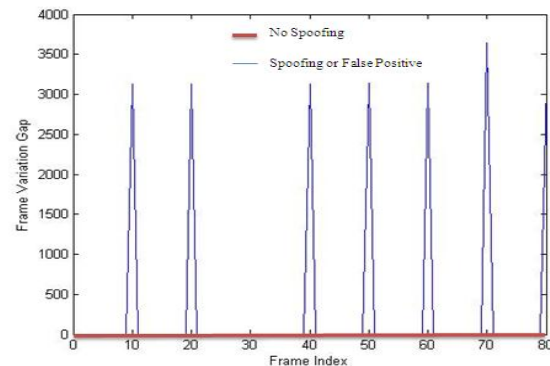


**Figure 4.** SN-R-SS detection method.

## 4.2 STAs with QoS Property

Three cases will be studied in this section:

- An attacker has QoS property while the victim does not have it.
- An attacker does not have QoS property while the victim has this property.
- Both of them (an attacker STA and the victim STA) have QoS property.

The results shown in Figures (5 to 13) illustrate the performance of FRR, FRR-RA and the SN-R-SS detection methods, respectively. In terms of false positive alarms and spoof detection, it is observed from the figures that the SN-R-SS detection method gives better performance than FRR and FRR-RA methods. FRR and FRR-RA generate large number of false positive alarms. The main reason of these alarms is the QoS property in the WLAN card of STAs.

- **attacker with QoS / victim without QoS**

In this case an attacker STA has QoS property in its WLAN card, but the victim does not have this property in its WLAN card. Figures (5, 6 and 7) illustrate the results performance of applying FRR, FRR-RA and the SN-R-SS detection methods, respectively.

**Fig. 5** shows the result performance which is obtained from FRR method. The FRR method produces 22.5% spoofing and false positive.The spoof and false positive alarms signs, shown in the figure, is very high compared to other methods. The reasons for generating false positive alarms, in FRR method, are:

- Frame loss.

- Out of order frames.

- One of duplicate frames is spoofed.

- Retransmitted frame due to the loss of an ACK frame.

- The QoS property of an attacker STA.



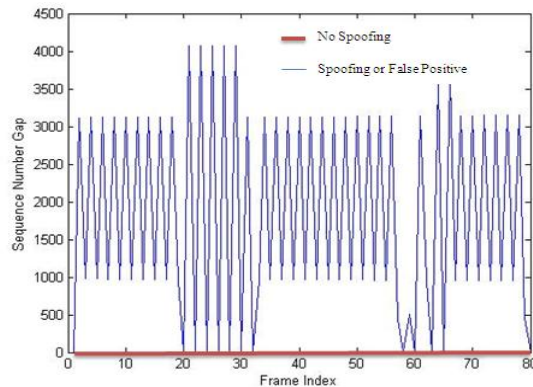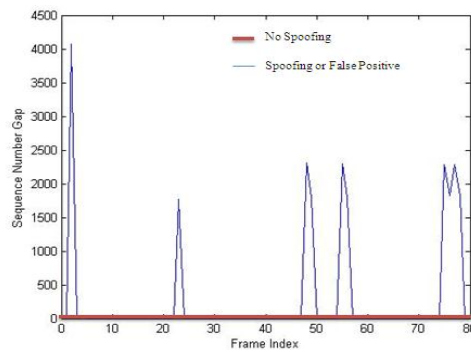**Figure 5.** FRR method.

The results performance which are obtained from the FRR-RA method are shown in **Fig. 6**. The FRR-RA method produces 17.5% spoofing and false positive. The spoof and false positive signs are less than the spoof and false positive signs shown in **Fig. 5** of FRR method. FRR-RA method fails to overcome the false positive alarms generated due QoS property of WLAN card.
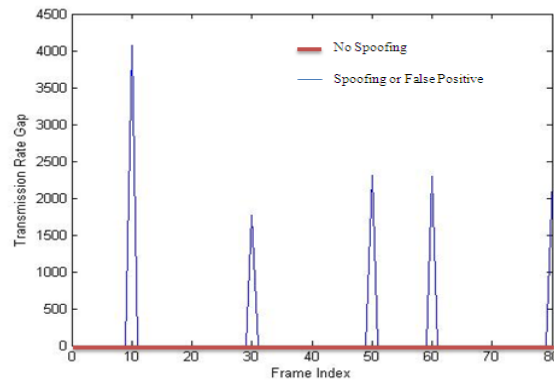
**Figure 6.** FRR-RA method.

**Fig. 7** shows the result of the performance which is obtained from SN-R-SS detection method. The SN-R-SS detection method produces 13.75% spoofing and false positive. The SN-R-SS detection method gives better results than the other two methods (FRR and FRR-RA). As shown in the Figure, the spoof and false positive signs are less than the spoof and false positive signs shown in **Fig. 5** and **Fig. 6** respectively.

The following are the reasons for generating false positive alarms that are faced totally in FRR and partially in FRR-RA and solved by the SN-R-SS detection method:

- It treats the case of frame loss.
- It treats the problem of out of order frames.
- It treats the problem of spoofing existence in duplicate frames.
- It treats the problem of the retransmitted frame due to the loss of an ACK frame.
- It treats the problem of QoS property in an attacker STA WLAN card.

Although the SN-R-SS detection method has better spoof detection capability than FRR and FRR-RA, as indicated by the rising edge signs shown in **Fig. 7**, but also the rising edge signs could partially indicates false positive alarms. The false positive alarms signs shown in **Fig. 7** are generated due to the RSS environmental variation, calibration drift, and other factors that make it difficult to trace the RSS value as these disturbances make it unstable and noisy.
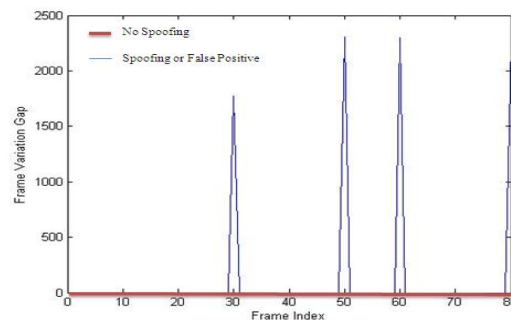


**Figure 7.** SN-R-SS detection method

- **Victim with QoS / Attacker without QoS**

In this case, an attacker STA has no QoS property and the victim STA has QoS property.  Figures (8, 9 and 10) illustrate the results performance of applying FRR, FRR-RA and the SN-R-SS detection methods, respectively. The results show that the SN-R-SS detection method gives better result than

FRR and FRR-RA methods. The same analysis and performance results discussed in the previous case are applied for this case, for the three detection method FRR, FRR-RA and SN-R-SS detection method, are shown in Figures (8, 9 and 10) respectively.

**Fig. 8** shows the results which are obtained from FRR method. The FRR method produces 90% spoofing and false positive.
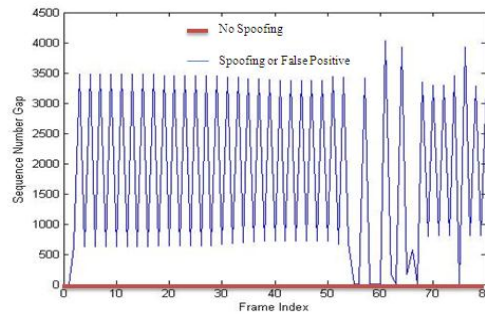


**Figure 8.** FRR method.

**Fig. 9** shows the results which are obtained from applying FRR-RA method on the data file. The FRR-RA method produces 28.75% spoofing and false positive.
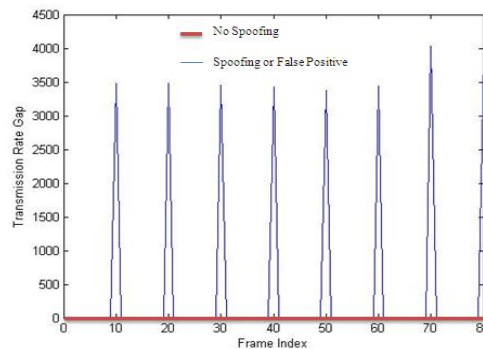


**Figure 9.** FRR-RA method.

**Fig. 10** shows the results which are obtained from applying SN-R-SS detection method on the data file. The SN-R-SS detection method produces 25% spoofing and false positive.
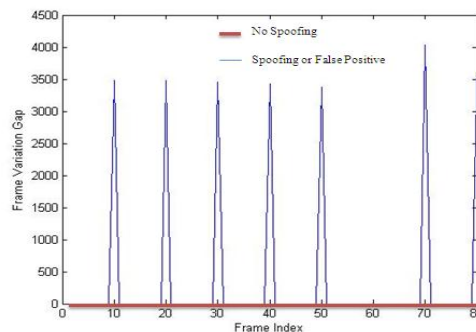


**Figure 10.** SN-R-SS detection method.

152

- **Victim and Attacker with QoS Property**

In this case both attacker and victim STAs have QoS property in their WLAN cards.  Figures (11, 12 and 13) illustrate the results performance of applying FRR, FRR-RA and the SN-R-SS detection methods, respectively. By applying the three methods (FRR, FRR-RA and the SN-R-SS detection method) on the data file. The SN-R-SS detection method gives better results than the other methods (FRR and FRR-RA). All the analysis and performance results discussed in the first case are also applied to this case for the three detection method FRR, FRR-RA and SN-R-SS detection method, are shown in  Figures (11, 12 and 13) respectively.

**Fig. 11** shows the results which are obtained from FRR method. The FRR method produces 36.25% spoofing and false positive.
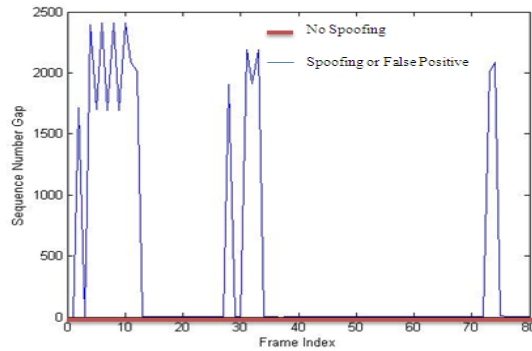


**Figure 11.** FRR method.

**Fig. 12** shows the results which are obtained from FRR-RA method. The FRR-RA method produces 17.5% spoofing and false positive.
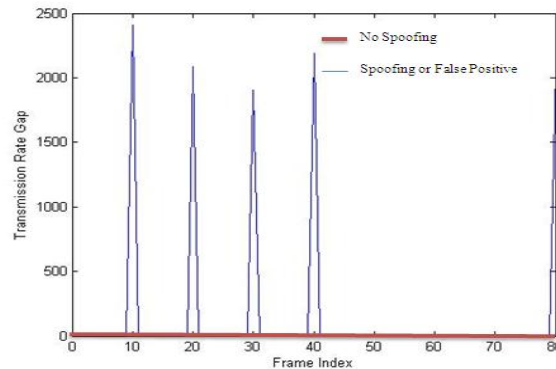


**Figure 12.**  FRR-RA method.

The results which are obtained from applying SN-R-SS detection method on data file are shown in **Fig. 13**. The SN-R-SS detection method produces 13.75% spoofing and false positive.
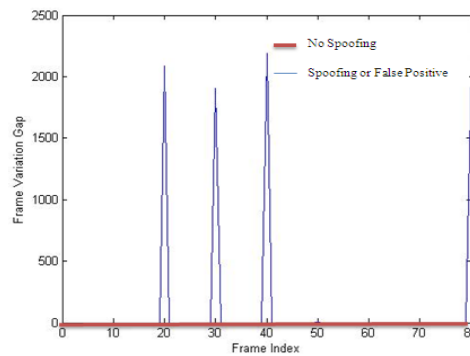
**Figure 13.**SN-R-SS detection method.

## 5. CONCLUSION

During the study and development of the proposed system, several points observed and noticed:

After deep analysis and inspection of the existing MAC spoof detection systems, it is found and realized that one mechanism such as FRR, FRR-RA or RSS alone is not sufficient to build efficient MAC spoof detection system. Each one of the mentioned detection system has its drawbacks in detecting MAC spoof. To enhance the MAC spoofing detection system, many factors has to be taken into account to design reliable detection system.

The results that have been obtained from SN-R-SS detection method after compared with two detection methods (FRR and FRR-RA) indicate that the SN-R-SS detection method gives better results performance than FRR and FRR-RA MAC spoof detection methods.

SN-R-SS detection method treats the problems when an attacker STA and victim STA have QoS property in the WLAN card, when attacker STA has QoS property while the victim STA does not have this property and the case when an attacker STA does not have QoS property while the victim STA has this property. The SN-R-SS detection method produced better results performance than FRR and FRR-RA when wireless station is equipped with Qos property WLAN interface card.

SN-R-SS detection method does not work well when the attacker and genuine STA are placed near enough to each other. This is because the final phase of SN-R-SS detection method depends on RSS value. In other satuation, when an attacker and the victim close to each other, the RSS value of an attacker STA is approximately equal to the RSS value of the victim STA. This statuation causes the RSS phase genrates false positives and negatives alarms.

SN-R-SS detection method does not work well when the victim STA is mobile. This is because the final phase of SN-R-SS detection method depends on RSS value. In case, when the victim STA is mobile STA, This causes oscilating of the RSS value received at the monitor STA that could generate false positives and negatives alarms.

SN-R-SS detection method unable to detect the attacker presence if victim not communicating. This results in false negative alarms.

Due the three phases of checking embedded in the SN-R-SS detection method which requires a lot of computation. The SN-R-SS detection method will not be able to conform in the real time spoof detection. But there is always tradeoff between security required and time consuming.

In this paper, the third phase is RSS phase; the researchers can use other fingerprinting tools in the STA to enhance the system. Other attributes can be used to uniquely identify WLAN station. Such attributes like wireless driver fingerprinting.

The researcher can use backpropagation neural network to obtain required values of threshold and window size which are used in first phase of SN-R-SS detection method algorithm instead of fixed values. In this case the system will be enhanced.

**REFERENCES**

➢ Bansal, R., etal., *2008, Non-Cryptographic Methods of MAC Spoof Detection in Wireless LAN*, Networks. ICON 2008.16th IEEE International Conference on, ISSN 1556-6463.

➢ Chandrasekaran, G., etal., *2009, Detecting Identity Spoofs in IEEE 802.11e Wireless Networks*, Global Telecommunications Conference,.Globecom 2009.IEEE , ISSN 1930-529X.

➢ Chumchu, P., etal., *2011, A new MAC Address Spoofing Detection Algorithm using PLCP Header*, Information Networking (ICOIN), 2011 International Conference on, ISSN 1976-7684.

➢ Goel, S., etal., *2009, An Improved Method of Detecting Spoofed Attack in Wireless LAN*, Networks and Communications. NETCOM '09.First International Conference on.

➢ Guo, F., etal., *2006, Sequence Number-Based MAC Address Spoof Detection*, Recent Advances in Intrusion DetectionLecture Notes in Computer Science, Vol 3858.

➢ Idland, C., *June 2011, Detecting MAC Spoofing Attacks in 802.11 Networks Through Fingerprinting on MAC Layer*, M.Sc. Thesis, Norwegian University of Science and Technology.

➢ Konings, B., etal., *2009, Channel Switch and Quiet Attack: New DoS Attacks Exploiting The 802.11 Standard*, Local Computer Networks. LCN 2009.IEEE 34th Conference on.

➢ Li, Q., etal., *December 2007, Detecting Spoofing and Anomalous Traffic in Wireless Networks via Forge-Resistant Relationships*, Ieee Transection on Information Forensics and Security, VOL. 2, NO. 4.

➢ Madory,D., *June 2006, New Methods of Spoof Detection in 802.11b Wireless Networking*, M.Sc. thesis, Thayer School of Engineering.

➢ Sheng, Y., etal., *April 2008, Detecting 802.11 MAC Layer Spoofing Using Received Signal Strength*, NFOCOM 2008. The 27th Conference on Computer Communications. IEEE,ISSN 0743-166X.

# Batch and Fixed-Bed Modeling of Adsorption Reactive Remazol Yellow Dye onto Granular Activated Carbon

**Mohammed Sadeq Salman**
Instructor
Computer Center
University of Baghdad
Iraqmas68@ yahoo.com

**Waleed Mohammed Abood**
Head of Engineering
Head of engineers
Ministry of industry-Iraq
Env_eng_waleed@yahoo.com

**DhaferFaza Ali**
Head of Chemists
Ministry of industry-Iraq
Dhaferali32@yahoo.com

## ABSTRACT

**I**n this work, the adsorption of reactive yellow dye (Remazol yellow FG dye) by granular activated carbon (GAC) was investigated using batch and continuous process. The batch process involved determination the equilibrium isotherm curve either favorable or unfavorable by estimation relation between adsorption capacity and concentration of dye at different dosage of activated carbon. The results were fitted with equilibrium isotherm models Langmuir and Freundlich models with $R^2$ value (>0.97). Batch Kinetic study showed good fitting with pseudo second order model with $R^2$ (0.987) at contact time 5 h. which provesthat the adsorption is chemisorptions nature. Continuous study was done by fixed bed column where breakthrough time was increased at flow rates (21.67, 12.5 and 6 ml/min) and initial dye concentration (80, 40, 20 and 10 mg/l) were decreased and bed depth was increased (5, 10, 15 and 20 cm). The adsorption data were fitted to the fixed-bed adsorption mathematical models Thomas and Yoon-Nelson models. The results fitted well to the Thomas and Yoon-Nelson models with correlation coefficient, $R^2 \geq 0.944$. Average relative error ARE% was applied to examine the theoretical and experimental results.

**Key Words:** Adsorption, Reactive Yellow dye, Granular activated carbon, Fixed bed column

## النمذجة الرياضية لامتزاز الصبغة الصفراء الفعالة باستخدام الفحم المنشط في تجارب الوجبة و تجارب الحشوة الثابتة

**ظافر فزع علي**
رئيس كيميائيين
هيئة البحث والتطوير
وزارة الصناعه

**د. وليد محمد عبود**
رئيس مهندسين
هيئة البحث والتطوير
وزارة الصناعه

**محمد صادق سلمان**
مدرس
مركز الحاسبه الالكترونيه
جامعة بغداد

### الخلاصة

في هذا البحث تم امتزاز الصبغة الصفراء الفعالة  باستخدام الفحم المنشط الحبيبي خلال تجارب وجبية و مستمرة حيث تضمنت التجربة الوجبية عملية تحديد منحني التوازن عند ثبوت درجة الحرارة وبيان هل نوعه مفضل ام غير مفضل من خلال احتساب علاقة مابين سعة الامتزاز وتركيز الصبغة المتبقية في المحلول بعد الامتزاز بعد استخدام اوزان مختلفة من الفحم المنشط حيث وضحت النتائج مطابقة مع موديل لانكمير بقيمة مربع معامل ارتباط اكثر من 97%   في حين تطابقت تجارب تغيير زمن التلامس عند ثبوت الحجم مع موديل سيدو ذا المرتبة الثانية بقيمة مربع معامل الارتباط 98.7% في اقصى زمن تلامس مقداره 5 ساعات والذي يثبت ان طبيعة الامتزاز بين الصبغة والفحم المنشط هو امتزاز كيمياوي.

التجارب المستمرة من خلال استخدام حشوة ثابتة عند عدة متغيرات مثل معدل جريان محلول الصبغة من الاعلى الى الاسفل
بمقدار ( 6 , 12.5 , 21.67) مل/دقيقة و عند تغيير تركيز الصبغة ( 10 , 20 , 40, 80 ) ملغم/لتر وعند عمق حشوات
( 5 , 10 , 15 , 20) سم     واحتساب منحني الانكسار ومقارنة النتائج مع موديلين  ثوماس  و يوون نيلسون و احتساب
معدل الخطاء بين النتائج النظرية والعملية .

## 1- INTRODUCTION

Water is one of most important commodities which man has exploited a other resources for sustenance of his life. Water can be regarded polluted when it changes its quality or composition either or as a result human activities. **Goal, 1997.**

Many materials can cause pollution like inorganic salts, acids, alkaline, organic matter, suspended solid, floating (solid or liquid), heat, color, toxic material, microorganisms, radioactive material and foam-reducing matter. **Nemerow, 1971.**

 Pure water is colorless, but water in nature often colored by foreign substances. Color contributed by dissolved solid that remain after removal of suspended matter is known as true color. Highly colored water is unsuitable for laundry, dying, paper making, dairy production and other industries. Thus the color water effects its marketability for both domestic and industrial use**. Peavy et al., 1986.**

The azo dyes are by far the most important class, accounting for over 50% of all commercial dyes, and having been studied more than any other class. The most important distinguishing characteristic of reactive dyes is that they form covalent bonds with the substrate that is to be colored during the application process. Thus, the dye molecule contains specific functional groups that can undergo addition or substitution reactions with the OH, $SO_3$, and $NH_2$ groups present in textile fibers. Most reactive dyes fall in the category of azo dyes. Virtually every hue in the dye spectrum can be achieved by appropriate structural modifications (mono- and di-azo dyes, combinations involving either single or multiple aromatic and heterocyclic ring systems). **Hunger, 2003.**

Wastewater effluent from the textile industries can be particularly problematic due to the presences of color in the final effluent. This color in the water system is highly visible and thus undesirable. Textile industries consist of multi-processes which produce wastewater which generally colored, different pH value, high chemical oxygen demand COD, high suspended solid and high temperature. **Nemerow, 1971.**

There are many technologies currently available for treating wastewater from textile industry which include Biological treatment,\Chemical precipitation, Ultra filtration, Adsorption and Advanced Oxidation. **Abood, 2012.**

Adsorption is a widely used method to treat industrial waste gas and effluent due to its low cost, high efficiency and easy operation. Particularly, the adsorption process is suitable for decontaminating those compounds of low concentration or high toxicity, which are not readily treated by biological processes. Based on the operation mode, adsorption can be generally classified into static adsorption and dynamic adsorption. Static adsorption, also called batch adsorption, occurs in a closed system containing a desired amount of adsorbent contacting with a

certain volume of adsorbate solution, while dynamic adsorption usually occurs in an open system where adsorbate solution continuously passes through a column packed with adsorbent.

For column adsorption, how to determine the breakthrough curve is a very important issue because it provides the basic but predominant information for the design of a column adsorption system. Without the information of the breakthrough curve one cannot determine a rational scale of a column adsorption for practical application. There are two widely used approaches to obtain the breakthrough curve of a given adsorption system: direct experimentation or mathematical modeling. The experimental method could provide a direct and concise breakthrough curve of a given system. **Zhe, 2013.**

Reactive yellow dye was investigated as an adsorbate to be removed onto activated carbon during batch and the result shows good removal of dyes when increasing adsorption capacity at increasing initial concentration and temperature and the adsorption is considered as an endothermic. **Sulyamon and Abood 2013.**

The aim of this study is examining the reactive yellow dye as adsorbate and granular activated carbon as adsorbent in batch process using Langmuir and Freundlich models as equilibrium isotherm models and for kinetic study tested pseudo first and second order models were applied to investigate mechanism of adsorption, while for the continuous adsorption the fixed bed column was used with different condition ( initial dye concentration , bed depth and flow rates)and the results were tested with most widely used models (Thomas and Yoon- Nelson) and the validity of results were approved according to the average relative error (ARE%) as a error function.

## 2- ADSORPTION ISOTHERMS MODELS

In general, an adsorption isotherm is an invaluable curve describing the phenomenon governing the retention (or release) or mobility of a substance from the aqueous porous media or aquatic environments to a solid-phase at a constant temperature and pH. Adsorption equilibrium (the ratio between the adsorbed amount with the remaining in the solution) is established when an adsorbate containing phase has been contacted with the adsorbent for sufficient time, with its adsorbate concentration in the bulk solution is in a dynamic balance with the interface concentration.

Typically, the mathematical correlation, which constitutes an important role towards the modeling analysis, operational design and applicable practice of the adsorption systems, is usually depicted by graphically expressing the solid-phase against its residual concentration. **Foo and Ahmed 2010**

### 2-1 Langmuir Isotherm

Considered sorption as a chemical phenomenon by assuming that the forces that are exerted by chemically unsaturated surface atom (total number of binding sites) do not extend further than diameter of one sorbet molecules and therefore sorption is restricted to a monolayer.

The Langmuir isotherm relationship is shown in Eq. (1) :

$$q_e = q_m \frac{K_L \ C_e}{1 + K_L \ C_e}$$ *(1)*

Where $q_e$ adsorption capacity mg adsorbate / g adsorbent, $C_e$ final concentration at Equilibrium mg/l. $q_m$ maximum adsorption capacity in forming complete monolayer on the surface mg/g. $K_L$ is coefficient related to the affinity between the adsorbate and adsorbent (L/mg)

Langmuir relationship can be linearized by plotting ($1/q_e$) vs. ($1/C_e$) where $1/q_m$ is intercept ($1/q_m$ $K_L$) is slope in Eq.(2).

$$\frac{1}{q_e} = \frac{1}{q_m K_L C_e} + \frac{1}{q_m}$$ (2)

The essential characteristics of the Langmuir isotherm can be expressed in terms of a dimensionless constant separation factor $R_L$ that is given by the following Eq. (3)

$$R_L = 1/(1 + K_L C_o)$$ (3)

where $C_o$ (mg/l) is the initial concentration of adsorbate, and $K_L$ (L/mg) is Langmuir constant. The value of $R_L$ indicates the shape of the isotherm which is unfavorable ($R_L > 1$), linear ($R_L = 1$), favorable ($0 < R_L < 1$) or irreversible ($R_L = 0$)

**2-2 Freundlich Model .**

The Freundlich's Equation has been widely used for many years. This Equation is special case for heterogeneous surface energies in which the energy term ($K_F$) in Langmuir's Equation varies as a function of surface coverage ($q_e$) strictly due to variation in heat of adsorption. This relationship is empirical Eq. (4). It doesn't indicate a finite uptake capacity of the adsorbent and can thus only be reasonably for low and intermediate concentration range.

$$q_e = K_F C_e^{1/n}$$ (4)

Where $q_e$ and $C_e$ are as above and $K_F$ and n are constants. n is larger than zero.
The linearization equation of Freundlich can be Eq.(5):

$$Log \ q_e = log \ K_F + 1/n \ log \ C_e$$ (5)

Where 1/n is slope and log $K_F$ is intercept

**3- ADSORPTION KINETICS**

The transport and subsequent adsorption of adsorbate onto an adsorbent particle is usually described by one of the following transport mechanism or by combination of them film diffusion and intrapartical diffusion (**Thomas and Crittenden, 1998**). Variations among such models are

distinguished according to the rate limiting mass transport step. Examples of those kinetic models include; the linear driving force model, the surface diffusion model, the pore diffusion model, and the film pore and surface diffusion model. **Ho et al., 2000**
kinetic modeling was examined by researchers to investigate the mechanism of adsorption and potential rate–controlling process such us mass transfer and chemical reaction. The pseudo-first order and pseudo-second order kinetics models were used to analyze the adsorption kinetic of textile dyes. **Isa, et al., 2007**

**3-1- Pseudo first order model**
This model assumes a first order adsorption kinetic and can be represented by the Equation (6):

$$\frac{dq_t}{dt} = K_1(q_e - q_t) \tag{6}$$

Where: $q_e$ and $q_t$ are adsorption capacity at equilibrium and at time t, respectively (mg g$^{-1}$), $K_1$ is the rate constant of pseudo first order adsorption (min$^{-1}$).

After integration and applying boundary conditions:
$q_t$=0 at t=0 and $q_t$=$q_e$ at  t=t.
The integrated form becomes Eq (7):

$$\ln(q_e - q_t) = \ln(q_e) - Kt \tag{7}$$

The values of ln ($q_e$– $q_t$) were linearly correlated with *t*. The plot of ln ($q_e$– $q_t$) versus t should give a linear relationship from which $K_1$ and $q_e$ can be determined from the slop and intercept of the plot, respectively. The applicability of the pseudo-first order equation to experimental data generally, differs in two ways; the parameter $K_1$ ($q_e$-$q_t$) does not represent the number of available sites and the parameter log ($q_e$) is an adjustable parameter and often found not equal to the intercept of the plot log ($q_e$– $q_t$) versus t, whereas in true first order, log ($q_e$) should be equal to the intercept.

**3-2 Pseudo second order model.**
The pseudo second-order adsorption kinetic rate Equation is expressed as Eq (8):

$$\frac{dq_t}{dt} = K_2(q_e - q_t)^2 \tag{8}$$

Where:
 $K_2$ is the rate constant of the pseudo second order adsorption (g.mg$^{-1}$.min$^{-1}$).
For the boundary conditions:
$q_t$=0 at t=0 and $q_t$=$q_e$ at t=$t_e$
The integrated form of the Eq (8) which can be rearranged to the linear form as Eq (9):

$$\frac{t}{q_t} = \frac{1}{K_2 q_e{}^2} + \frac{1}{q_e} t \qquad (9)$$

The plot of $(t/q_t)$ and t of Eq (9) should give a linear relationship from which $q_e$ and $K_2$ can be determined from the slope and intercept of the plot, respectively.

## 4- DYNAMIC ADSORPTION

The adsorption equipment is the heart of the system. Three types of adsorber are generally used in wastewater application: down flow fixed bed, packed moving bed an up flow expanded – bed **Cavaseno, 1980**. Down flow fixed bed adsorbers offer the advantage of simple operation plus the ability to serve as a filter and can be operated either under pressure or by gravity flow. Typical superficial linear velocity for liquid in bed is 0.3 (m/min) in vertical direction to prevent settling **Tchohanoglous et al., 2003.** Empirical or short cut models are still used extensively for the design of fixed beds. This is not only due to their simplicity and reliability but also because of the formidable nature of more rigorous alternative. **Thomas and Crittenden, 1999**

**4-1 Thomas Model** was developed for adsorption processes in which external and internal diffusion limitations are not present. The linearized form of the Thomas model can be expressed as in Eq. (10) . **Sachin et al., 2010**

$$\ln\left(\frac{C_o}{C} - 1\right) = \frac{K_T q_{cal} m}{Q} - \frac{K_T C_o}{Q} V_{eff} \qquad (10)$$

where $K_T$ is the Thomas rate constant (mL/min.mg), $q_e$ is the equilibrium of reactive yellow dye uptake (mg/g), $C_o$ is the inlet reactive yellow dye concentration (mg/L), $C_t$ is the effluent reactive yellow dye concentration at time t (mg/L), W is the mass of adsorbent (g), Q is the inlet flow rate (mL/min) and t is the flow time (min). The value of Co/Ct is the ratio of inlet to outlet reactive yellow dye concentrations. A linear plot of ln $[(C_o/C_t) − 1]$ against time (t) was drawn to determine the values of qe and $K_T$ from the interception point and slope of the plot, respectively.

**4-2 The Yoon–Nelson** model was developed model to describe the adsorption behavior in the continuous column adsorption. The linearized form of the Yoon-Nelson model is given in Eq.(11). **Yahaya et al., 2011**

$$\ln\left(\frac{C_t}{C_o - C_t}\right) = K_{YN} t - K_{YN} T \qquad (11)$$

where, $K_{YN}$ is the rate velocity constant(L/min) and T is the time in (min) required for 50% adsorbate breakthrough. A linear plot of ln $[C_t / (C_o − C_t)]$ against sampling time (t) was used to determine the values of $K_{YN}$ and $\tau$ from the slope and intercept of the plot. $q_e$ is the amount of adsorbate being adsorbed in a fixed bed is half of the total adsorbate entering the adsorption bed

within 2Tperiod. Hence, the following Equation (12) can be obtained for a given bed**. Sotelo, et al, 2012.**

$$q_e = \frac{q_{adsorbed}}{m} = \frac{C_o[(Q/1000)t]}{2m} = \frac{C_o.Q.T}{1000.m}$$

(12)

The validity of the adsorption model was further determined by using normalizedaverage relative error (ARE%) Eq.(13) for experimental and theoretical results of ( $C_t/C_o$). **Foo and Hameed, 2010**

$$ARE\% = \frac{100}{N} \sum \left[ \frac{|X_{exp} - X_{cal}|}{X_{exp}} \right]$$

(13)

Where X represent the result and N number testing time.

## 5- EXPERIMENTAL MATERIALS AND METHOD

### 5-1-Adsorbent

Granular activated carbon GAC was used as adsorbent with particle size (0.5–0.75 mm), bulk density 711.8 kg/m$^3$, porosity 53.44%, and surface area 911.56m$^2$/g.

AC was washed with distilled water to remove dust and fine particles then dried at 100°C.

### 5-2-Adsorbate

A yellow FG reactive dye (Remazol yellow 42) was obtained from Iraqi textile factory as a powder with solubility 150 g/l (manufacture companies). A stock of dye solution was prepared by dissolving the required amount of dye in distilled water. The dye was measured at a maximum wave length 420 (nm) using double beam spectrophotometer (Labomed, UVD. 3, 500 USA) and single beam spectrophotometer type (APEL PD- 303 UV JAPAN) which was used for the analyzing of samples. **Al-Degs, et al, 2009**

### 5-3 Isotherm Experiments

The batch adsorption isotherm experiments were carried out by varying adsorbent dosage m (0.05,0.1, 0.15, 0.2, 0.3and 0.4) g of activated carbon GAC which were added to 50cm$^3$ of aqueous dye solution with initial yellow concentrations $C_o$ 10 mg/l in a 100 cm$^3$conical flask. The mixture was agitated at 200 rpm in a shaker at a constant temperature and pH for 5 h. The suspensions were decanted and the solutions were analyzed for yellow reactive dye concentrations $C_e$ at equilibrium while adsorption capacity $q_e$ at equilibrium is calculated for each using Eq.(14)

$q_e=(C_o-C_e)*50/1000*m$

(14)

**5-4  Kinetic Experiments**

Effect of contact time was determined by the "limited bath" technique. A 5 g sample of GAC (m) was added to 500 ml volume of reactive dye solution with initial dye concentration 10 mg/l, under stirring for 5 h. The temperature was room temperature. After different time intervals (5, 15, 30,60,90,120,180,240 and 300 minutes) volumes of 5 ml of each sample analyzed for yellow reactive dye concentrations $C_t$ at time t then adsorption capacity were estimated using Eq.(15) for each sample.

$$q_t=(C_o-C_t)*50/1000*m \tag{15}$$

**5-5 Fixed Bed Column Experiments**

Removal of yellow dye in continuous process was investigated using fixed- bed of GAC in Perspex column with internal diameter  1.25 cm and length  50 cm **Fig. 1** at different conditions, bed height (5, 10, 15 and 20 cm), dye concentration (10, 20,40 and 80 mg/l), and flow rate (21.67, 12.5  and 6 ) ml/min. At the top of the fixed-bed, a layer of glass bed was used to provide uniform inlet flow to the column and the same layer was placed at the bottom to prevent discharging any AC particles during sampling. Dye solution was introduced into the top column and was controlled by perstatic pump range (1-10) ml/min which is adjusted for desired flow rates. Samples were collected at regular time intervals for analyzing.

**6-RESULTS and DISSCUSSION**

**6-1 -Equlibruim Isothrm**

**Fig. 2** shows $q_e$ vs. $C_e$ as a favaroble curve for reactive yellow dye adsorption by activated carbon due to  the  separation factor $R_L$ vlaue ( 0.69) when the standard range  is ( $0<R_L<1$).

Using $q_e$ and $C_e$ values of equilibrium isotherm were applied in Eqs. (2) and (5) to estimate Langmuir and Freundlich models constants and regression coefficients as shown in **Table 1**.

$R^2$ values show good fitting for both models with slightly larger for Freundlich than Langmuir, while deviation by average relative error shows good fitting with Freundlich model.

**6-2 Contact Time Effect**

The objective of adsorption kinetic study is to investigate the possible mechanisms for the adsorption process and to determine the time required to attain equilibrium. **Fig. 3** show the decrease of dye concentration $C_t$ and adsorption capacity at each sampling time were calculate by Eq. (15) and adsorption capacity at equilibrium $q_e$ equal to 0.865 mg/g at end of contact time (300 min).

The kinetics data of **Fig. 3** were analyzed using the linearized pseudo first and second order models presented in Eqs. (7) and (9). The parameters of the models are listed in **Table 2**

Results in **Table 2** show good correlation coefficients $R^2$ (0.978 and 0.987) by fitting the experimental data to pseudo-first and second order kinetic models. Comparing ARE% value shows low value for calculated $q_e$ by pseudo second order model Therefore, the adsorption is more favorably by pseudo second order kinetic model which is based on the assumption that the rate limiting step may be chemisorptions involving valence forces through sharing or exchange of electron between reactive yellow dye as asdorbate and activated carbon as adsorbent and these result with agreement conclusion by **(Ong et al. 2010)** and **( Sulyamon and Abood 2013**)

**6-3 Fixed –Bed Column**
**6-3-1 Effect of flow rates**
**Fig. 4** shows low effect of flow rate higher than 12.5 ml/min even though increasing flow rate decrease breakthrough time (the position at $C/C_0 = 0.1$) which were ( 25.67 , 16 and 13 min) and contact time (volume of bed/ flow rate ) (0.566 ,1 and 2.05 min) for flow rates (21.67,12.5 and 6ml/min) respectively. This is due to decreased contact time between the dye and the adsorbent at higher flow rates. When the flow-rate has smaller values, equilibrium correspondent with batch experimental data could be reached, and the shape of the curves is more like an ideal breakthrough curve, this result is in agreement explaining by **Liljana, 2001**

**6-3-2 Effect of bed depth.**
**Fig. 5** shows the breakthrough curve obtained for reactive yellow dye adsorption on the GAC for different bed height at a constant flow rate of 21.67 ml/min and dye inlet concentration of 10 mg/l where the breakthrough time increased (0, 15, 40, and 120 min) and contact time increased (0.283, 0.566, 0.849 and 1.039 min) for bed depth ( 5, 10, 15 and 20 cm) respectively. Increasing bed depth will provide more binding sites will be available for the yellow reactive dye to be adsorbed which will eventually lead to the attainment of a higher bed capacity. Also, an increased bed height results in more contact time being available for the dye to interact with the adsorbent. This phenomenon has allowed the yellow dye molecules to diffuse deeper into the adsorbent. Subsequently, the percentage of dye removal increased (low $C_t/C_o$) when the bed height was increased. Faster breakthrough curves were observed for a bed height of 5 cm, while the slowest breakthrough curve was observed at a bed height of 20 cm. The bed capacity ($q_e$) increased from 4.74 to 17.14 mg/g when the bed height increased from 5 to 20 cm. This results are in agreement with conclusion by **Zulfadhly et al., 2001.**

**6-3-3 Effect of initial dye concentration**
The initial dye concentration of the effluent is important since a given mass of adsorbent can only adsorb a fixed amount of dye. Therefore, the more concentrated an effluent, the smaller is the volume of effluent that a fixed mass of adsorbent can purify.
**Fig. 6** shows decreasing in breakthrough time (service time) (18, 5, 0, and 0) for increasing initial inlet reactive dye concentration (10, 20,40 and 80 mg/l) respectively due to initial dye concentration in the inlet constant flow ( constant contact time) is one of the limitation factors

and main process variables. An increase in the inlet dye concentration increased the slope of the breakthrough curve, reducing the efficiency of bed This may be caused by high yellow dye concentrations saturating the adsorbent more quickly, thereby decreasing the breakthrough time **Banat et al., 2007.** The dye concentration play driving force to mass transfer of dye from liquid phase ( yellow dye solution) to solid phase (adsorbent GAC) therefore high concentration increase rate constant and rapid saturation of adsorbent.

### 6-4 Mathematical Mode

Constants of ( Thomas and Yoon-Nilson) model were calculated using Eq.(10) and Eq.(11) at different variable  flow rate ,reactive yellow dye initial concentration and  bed depth as shown in **Table 3** while $T_{exp}$ values (50% $C_t/C_o$) were calculated approximately by breakthrough curves.

Examining results of **Table 3** show accepted values of $R^2$ (>0.944) at all conditions for both mathematical models Thomas and Yoon-Nelson. Adsorption capacity $q_o$ were approximately equal in both models which explain the harmony application of two models. The actual value shows fitting at low flow rate, initial yellow dye initial concentration and high bed depth $T_{cal}$ values for Yoon-nelson model show increasing at decreasing flow rate and initial yellow dye concentration and increasing bed depth and this is in match with $T_{exp}$. This result is in agreement with **Nwabanne, 2012** and **Sotelo et al., 2012.** ARE% for calculated and experimental T (50% $C_t/C_o$) which show good fitting with most variables.

The calculated adsorption capacity $q_o$ values were increased at increasing flow rate due to the larger mass transfer driving force at high flow rates where high velocity reduce resistance of molecule transfer of yellow dye from solution phase to solid phase. This is the same as at increasing inlet yellow dye concentration leading to the increasing of $q_o$ by models due to the fact that the mass transfer driving force increases with increasing the feed concentration which is in agreement with results by **Banat et al., 2007**. Calculated and experimental $q_e$ show increasing value at increasing bed depth (5-15 cm) and this disagrees with result at **Nwabanne, 2012** but was in agreement with results by **Sotelo et al., 2012**. This is may be due to more available adorable site will be provided at exact bed depth which lead to increasing mass of adsorbent then reduce $q_o$ value at constant initial dye concentration and flow rate.

Eq.(16) and Eq.(17) are used for the theoretical breakthrough curves using Thomas and Yoon-Nelson models **Trgo et. al., 2011** and comparing them with experimental one as shown in Figs. 7 and 8 respectively according to obtained parameters in **table 3**.

Thomas breakthrough curve is shown in Eq. (16)

$$\frac{C_t}{C_o} = \frac{1}{1+\exp\left[K_T(\frac{q*m}{Q} - Co*t)\right]}$$

(16)

Yoon-Nelson breakthrough curve is shown Eq. (17)

$$\frac{C_t}{C_o} = \frac{1}{1 + \exp\left[K_{YN} * (t - T)\right]}$$

(17)

The validity of models is shown in **Fig. 7 and 8** and Eq. (16) and Eq. (17) are used to estimate ARE% values at different flow rate, initial reactive yellow dye and bed depth.

**Table 4** shows that ARE% value for Thomas model less than Yoon- Nelson model for flow rate (>6 ml/min) and initial dye concentration except 20 mg/l while ARE% values are lower by Yoon-Nelson model than Thomas model, generally both models are considered acceptable due to that  Thomas model is widely used to predict adsorption in column study and Yoon –Nelson less complicated than the other models but also requires no detailed data concerning the characteristics of adsorbate, the type of adsorbent, and the physical properties of the adsorption bed like Thomas model. **Mohammad, 2013**

## 7-CONCLUSIONS

**-** Adsorption of reactive yellow dye onto granular activated carbon show good fitting with Langmuir and Freundlich equilibrium isotherms as chemisorptions process.

- Kinetic study shows good fitting with first and second order models but the ARE % shows the best results for second order model.

- Increasing breakthrough time with decreasing flow rates and initial yellow dye concentration and increasing bed depth of activated carbon in fixed bed experiments due to slowly bed saturation and more contact time respectively.

- Shortcut breakthrough curves models ( Thomas and Yoon-Nilson) show good fitting with all of experiment variables according to the ARE% values in fixed bed continuous process.

- Calculated adsorption capacity by (Thomas and Yoon -Nilson) models show increasing at increasing flow rate due to elimination of film thickness effect at high velocity.

- $T_{cal}$ and $T_{exp}$ by (Yoon –Nilson) model show good fitting at bed depth due to increasing contact time at constant velocity.

## REFERENCES

➢ Abood W. M., 2012, PhD. thesis, Baghdad University , College of engineering, Baghdad Iraq.


➢ Al–Degs Y. S., KhraishehM. A., Allen S.J. and Ahmed M., 2009, *Adsorption characteristics of reactive dyes in column of activated carbon*, J. Hazard. Mater. Vol. 165, pp.  944–949.

➢ Banat F. a, Al-Asheh S. b, Al-Ahmad R. a and Bni-Khalid F., 2007, *Bench-scale and packed bed sorption of methylene blue using treated olive pomace and charcoal,* l Bioresource Technology, Vol. 98, pp. 3017–3025

➢ Cavaseno, V., 1980, *Industrial Waste Water and Solid Waste Engineering*, Mc Craw-Hill Publication Co., New York, USA.

➢ Foo. K.Y. and Ahmed B. H , 2010, *Insight into the Modeling of Adsorption Isotherm Systems*, Chemical Engineering J.,  Vol. 156, pp.2-10.

➢ Goel, P. K., 1997, Water Pollution- causes, effects and control, New Age International Publishers, New Delhi, India.

➢ Ho, Y.S.  Ng, J.C.Y.  and McKay, G., 2000, *Kinetics of Pollutant Sorption By Biosorbents*: Review , separation and purification methods, vol.29, No.2 , pp.189–232.

➢ Hunger, K., 2003, *Industrial Dyes Chemistry, Properties, Applications* ,  WILEY-VCH Verlag GmbH & Co. KGA, Weinheim

➢ Isa, M. H., Lang, L. S., Asaari, F., Aziz, H., Ramli, N. and Dhas, J., 2007, *low Cost Removal of Disperse Dyes from Aqueous Solution Using Palm Ash* , Dyes and Pigments, vol. 74, pp. 446-453.

➢ Liljana Markovska, Vera Meshko and Vladimir N., 2001,  *Adsorption of Basic Dyes in a Fixed Bed Column*, Korean J. Chem. Eng., Vol. 18, No. 2, pp. 190-195 .

➢ Mohammad H. S., Mahmoud V. and Mohammad H. E., 2013, *A comparative study of copper (ii) removal on iron oxide, aluminum oxide and activated carbon by continuous down flow method*, Journal of Toxicology and Environmental Health Sciences, Vol. 5, No. 8, pp. 150-155.

➢ Nemerow N. L., 1971, *IndustrialWater Pollution-Origins, Characteristics and Treatment*, Addison-Wesley publishing company, Canada.

➢ Nwabanne, J. T., Igbokwe and P. K., 2012, *Adsorption Performance of Packed Bed Column for the removal of Lead (ii) using oil Palm Fibre International*, Journal of Applied Science and Technology Vol. 2, No. 5, pp106-117

➢ Ong S., Lee W., Keng P. and Ha S. T., 2010, *Equilibrium studies and kinetics mechanism for the removal of basic and reactive dyes in both single and binary systems using EDTA modified rice husk*, International, J. Phys. Sci.  Vol. 5, pp. 582–595.

- Peavy, H. S., Rowe, D. R., and Techobanoglous, G., 1986, *Environmental Engineering*, McGraw-Hill book company, New York, USA.

- Sachin M., Kanawade, Gaikwad, R.W. and Misal, S. A., 2010, *Low cost Sugarcane Bagasse Ash as an Adsorbent for Dye Removal from Dye Effluent*, International Journal of Chemical Engineering and Applications, Vol. 1, No. 4, December 2010, ISSN: 2010-0221

- Sotelo, J. L., Rodríguez, A., Álvarez, S. and García, J., 2012, *Modeling and Elimination of Atenolol on Granular Activated Carbon in Fixed Bed Column*, International Journal of Environmental Research, Vol6, No. 4 pp.961-968,.

- Sulyamon A. H. and Abood W. M. , 2013, *Competitive Adsorption of Three Reactive Dyes by Activated Carbon* , Journal of Engineering, Vol. 19, No. 6, pp. 655-670.

- Sulyamon A. H. and Abood W. M., 2013, *Removal of reactive yellow dye by adsorption onto activated carbon using simulated wastewater* , Journal of desalination and waste water treatment , Published online: 05 Jun 2013, pp.1-11.

- Tchohanoglous, G., Burton F. L. and Stensel, D., 2003, *Waste Water Engineering-Treatment and reuse*, Mc-Craw-Hill Co., 4th edition, Hong Kong, China.

- Thomas, W. J. and Crittenden, B., 1998, *Adsorption technology and Design*, Butterworth Heinemann, Oxford, UK.

- Trgo, M., Medvidovic, N. and Peric, J., 2011, Application of Mathematical empirical Models to Dynamic Removal of Lead 0n Natural Zeolite in Fixed Bed, Indian Journal of Chemical Technology, March, vol. 18, pp. 123-131.

- -ahaya, N. K., Latiff, M. F., Bello, O. S. and Ahmed, M., 2011, *Fixed-Bed Column Study Cu Removal from Aqueous Solution Using Rice Husk Based Activated Carbon*, International Journal of Engineering &Technology, vol. 11, No. 1, pp. 248-252.

- Zhe XU, Jian-guo CAI, and Bing-cai PAN, 2013, *Mathematically modeling fixed-bed adsorption in aqueous systems*, Journal of Zhejiang University-SCIENCE A (Applied Physics & Engineering) Vol. 14, No. 3, pp3.155-176.

- Zulfadhly, Z., Mashitah, M.D. and Bhatia, S., 2001, *Heavy metals removal in fixed-bed column by the macro fungus Pycnoporussanguineus*, Environmental Pollution, Vol. 112, No. 3, pp. 463-470.

### NOMENCLATURES

C     Dye concentration in aqueous solution(mg/l) .

$C_e$     Dye concentration in liquid phase at equilibrium (mg/l).

$C_t$     Dye concentration in liquid phase at time of sampling (mg/l).

$C_o$     Initial dye concentration in aqueous solution(mg/l).

$K_1$     Pseudo-first-order rate constant $(min^{-1})$.

$K_2$     Pseudo-second order rate constant$(g\ mg^{-1}\ min^{-1})$

$K_F$     Freundlich constant $(mg\ g^{-1})$

$K_L$     Langmuir adsorption constant $(l\ mg^{-1})$

$K_T$     Thomas rate constant (mL/min.mg)

$K_Y$     Yoon-Nelson rate constant(1/min)

N

m     Adsorbent dosage (g)

n     Freundlich parameter

N     Number of tested sampling

Q     Flow rate $(m^3/min)$

q     Adsorption capacity  mg/g

$q_e$     Aquilibrium dye concentration in solid phase$(mg\ g^{-1})$ .

$q_o$     Adsorption capacity (calculated by model and estimated by experimental results)
(cal    mg/g)

$q_t$     Amount of dye adsorbed per unit mass of adsorbent at time t $(mg\ g^{-1})$

$q_m$     Langmuir isotherm parameter, maximum dye adsorbed/unit mass of adsorbent (mg $g^{-1}$)

$R_L$     Separation factor( favorability index of Langmuir  isotherm model  curve)

T     Time of (50% Ct/Co removal in fixed bed)  Yoon model parameter. min

t     Time (min)

V     Treated water volume (ml)
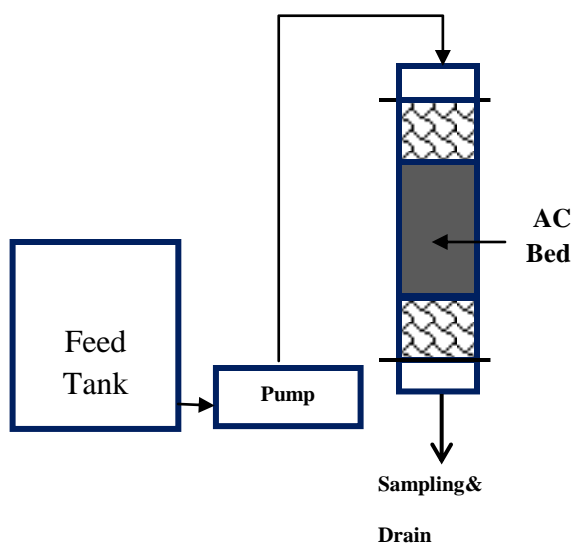
**Figure 1.** Fixed bed column diagram.
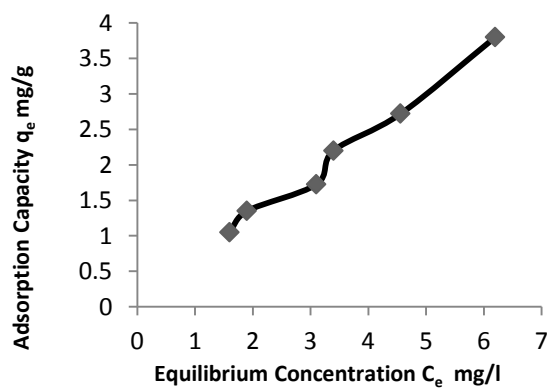


**Figure 2.** Equilibruim isotherm curve.
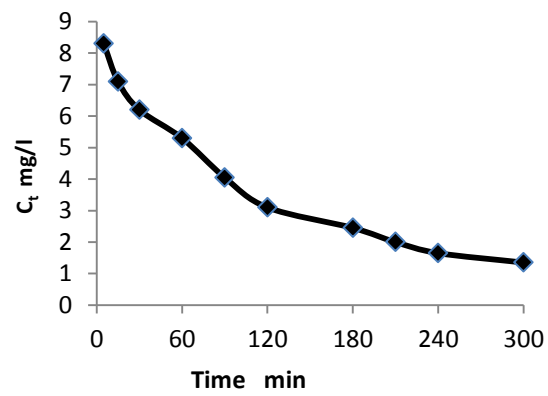
**Figure 3.** kinetic curve
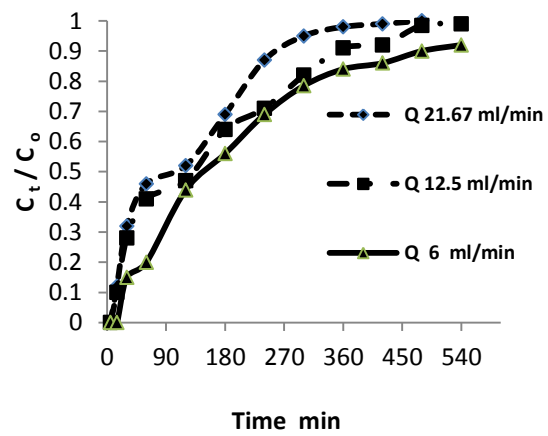


**Figure 4.** Effect flow rate in fixed bed column
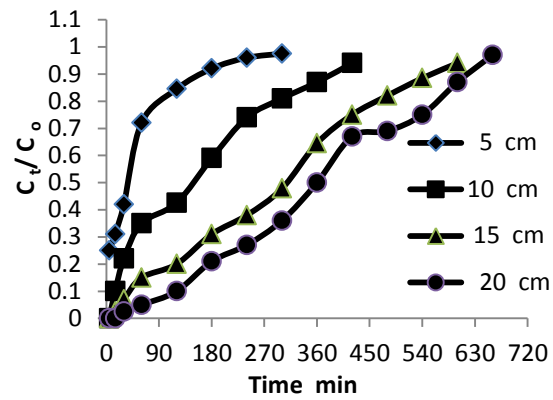
**Figure 5.** Effect bed depth column
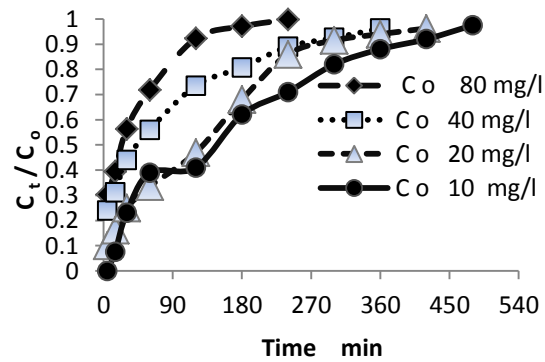


**Figure 6.** Effect of concentration dye

172

**breakthrough curve**
**Q 6 ml/min   Co 10 mg/l   bed depth 10 cm**

Exprimental curve

Thomas theoritecal curve

**C_t / C_o**

**Time  min**

**breakthrough curve**
**Q  21.67  ml/min    Co 20mg/l   bed depth**
**10 cm**

Exprimental curve

Thomas theoritecal curve

**C_t / C_o**

**Time  min**

**breakthrough curve**
**Q 21.67 ml/min  Co 10 mg/l  bed depth 20cm**

Experimental curve

Thomas theoritecal curve

**C_t / C_o**

**Time min**
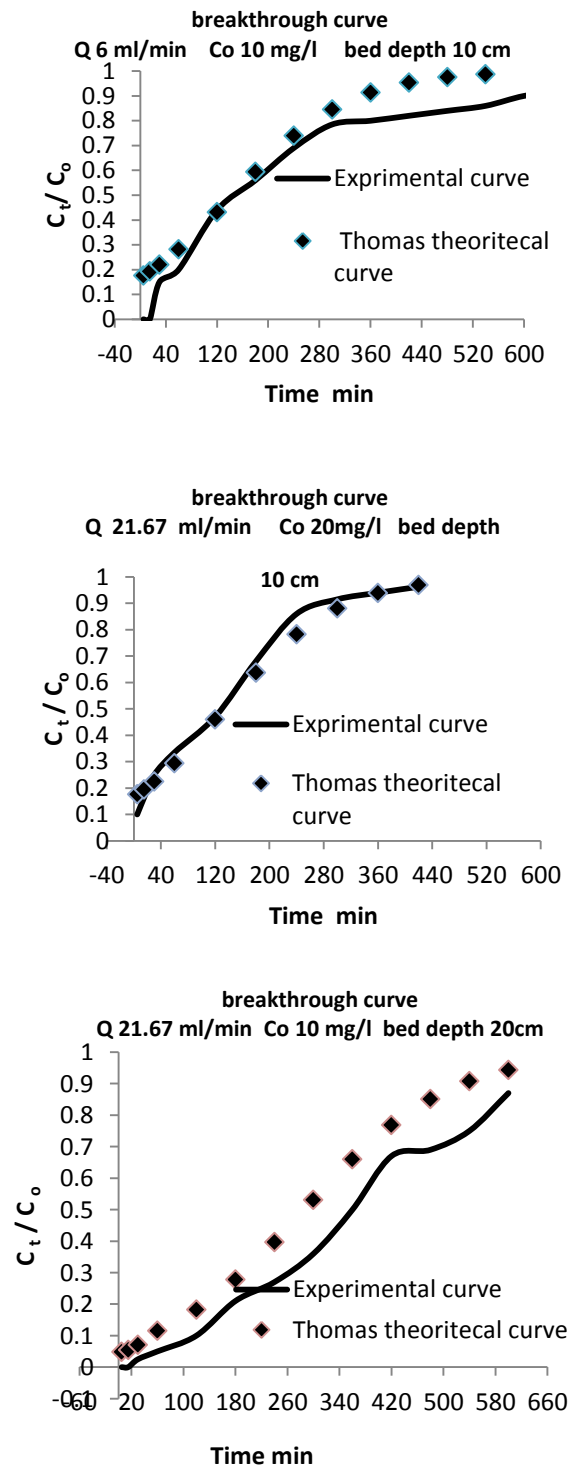
**Figures 7** . Thomas model application of fixed bed column.

173

**breakthrough curve**
**Q  6 ml/min  Co 10 mg/l bed depth  10 cm**



**breakthrough curve**
**Q 21.67 ml/min  Co 20 mg/l     bed depth 10 cm**
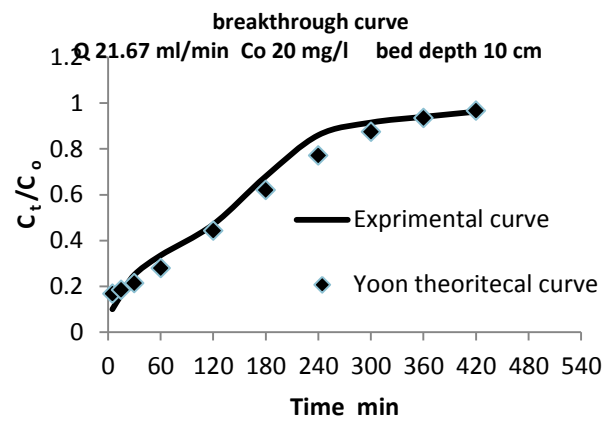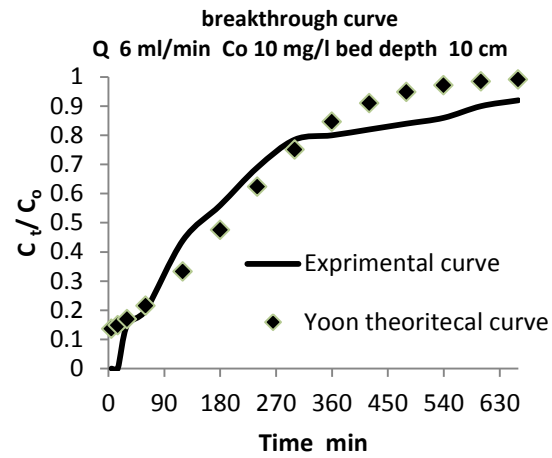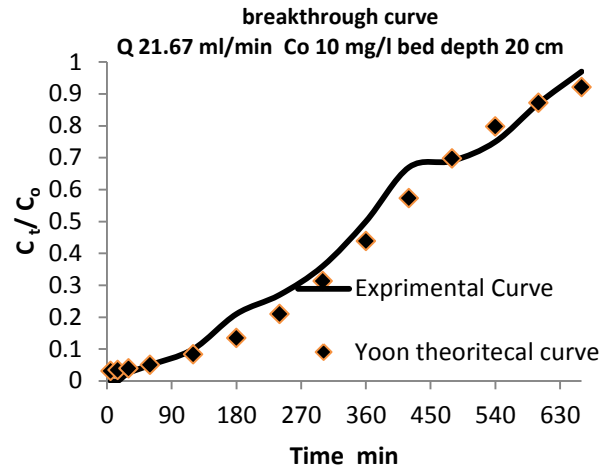
**Figures 8.** Yoon-Nelson model application of fixed bed column

**Table 1.** Equilibrium isotherm models constants.

| Langmuir model | Freundlich model |
|---|---|
| $K_L$ (l/mg)0.045 $R_L$0.69 | $K_F$(mg/g) 0.699 |
| $q_{m(}$mg/g)16.13 | N1.1 |
| $R^2$0.972 | $R^2$0.977 |
| ARE %4.7 | ARE%2.15 |

**Table 2.** kinetic models parameters.

| pseudo first order | Pseudo second order |
|---|---|
| $K_1$ (1/min)0.012 | $K_2$(g/mgmin )0.023 |
| $q_{e(cal)(}$mg/g)0.756 | $q_{e(cal)}$ (mg/g) 0.97 |
| $R^2$0.978 | $R^2$0.987 |
| ARE %12.2 | ARE %12.1 |

**Table 3.** Calculated parameters of mathematical breakthrough models.

| Models | Flow rates ml/min | | | Yellow dye Conc. mg/l | | | | AC Bed depth cm | | |
|---|---|---|---|---|---|---|---|---|---|---|
| | 21.67 | 12.5 | 6 | 80 | 40 | 20 | 10 | 20 | 15 | 10 |
| Thomas $K_T$ (ml/min/mg) | 1.1 | 1.1 | 1 | 0.275 | 0.325 | 0.6 | 1.05 | 0.9 | 0.9 | 1 |
| $q_{ocal}$ (mg/g) | 4.137 | 2.03 | 1.15 | 6.87 | 6.7 | 6.42 | 4.168 | 4.168 | 4.85 | 4.04 |
| $R^2$ | 0.952 | 0.959 | 0.989 | 0.985 | 0.967 | 0.972 | 0.947 | 0.968 | 0.962 | 0.96 |
| Yoon- nelson | | | | | | | | | | |
| $K_{YN}$ (min$^{-2}$) | 0.011 | 0.011 | 0.01 | 0.026 | 0.012 | 0.011 | 0.0105 | 0.009 | 0.009 | 0.01 |
| $q_o$ (mg/g) | 3.07 | 2.02 | 1.15 | 5.78 | 6.36 | 6.74 | 4.165 | 4.66 | 4.85 | 4.08 |
| $T_{cal}$min (%50$C_t/C_o$) | 127.2 | 145.7 | 172.7 | 30.2 | 66.4 | 140 | 165 | 387 | 313.4 | 168 |
| $R^2$ | 0.95 | 0.96 | 0.988 | 0.985 | 0.967 | 0.972 | 0.965 | 0.968 | 0.96 | 0.96 |
| $T_{exp}$ min (%50 $C_t/C_o$) | 100 | 130 | 155 | 25 | 42 | 130 | 150 | 360 | 312 | 145 |
| ARE% ($T_{cal}$&$T_{exp}$) | 27.2 | 12. | 11.4 | 20.8 | 56 | 7 | 10 | 7.5 | 0.4 | 15 |
| $q_{oexp}$.(mg/g) | 2.85 | 1.89 | 1.05 | 5.99 | 7.03 | 5.51 | 3.48 | 4.03 | 4.25 | 3.44 |

**Table 4.** ARE Percentage

| **Model** variable | Thomas ARE% | Yoon-Nelson ARE% |
|---|---|---|
| Flow rates ml/min 21.67 12.5 6 | 2,17 7.7 1.9 | 9.8 7.6 0.9 |
| Initial dye Conc.mg/l 80 40 20 10 | 0.2 2.7 1.9 11.1 | 1.7 4.4 6.6 11.6 |
| Bed depth cm 5 10 15 20 | 5.9 10.1 21.2 14.1 | 5.1 7.8 1.2 4.5 |

# Corrosion Study of the Injection Equipments in Water in Al-Ahdeb Wells -Iraq

**Hassan Abdulkadhim Alwan Alsaadi**
Assistant Lecturer
Engineering College-Baghdad University
E-mail: alwan_hassan@yahoo.com

## ABSTRACT

**W**ater injection equipments such as pipelines, which are used in the second recovery of oil in the Al-Ahdeb wells, suffer from the corrosion in water during maintaining vacuum deoxygenated tower that used to decrease concentration of the dissolved oxygen gas in the water from 6.2-9.1 ppm to o.5 ppm. This study involved calculation the corrosion rates of the internal surfaces of the pipelines either during operation of the vacuum unit or when the tower out of operation. Finally, find the solution by one of the following suggestions. In the first suggestion removal of the dissolved $O_2$ from water is achieved by increasing the dosage of the oxygen scavenger (sodium sulphite). The second suggestion involves removing the dissolved $O_2$ from water by bubbling the oxygenated water with nitrogen gas. The study showed that the corrosion rates of various inside diameter pipelines are between 0.13 mm/yr and 1.5 mm/yr during operation of the vacuum tower and between 3.2 mm/yr and 18.5 mm/yr when the tower out of the operation. While the results showed that the corrosion rate of the pipelines when the tower out of operation reached to the acceptable value of 0.1 mm/y when the dissolved oxygen in the injected water removed by increasing the dosage of the sodium sulphite ($Na_2SO_3$) to 48-72 ppm. The results also explained that corrosion rates of the pipelines reached to 0.5 mm/y when the dissolved oxygen removed by bubbling the water with nitrogen gas.

**Key Words:** Corrosion, deaerated water, oxygen scavenger, aerated water

**الخلاصة**

معدات وانابيب حقن الماء المستخدمة ففي عملية زيادة انتاج النفط في حقول الاحدب تعاني من مشكلة التأكل في الماء الحاوي على الأوكسجين ويصل معدل التأكل الى اعلى قيمة له خلال فترة صيانة وحدة التفريغ المستخدمة لتقليل تركيز الأوكسجين الذائب في الماء من 6.2-9.1 جزء بالمليون الى 0.5 جزء بالمليون. هذه الدراسة اشتملت على حساب معدلات التأكل لسطح الأنابيب الداخلية في حالة ان تكون وحدة تفريخ الأوكسجين في الخدمة او خلال فترة صيانتها. هذه الدراسة اشتملت على اقتراح تقنيتان من اجل التخلص او تقليل تركيز الأوكسجين في الماء خلال فترة صيانة وحدة تفريغ الأوكسجين. في المقترح الأول تقليل تركيز الأوكسجين بواسطة زيادة كمية المواد الكيمياوية (مادة كبريتيد الصوديوم) التي تتفاعل مع الأوكسجين وينتج عنه مادة غير أكلة للمعادن. المقترح الثاني اشتمل على تقليل تركيز الأوكسجين في الماء عن طريق تعريض الماء الى غاز النتروجين. الدراسة اوضحت على ان معدلات تأكل السطوح الداخلية الأنابيب ذات اقطار داخلية مختلفة يتراوح بين 0.13ملم/سنة و1.5 ملم/سنة في حالة التي تكون وحدة التفريغ في الخدمة. بينما معدلات تأكل السطوح الداخلية الأنابيب ذات اقطار داخلية مختلفة تراوح بين 3.2 ملم/سنة الى 18.5 ملم/سنة عندما تكون وحدة التفريغ تحت الصيانة. نتائج هذه الدراسة ايضا اوضحت بان معدلات تأكل الانابيب وصلت الى الحدود المسموح بها وهي اقل من 0.1 ملم/سنة عندما تم تقليل تركيز الاوكسجين عن طريق اضافة بين 48 الى 72 جزء بالمليون من مادة كبريتيد الصوديوم . اخيرا بينت النتائج ايضا بان معدل تاكل الانابيب اصبح 0.5 ملم/سنة عن طريق تقليل تركيز الاوكسجين في الماء بواسطة غاز النتروجين.

**الكلمات الرئيسية :** ألتأكل, الماء الغير مهوى (الخالي من الاوكسجين), قانص الاوكسجين, الماء المهوى (الحاوي على الاوكسجين)

## INTRODUCTION

Generally the water injection systems are used in oil industries in order to increase the oil production. This occurs when the water is injected into the reservoir at high flow rate or at high pressure. As result, the pressure of the oil reservoir rises. Consequently, the quantity of the oil recovery from the well increases. The sources of water, which are used in this process, vary from seawater, produced water, lake, and river **Havard, 2oo6, Stephen et al.,1989**. All these types of water contain dissolved oxygen approximately 8-9 ppm at 20 C° which causes corrosion of the internal surface of the injection system equipments such as pipelines. The cathodic reaction is oxygen reduction Eq. (1), while the metal dissolution is the anodic reaction Eq. (2).

The corrosion rate of the metal is controlled by rate of the mass transport of the dissolved oxygen from bulk to the solution/metal interface. Therefore, $O_2$ should be removed from the Injected water before pumping into the reservoir. There are many methods that are used in the oil production in order to eliminate the concentration of the dissolved oxygen in the water such as mechanical deaeration combination with the chemical process. The former process is used before the chemical treatment. In the mechanical deaeration removal oxygen can be established by either introducing steam into the water that leads to increase the temperature of the water. As a result, oxygen will releases from the water to the atmosphere and consequently the concentration of oxygen decreases or by using vacuum process such as that uses in the Al-Ahdeb wells. In this process vacuum pumps are utilized in order to reduce the partial pressure of $O_2$ in the gas phase. Hence, concentration of the dissolved $O_2$in the feed water will reduce [Havard, 2oo6, Stephen et al.,1989].While removal oxygen by chemical process is achieved by adding a small amount of chemical substance {either hydrazine ($N_2H_4$) or sodium sulfite ($Na_2SO_3$)} to the water which reacts with oxygen **Stephen et al.,1989,Zaki, 2006, Nathan,1981**.

Three vacuum deoxygenation packed towers, which have installed recently by Al-Waha company one of the Chinese companies, uses to remove the gas of $O_2$ from water that utilized to enhance the oil production in the Al-Ahdeb wells in the Al-Kut city. According to the Al-Waha document, this process leads to decrease concentration of $O_2$ in the water to 500 ppb (0.5 ppm) [Al Ahdeb Wells, 2013]. Although the corrosion rate of the system equipment will decrease, but it not within the acceptable value 0.1 mm/yr. In addition to the aggressive environment (dissolved $O_2$), the pipe lines, which transport the water from the water tank to the wells, are subjected to the high stress (water pressure). The stress values reaches to 17 Mpa at the high pressure section and 12 Mpa at sub high pressure section. Hence, the pipelines will susceptible to the stress corrosion cracking (SCC), which takes place when a metal/an alloy is subjected to the combination of aggressive environment ($O_2$) and stress (water pressure) **Zaki,2006, Nestor,2004**.

The aim of this research is to study and calculate the corrosion rates of the internal surface of the water injection components (pipelines) when the Vacuum deoxygenation tower will be out of operation and then find the solution.

## 1- OPERATION OF THE SYSTEM

In Al-Ahdeb wells, removing dissolved oxygen from water takes place in two processes, vacuum and chemical processes. The vacuum process carries out in three vacuum deoxygenation packed towers that are parallel operated. Each tower consists of two stages. In the first stage most of the dissolved $O_2$ gas is removed from feed water to the gas phase by vacuum process. In the second stage the oxygen scavenger is added to the deaerated water. Hence, further removing of dissolved $O_2$ from water takes place by the chemical process **Al Ahdeb Wells, 2013**.

The O$_2$-free water is transported to the deaerated water tank through 18-20 in. inside diameter of carbon-steel pipe at flow rate 900-1075 m$^3$/h. In addition to the deaerated water, the deaerated water tank is also supplied with formation water (produced water) after treatment. Then, the deaerated water and produced water (injected water) pumping to the high pressure section and sub high section through 28 in. id pipe at flow rate 4200 m$^3$/h. At the high pressure section, the injected water is transported to the oil gathering main field (OGM) through 8 in. id steel pipes at flow rate 150 m$^3$/h and pressure 17 Mpa (170 bar). While, at the sub high section the injected water is transported to the different (OGM) through pipes, which have the same inside diameter (16 in), and at equal flow rate 650 m$^3$/h and pressure 12 Mpa. Finally, the injected water is pumping from the (OGM) to the many wells through pipes, which have the same inside diameter (6 in), and at equal flow rate 5000 bbl/day and pressure either 17 MPa. or 12 MPa. depending on the source of the water injection **Al Ahdeb Wells, 2013**.

## 2- OPERATION CONDITION OF THE TOWER

According to the Al-Waha documents, operation conditions of the unit are represented in the Table1. As can be seen from the Table, concentration of the dissolved O$_2$ in the inlet water is not recorded. This is because of it depending on the solubility of the gas in the water which is function to the temperature of water (i.e operating temperature). As the temperature of water increases, the solubility of dissolved O$_2$ in the water decreases. Consequently, concentration of dissolved O$_2$ decreases. The concentration of dissolved oxygen in the outlet water is 500 ppb (0.5 ppm) as recorded in the Table1. In order to treat the microbiological induced corrosion (MIC), which forms on the surface of the structure of the system such as sulfate reducing bacteria (SRB), the chemical removal oxygen process will be stopped for a certain time and adds biocide species.

## 3- PROBLEM

In the water injection system there is a problem will appear during either shutdown of the deaeration unit or normal maintenance when the concentration of the oxygen in the water will be at high value. This leads to
corrode the internal surfaces of the system equipments as shown in Fig.1 Therefore, it should calculate the corrosion rate of internal surface of the system components when the deaeration unit will be out of operation and find the solution.

## 4- EXPERIMENTAL WORKWS

The experimental works consist of two steps. In the first step, the lowest concentration of the dissolved O$_2$ gas in the water, which can be obtained by bubbling water with nitrogen gas, was estimated by doing an experimental work. In the second step corrosion rate of the internal surfaces of the pipelines, which made of carbon steel, are calculated under aeration and deaeration conditions of water.

First step, The experimental work of dissolved oxygen removal from water by using nitrogen gas stream was done in order to estimate the lowest concentration of dissolved gas of oxygen in water that can be obtained after the deaeration process. The experiment includes preparation an electrochemical cell that consists of a calomel electrode as a reference electrode and two platinum wires as working and auxiliary electrodes (note, in this step it is not necessary to use iron as working electrode). All electrodes were immersed in electrolyte that prepared by dissolving 4.5% of NaCl in one liter of distilled water. Then, the electrochemical cell was connected to a potentiostat in order to polarise the cell during deaeration process as shown in **Fig. 2.**a nitrogen gas stream was used to deaerate the system. This was achieved by bubbling a

solution with pure nitrogen gas which caused removal of a high proportion of the dissolved oxygen gas from the system to the water-containing flask and then to the atmosphere through a vent present at the top of the flask. As a result, a decrease in the concentration of the dissolved oxygen gas in an electrolyte (water) is obtained according to the Henrys law. Residual dissolved oxygen in the system can be controlled by the period of deaeration process and preventing an oxygen gas from entering to the system either during or after deaeration process.

Second step, corrosion rates of the pipelines are calculated during aerated condition and deaerated condition by using equations that derived experimentally by scientists. Concentration of O2, which used in the calculation, are obtained from the references and from the experimental work of this study.

## 5- CALCULATION AND RESULTS

Calculation and result can be divided into two parts, the first part includes prediction corrosion of the injection equipments (i.e. pipelines) in injected water at flow condition and in either deaerated or aerated condition. While the second part of calculation involves estimate the lowest concentration of dissolved oxygen in the injected water after deoxygenated of water with nitrogen gas.

First part, corrosion of the pipelines in injected water at flow condition and in either deaerated or aerated condition can be predicted by studying the effect of flow velocity of the water on the mass transfer of the dissolved $O_2$. As result, the corrosion rates of the pipelines increase .

Flow in pipes is usually turbulent that destroys the concentration gradients in the bulk of the fluid, and all the action affecting  then takes place in a very thin boundary layer of fluid adjacent to the pipe wall. Consequent, the flux of the dissolved $O_2$ increases **Scheers,1992**.

Equations relating mass transport and flow velocity for various geometries have been derived by several authors. While several equations describing mass transfer in pipes have been deduced theoretically, others have been derived experimentally. These equations, which are classified according to the value of Schemidt number ( $Sc$ ) **Scheers,1992, Van den Berg et al.,1989**.

Chilton-Colburn relation Eq. (3) is used for SC< 1, for 1 <SC< 1000 Deissler equation is used see Eq. (4), and Harriott-Hamilton relationship is used for SC>1000  see Eq. 5.

Hence, in the first step of the calculation, it is required to select one of the above equations by calculation Schemidt number ($Sc$) for injected water by using Eq. (6).

At T = 20°C, $v$ = 1x10$^{-6}$  (m$^2$/sec), $D$ = 1.8x10$^{-9}$ (m$^2$/sec)     (see **Table 3**)
At T = 40°C,  $v$ = 6.6x10$^{-7}$ (m$^2$/sec), $D$ =3.7x10$^{-9}$ (m$^2$/sec)     (see **Table 3**)
$Sc$ = 555.55 at 20°C and $Sc$ = 178.38 at 40°C.
According to the above values of $Sc$ either Eq. (4) or Eq. (7) is used for calculation the mass transfer coefficient ($K$).

As it is mentioned before that the corrosion rate of the metal in water is controlled by the rate of transport of the oxygen to the surface of the metal and the cathodic current density reaches to the limiting value. Therefore, the second step of this calculation includes calculation the limiting current density ($I_{lim}$) by using equation Eq. (10) **Hongwei, 2000**.

Third step involves converting the limiting current density ($I_{lim}$) into a rate of dissolution of the internal surfaces of the pipe lines, which made of carbon steel, by using the Faraday's law Eq. (11) **Zaki,2006**:

The results are represented in the **Table 3**, while corrosion rates of the equipments during operation of the deaeration unit are represented in the **Table 2**.

The second part of this calculation involves estimate the lowest concentration of dissolved oxygen in the injected water after deoxygenated of water with nitrogen gas. **Fig. 3** shows polarization curve of the working electrode (platinum wire) after deaerating the cell for certain time.

As can be seen from **Fig. 3**, the limiting current density at aerated condition is 8.68 A/m$^2$ at potential -0.85V SCE, whereas the limiting current density at deaerated condition is 0.462 A/m$^2$ at -0.55V SCE .The lowest oxygen concentration achieved by deaerating the water with nitrogen gas can be calculated from the cahodic current density. It was limited by the diffusion rate of oxygen to the platinum surface according to Fick's firs law see Eq. (12).

The cathodic limiting current density was achieved when the concentration of dissolved species at the WE became depleted, i.e. $C_s$ = zero see Eq. (13).

Since thickness of the diffusion layer in the case of deaeration is similar to that in the aerated condition, therefore it can be calculated by using Eq.(13) for aerated system according to the following data at room temperature:

$C_b$ = 8 ppm (mg/l or g/m$^3$).

$C_b$ = 0.25 mole/m$^3$ (atomic mass of O$_2$ 32 g/mole).

$D_{O2}$ = 2 x10$^{-9}$ m$^2$/s (diffusion coefficient of O$_2$ in water).

$I_{lim}$= 8.68 A/m$^2$ from Figure3(i.e for aerated curve)

$F$ = 96,500 C/mole

$n$ = 4 electrons that required for oxygen reduction

$$8.68 \text{ A/m}^2 = \frac{2\text{x}10^{-9}\,\text{m}^2/\text{s}*4*96,500\,\text{C}/\text{mole}*0.25\,\text{mole}/\text{m}^3}{x}$$

$x$ = 2.22x10$^{-5}$ m

Now calculate concentration of dissolved oxygen in solution under deaerated condition. The lowest I$_{lim}$, which was achieved after aerating process, was 0.462 A/m$^2$ at E -0.55 V SCE (see **Fig. 3**). Using Eq.(13) to calculate $C_b$ in deaerated condition:

$$0.462 \text{ A/m}^2 = \frac{2\text{x}10^{-9}\,\text{m}^2/\text{s}*4*96,500\,\text{C}/\text{mole}*C_b}{2.22\text{x}10^{-5}\,\text{m}}$$

$C_b$ = 0.013 mole/m$^3$

$C_b$ = 416 ppb

The corrosion rate of injection pipelines can be calculated by using Eq. (11)

$CR$ = 0.5 mm/year

## 6- DISCUSSION AND SOLUTIONS

**Fig. 1** shows the limiting current densities for aerated and deaerated conditions. While **Table 2** and Table3 show the corrosion rates of various pipelines during operation the vacuum deoxygenation packed towers and during maintenance respectively. It can be seen from **Table 2** that although most of the dissolved $O_2$ gas is removed from water by the deaeration process, but the corrosion rates of the pipe lines are still higher than the acceptable value that is 0.1 mm/yr. This because of the concentration of the remaining dissolved oxygen in the water, which leaves the vacuum towers after deoxygenation process, is high 0.5 ppm (500 ppb) as shown in the **Table 1**. Whereas **Table 3** explains that the $O_2$ related corrosion rates of various diameter pipelines are high when the vacuum deoxygenation tower is out of the operation. **Table 3** also explains that the corrosion rate of a pipeline strongly depends on the water flow rate. As the flow rate of injected water increases, thickness of the diffusion layer decreases and hence the flux of the oxygen increases **Coulson et al.,1999**. Therefore, the corrosion rate of a pipe lines increase. It can be seen from the same **Table** that the CR of 8 in. id pipeline is 7 mm/yr at 150 m$^3$/hr, while the CR of 28 in. id pipeline is 18.5 mm/yr at 4200 m$^3$/hr. On the other hand, the corrosion rate of a pipeline decreases with increasing the diameter of a pipeline.

It also can be seen from the **Table 3** the effect of the temperature of the injected water on the corrosion rate. Although the concentration of dissolved oxygen in water decreases with increasing temperature, but the corrosion rate of a pipeline increases. This because of increasing temperature leads to increase the diffusivity of the oxygen in the water. Consequently, the oxygen flux increases and hence the corrosion rate increases **Coulson et al.,1999**. The corrosion rates of a pipelines during maintenance of the deaeration unit can be calculated by multiplying the corrosion rate of a pipe line in mm/month by a period of a maintaining.

In both cases when either the vacuum towers operate or out of operation, in additional to the general corrosion, the pipe lines will susceptible to the stress corrosion cracking (SCC) as it be mentioned in the introduction. Therefore, it is necessary to remove or to eliminate quantity of dissolved $O_2$ gas in the injected water to acceptable value 0.01 ppm (10 ppb) especially when the water injection system operates without the deaeration process (i.e. vacuum towers are out of operation). These can be achieved either by increasing the amount of the chemical species that acts as oxygen scavenger or by bubbling the water with nitrogen gas. Each option will be discussed separately.

The first recommendation involves increasing the amount of the scavenger added to compensate for the loss of the dearation unit. The new amount of the oxygen scavenger, which will be added to the system, should be sufficient to reduce the concentration of dissolved oxygen from either 9.1 ppm at 20°C or 6.2 ppm at 40°C into 0.01 ppm (10 ppb). This will reduce the reduction of $O_2$ (cathodic reaction) and iron dissolution (oxidation reaction) that take place on the internal surfaces of the injection system pipelines and oil production during the repair of the dearation unit. There are many chemical species that are used as oxygen scavenger but sulfite and hydrazine are the most common oxygen scavengers agent for water system. It prefers to use sodium sulfite ($Na_2SO_3$) to remove the $O_2$ from water. This is because hydrazine is very toxic and dangerous **Zaki, 2004, Nathan,1984**.

According to the chemical equilibrium reaction Eq. (14), two mole of $Na_2SO_3$ are required for remove one mole of dissolved oxygen.

Where the atomic mass of $2Na_2SO_3$ = 252 gm/mole, and atomic mass of $O_2$=32 g/mole. Then, the number of parts (grams) of sodium sulfite that required to remove one part of dissolved oxygen from water = 8 parts (grams) of $Na_2SO_3$ per part (gram) of $O_2$. Therefore, it is required to add 48-72 ppm of sodium sulfite for reduce the concentration of dissolved oxygen from 6.2-9.1

ppm to 0.01 ppm. As result the corrosion rate of the pipelines and other equipments of the injection system decrease to acceptable values as shown in **Table 4**.

On the other hand, the performance of the sodium sulfite affects by presence of the anearobic sulphate reducing bacteria (SRB) in the system which utilise sulphate to produce high aggressive substance such as $H_2S$. It forms unprotective sulphide corrosion product. This is can be treated by adding Biocide to the injected water in order to prevent formation the SRB on the inner surface of the pipelines and other structure.

The second suggestion is deaerated the injected water, which is utilized to enhance the oil production, by using nitrogen gas stream and this process should take place in the water injection tank before transport through pipelines into the wells **Barnhart,1995**. This was achieved by bubbling a solution with pure nitrogen gas which caused removal of a high proportion of the dissolved oxygen gas from the water to the atmosphere. As a result, a decrease in the concentration of the dissolved oxygen gas in an electrolyte (water) is obtained according to the Henrys law. The experimental result showed that the residual dissolved oxygen in the water was 0.013 mol/m$^3$(416 ppb) and the corrosion rate of metal was 0.5 mm/year. Amount of the residual dissolved oxygen in the injected water can be controlled by the period of deaeration process and preventing an oxygen gas from entering to the system either during or after deaeration process.
This process can be used combine with chemical species in order to reduce the quantity of oxygen scavenger, which used to eliminate the concentration of dissolved $O_2$ in water. Hence, the cost of using oxygen scavenger will be reduced and the dangerous of SRB also will be eliminated.

## 7- CONCLUSION
It can be concluded that presence dissolved oxygen in the water which is injected to the oil wells, without treating causes severe damage of its structure. The $O_2$ related corrosion rate is predicted to be higher during the repair of the deaeration unit. This influence can be reduced by increasing the amount of the oxygen scavenger between 48 to 72 ppm which reacts chemically with the dissolved $O_2$. This influence also can be overcome by bubbling the water with oxygen-free nitrogen gas which caused removal of a high proportion of the oxygen gas from the system to the atmosphere through a vent present at the top of the water injection tank and experimental result showed that the residual dissolved oxygen in the water was 0.013 mol/m$^3$(416 ppb) and the corrosion rate of metal of the internal surfaces of the pipelines, which is made of carbon steel, was 0.5 mm/year.
The first and second recommendations could be used together in order to decrease the cost of the chemical substance, which be used as $O_2$ scavenger, and the dangerous of SRB also will be eliminated.

## REFERENCES
- Al Ahdeb Well Documents, 2013, Al Kut, Iraq.

- Barnhart, M. C., 1995, *An Improved Gas Stripping Column for Deoxygenating Water*, J. N. Am. Benthol. Soc., Vol.14, No. 2, pp. 347-350.

- Coulson, J.M., Richardson, J.F., Marker, J. H., Backhurst, J. R., 1999, *Chemical Engineering* Vol. 1, 6$^{th}$ edition, UK.,
- p. 279.

- Havard, D., 2006, *Oil and Gas Production HandBook*, ABB ATPA Oil and
- Gas.

- Hongwei, W., Tao,  H., Ji-Yong, C.,Howard,  D.D., William, P.J., 2000, *Enhancement of the Instantaneous Mass-Transfer Coefficient in Large Diameter Pipeline under Water/Oil Flow*,Journal of The Electrochemical Society, Vol. 147, no. l, pp. 2552-2555.

- Josepn, K., Mordechai, S., William, A.w., 1978, *Viscosity of Liquid Water in the Range -8°C to 150°C*, J. Phys. Chem., Vol. 7, No. 3, pp. 941-948.

- Nathan, C. C., 1981, *Corrosion Inhibitors*, 5[th]edithion, NACE.

- Nestor, P., 2004, *Electrochemistry and Corrosion*", Kluwer Academic Publishers, Boston, USA.

- Scheers, P.V., 1992, *The Effects of Flow Velocity and pH on the Corrosion Rate of Mild Steel in a Synthetic Mine Water*, J. S. Afr. Inst. Min. Metall., vol. 92, no.10, Oct.  pp. 275-281.

- Stephen, C.R., John, F.B., Robert, J.W., 1989, *The Design Engineering Aspects of Water Flooding*, Society of Petroleum Engineers Inc., Vol.11, USA.

- Van den Berg, G.B., Racz, I.G., Smolders, C.A., 1989, *Mass Transfer Coefficients in Cross-Flow Ultrafiltration*, Journal of Membrane Science, vol.47, pp. 25-51.

- Verhallen, P.T.H.M., Oomen, L.J.P.,  Elsen, A.J.J.M.v.d., Kruger, A.J., Fortuin, J. M. H., 1984, *The Diffusion Coefficients of Helium, Hydrogen, Oxygen and Nitrogen in Water Determined from the Permeability of a Stagnant Liquid Layer in the Quasi-Steady State*, Chemical Engineering Science, Vol. 39, No. 11, pp. 1535-1541.

- Zaki, A., *Principle of Corrosion Engineering and Corrosion Control*, 1st edition, printed in UK, 2006, p. 370.

**EQUATIONS**

$$Fe \rightarrow Fe^{2+} + 2e^- \tag{1}$$

$$O_2 + 2H_2O + 4e^- \rightarrow 4OH \tag{2}$$

$$Sh = 0.023 Re^{0.8} Sc^{0.33} \tag{3}$$

$$Sh = 0.023 Re^{0.875} Sc^{0.25} \tag{4}$$

$$Sh = 0.0096 Re^{0.91} Sc^{0.35} \tag{5}$$

$$Sc = v/D \tag{6}$$

$$\frac{K.d}{D} = 0.023 * \left(\frac{d.u}{v}\right)^{0.875} * \left(\frac{v}{D}\right)^{0.25} \tag{7}$$

$$u = \frac{Q}{A} \tag{8}$$

$$A = \frac{\pi}{4}d^2 \tag{9}$$

$$I_{lim} = n.F.K.C_b \tag{10}$$

$$CR(mm/yr) = \frac{I_{lim}.t.m}{n.F.\rho} * 1000 \tag{11}$$

$$I_{lim} = \frac{DnF(C_b - C_s)}{x} \tag{12}$$

$$I_{lim} = \frac{DnFC_b}{x} \tag{13}$$

$$2Na_2SO_3 + O_2 \rightarrow 2Na_2SO_4 \tag{14}$$

## NOMENCLATURE

$A =$ Cross-section area of the pipe    $(m^2)$

$C_b =$ Concentration of the oxygen in the bulk of feed water $(mole/m^3)$.

$C_s =$ concentration of dissolved species at surface of the WE $(mole/m^3)$.

CR: corrosion rate in mm/yr.

$D =$ diffusion coefficient of oxygen in water   $(m^2/s)$.

$d =$ Diameter of the pipe   (m).

$F =$ Faraday's constant   (96,500 C/mole).

$K =$ Mass transport coefficient of the oxygen   (m/sec).

$I_{lim} =$ Limiting current density    $(A/m^2)$.

$m =$ Atomic mass of iron $= 55.845$ g/mol.

$n =$ number of the electrons that are consumed or released.

$Q =$ Volumetric flow rate    $(m^3/s)$.

$Re =$ Reynold number and is related to the fluid flow rate.

$Sc =$ Schemidt number and is related to the fluid properties.

$Sh =$ Sherwood number and is related to the   mass transport.

$t =$ Time   (year)

$u =$ Velocity of the fluid    (m/s).

$v =$ Kinematic viscosity   $m^2/sec$

x = thickness of the diffusion layer   m

$\rho =$ Density of the iron $= 7.874$ g/cm$^3$

| Parameter | unit | Range | Parameter | unit | Range |
|-----------|------|-------|-----------|------|-------|
| Operating Temperature | °C | 20-40 | Inlet Water Flow Rate (per tower) | m³/h | 300 |
| Operating Pressure | Mpa | -0.098 | Dissolved Oxygen in Inlet Water | ppm | - |
| Design Life | year | 20 | Dissolved $O_2$ in outlet Water | ppm | 0.5 |



**Figure 1.** Internal corrosion of water injection pipeline.
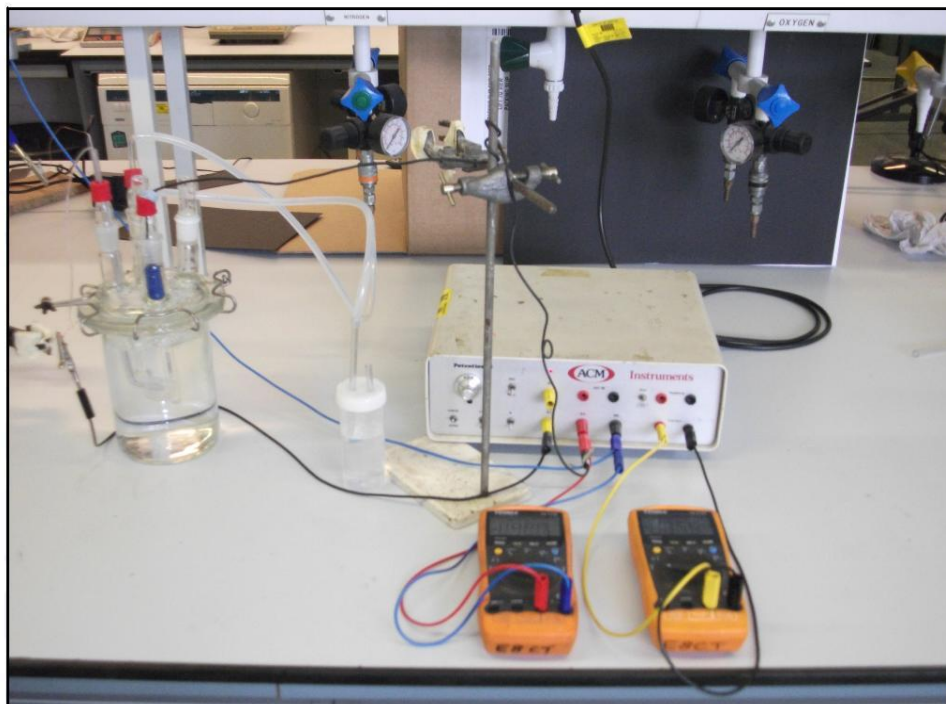
**Figure 2.** Electrochemical cell during deaerated process at -200 mV SCE.

**Table 2.** Corrosion rate of the water injection system during operation of
the vacuum deoxygenation tower.

| | CR | | | | | | | | | |
|---|---|---|---|---|---|---|---|---|---|---|
| | At 20 °C | | | | | At 40 °C | | | | |
| | Inside diameter (in.) | | | | | Inside diameter (in.) | | | | |
| Parameter | 6 | 8 | 16 | 18 | 28 | 6 | 8 | 16 | 18 | 28 |
| $C_{O2}$ (ppm) | 9.1 | 9.1 | 9.1 | 9.1 | 9.1 | 6.2 | 6.2 | 6.2 | 6.2 | 6.2 |
| $C_b$ (ppm) | 0.5 | 0.5 | 0.5 | 0.5 | 0.5 | 0.5 | 0.5 | 0.5 | 0.5 | 0.5 |
| CR (mm/yr) | 0.18 | 0.13 | 0.37 | 0.46 | 0.67 | 0.38 | 0.84 | 0.84 | 1 | 1.5 |

**Table 3.** Corrosion rate of the water injection system equipments during maintenance.

| | CR | | | | | | | | | |
| --- | --- | --- | --- | --- | --- | --- | --- | --- | --- | --- |
| | At 20 °C | | | | | At 40 °C | | | | |
| | Inside diameter (in.) | | | | | Inside diameter (in.) | | | | |
| Parameter | 6 | 8 | 16 | 18 | 28 | 6 | 8 | 16 | 18 | 28 |
| Flow rate ($m^3$/hr) | 33 | 150 | 650 | 1075 | 4200 | 33 | 150 | 650 | 1075 | 4200 |
| Area of a pipe ($m^2$) Eq.(9) | 0.0182 | 0.032 | 0.13 | 0.164 | 0.397 | 0.0182 | 0.032 | 0.13 | 0.164 | 0.397 |
| $u$ (m/s) Eq.(8) | 0.503 | 1.3 | 1.39 | 1.82 | 2.94 | 0.503 | 1.3 | 1.39 | 1.82 | 2.94 |
| $C_{O2}$(ppm) | 9.1 | 9.1 | 9.1 | 9.1 | 9.1 | 6.2 | 6.2 | 6.2 | 6.2 | 6.2 |
| $C_b$ mol/$m^3$ | 0.284 | 0.284 | 0.284 | 0.284 | 0.284 | 0.1937 | 0.1937 | 0.1937 | 0.1937 | 0.1937 |
| $D$ ($m^2$/s) | 1.8E-9 | 1.8E-9 | 1.8E-9 | 1.8E-9 | 1.8E-9 | 3.7E-9 | 3.7E-9 | 3.7E-9 | 3.7E-9 | 3.7E-9 |
| $v$ ($m^2$/s) | 1.0E-6 | 1.0E-6 | 1.0E-6 | 1.0E-6 | 1.0E-6 | 6.6E-7 | 6.6E-7 | 6.6E-7 | 6.6E-7 | 6.6E-7 |
| Re | 76428 | 263369 | 563206 | 829615 | 2084674 | 116500 | 400242 | 855903 | 1264596 | 3168072 |
| $K$ (m/s) Eq.(7) | 2.5E-5 | 5.5E-5 | 5.3E-5 | 6.6E-5 | 9. 6E-5 | 5.5E-5 | 1.2E-4 | 1.2E-4 | 1. 5E-4 | 2. 1E-4 |
| $I_{lim}$ Eq.(10) | 2.74 | 6.0 | 5.81 | 7.24 | 10.52 | 4.11 | 9.0 | 8.97 | 11.21 | 15.95 |
| CR(mm/yr) Eq.(11) | 3.2 | 7 | 6.7 | 8.4 | 12.2 | 4.8 | 10.42 | 10.4 | 13 | 18.5 |
| CR (mm/month) | 0.265 | 0.6 | 0.56 | 0.7 | 1.0 | 0.4 | 0.87 | 0.86 | 1.1 | 1.54 |
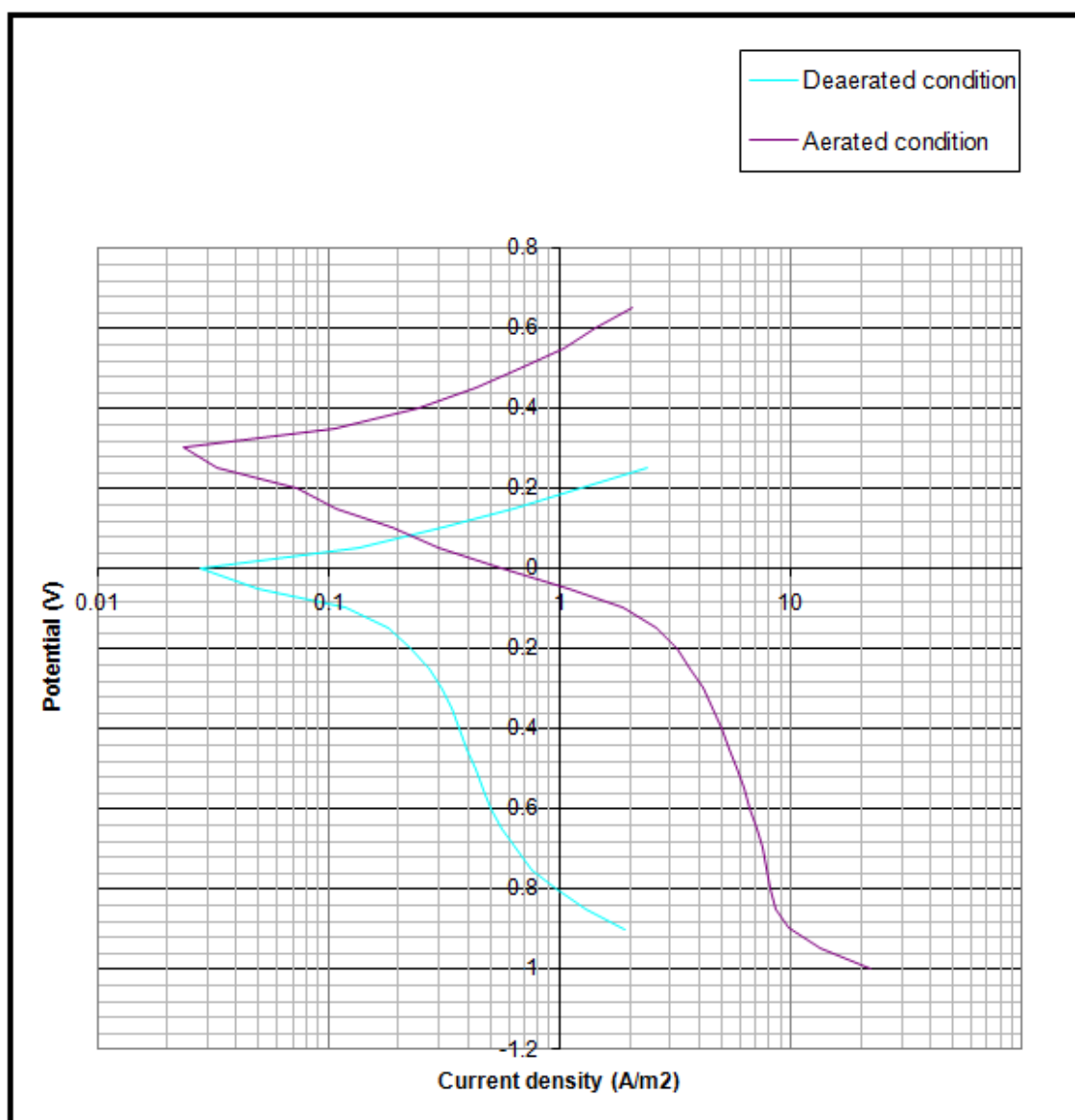
**Figure 3.** Polarization curve of platinum in solution of sodium chloride.

**Table 4.** Corrosion rate of the water injection system equipments after   increasing the amount of the $O_2$ scavengers.

| | CR | | | | | | | | | |
|---|---|---|---|---|---|---|---|---|---|---|
| | At 20 °C | | | | | At 40 °C | | | | |
| | Inside diameter (in.) | | | | | Inside diameter (in.) | | | | |
| Parameter | 6 | 8 | 16 | 18 | 28 | 6 | 8 | 16 | 18 | 28 |
| Flow rate (m³/hr) | 33 | 150 | 650 | 1075 | 4200 | 33 | 150 | 650 | 1075 | 4200 |
| Area of a pipe (m²) Eq.(9) | 0.0182 | 0.032 | 0.13 | 0.164 | 0.397 | 0.0182 | 0.032 | 0.13 | 0.164 | 0.397 |
| $u$ (m/s) Eq.(8) | 0.503 | 1.3 | 1.39 | 1.82 | 2.94 | 0.503 | 1.3 | 1.39 | 1.82 | 2.94 |
| $C_{O2}$(ppm) | 0.01 | 0.01 | 0.01 | 0.01 | 0.01 | 0.01 | 0.01 | 0.01 | 0.01 | 0.01 |
| $C_b$ mol/m³ | 3.1E-4 | 3.1E-4 | 3.1E-4 | 3.1E-4 | 3.1E-4 | 3.1E-4 | 3.1E-4 | 3.1E-4 | 3.1E-4 | 3.1E-4 |
| $D$ (m²/s) | 1.8E-9 | 1.8E-9 | 1.8E-9 | 1.8E-9 | 1.8E-9 | 3.7E-9 | 3.7E-9 | 3.7E-9 | 3.7E-9 | 3.7E-9 |
| $v$ (m²/s) | 1.0E-6 | 1.0E-6 | 1.0E-6 | 1.0E-6 | 1.0E-6 | 6.6E-7 | 6.6E-7 | 6.6E-7 | 6.6E-7 | 6.6E-7 |
| Re | 76428 | 263369 | 563206 | 829615 | 2084674 | 116500 | 400242 | 855903 | 1264596 | 3168072 |
| $K$ (m/s) Eq.(7) | 2.5E-5 | 5.5E-5 | 5.3E-5 | 6.6E-5 | 9. 6E-5 | 5.5E-5 | 1.2E-4 | 1.2E-4 | 1. 5E-4 | 2. 1E-4 |
| $I_{lim}$ Eq.(10) | 3E-3 | 6.6E-3 | 6.3E-3 | 7.9E-3 | 1.15E-2 | 6.6E-3 | 1.4E-2 | 1.4E-2 | 1.79E-2 | 2.5E-2 |
| CR(mm/yr) Eq.(11) | 3.4E-3 | 7.6E-3 | 7.3E-3 | 9.1E-3 | 1.3E-2 | 7.6E-3 | 1.6E-2 | 1.6E-2 | 2E-2 | 2.9E-2 |

Diffusivity coefficient of $O_2$ in the water at 20°C and at 40°C are obtained from Coulson et al.,1999, Verhallen et al.,1984].

 Kinematic viscosities of water at 20°C and 40°C are obtained from [Josepn et al.1987]

# قـائـمـة الـمـحـتـويـات

**القسم العربي:**

ة

<div dir="rtl">

# تطوير نظام مقترح للهيكل التنظيمي لإدارة مشاريع إنشائية متعددة

**المشرف**                      **المهندس**

**أ.م.د. سوسن رشيد محمد**          **هيثم عبد الرزاق بوهان**

**قسم الهندسة المدنية**            **قسم الهندسة المدنية**

**كلية الهندسة – جامعة بغداد**      **كلية الهندسة – جامعة بغداد**

## الخلاصة

يهدف البحث إلى ضرورة وضع الهيكل التنظيمي الملائم لمؤسسات قطاع التشييد العراقية التي تقوم بتنفيذ مشاريع إنشائية متعددة, والذي يفي بمتطلبات الإدارة والإشراف للسيطرة على تنفيذ هذه المشاريع في حدود الكلفة والمدة المحددة وبالجودة المطلوبة. وإستنادا إلى المعلومات الأولية والبيانات الإستطلاعية التي تم جمعها, فقد تم صياغة فرضية البحث كما يأتي: "حاجة مؤسسات قطاع التشييد العراقية التي تقوم بتنفيذ مشاريع إنشائية متعددة في آن واحد الى إعادة هيكلتها التنظيمية لتكون أكثر ملائمة للإدارة والسيطرة على هذه المشاريع". وقد تضمن البحث جزء نظري شمل استعراض لأهم المصادر المحلية والعالمية ذات الصلة المباشرة بموضوع البحث والتطرق فيه لمفهوم التنظيم وأنواع الهياكل التنظيمية لإدارة المشاريع الإنشائية المتعددة والسيطرة عليها. وجزء ميداني شمل في قسمه الأول دراسة الهيكل التنظيمي والتنظيم الوظيفي المتبع في واحدة من مؤسسات قطاع التشييد العراقية التي تقوم بتنفيذ مشاريع إنشائية متعددة في آن واحد وإبراز سلبيات هذا التنظيم. أما القسم الثاني فقد تضمن إستعراض للهياكل التنظيمية التي تستخدمها بعض مؤسسات التشييد والشركات الأجنبية في تنفيذ مشاريع إنشائية متعددة. وعليه فقد تم تحديد نقاط الضعف في التنظيم المتبع في مؤسسات قطاع التشييد العراقية وما يسببه من إخفاقات في السيطرة على محددات هذه المشاريع. وتم التغلب عليها بتطوير نظام مقترح للهيكل التنظيمي للإدارة والسيطرة على مشاريع إنشائية متعددة, يتم فيه السيطرة على تنفيذ هذه المشاريع من مرحلة التخطيط مرورا بمرحلة التصميم والإحالة ومرحلة التنفيذ لغاية التسليم الأولي.

**كلمات رئيسية:** إدارة, تنظيم, هيكل تنظيمي, سيطرة, إشراف ميداني, تخصص وظيفي.

</div>

# Development a Proposed System of Organization Structure to Management Multi Construction Projects

**Haitham Abdulrazzq**          **Assist. Proff. Dr. Sawsan Rasheed Mohammed**
Civil Engineering                  Civil Engineering
Engineering Collage-Baghdad University     Engineering Collage-Baghdad University
eng_haitham1981@yahoo.com            Sawsan_2@yahoo.com

## ABSTRACT

**T**he purpose of this study is aimed to lay down an arranged platform suited to Iraqi constructional associations which in charge to carry out multi constructional projects, as it fulfilled management requirements and supervising, so that low - cost projects will be controlled in due term and quality. Based on primary info and observed data collected, the study thesis has been formulated in this way: Iraqi constructional sector bodies which are in charge to implement simultaneously multi constructional projects in need to reformulate its organized structure so that it will be more fitted to management and control of these projects. This thesis includes a theoretical part contained presenting the most important resources locally and internationally where it has direct relation with this study

subject. Also it touches on the arrangement term and the kinds of organized structure of the multi constructional projects and control it. And its field part included in its first section studying the organized structure and functional arrangement practised in one of the Iraqi constructional projects. in charge of implemented simultaneously multi construction and exposing the defection of this arrangement. The second section of this study included reviewing the organized structure used by some of constructed corporations and foreign companies of implementing multi constructional projects .Thus, the deficiency points of the organized structure and the arrangement followed in Iraqi conduction sectors recognized and what it causes of control defections in the limitation of these projects. The deficiency points have been solved by developing a proposed system of the organized structure to administering and controlling of the multi constructional projects. The implementation of these projects have been controlled from its draw phase and passing the design phase and reference and implementation phase till the first deliver.

**Keywords: Management. organization structure. Control. Superintendence. Specialty functional**

## 1.المقدمة

إن من أهم الخطوط العريضة لإدارة المشاريع الإنشائية هو حسن استخدام الموارد البشرية المتاحة, التي تستوجب توفر الإدارة الكفوءة التي تقوم بتوفير فريق العمل المناسب ووضع الهيكل التنظيمي الملائم لإدارة المشاريع, ووضع الأشخاص المناسبين في الأماكن المناسبة لهم, وتوزيع الصلاحيات والواجبات حسب الاختصاصات الوظيفية, ودراسة المعوقات والمشاكل التي يمكن أن يتعرض لها المشروع سواء المشاكل المالية أو المشاكل الفنية أو غيرها من المشاكل التي تؤدي إلى تلكؤ وتعطيل وقت إنجاز المشاريع أثناء التنفيذ, مع دراسة إيجاد الحلول العلمية لها التي تؤدي إلى زيادة احتمالية تنفيذ المشاريع بالكلفة المقررة لها والمدة المحددة والجودة المطلوبة.

## 1.1.مبررات البحث:

1-ضعف الهيكلية التنظيمية لفرق الاشراف على المشاريع الإنشائية في مؤسسات قطاع التشييد العراقية.

2-عدم الإهتمام بالتخصص الوظيفي.

3-كثرة مهام هذه اللجان مما يسبب عرقلة العمل وإرتباكه.

4-قلة عددهم أحيانا الذي يؤدي الى تحملهم مهمة الإشراف على أكثر من مشروع.

5-المسؤولية القانونية الضخمة المترتبه على كاهل هذه اللجان.

6-تأثير ذلك على تفشي ظاهرة الفساد الإداري والمالي.

## 1.2.أهداف البحث

إن الهدف الرئيس من هذا البحث هو : تطوير نظام مقترح للهيكل التنظيمي لإدارة مشاريع إنشائية متعددة, يمكن من خلاله السيطرة على تنفيذ هذه المشاريع وتحقيق مايأتي:

1- تجنب حدوث تعديلات في التصاميم تؤدي الى حدوث تغييرات أثناء التنفيذ مما يسبب زيادة كلفة المشروع ووقته.

2- تجنب مشاكل الإحالة على المقاولين التي تسبب تردي جودة الأعمال وتأخر إنجاز المشاريع.

2

3- السيطرة على كلفة ووقت وجودة المشاريع أثناء التنفيذ.

4- تخصص الأفراد العاملين في المشاريع بنوع معين من النشاط يلائم تخصصهم الوظيفي.

5- تحسين الاتصال والتنسيق بين أعضاء فرق العمل في المشاريع.

6- سيطرة كاملة على كل جانب من جوانب المشروع.

7- تخفيف حمل المسؤولية القانونية عن لجان الإشراف والسيطرة على قضايا الفساد الإداري والمالي.

## 2.الهياكل التنظيمية لإدارة المشاريع الإنشائية

لكلمة التنظيم مفهوم عام يعني وضع كل شي في مكانه وكل شخص في مكانه وربط الأشياء ببعضها, والأشخاص ببعضها البعض من أجل تكوين وحدة متكاملة الفاعلية. حيث يعرف التنظيم بأنه "عملية ترتيب العلاقات بين وظائف المنظمة وواجبات كل منها وتحديد الإختصاصات والمسؤوليات والإتصالات بين الأفراد العاملين في الوحدة التنظيمية(Maylor-1990). أما الهيكل التنظيمي فهو الإطار الرسمي أو الهرمي الوظائفي, حيث يتم تجميع الأنشطة المتشابهة في وحدات وتجميع الوحدات في اكبر وهكذا حتى يكون هناك شخص واحد في قمة الهرم الوظيفي تتركز في يده السلطة والمسؤولية, فالهيكل التنظيمي يوضح بمجرد النظر : المناصب الإدارية المختلفة,عدد المستويات الإدارية, التسلسل الرئاسي, خطوط الإتصالات, نطاق الإشراف لكل مدير(محمد-2008).

## 1.2. أنواع الهياكل التنظيمية

هناك ثلاثة أنواع رئيسية من الهياكل التنظيمية (Albert-2006):

1-الهيكل التنظيمي الوظيفي Funactional Organization Structure

2-الهيكل التنظيمي النموذجي أو المشروعي Pure Project Organization structure

3-هيكل تنظيم المصفوفة Matrix Organization Structure

## 1.1.2. الهيكل التنظيمي الوظيفي

ويتم بموجبه تقسيم الوحدات التنظيمية الرئيسة والوحدات الفرعية المرتبطة بها ضمن الهيكل التنظيمي على أساس الوظائف المطلوب القيام بها إعتماداً على مبدأ التخصص وتقسيم العمل (2006-محمد). في ظل هذا النوع يتم تجميع الأنشطة والأعمال طبقا لطبيعة العمل في المشروع ويلزم تحديد الوظائف الرئيسة وبناء وحدات تنظيمية رئيسة لها ثم تقسم هذه الوحدات إلى وحدات فرعيه تقوم كل منها بوظيفة فرعية تندرج تحت الوظيفة الرئيسة . (محمد-2008)**بين الشكل (1) الهيكل التنظيمي الوظيفي.**

## 2.1.2.الهيكل التنظيمي النموذجي

يتم اللجوء إلى هذا التنظيم عندما يتم معاملة القسم الوظيفي كوحدة مستقلة عن المنظمة الأم بحيث يتم إستخدام نفس الموارد والمصادر المستخدمة في المنظمة (صويص-2010). يعتمد هذا التنظيم على إن كل مشروع وحده مستقلة بذاتها لها مدير مشروع مسؤول مسؤولية كاملة عن المشروع من حيث النتائج والربحية وتنتهي مسؤوليته بإنتهاء المشروع ويعمل معه فريق عمل يتم إختياره من الإدارات الوظيفية الفنية المتخصصة طبقا لإحتياجات المشروع (مالي, إداري, كهربائي ....الخ) (محمد-2008). **يبين الشكل (2) الهيكل التنظيمي النموذجي أو المشروعي.**

## 2.1.3.هيكل تنظيم المصفوفة

هو مزيج من الهيكل التنظيمي النموذجي والهيكل التنظيمي الوظيفي (صويص-2010). إن هذا الأسلوب التنظيمي في أبسط أشكاله يجعل كل الأقسام مفصولة عن بعضها البعض, ويكون تدفق المعلومات رأسيا وأفقيا ويحتاج إلى تعيين مدير المشروع لكي يكون محفزا رئيسا في التأكد من تحقيق أهداف المشروع والتنسيق بين العديد من المجموعات ( James-1996 ). حيث تحتل المجموعات الوظيفية موقعها تحت إشراف المدير العام أو المدير التنفيذي وبذلك تكون المسؤولية بالإتجاه العمودي متعلقة بالاختصاص الوظيفي في حين إن المسؤولية بالاتجاه الأفقي تكون متعلقة بمجموعة المشاريع بصورة مستقلة ويعتبر من أحدث أشكال التنظيم (2006-محمد). **يبين الشكل (3) هيكل تنظيم المصفوفة.**

## 2.2.إختيار الهيكل التنظيمي الملائم للمشاريع

يمكن تحديد الهيكل التنظيمي للمشروع بشكل عام عن طريق إتباع الخطوات التالية (صويص-2010):

1- تعريف أهداف المشروع وتحديدها.

2- تعريف المهام الأساسية المتعلقة بكل هدف وتحديدها.

3- تحديد الأقسام الوظيفية المسؤولة عن القيام بمهام المشروع وذلك بالرجوع إلى المنظمة الأم ومعرفة الأقسام الموجودة فيها.

4- تحديد فريق العمل الذي سيعمل في المشروع.

5- تحديد أي قضايا خاصة تتعلق بالمشروع مثل الحاجة إلى تقنية معينة.

6- تحديد إيجابيات وسلبيات انواع الهياكل التنظيمية وإختيار الهيكل الذي يلائم المشروع أكثر من غيره.

## 3.بناء فريق المشروع

بناء فريق المشروع هو عملية التأثير على مجموعة متنوعة من الأفراد ،كلٌ له الأهداف الخاصة، ووجهات النظر، للعمل معا على نحو فعال لصالح المشروعى[7]. تكمن أهداف بناء فريق العمل في زيادة التماسك وفعالية وحدة العمل الوظيفي داخل المنظمة. وتكمن جهود بناء الفريق في إنجاز المهام, حل المشاكل، توضيح الأهداف، تحديد الأولويات، تخطيط الأنشطة، تخصيص المهام وإستخدام الموارد على نحو فعال [6] يتكون فريق المنظمة من فرق متعددة مثل فرق الإدارة وفرق التصميم وفرق الإنشاء وغيرها رغم أن لكل من هذه الفرق أهدافها الخاصة وخبراتها المتنوعة وتنفيذها لوظيفة مختلفة، لكن يجب أن تمتلك هذه الفرق التقارب في بيئة متداخلة وتوحيد للجهود المبذولة لتحقيق أهداف المشروع. ولا بد من مواصلة البناء والعمل الجماعي بغض النظر عن حجم وعدد الفرق، ومن الأهمية وجود رئيس واحد يرأس هذه الفرق لإتخاذ القرارات النهائية والتركيز على أهداف المشروع (Garold-2000).

## 4.الإشراف الميداني

إن جهاز الإشراف هو فريق العمل المعين رسمياً من قبل صاحب العمل، وهو المسؤول عن الإشراف على تنفيذ العقد أو جزء منه ضمن حدود الصلاحيات المخولة له ويكون على أحد الأشكال الآتية (دليل إجراءات الإشراف-2009)

1- جهاز إشراف مباشر من الإدارة الهندسية لصاحب العمل (تنفيذ مباشر).

2- جهاز إشراف مقيم مكون من مهندسين وفنيين من مختلف التخصصات يتبع صاحب العمل.

3- مكتب استشاري مع وجود ضابط اتصال من الإدارة الهندسية لدى صاحب العمل.

ومن بين الواجبات المهمة التي يتضمنها هذا النشاط ما يلي (ستانلي-1982):

1-تنسيق نشاطات المقاولين.

2-مراجعة جداول المقاولين الزمنية والتأكد من تقيدهم بها.

3-إقتراح أساليب التنفيذ بغرض الإسراع بانجاز العمل.

4-وضع التوصيات الخاصة بدفع مبالغ تقدم العمل للمقاولين.

5-حضور وعقد الإجتماعات التنسيقية في موقع العمل.

6-إجراء التفتيش الكامل في المواعيد المناسبة.

7-التأكد من الحصول على خرائط الموقع والمرافق كما تم إنشاؤها.

8-  التأكد من التنفيذ وفق بنود شروط المقاولة لأعمال الهندسة المدنية والكهربائية والميكانيكية.

9-  وضع التوصيات الأولية حول أوامر التغيير.

## 5.السيطرة على المشاريع الإنشائية

تتضمن السيطرة على المشروع الإنشائي عمليات قياس الأداء والفحص والمراقبة والتعديل وإصدار التقارير التحليلية الضرورية لكافة نواحي العمل من أجل إنجازه على اتم وجه. حيث إنه على مدير المشروع وفريقه متابعة هذه العمليات بشكل دائم وذلك من أجل التحكم في أي انحرافات عن الأهداف, إذ يمكن مواجهة هذه الإنحرافات عن طريق إتخاذ إجراءات تصحيحيه مناسبة لإعادة العمل إلى ما كان عليه أساسا (صويص-2010). لذا فان أعمال السيطرة على المشاريع الإنشائية بشكل خاص تتم من خلال المحاور التالية (احسان-1989):

1-  السيطرة على الكلفة Cost Control: تتم من خلالها تسجيل كافة المصاريف المالية والمبالغ الفعلية التي تستنفذها كل فعالية من فعاليات المشروع ومقارنتها مع المبالغ المخمنة لها.

2-  السيطرة على الوقت Time Control: تتم خلالها متابعة المدة الفعلية لكل فعالية وتسجيلها ومقارنتها إزاء المنهاج الزمني المعد مسبقاً.

3-  السيطرة على الجودة Quality Control: تتم خلالها مراقبة المواصفات الفنية للعمل المنجز ومقارنتها مع المواصفات المطلوبة والمثبتة في الوثائق الفنية للمشروع.

وتوضح طبيعة العلاقة والترابط بين هذه العوامل كما يأتي (حوا-2008):

1- إن تقليص المدة سيؤدي إلى زيادة الكلفة بالإضافة إلى التأثير السلبي على الجودة.

2- خفض الكلفة يؤدي إلى التأخير في البرنامج الزمني كما إن له تأثير سلبي على الجودة.

3- خفض معايير الجودة قد لا يؤدي إلى إرجاع المشروع إلى البرنامج الزمني وضمن الميزانية وعادة ما يؤدي إلى جودة غير ملائمة أو غير مستوفية للمواصفات.

## 6.الدراسة الميدانية

لأجل مقارنة الهياكل التنظيمية والتنظيم الوظيفي في العراق وخارجه قام الباحث بإجراء حالتين دراسيتين, الأولى مختصة بدراسة الهيكل التنظيمي والتنظيم الوظيفي لواحدة من مؤسسات قطاع التشييد العراقية والأخرى لشركات أجنبية. كان الهدف من الدراسة تحليل واقع

الحال وإيجاد نقاط الضعف في التنظيم المتبع في مؤسسات قطاع التشييد العراقية والعمل من أجل التغلب عليها ببناء نظام مقترح يتضمن وضع هيكل تنظيمي وتنظيم وظيفي يلائم مؤسسات قطاع التشييد العراقية.

## 1.6.حالة دراسية لواحدة من مؤسسات التشييد العراقية

أجريت هذه الدراسة في قسم الشؤون الهندسية التابع لأحدى الجامعات العراقية الفتية والتي تمثل نموذجا اختير لأجل تسليط الضوء على الطرق المتبعة لإدارة تنفيذ المشاريع الانشائية في مؤسسات قطاع التشييد العراقية. حيث تم إجراء هذه الدراسة على مرحلتين, **الأولى:** دراسة الهيكل التنظيمي والتنظيم الوظيفي المتبع لقسم الشؤون الهندسية لسنة 2011 وكيفية توزيع فرق الإشراف على المشاريع ومهام القسم في تنفيذ مشاريع الجامعة وبيان سلبيات هذا التنظيم.**الثانية:** دراسة المشاريع المنجزة للجامعة خلال المدة التي قامت فيها الجامعة ببناء مدينة جامعية جديدة تشمل على عدد من مباني الكليات والأقسام الداخلية والبنى التحتية والمرافق الأخرى للمدينة

## 1.1.6.هيكلية قسم الشؤون الهندسية وشعبة العقود الحكومية

يتكون الهيكل التنظيمي لقسم الشؤون الهندسية من مدير القسم ومعاونه ومكتب رئيس القسم وثلاث شعب تتكون من عدة وحدات مع بعض اللجان **وكما مبين في الشكل(4)** . وتتكون شعبة العقود الحكومية من خمس وحدات هي: وحدة المتابعة, وحدة الإستثمار, وحدة التعاقدات, وحدة الإرشيف ووحدة الإستيراد.

## 2.1.6.فرق الإشراف المكونة لقسم الشؤون الهندسية

يتكون قسم الشؤون الهندسية في سنة 2011من عدد من المهندسين بمختلف الاختصاصات وعدد من مراقبي العمل وعدد من الإداريين والمحاسبيين. حيث يتكون القسم من 20 مهندس منهم 8 مدني, 4 ميكانيك, 3 كهرباء, 2 مواد, 2 معماري, 1 كيمياوي, و خمسة مراقبي عمل, و أربعة إداريين و ثلاث محاسبيين.

حيث قامت هذه الفرق بالإشراف على تنفيذ 16 مشروع متوسط الحجم تشمل مباني الكليات والأقسام الداخلية والبنى التحتية للمدينة الجامعية ,نفذت بأسلوب المقاول العام, بالإضافة الى الإشراف على تنفيذ تسعة مشاريع صغيرة منفذة بأسلوب التنفيذ أمانة.

## 3.1.6.سلبيات التنظيم المتبع في قسم الشؤون الهندسية

بعد دراسة التنظيم المتبع للإشراف على المشاريع في هذا القسم والمعايشة الميدانية والمقابلات الشخصية للمهندسين فيه توصل الباحث إلى تسجيل الملاحظات الآتية:

1-  إن شكل الهيكل التنظيمي المتبع في هذه المؤسسة هو مزيج من الهيكل التنظيمي الوظيفي والهيكل التنظيمي النموذجي.

2-  هناك عدد من المشاريع يوجد فيها عنصر واحد على الإشراف. ويتولى بعض المهندسين رئاسة الإشراف على أكثر من مشروع.

3-  تم توزيع فريق الإشراف على المشاريع بشكل لا يتناسب مع الإختصاص الوظيفي بسبب قلة فرق القسم.

4-  تتحمل اللجنة المشرفة اغلب الأعمال الإدارية والكتابية.

5-  أغلب المشاريع لا يتوفر فيها مهندسي الإختصاص المشرفين على الأعمال الجزئية.

6- تغيير مدير الشؤون الهندسية بين مدة وأخرى, يؤدي إلى تغير سياسة القسم والسياقات المعمول بها, مما يؤدي إلى ضعف في الارتباط بين الفرق والمدير.

7- شعور الفريق المشرف بالولاء لإداراتهم والإهتمام بالأمور الإدارية وليس للمشروع ككل.

8- عزوف المهندسين عن العمل بسبب التشدد والإجراءات التدقيقية التي تقوم بها الإدارة العليا ولجان المفتش العام وغيرها التي تجعل المهندس عرضة للإتهام.

9- قلة وضعف الدعم المعنوي والمادي من قبل الإدارة العليا لفرق الإشراف.

## 6.1.4.دراسة وتحليل المشاريع المنجزة

أنجزت هذه المؤسسة لنهاية سنة 2011 إثني عشر مشروع ضمن خطة بناء المدينة الجامعية. نفذت هذه المشاريع بأسلوب المقاول العام, حيث تمت دراسة أبرز المشاكل التي تؤدي إلى الزيادة في كلفة المشاريع ومددها الزمنية والعوامل التي تؤدي إلى الإخفاق في تحقيق الجودة المطلوبة للمشروع. حيث وجد من خلال دراسة تنفيذ هذه المشاريع وبعد الإطلاع على ملفات المشاريع والمقابلات الشخصية للعديد من المهندسين إن أسباب كثيرة تؤدي إلى العديد من المشاكل وعرقلة سير عمل المشاريع بالدرجة المطلوبة, كما وجد الباحث عدة عوامل مشتركه تؤدي إلى مشاكل فنية ومالية ووقتية تسببها الإدارات والمقاولين وأيضا تسببها الإجراءات المتبعه في الإدارة العليا, حيث تؤدي عملية نقص البيانات أثناء مرحلة تخطيط المشروع إلى ظهور العديد من المشاكل التصميمية التي تؤدي بالتالي إلى زيادة مدة وكلفة المشروع, ووجد في اغلب المشاريع العديد من الأخطاء التصميمية التي تؤدي إلى حصول العديد من التغييرات أثناء التنفيذ والتي تؤدي بالتالي الى زيادة كلفة المشروع ومدته, والتزام الدائرة بالإحالة إلى أوطأ العطاءات في مرحلة الإحالة التي غالبا ما تكون أقل من الكلفة التخمينية للمشروع بكثير, مما يؤدي هذا إلى تأخر المشروع مده طويلة في مرحلة التنفيذ بسبب إنخفاض أسعار تنفيذ فقرات المشاريع, إن سبب زيادة كلفة المشروع أثناء التنفيذ هي التغييرات الحاصلة بالأعمال, ولزيادة المدة أيضا أسباب كثرة تعود لهذه التغيرات وأخرى لأسباب خارجة عن ارادة أطراف العقد وأخرى تعود للمقاول وأخرى بسبب الإجراءات الروتينية من قبل الإدارة العليا والوسطى, أما أسباب وجود بعض الإخفاقات في الجودة فتعود الى توفير المقاول لعمال غير ماهرين وغير كفوئين بسبب إنخفاض سعر الفقرات, كما لاحظ الباحث إن من أهم أسباب تلكؤ المشاريع هو إحالة المقاولة كليا من الباطن إلى مقاولين ثانويين, حيث تصل المقاولة إلى المقاول الثانوي بمبلغ اقل من المتعاقد عليه وهذا بدوره يؤثر سلبا على العمل ويؤدي إلى دخول المشروع في الغرامات التأخيرية والإخفاقات النوعية.

## 6.2.حالات دراسية لبعض الشركات الأجنبية

تم إجراء دراسة للهياكل التنظيمية التي تستخدمها بعض الشركات الأجنبية والتي تقوم بالإشراف على تنفيذ مشاريع إنشائية متعددة في آن واحد. واحدة من هذه الشركات (شركة نيت ورك ريل) البريطانية صاحب عمل أما بقية الشركات فهي مقاول رئيسي يشرف على أعمال المقاول الثانوي, وتم الإستفادة من سلوكه في الإشراف على تنفيذ المشاريع, تم التوصل لهذه البيانات عن طريق المقابلات الشخصية مع بعض المهندسين الذين يشغلون مناصب رفيعة في هذه الشركات.

### 6.2.1.شركة(Net work Rail)البريطانية

تقوم هذه الشركة الخاصة باعمال السكك الحديدية للقطارات في بريطانيا في سنة 2009 بتنفيذ مشروع ضخم لسكك الحديد يضم منطقتي ويلز وويسترن والتي تقسم إلى أربعة مشاريع رئيسة هي:

1- مشروع أعمال كروسريل  Crossrail Surface Works
2- مشروع إعادة تطوير محطات ريدينغ (RSAR) Reading Station Area Redevelopment
3- مشروع تكامل المنطقة الغربية Western Integration
4- مشروع القطارات الكهربائية Electric Trains

يضم المشروع الواحد عدة مشاريع فرعية مكونة من أعمال مختلفة لتطوير سكك الحديد وتحسين الأداء ورفع مستوى الإنتاج وتسريع القطارات. قامت هذه الشركة بالتعاقد مع شركة بكتل الأمريكية لإدارة المشاريع بطريقة الإدارة الإنشائية, وكان الفريق الفعلي لشركة بكتل مكون من 95 فريق بمختلف الإختصاصات بالإضافة إلى فرق الشركة الحكومية المكونة من  392 فريق, قامت شركة بكتل بوضع الهياكل التنظيمية لإدارة المشاريع الاربعة المجزءة الى مشاريع صغيرة والمحالة الى عدد كبير من المقاولين بطريقة هيكل تنظيم المصفوفة حيث يخضع كل عضو من فرق الإشراف إلى سلطة المدير الوظيفي وسلطة مدير المشروع.

### 6.2.2.شركة تارماش التركية

قامت وزارة التربية العراقية في سنة 2011 بإستحداث مشروع إنشاء مائة وست وعشرون مدرسة في المحافظات الجنوبية وقد قامت بإحالة هذا المشروع على وزارة الصناعة والمعادن والتي بدورها أحالت هذا المشروع على الشركة التركية تارماش الإنشائية كمقاول ثانوي. يتكون مشروع مدارس الجنوب من 126 مشروع  صغير الحجم (مدرسة) موزعة في مناطق متفرقة ومتباعدة في محافظة ذي قار وعدد قليل في المحافظات المجاورة لها. قامت شركة تارماش بإحالة بعض هذه المشاريع على عدد من المقاولين الثانويين والبعض الآخر قامت بتنفيذه بأسلوب التنفيذ المباشر, وقامت هذه الشركة بفتح مكتب لها في محافظة ذي قار, مدينة الناصرية الذي يعتبر هو مقر الشركة لإدارة هذه المشاريع, وقامت بتنظيم هيكلية للمكتب مكونة من: مدير المكتب و قسم التخطيط و القسم الفني و قسم الإدارة والحسابات و قسم التنفيذ. قام المكتب بتوزيع المشاريع إلى قطاعات حسب المنطقة التي تضم مجموعة متقاربة من المشاريع. ووضع المكتب على إدارة كل قطاع مدير يرأس مجموعة من المهندسين الذين يدعون بمهندسي المواقع يختلف عددهم حسب القطاعات, يتولى مهندسو المواقع المكونين للقطاع الواحد مهمة الإشراف على أكثر من مشروع حسب المسافات بين هذه المشاريع. ومراقب عمل لكل مشروع ومهندس كهرباء لكل قطاع. إن نوع الهيكل التنظيمي الذي إستخدمته هذه الشركة هو هيكل تنظيمي وظيفي.

### 6.2.3.شركة محادين الأردنية

قامت وزارة الصحة العراقية بإحالة خمسة مشاريع إنشائية ضخمة كل مشروع هو عبارة عن مستشفى 400 سرير على إحدى الشركات الإنشائية التركية ( شركة يونيفرسل أجارسن) والتي باشرت بتنفيذ هذه المشاريع بتاريخ 2009/7/1  وكان أسلوب الإحالة بطريقة التصميم/التنفيذ.

قامت الشركة المنفذة بالتعاقد مع شركة محادين الأردنية للإستشارات الهندسية لغرض الإشراف على تنفيذ هذه المشاريع ووضع الحلول الإستشارية للمشاكل المتوقعة أثناء التنفيذ, فقامت شركة محادين بتوزيع فرق الإشراف الخاصة بها على هذه المشاريع الخمسة مع وضع ارتباط لهذه الفرق بالمكتب الرئيس للشركة في  بغداد الذي يتكون من مجموعة من المهندسين الاستشاريين بمختلف الاختصاصات

الهندسية. إن شكل الهيكل التنظيمي المستخدم للإشراف هو هيكل تنظيمي نموذجي أو مشروعي حيث تقوم شركة محادين بتوفير فريق عمل كامل من مختلف الإختصاصات مع مدير مشروع لكل موقع. يتكون فريق إشراف شركة محادين داخل الموقع لأحد المشاريع الخمسة من: مهندس معماري, مهندس إنشائي, مهندس سيطرة نوعية, مهندس مساحة, مهندس كهرباء, مهندس ميكانيك, ثلاث مراقبي عمل بمختلف الإختصاصات, موظف إداري, موظف محاسبي

## 7.الهيكل التنظيمي المقترح

بعد دراسة أنواع الهياكل التنظيمية وبعد دراسة ملائمتها لأنواع المشاريع الكبيرة والمتوسطة والصغيرة الحجم, وبعد تحليل النماذج المعمول بها في الحالات الدراسية, قام الباحث بتطوير نوع مقترح من الهياكل التنظيمية لإدارة فرق الإشراف على المشاريع الإنشائية المتعددة, يتم فيه الإهتمام بالتخصص الوظيفي بدرجة عالية, وأطلق عليه الباحث اسم **الهيكــل التنظيمــي المــرن flexible Organizational Structure**.

وهو يجمع بين مزايا الهيكل التنظيمي النموذجي وهيكل تنظيم المصفوفة وسمي بالمرن من حيث: ملائمته للمشاريع بجميع أحجامها ومرونته لعدد الفرق المكونة للإشراف حسب نوع الأعمال المكونة للمشاريع الإنشائية ودرجة تعقيدها وملائمتة لعدد كل فرقة من فرق الإشراف المتوفرة سواء كانت قليلة أو كثيرة العدد. **ويوضح الشكل (5) تفاصيل الهيكل التنظيمي المرن**

## 1.7.ملائمة الهيكل التنظيمي المرن لحجم المشاريع الإنشائية

لا توجد معادلة رياضية لحساب العدد المطلوب توفره من الفرق المشرفة على المشاريع بل يعتمد هذا التوزيع على: حجم المؤسسة الإنشائية, عدد المشاريع المتوفرة, عدد وحجم الأنشطة المكونة للمشاريع ودرجة تعقيدها, نوعية المشاريع, الموقع الجغرافي للمشاريع, الخبرة المتراكمة للشخص المسؤول عن التخطيط وقدرة الشخص المرشح للإشراف. لذا فان المستطيلات المبينة في شكل الهيكل التنظيمي المرن تمثل عدد كل فرقة حيث إنه في المشاريع الكبيرة جدا يوضع في كل مشروع عضو أو أكثر من كل فريق فيصبح كادر الإشراف مكون من عدد كبير يلائم حجم المشروع. أما المشاريع المتوسطة الحجم فيمكن أن يكون لكل مدير مشاريع مشروعين أو أكثر تقع تحت إدارته حسب حجم هذه المشاريع, وكذلك يكون لكل مشروعين أو أكثر مهندس موقع ومراقب عمل لكل مشروع ومهندس مساحة لكل عدد من المشاريع ومهندس كهرباء لكل عدد من المشاريع أيضا وكذلك الحال مع مهندس الميكانيك ومهندس السيطرة على التخطيط والتصميم والتغييرات ومهندس السيطرة النوعية ومهندس المسح الكمي وإستلام الأعمال, وكذلك مع بقية الفرق الأخرى مثل مسؤول المشتريات, عضو الأعمال الإدارية والكتابية, عضو الأعمال المالية والمحاسبية وأي عضو آخر يتطلبه المشروع مثل المهندس المعماري أو مسؤول السلامة. أما في المشاريع الإنشائية الصغيرة فيكون العدد المطلوب للإشراف أقل بكثير, حيث يمكن أن يكون لمجموعة مشاريع صغيرة مدير مشاريع واحد ومهندس موقع لكل عدد معين من هذه المشاريع بالإضافة إلى مراقب عمل لكل مشروعين أو أكثر, وأيضا ممكن أن يكون لكل المشاريع الصغيرة مهندس مساحة واحد ومهندس كهرباء واحد وكذلك الحال مع مهندس الميكانيك ومهندس السيطرة على التخطيط والتصميم والتغييرات ومهندس السيطرة النوعية ومهندس المسح الكمي وإستلام الأعمال وكذلك مع بقية الفرق الأخرى مثل مسؤول المشتريات, عضو الأعمال الإدارية والكتابية, عضو الأعمال المالية والمحاسبية وأي عضو آخر يتطلبه المشروع مثل المهندس المعماري أو مسؤول السلامة, يمكن أن يزيد أو ينقص عدد الأشخاص المكونة للفرق حسب حجم المشاريع وطبيعة الأعمال المكونة لها ودرجة تعقيدها.

## 2.7.الهيكل التنظيمي المرن لمقر المؤسسة الإنشائية

إن هذا الهيكل التنظيمي لتنفيذ مشاريع إنشائية متعددة يقود إلى رسم هيكل تنظيمي خاص بالوظائف داخل مقر المؤسسة الإنشائية الذي يمكن من خلاله الخروج بهيكل تنظيمي متكامل من حيث الوظائف المركزية للفرق المكونة للمؤسسة الإنشائية داخلها والمهام الخاصة بالفرق المشرفة على المشاريع الإنشائية خارجها. حيث ستتكون المؤسسة من رئيس المؤسسة ومكتب رئيس المؤسسة, وعدة شعب هي: شعبة التخطيط والتصميم, شعبة العقود والمتابعة, شعبة الادارة والحسابات, شعبة التنفيذ وشعبة السيطرة. يترأس كل شعبة مسؤول الشعبة وتنطوي تحت كل شعبة عدة فرق يترأس كل فريق رئيس الفريق. **وكما موضح في الشكل (6).**

## 3.7.ملاحظات حول الهيكل التنظيمي المرن

1–     مستويات العمل داخل المكتب الحقلي للمشروع الواحد تكون كالآتي:

أولا: مهندس الموقع, مهندس المساحة, مهندس الكهرباء, مهندس الميكانيك, مهندس السيطرة على التخطيط والتصميم والتغييرات, مهندس السيطرة النوعية, مهندس المسح الكمي وإستلام الأعمال وغيرهم  حسب حاجة المشروع مثل المهندس المعماري يرتبطون بعلاقات جانبية مع بعضهم أي لا سلطة لأحدهم على الآخر بل يكون العمل كفريق واحد مع تعدد الرؤساء.

ثانيا: فريق مراقبي العمل يرتبطون بعلاقة مباشرة مع مهندس الموقع أي يعمل تحت إدارته.

ثالثا: فريق المشتريات, فريق الإدارة والأعمال الكتابية والفريق المالي والمحاسبي يعملون بمستوى واحد ويخضعون لإدارة مدير المشروع ورئيس الفريق.

رابعا: فريق الإرة والأعمال الكتابية يقوم بكافة الأعمال الإدارية والكتابية المتعلقة بكل المهندسين في المكتب الحقلي ويقوم بحفظ كافة الاعمال الكتابية المتعلقة بالمشروع والخاصة بعمل أي عضو في المشروع.

خامسا: الفريق المالي والمحاسبي يعمل مع فريق المسح الكمي وإستلام الأعمال بخصوص الأعمال المالية والحسابية المتعلقة بالمشروع.

2–     مفهوم واحد لواحد (النافذة الواحدة): يعتبر هذا المفهوم من أهم مبادئ إدارة المشاريع الإنشائية, وهو يقضي بحصر توجيه المقاول ليكون عبر شخص واحد فقط  في الموقع, يحرر الأوامر والتعليمات إلى المقاول, هذا الشخص هو مدير المشروع أو من يخوله مدير المشروع بالنطق نيابة عنه الذي يكون غالبا مهندس الموقع.

3–     إن علاقة العمل بين أعضاء المكتب الحقلي يجب أن تكون تعاونية و ينبغي التنسيق بين المهندسين في المكتب الحقلي  وأن لا يصدر من هو مخول من مدير المشروع أي أمر للمقاول إلا بعد مناقشة بقية المهندسين وفي حال تحفظ احدهم  يحيل المشكلة لرئيس الفريق الخاص به الذي يناقشها بدوره مع مدير المشروع ثم تعود مرة اخرى الى مهندس الموقع ليصدرها إلى ممثل المقاول وفي حال عدم التوصل إلى حل بين أعضاء المكتب الحقلي أو بين رؤساء الفرق يكون رأي مدير المشروع هو الحاسم والأخير .

4–     المهندس مابين التواجد الدائم والتواجد الجزئي في الموقع: قد يكون من غير المجدي في بعض المشاريع الإنشائية تكليف المهندسين بالتواجد الدائم في الموقع كأن يكون المشروع بسيطا من الناحية الإنشائية. ولهذا كثيرا ما نجد مهندس وحيد يشغل مهمة الإشراف  لأكثر من مشروع في الوقت نفسه.

5–     تأخذ الأعمال الإدارية والمكتبية 85% من وقت المهندس تقريبا وسيشغله ذلك عن التواجد في الموقع في كثير من الأوقات الحرجة مايعني إحتمالية وقوع المشاكل التنفيذية دون علمه في الوقت المناسب, ولما كانت الأمور المكتبية لا تتطلب أي خبرة وبإمكان

أي موظف القيام بها على الوجه الأكمل, حيث يمكن أن يضطلع بـ 70% منها أي موظف عادي [12], ولهذا السبب تم وضع أعضاء خاصين بالأعمال الإدارية والمكتبية داخل المشاريع في الهيكل التنظيمي المرن.

6- يمكن في هذا الهيكل التنظيمي تبادل المسؤوليات بين الفرق دوريا: على سبيل المثال يمكن تغيير فرقة السيطرة النوعية كلا أو جزءا إلى فريق مهندسي الموقع أو بالعكس أو تغيير فريق السيطرة على التخطيط والتصميم والتغيرات إلى فريق المسح الكمي وإستلام الأعمال أو بالعكس أو تغيير رؤساء الفرق إلى مدراء للمشاريع أو بالعكس وهكذا, وهذا يؤدي إلى تراكم الخبرات في كل الاختصاصات لدى الفرق المشرفة.

7- في حالة تعدد فقرات إنشاء المشروع وزيادة تعقيده يمكن زيادة الإختصاصات اللازمة للإشراف على التنفيذ, حيث يمكن مثلا إدخال فريق هندسي يختص بالإشراف على الأعمال الصحية أو فريق يختص بالإشراف على الأعمال الكيمياوية وغيرها حسب درجة تعقيد المشروع.

8- في حال كون الفريق الخاص بالإشراف على المشاريع قليل العدد أو غير كافي لأن يملأ الوظائف المكونة للهيكل التنظيمي المرن يمكن في هذه الحالة دمج مهام بعض الفرق لتكون من واجبات فريق واحد, مثلا دمج مهام فريق مهندسي المواقع مع مهام فريق مهندسي السيطرة النوعية أو دمج مهام فريق السيطرة النوعية مع مهام فريق المسح الكمي وإستلام الأعمال وهكذا حيث يمكن دمج مهام ثلاث فرق حسب ما تراه المؤسسة مناسبا.

## 4.7.مميزات الهيكل التنظيمي المرن

1-يصلح لكافة المشاريع الإنشائية الصغيرة والمتوسطة والكبيرة الحجم.

2-ملائمة لعدد الأعضاء المكونين لفرق الإشراف المتوفرة سواء كانت قليلة أو كثيرة العدد.

3-يخضع أغلب الموظفين فيه إلى سلطة رئيسين في وقت واحد (سلطة المدير الوظيفي وسلطة مدير المشروع). حيث تتدفق المعلومات بسهوله وكفاءة حيث إنها تأتي راسيا وأفقيا داخل فريق المشروع.

4-يتبادل فريق العمل عدة أمور مهمة كالمعرفة والخبرات المتنوعة.

5-يتيح الفرصة لان يتخصص مجموعه من الأفراد في نوع معين من النشاط لتكون المشاكل التي تواجههم ذات طبيعة واحده تستدعي قدر محدد من المعرفة.

6-سيطرة كاملة على كل جانب من جوانب المشروع.

7-يحسن الاتصال والتنسيق بين أعضاء فرق العمل.

8- الولاء الأساس للمشروع بالإضافة الى الولاء للإدارة,

9- يوفر المرونة التي تمكن الإدارة من الاستجابة السريعة للتغيرات في نطاق المشروع.

10-يوزع الهيكل الوظائف بين الفرق بحيث يعلم كل شخص مهامه وصلاحياته بشكل جيد.

11-يتم تحديد الفرد الذي تقع عليه المسؤولية عن أي خطا يحدث في المشروع.

12-يمكن لأعضاء العمل بأكثر من مشروع وبإختصاص واحد.

13-تخفيف العبء والمسؤولية القانونية عن كاهل أعضاء الإشراف حيث يخضع كل شخص من هذه الأعضاء إلى مسؤولية محددة يمكنه السيطرة عليها.

14- إن العمل بالهيكل التنظيمي المرن الذي يضع فرق متعددة ويخصص ويحدد مهامها, يمكن مؤسسات التشييد من السيطرة على ظاهرة الفساد الإداري والمالي الحاصل في هذه المؤسسات وحصرها, من خلال النظام الرقابي الناتج عن تعدد الفرق حيث تكون كل فرقة رقيبة على الأخرى.

## 7.5.السيطرة على المشاريع في الهيكل التنظيمي المرن

1-السيطرة على المشاريع في مرحلة التخطيط

إن المعلومات المتكاملة في مرحلة التخطيط للمشاريع تؤدي إلى تصاميم خالية من الأخطاء  حيث تؤدي البيانات الدقيقة إلى وصول المعلومات الدقيقة للمصمم التي تؤدي إلى تصميم ناجح خالي من العيوب والنواقص الذي بدوره لا يحتاج إلى أي تغييرات أثناء التنفيذ تؤدي إلى زيادة في الكلفة والوقت للمشروع.

2-السيطرة على المشاريع في مرحلة التصميم

يتم تصميم المشاريع عن طريق مكتب إستشاري أو عن طريق فريق التصميم في المؤسسة أو عن طريق المقاول الذي ينفذ المشروع بطريقة التصميم/ التنفيذ, وتتم السيطرة على التصاميم من خلال واحدة من النقاط الآتية:

أ-   إحالة المشروع بطريقة التصميم/ التنفيذ وبذلك يتخلص صاحب العمل من كافة مطالبات المقاول للزيادة بالكلفة والوقت.

ب- إحالة التصاميم على مكتب استشاري آخر بعد التصميم عند احد المكاتب الإستشارية, لغرض تحليل التصميم وتدقيقه والقضاء على المشاكل فيه التي تؤدي إلى زيادات في الكلفة والمدة, وتكون نفقات تحليل التصاميم على حساب المكتب الاستشاري الأول (المصمم).

ت- قيام فريق التصميم في الدائرة بالتحليل والتدقيق لكافة التصاميم ومعرفة مدى تطابقها مع بعضها ومعرفة مدى تطابق الكميات في المخططات مع جدول الكميات في الكشف المعد من قبل المكتب الإستشاري وكذلك مراجعة التصاميم لمعرفة مدى قابليتها للتطبيق وتلائمها مع متطلبات وظروف التنفيذ.

3-السيطرة على المشاريع في مرحلة الإحالة

أ-إعتبار الكلفة والمدة المخمنة حجر الأساس عند الإحالة.

ب- حصر التنافس بين ثلاث شركات فقط من مجموع الشركات المتنافسة تكون مبالغ عطاءاتها اقرب للمبلغ التخميني للمشروع.

ت- تجنب إحالة عدد من المشاريع على نفس الشركة لأن هذا يؤدي إلى عدم قدرة الشركة الإدارية والمالية على التنفيذ وبالتالي يتأخر تنفيذ هذه المشاريع.

4-السيطرة على المشاريع في مرحلة التنفيذ:

تقع مهمة السيطرة على محددات المشاريع, الكلفة والوقت والجودة في مرحلة التنفيذ داخل هذا الهيكل التنظيمي ضمن مهام شعبة السيطرة المكونة من فرق السيطرة المختلفة: فريق السيطرة على التخطيط والتصميم والتغييرات, فريق السيطرة النوعية و فريق المسح الكمي وإستلام الأعمال, حيث تتلخص مهام هذه الفرق في السيطرة على محددات المشاريع **في الشكل رقم (7)**

## 8.الإستنتاجات

**1-** ضعف الهيكل التنظيمي في أغلب مؤسسات قطاع التشييد في العراق, وإن إنخفاض السيطرة على تنفيذ المشاريع يعود أساسا لضعف الاهتمام بعملية تنظيم فرق إدارة المشاريع, إضافة إلى عدم تأهيل وتدريب العاملين بما يضمن مواكبتهم للتطور العلمي المطلوب لتنفيذ الفعاليات المختلفة في المشروع الإنشائي

**2-** بصورة عامة ،هناك ضعف في عملية أدارة وتخطيط مشاريع التشييد والسيطرة عليها (ضعف دور الأقسام الإدارية كالتخطيط والتصاميم والعقود والمتابعة في السيطرة على المشاريع) تؤدي إلى تجاوز كلف ومدد هذه المشاريع وكذلك تولد إخفاقات في تحقيق الجود .

**3-** يعتبر الهيكل التنظيمي المرن تنظيم أمثل يصلح لكل المشاريع وفي كل الأوقات وهو خطوة متقدمة لأنواع الهياكل التنظيمية الأخرى (الوظيفي والنموذجي والمصفوفي)  فهو يجمع قدر الإمكان بين إيجابياتها ويبتعد عن سلبياتها ويحقق التنظيم الوظيفي الملائم لفرق إدارة المشاريع الإنشائية التي تهتم بإختصاص محدد وواجبات معينة تقلل من الأعباء والمسؤوليات عن كاهل الفرق المشرفة. ويوفر سيطرة كاملة على كل جانب من جوانب المشروع وكذلك يهيأ الأرضية لتلافي ظاهرة الفساد الإداري والمالي.

## 9.التوصيات

1- يوصى بإعادة بناء الهيكل التنظيمي لفرق الإشراف على المشاريع الإنشائية في مؤسسات قطاع التشييد االعراقية وذلك بتبني الهيكل التنظيمي المقترح كنظام متكامل لمؤسسات التشييد.

2- لضمان التطبيق الناجح للهيكل التنظيمي المرن في مؤسسات قطاع التشييد يوصى بتعديل وإعداد التشريعات القانونية الملائمة لقيام صاحب العمل أو الجهات المسؤولة بتعديل هيكليتها التنظيمية.

3- لضمان التطبيق الناجح للهيكل التنظيمي المقترح يوصى ببناء القدرات البشرية في عموم مؤسسات التشييد بما يخدم تحقيق أهدافها من خلال إعداد دورات تطويرية لرفع المستوى الإداري والفني.

4- دعم العاملين في المشاريع بكافة المجالات والإمكانيات وخاصة مجال التحفيز المادي من اجل خلق جو ملائم لنجاح إدارتها للمشاريع .

5- فسح المجال أمام العديد من المهندسين للعمل في مؤسسات التشييد, وذلك من خلال العقود المؤقتة وتدفع النفقات من المبالغ المخصصة للإشراف على المشاريع لسد النقص الحاصل في الفرق.

6- التركيز على إحالة المشاريع على الشركات المنفذة بحدود الكلف والمدد المثلى المقاربة للكلف والمدد التخمينية لتجنب زيادة مدة المشاريع والإخفاقات النوعية.

7- التأكيد على تنفيذ التصاميم لدى جهات استشارية ضليعة بإعمال التصميم مع التأكيد على تدقيق هذه التصاميم قبل إعتمادها لتجنب التغييرات التي تحدث اثناء التنفيذ والتي تؤدي الى زيادة في كلفة ووقت المشاريع بسبب الأخطاء التصميمية.

8- ينبغي إعطاء الصلاحيات الكاملة من قبل الإدارات العليا للمؤسسات الإنشائية في إصدار الأوامر الإدارية الخاصة بتنفيذ المشاريع وخاصة الأوامر المتعلقة بالتغييرات وغيرها من المراسلات تلافيا للتأخيرات والمطالبات الحاصلة بسببها.

<u>المصادر</u>

➢ Maylor, Harvey "Project " Financial times, pitman, 1$^{st}$ED–1990 – UK

➢ محمد جمعة حسين "إدارة تنفيذ المشروعات الإنشائية" مكتب الدراسات والإستشارات الهندسية القاهرة 2008

➢ Albert Lester "Project , Planning and Control Managing Engineering, Construction and Manufacturing Projects" to PMI, APM and BSI St –andards Elsevier Science & Technology Books 2006

➢ محمد مشعل محمد "تطوير نظام إداري للسيطرة على المعلومات والمتابعة في المشاريع الإنشائية" رسالة ماجستير, هندسة البناء والإنشاءات, الجامعة التكنولوجية, 2006

➢ صويص غالب جليل "أساسيات إدارة المشاريع الهندسية" الأردن 2010

➢ James A. Bent ,Albert Thumann "Project  for Engineering And Cconstruction" 2nd Edition PennWell Publishing Company 1994

➢ Garold D. Oberlender "Project  for Engineering and Constru –ction" Second Edition, United States, McGraw–Hill Companies, Inc 2000

➢ المملكة العربية السعودية "دليل إجراءات الإشراف على تنفيذ المشاريع في المملكة العربية السعودية" 2009

➢ ستانلي غولد هابر ، مانويل ماسيدو " النظم الإدارية لهندسة التشييد " دار جون وايلي وأبناءه المملكة العربية السعودية 1982

➢ العطار إحسان إبراهيم "إدارة المشاريع الإنشائية والعلاقات المهنية" بغداد, الجامعة التكنولوجية  1989م

➢ Linda, Sllai "a sunergistic approach to project  in information systems development international Journal of project . Vol. 15 No. 3, June 1997.

➢ حوا عمار مصطفى "إدارة مشاريع التشييد" سوريا, حلب, شعاع للنشر والعلوم,  2008

➢ Harvey A. Levine  "Practical Project  Tips, Tactics, and Tools" John Wiley & Sons, INC New York. 2002

➢ Dennis Lock "Project  in construction" 2004
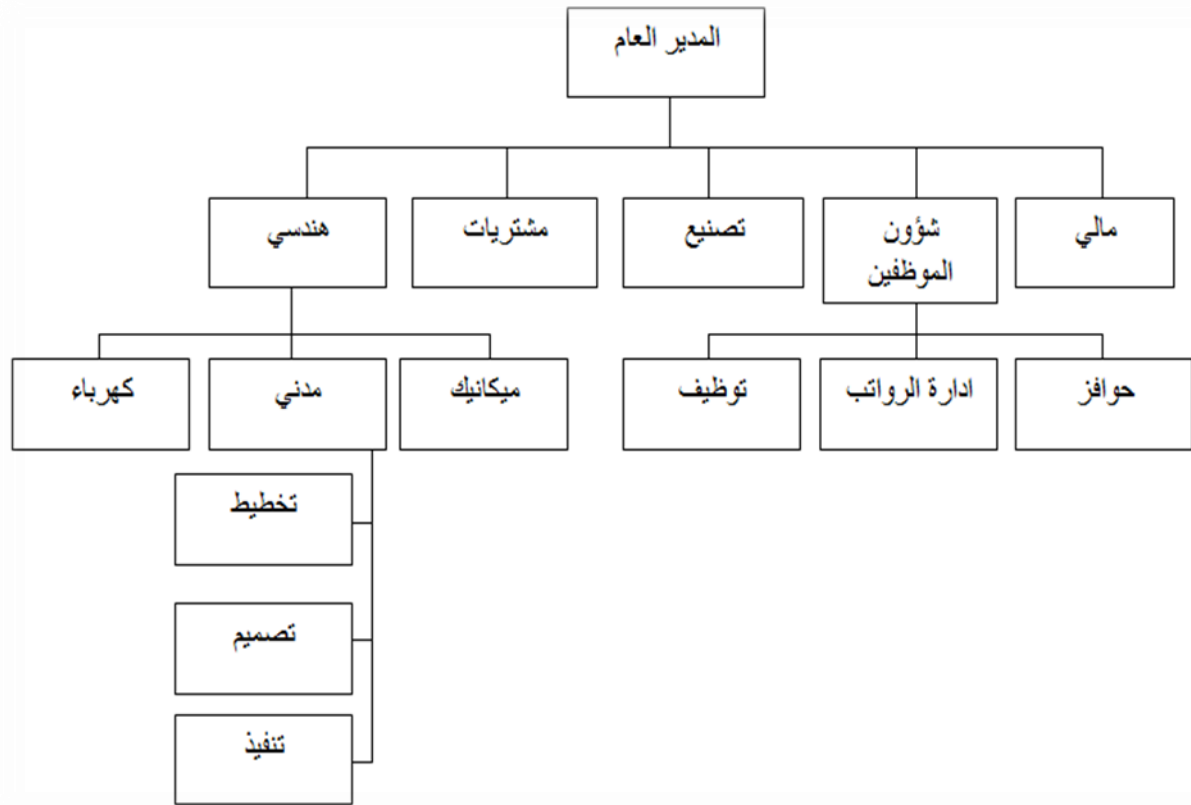
شكل (1) الهيكل التنظيمي الوظيفي (Harvey-2002)
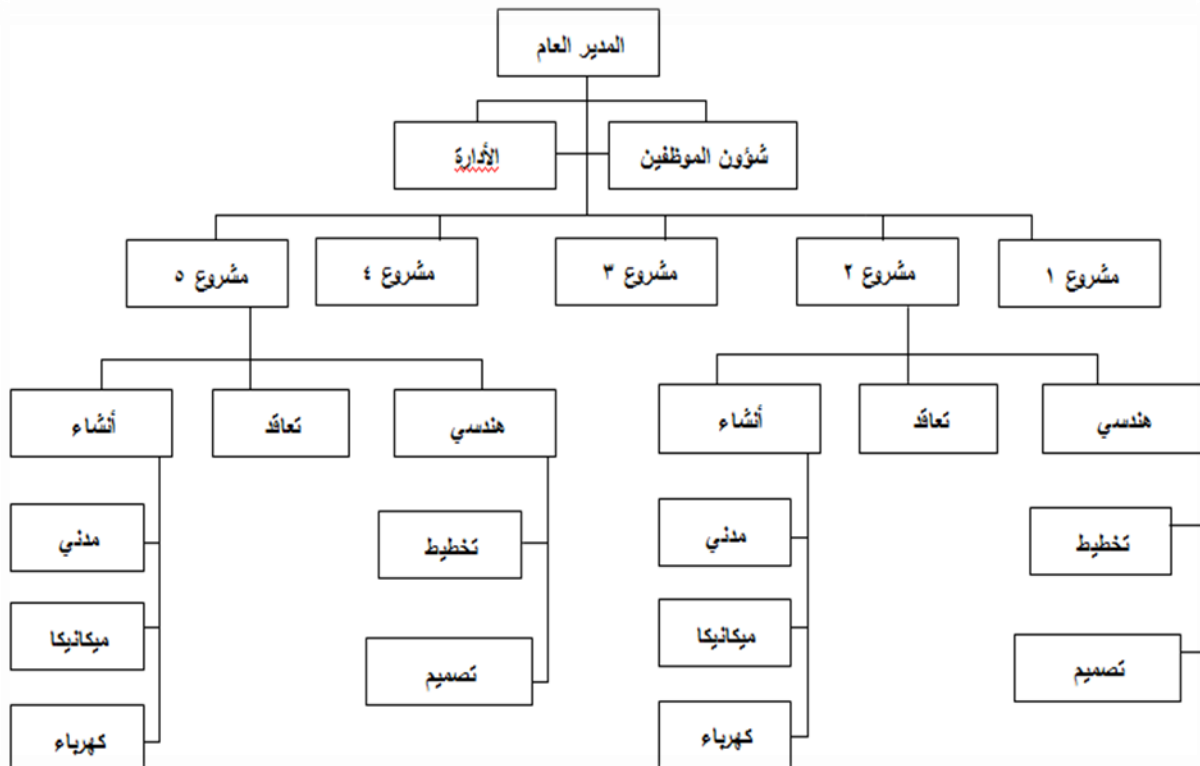


شكل(2) الهيكل التنظيمي النموذجي أو المشروعي (Harvey-2002)

شكل (3) هيكل تنظيم المصفوفة(Dennis-2004)
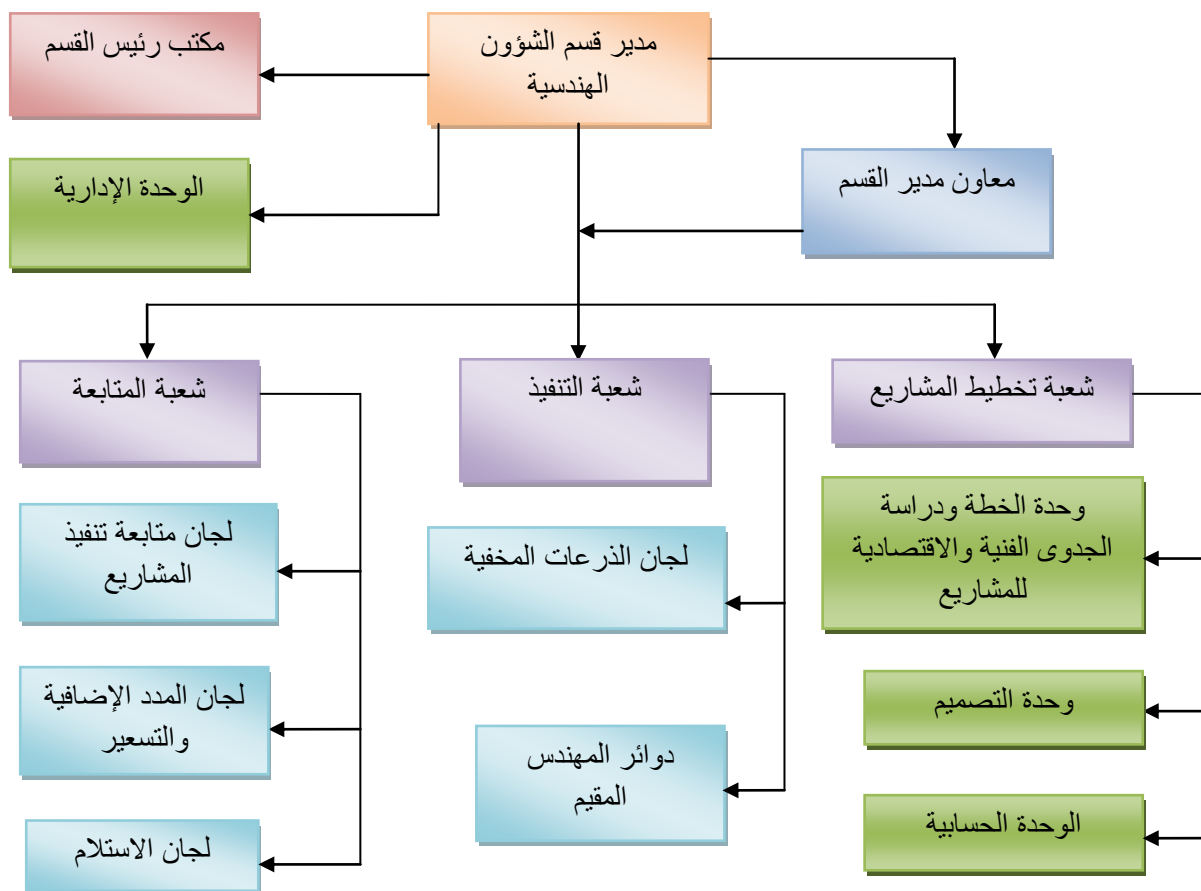


شكل (4) الهيكل التنظيمي لقسم الشؤون الهندسية(الباحث)
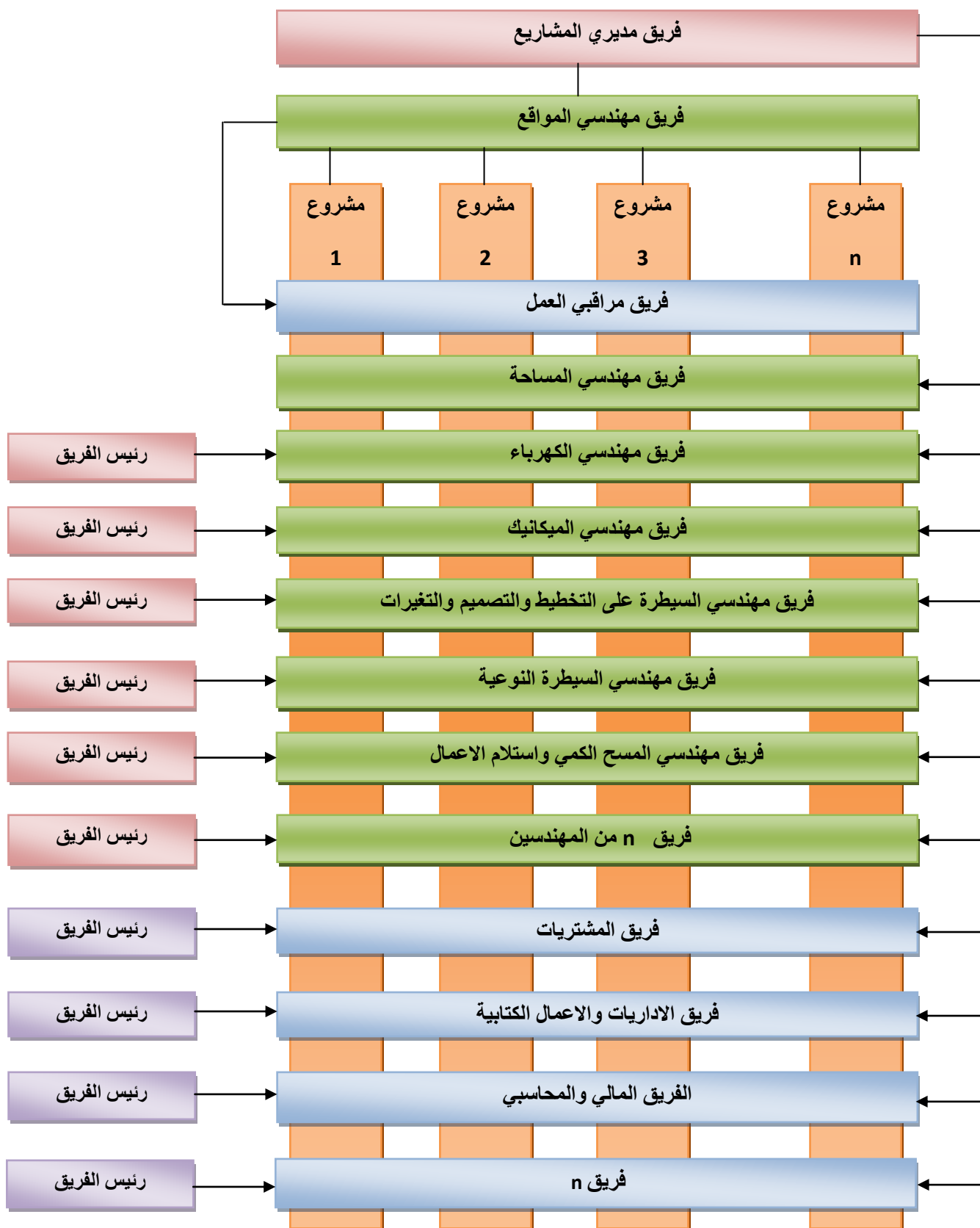
شكل (5) الهيكل التنظيمي المرن للإشراف [
(الباحث) على تنفيذ مشاريع إنشائية متعددة
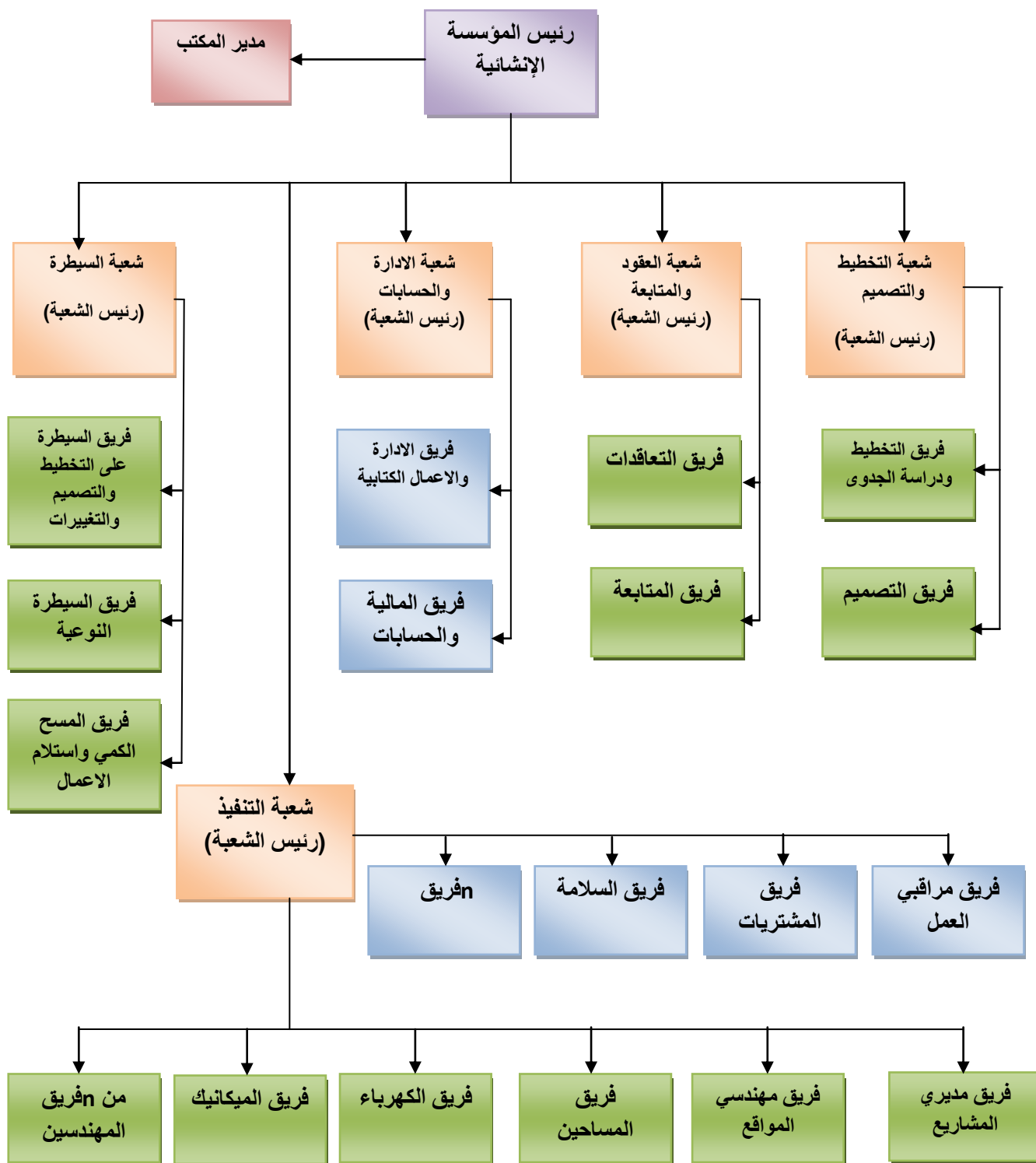
شكل (6) الهيكل التنظيمي المرن لمركز المؤسسة الإنشائية(الباحث)

| خط أساس الجودة | خط أساس الجدول الزمني | خط أساس الكلفة (الموازنة) |
|---|---|---|
| تقارير الأداء | وضع البرامج الزمنية الخطية | تقارير الأداء |
| مخطط التباين | تقارير الأداء | تحليل التباين |
| خطط الإجراءات الوقائية والتصحيحية | تحليل التباين | التنبؤ |
| تطبيق الإجراءات الوقائية والتصحيحية | التنبؤ | الإجراءات التصحيحية |
| قائمة التغييرات المستحدثة | الإجراءات التصحيحية | قائمة التغييرات المستحدثة |
| مراجعة إصلاحات العيوب | قائمة التغييرات المستحدثة | تحديث تقديرات الكلفة |
| تحديث خط أساس الجودة | تحديث خط أساس الجدول الزمني | تحديث خط أساس الكلفة (الموازنة) |

خطة إدارة المشروع

تحديث خطة إدارة المشروع

شكل (7) خطوات السيطرة على المشاريع الانشائية في مرحلة التنفيذ(الباحث)

19

تأثير البولي ايثيلين ذو الكثافة المرتفعة و المنخفضة على بعض الخواص الميكانيكية للخرسانة

هديل ابراهيم احمد
مدرس مساعد
معهد التكنولوجيا / هيئة التعليم التقني

د. ندى مهدي الجيلاوي
استاذ
كلية الهندسة / جامعة بغداد

**الخلاصة**

ان تزايد استخدام اللدائن البلاستيكية في مختلف جوانب الحياة العصرية اسفر عن توفر كم هائل من مخلفاتها وبما يؤثر بشكل سلبي على البيئة و الانسان . لذا كان لابد من ايجاد حلول لمعالجة هذه المخلفات وبما يضمن الاستفادة منها وكأحد هذه الحلول محاولة استخدامها الخلطة الخرسانية .

تم في هذا البحث استخدام الفحوصات المختبرية لإنتاج خرسانة حاوية على مثروم البولي ايثيلين ذو الكثافة المرتفعة و المنخفضة وقد استخدم بمقدار (5 ، 10 ، 15) % كنسبة استبدال جزئي من حجم الرمل وذلك للحصول على خرسانة اخف وزناً وذات مقاومة انضغاط جيدة فضلاً عن فوائد اخرى مثل تحسين امكانية ضخ الخرسانة وتقليل سرعة فقدان الخرسانة لقابلية تشغيلها كون ان هذا البوليمر مادة غير قابلة لامتصاص الماء والاستفادة ايضاً من هذه المخلفات الضارة بشكل ايجابي يحقق فوائد للبيئة و الانسان على حد سواء .

**الكلمات الرئيسية** : الخرسانة , البولي ايثيلين ذو الكثافة المرتفعة , البولي ايثيلين ذو الكثافة المنخفضة , مقاومة الانضغاط , الكثافة .

# Effect of high and low density polyethylene on some mechanical properties of concrete

**Assist Lecturer.Hadel Ibraheem Ahmad**
Institute of Technology-Foundation of Technical Education
Email : hadeel_ebraheem @yahoo.com

**Prof.Nada Mahdi Algalawi**
College of Engineering-Baghdad University
Email : naljalawi @yahoo.com

## ABSTRACT

The increasing use of plastics in various aspects of modern life resulted in the availability of enormous amount of wastes, including a negative effect on the environment and humans. So it is necessary to find solutions to deal with these wastes and ensure to use them as solutions to use in concrete mix .

In this research the production of concrete containing high and low density polyethylene has been used by (5, 10, 15)% as a replacement of part of the volume of sand, so as to obtain concrete good compressive strength as well as other benefits such as improved possibility of pumping concrete and reduce the loss of concrete for workability polymer is a material that is non-absorbable of water . It is also intended to dispose of these wastes positively to achieve benefits to the environment and humans alike .

**Keywords :** Concrete , High Density Polyethylene , Low Density Polyethylene ,Compressive Strength , Density .

## 1. المقدمة

الخرسانة  تعبير إنشائي مكون من خليط متدرج من الركام مثل الحصى والرمل المترابطة حبيباته بواسطة مادة رابطة وهذه المواد الرابطة يمكن ان تكون مواد غير عضوية مثل السمنت و كما يمكن تسمية الخرسانة طبقاً لنوع الحصى المستخدم مثل  الخرسانة الخفيفة والثقيلة وعادة يطلق اسم الخرسانة على الخرسانة السمنتية التي يدخل في تركيبها السمنت والركام والماء .

تعتبر الخرسانة هي المادة الوحيدة التي يمكن ان تفي باحتياجات الانشاءات من الوحدات السكنية الصغيرة والبسيطة الى الهياكل الكبيرة والمعقدة ومن المعروف ان استعمالات الخرسانة لا تقتصر على المباني و انما تمتد الى انشاء السدود والطرق والجسور والمطارات وكذلك في مشاريع الري والصرف والموانئ وغير ذلك مما لا يمكن حصره وتعتبر صناعة الخرسانة وخاصة في المنشأت الصغيرة المحدودة من اهم العوامل التي ادت الى انتشار الانشاء في مجال المباني السكنية حيث لا توجد مادة بديلة يمكن ان تستوعب وتخدم هذا الانتشـــار العمراني الكبير الذي يحدث في جميع انحاء العالم ، الا ان مادة الخرسانة يمكن ان تصنع بمهارات بسيطة  من خلال التفاعل الكيميائي (Hydration) فان العجينة تتصلب وتكتسب قوة لتشكل كتلة كالصخرة ولها خصائص تتحدد بجودة العجينة السمنتية المستخدمة ، وقوة الخرسانة تعتمد على  نسبة المـاء الـى السمنت (w\c) في العجينـة ولكن معظم انواع الخلطات تحوي اضافات عديدة ذات تأثير هام على مواصفاتها ، وللحصول علـى افضل المواصفات يجب ان تستعمل الاضافات المناسبة في المكـان المناسب ، ومن المهم معرفـة كل الاثار الممكنة لأنها يمكن ان تغير من سلوك الخرسانة المطلوبة وربما يكون ضرورياً تعديل اسلوب الصب ليكون ملائماً للصفات المميزة المطلوبة **(الخلف و يوسف ، 1982) (ليفون ، ساكو ،1983)** .

## 2. تطور علم وتكنولوجيا البوليمرات (اللدائن)

يتزايد استعمال منتجات اللدائن في مختلف جوانب الحياة العصرية بصور و اشكال مختلفة يصعب حصرها وتحديدها سواء بشكل مواد ومنتجات بلاستيكية او مطاطية او الياف تركيبية وصناعية و خلائط بوليمرية ذات خصائـص تتفوق كثيراً علـى المعـادن والمـواد التقليدية المعروفة ، وبدأت تحل تدريجياً محل الكثير من المواد في مجالات مختلفة مثل الملبس والسكن والنقل والتجهيزات المنزلية و الاثاث ، وفي الكثير من اجزاء السيارات والطائرات والمعدات المختلفة ، وحيث كانت المادة الاشارة الدالة على عصور التقدم في الحضارة البشرية وكثيراً ما سميت العصور بأسمائها مثل الحجر والقصدير والبرونز والحديد والفولاذ ، فان الاعتقاد يسود في العالم بأننا مقبلون على عصر اللدائن ، وان عالم الغد ستغزو فيه البوليمرات ومنتجاتها العديد من جوانب حياتنا وتلبي متطلبات التقدم ، مثل الكثير من العلوم ، وكان للطبيعة الفضل الاول في تطور البوليمرات (اللدائن) اذ انه من المعلوم وجود العديد من البوليمرات الطبيعية  "Natural Polymer"  المستعملة من قبل الانسان منذ قرون عديدة مثل القطن والحرير والخشب والمطاط مما دفع العلماء قديماً الى محاكاة الطبيعة ومحاولة تقليد ودراسة ما هو موجود .

## 3. البولي ايثيلين

### 1.3 البوليمــر

ان كلمة البوليمر لاتينية الاصل وهي مركبة من مقطعين هما "poly" وتعني متعدد ، ومير "mer" تعني الوحدة ، لذلك ال "polymer"  يعني متعدد الاجزاء ، ولغرض السهولة تستعمل كلمة بوليمر بدلاً من متعدد

الاجزاء . ان علم البوليمرات يبحث عن المواد التي تكون جزيئاتها كبيرة وبوليمرية والتي تتكون عادة نتيجة لارتباط جزيئات صغيرة ببعضها كيميائياً ، وتدعى واحدة من هذه الجزيئات الصغيرة بالمونومير "Monomer" ، فالوحدة البنائية الصغيرة للبوليمر والمسماة بالمونومير يمكن ان تمثل بحلقة واحدة في سلسلة معدنية طويلة . فالجزيئة او السلسلة البوليمرية "Polymer chain" تنتج عن ارتباط كيميائي بين عدد كبير من الجزيئات الصغيرة والتي سميت بالمونومرات مكونة السلاسل البوليمرية الطويلة، ويجوز ان تكون الجزيئة الناتجة متفرعة ويدعى عندئذ البوليمر بالبوليمر المتفرع "Branched polymer" ويشار عادة الى عدد الوحدات المتكررة "Repeating units" او عدد الوحدات البنائية والتي هي في الواقع عدد المونومرات المتحدة في سلسلة واحدة ، بالمصطلح "درجة البلمرة""Degree of polymerization" ويرمز لها بـ Dp او Xn ولما كانت جزيئات البوليمر الواحد غير متساوية جميعاً في درجة البلمرة لذلك يعبر عم درجة البلمرة بمعدل درجة البلمرة ويرمز بـ Dp او Xn. وتكون في بعض الاحيان درجة البلمرة واطئة ، وبذلك يكون الوزن الجزيئي للبوليمر واطئاً وتتراوح درجة البلمرة هذه بين (10 – 20) .

## 4. استعراض البحوث السابقة

ان التطور الصناعي والتكنولوجي يعتمد بشكل كبير على تقدم المواد ونتيجة لهذا التطور الصناعي الكبير الذي شهده العالم في كافة المجالات ظهرت الحاجة لإيجاد البدائل للمواد ذات الاستخدامات الصناعية المتعددة بحيث تكون تلك البدائل ذات مواصفات جيدة من حيث الكلفة وخفة الوزن والخواص بصورة عامة وذلك لاستخدامها في التطبيقات الصناعية المتعددة (سعيد ، رفيق ، 2011) . ومن هذه البدائل هي المواد البلاستيكية التي زاد استهلاكها سنوياً الى ما يقارب 5 مليون طن في عام 1950 الى ان وصل الى مـــا يقارب 100 مليـون طن في 2001 . وان المـــواد البلاستيكـ 3 غير ضارة بالبيئة حتى بعد فترة طويلة من التعرض للظروف البيئية . فان عملية التحلل البطيئة لهذه المواد تتسبب في مشكلة التخلص من هذه المخلفات من جهة نظر بيئية . وبالتالي فان استخدام مخلفات هذه المواد في الخرسانة يكون حلاً جيداً لهذا الخطر البيئي . وقد اجريت بحوث عـديدة حــول استخـدام المخلفات البوليميرية المعادة تدويرها (Batayneh, et al, 2007) .

بين الباحثان (Kumar and Praksh,2006) ان اختيار الركام للخرسانة العادية مهم جداً وذلك لان خواص الركام المتوعة تؤثر على اداء الخرسانة حيث استخدمت المخلفات البلاستيكية و هي البولي ايثيلين ذات الكثافة المرتفعة و بنسب ( 6,4,2 ) % كنسبة استبدال من الرمل و السمنت . و قد لاحظوا ان قيم مقاومة الانضغاط للخلطات الخرسانية تزداد بإضافة المضافات المعدلة لخواص الخرسانة , فان مقاومـة الانضغاط زادت بمقدار 20% مقارنة بخلطات الخرسانة العادية .

وقد استخدم الباحثون ( Batayneh et al., 2007 ) في تلك الدراسة ثلاثـة انواع من مخلفات المواد و هي الزجاج , البلاستك و الخرسانة المعادة . فالبلاستك و الزجاج تم استخدمهما كنسبة استبدال كحد اعلى 20% من الركام النـاعم و استخدمت الخرسانة المعادة كنسبة استبدال كحـــد أعلى 20% من الركام الخشن . وقد استخدم السمنت البورتلاندي في الخلطات الخرسانية بمحتوى 446 كغم/م³ و نسب الاستبدال الحجمي تتراوح ما بين ( 5–20 )% . و قد بينت الدراسة ان اعادة استخدام مثل هذه المواد تحسن و بنجاح خواص الخرسانة من مقاومة الانضغاط و الانثاء و الشد المباشر .

وقد استخدم الباحثون **( Rahman, et al., 2012 )** انواع من المخلفات البوليميرية مثل , البولي استايرين و مطاط الاطارات و على نسب ( 10–40 )% كنسبة استبدال حجمي من الحجم الكلي للنموذج و قد اظهرت لنتائج ان هذه المواد تقلل من مقاومة الانضغاط و الكثافة و امتصاص الماء و المسامية للخرسانة .

## 5. المواد المستخدمة

### 1.5 السمنت

السمنت المستخدم في هذا البحث هـــو سمنت بورتلاندي اعتيادي (Type I ) المصنع من قبل شركة الماس للاستثمار الصناعي . و قد أجريت له الفحوصات الفيزيائية والكيميائية في مختبر الشركة العامة للسمنت العراقية والنتائج موضحة في الجدولين ( 1 ) و (2) على التوالي و يــلاحظ ان الخــواص الفيزيائية و الكيميائية مطابقة للمواصفة العراقية ( م.ق.ع /5 / 1984 ) .

### 2.5 الركام الناعم

تــم استخدام الركام الناعم ( الرمل ) من مقالع منطقة الاخيضــر و تــم فحص خواصــه الفيزيائيــة فــي مختبر الخرسانة التابع لمعهد التكنولوجيا وهو مطابق للمواصفة العراقية القياسية ( م.ق.ع /45 / 1984 ) كما موضح بالجدول (3) و ( 4 ) على التوالي .

### 3.5 الركام الخشن

تم استخدام حصى مكسر مقاسه الاسمي ( 14ملم) و قد تم الحصول عليه من منطقة النباعي. و تم فحص خواصه الفيزيائية في مختبر الخرسانة التابع لمعهد التكنولوجيا وهو مطابق للمواصفة العراقيــة القياسيــة ( م.ق.ع /45 / 1984 ) كما موضح بالجدول (5) و (6) على التوالي.

### 4.5 المـــاء

تم استخدام ماء بغداد الصالح للشرب في جميع الخلطات التجريبية في هذا البحث .

### 5.5 الملدن المتفوق

استخدم في هذا البحث ملدن متفوق عالي الاداء والمعروف تجاريا ( Flocrete PC 200 ) وصمم خصيصاً لتقليل محتوى ماء الخرسانة لاداء اكثر فعالية و بهذا يعطي مقاومة عالية وانسيابية لجميع الخلطات الخرسانية وبذلك يحقق اعلى ديمومة و اداء للخرسانة . ان المحتوى الأمثل للملدن المتفوق المستخدم في هذا البحث هي 0.9 لتر لكل 100 كغم من السمنت لجميع الخلطات التجريبية التي سوف يتم ذكرها في فقرة خلطات الخرسانة . يوضح الجدول (7) الخصائص التقنية للملدن المتفوق المستخدم في هذه الدراسة .

### 6.5 البولي ايثيلين

استخدم مثروم البولي ايثيلين ذو الكثافة المرتفعة و المنخفضة وبنسبة( 5 , 10 , 15 )% كنسبة استبدال حجمي من الرمل . تم الحصول عليه من الشركة العامة لصناعة الزيوت النباتية . و يوضح الجدول (8) بعض خواص البولي ايثيلين ذو الكثافة المرتفعة و المنخفضة.

### 7.5 الخلطات الخرسانية

تم تقسيم التجارب المختبرية إلى أربعة خلطات تم تصميمها بموجب المعهد الاميركي للخرسانة ( ACI 211 1R/91 ) و مزجها و صبها و فحصها . و تفاصيل هذه الخلطات تم عرضها بالجدول ( 9 ) .

### 8.5 طريقة خلط و صب و إنضاج النماذج الخرسانية

عملية الخلط تمت بالمزج اليدوي بموجب المواصفة الأميركية(ASTM C-192-02) و بذلك يتم الحصول على خلطة خرسانية متماسكة,حيث تم خلط المواد التالية ( السمنت , الرمل , الحصى و البولي ايثيلين ذو الكثافة المرتفعة ) ثم اضيف جزء من ماء الخلط ومع الاستمرار بالمزج عدة مرات وبعدها اضيف الملدن المتفوق و من ثم اضافة الجزء الاخير من الماء و استمرت عملية الخلط لمدة 5 دقائق تقريبا حتى اصبحت المزجة الخرسانية متجانسة تماماً , و بعدها تم وضع الخرسانة بعدة طبقات و استعمال الهزاز لمدة ( 15-30 ) ثانية لغرض رص القوالب للتخلص مــن الفقاعات الهوائية بعد ان تم  طلاء الجدران الداخلية لها بالدهان (Grease) وذلك لمنع التصاق الخرسانة بعد تصلبها ثم تم تعديل سطح الخرســانة وبعد الانتهاء من عملية الصب تغطى القوالب بغطاء من النايلون لمنع تبخر الماء من الخرسانة الطرية مع تركها لمدة 24 ساعة و بعدها يتم إخراج النماذج من القوالب و يتم وضعها بالماء لفترة إنضاج قدرها (7 , 28 , 60) يوم . اما عن ابعاد النماذج المستخدمة فقد تم استخدام نماذج مكعبة الشكل أبعادها (100 × 100× 100 ) ملم لأجراء فحص مقاومة الانضغاط وفحص الموجات فوق الصوتية وفحص الكثافة .

**9.5 الفحوصات غير الاتلافية**

**1.9.5 فحص الكثافة**

تم إيجاد الكثافة الكلية للنماذج الخرسانية بموجب متطلبات ( الدليل الاسترشادي المرجعي 274) .

**9.5. فحص سرعة الذبذبات فوق الصوتية**

تم أجراء هذا الفحص في مختبر الخرسانة التابع لمعهد التكنولوجيـا و بموجـب المواصفـة البـريطانيـــة (BS:1881part 203:1986) . باستخدام جهاز (PUNDIT) لقياس سرعة الذبذبات فوق الصوتية خلال نماذج مكعبة الشكل بأبعاد (100×100×100) ملم للخلطات الخرسانية وكان تردد المجسات المستخدمة لهذا الجهاز ( 55 كيلوهرتز ) ويعتمد قياس سرعة الذبذبات فوق الصوتية في الخرسانة على قياس الزمن (T) الذي تستغرقه الذبذبات لعبور مسافة محددة (L) في الخرسانة ولغرض الحصول على درجة عالية من الدقة تقاس المسافة بالمليمترات ويقاس الزمن بواسطة جهاز (PUNDIT) والى حد جزء من المليون من الثانية ويمكن التعبير عن السرعة بوحدات كيلومتر/ ثانية كما في المعادلة الآتية :-

$$V = \frac{L}{T}$$

( 1 )

**10.5 الفحوصات الاتلافية**

**5-10-1 فحص مقاومة الانضغاط**

اجري فحص مقاومـة الانضغاط بموجب المواصفة البريطانية( BS1881:part116:1989 ) و باستعمال جهاز ( ELE Digital Testing ) و بسعة تحميل ( 2000 كيلونيوتن ) . وتــم استخــدام نماذج مكعبة الشكل بإبعاد (100×100× 100) ملم للخلطــات الخرسانية و تم الفحص بأعمار( 7 , 28 , 60 ) يوم واخذ معدل ثلاث مكعبات .

**6. النتائج و مناقشتها**

**1.6 فحص مقاومة الانضغاط**

تعد مقاومة الانضغاط من الخواص الرئيسية والمهمة للخرسانة المتصلبة والتي من خلالها يمكن تقييم اغلب الخواص لتحديد صلاحيتها كمادة إنشائية. ومن النتائج التي تم الحصول عليها ان مقاومة الانضغاط تقل مع

زيادة نسب الاستبدال الحجمي و لكلا نوعين البولي ايثيلين ( LDPE , HDPE ) و كما موضح **بالشكل** ( 1 ) وهذا السلوك يعود الى انخفاض مقاومة انضغاط جزئيات البولي ايثيلين مقارنتاً مـــع عجينة السمنت و طبيعة الركام الناعم و الخشن وهذا يشابه ما توصل اليه الباحث **(Naik et al. 1996)** واخرون . يوضح **الجدول (10)** نتائج فحص مقاومة الانضغاط للخرسانة الحاوية على البولي ايثيلين ذو الكثافة المرتفعة و ذو الكثافة المنخفضة. و بينت الدراسة ايضاً ان مقاومة الانضغاط للخرسانة الحاوية على البولي ايثيلين ذو الكثافة المرتفعة أفضل من مقاومة الانضغاط للخرسانة الحاوية على البولي ايثيلين ذو الكثافة المنخفضة بمقدار ( 16.6,12.5,14.8 ) % و يعزى ذلك الى الكثافة العاليـــة للمنتج يعني ان له بلورية عالية نتيجة تجمع السلاسل البلورية و تراصها بشكل قريب جدا من بعضها البعض ( **سعيد و رفيق** , **2011** ) .

## 2.6 فحص كثافة الخرسانة

تعتبر الكثافة من الخواص المهمة للخرسانة لعلاقتها بالخواص الميكانيكية ومن ضمنها مقاومة الانضغاط وسرعة الذبذبات فوق الصوتية . **الجدول ( 11 )** يوضح نتائج فحص كثافة الخرسانة الحاوية على البولي ايثيلين ذو الكثافة المرتفعة و ذو الكثافة المنخفضة . 7 انخفاض كثافة الخرسانة الحاوية على البولي ايثيلين ذو الكثافة المرتفعة و الخرسانة الحاوية على البولي ايثيلين ذو الكثافة المنخفضة مع زيادة نسب الاستبدال له وبمقدار(5 ، 10 ، 15) % من حجم الرمل . وذلك بسبب خفة وزن البولي ايثيلين فمثلا ذو الكثافة المرتفعة الذي تبلغ كثافته (970 − 950) كغم/ م$^3$ وهو اقل من كثافة الركام الناعم (الرمل) والبالغة (1630 كغم /م$^3$) وهذا بدوره يؤدي الى تقليل في الاحمال الميتة للمنشأ وبالتالي ادخال ذلك في حسابات التصميم . ومن النتائج ممكن ملاحظة ان العينات التي تحتوي البولي ايثيلين ذو الكثافة المرتفعة تمتلك كثافة اعلى من العينات التي تحتوي البولي ايثيلين ذو الكثافة المنخفضة كما موضح **بالشكل ( 2 )** و ذلك لتاثير الكثافة للبولي ايثيلين و ايضا لزيادة البلورية لمادة البولي ايثيلين .

## 3.6 فحص سرعة الذبذبات فوق الصوتية

يعد فحص سرعة الذبذبات فوق الصوتية هو احد الفحوصات غير الاتلافية التي يتم بواسطتها توقع بعض الخواص الفيزيائية للخرسانة وكذلك امكانية اعادة اجراء الفحوص للنماذج نفسها في فترات زمنية متعاقبة . **الجدول ( 12 )** يوضح نتائج فحص سرعة الذبذبات فوق الصوتية للخرسانة الحاوية على البولي ايثيلين ذو الكثافة المرتفعة و المنخفضة . يلاحظ انخفاض سرعة الذبذبات فوق الصوتية للخرسانة الحاوية على البولي ايثيلين ذو الكثافة المرتفعة و المنخفضة مع زيادة نسب الاستبدال له وبمقدار (5 ، 10 ، 15) % من حجم الرمل . و ايضاً يمكن ملاحظة تصرف عينات الخرسانة الحاوية البولي ايثيلين ذو الكثافة المرتفعة افضل و بمقدار ( 2.4,2.3,2 ) % اذا ما قورنت مع عينات الخرسانة الحاوية البولي ايثيلين ذو الكثافة المنخفضة و كما مبين **بالشكل ( 3 )** و ذلك لتأثير كثافة المادة الأساس حيث كلما زادت الكثافة كلما زادت السرعة .

## 7. الاستنتاجات

قد أظهرت النتائج ان زيادة نسبة هذا البوليمر في الخلطة الخرسانية يؤدي إلى :-

1-إعطاء مقاومة انضغاطية جيدة لكن ليس بقوة مقاومة الانضغاط للخرسانة المرجعية حيث كانت تتراوح بين ( 21.7 , 20 , 10 ) % للخرسانة الحاوية على البولي ايثيلين ذو الكثافة المرتفعـة و تتراوح بين ( 33.3 , 30 , 25 ) % للخرسانة الحاوية على البولي ايثيلين ذو الكثافة المنخفضة لنسب الاستبدال (5 ، 10 ، 15) % من حجم الرمل وبزمن انضاج 50

8

2– إنتاج خلطة خرسانية خفيفة الوزن حيث بلغت النسب المئوية للكثافة الخرسانية الحاوية على البولي ايثيلين ذو الكثافة المرتفعة (0.5 , 1.4 , 2.4 ) % للخرسانة الحاوية على البولي ايثيلين ذو الكثافة المرتفعة و تتراوح بين ( 0.8 , 2.3 , 3.2 ) % للخرسانة الحاوية على البولي ايثيلين ذو الكثافة المنخفضة لنسب الاستبدال (5 ، 10 ، 15) % من حجم الرمل وبزمن انضاج 60 يوم .

3– انخفاض سرعة الذبذبات فوق الصوتية للخرسانة الحاوية على البولي ايثيلين ذو الكثافة المرتفعة حيث تتراوح بين (5.6 ، 7.5 ، 9.4) % و تتراوح ( 7.5 , 11.3 , 13.2 ) % للخرسانة الحاوية على البولي ايثيلين ذو الكثافة المنخفضة لنسب الاستبدال (5 ، 10 ، 15) % من حجم الرمل وبزمن إنضاج 60 يوم .

## 8. المصادر العربية

➢ المواصفة القياسية العراقية رقم (5) لسنة 1984، السمنت البورتلاندي" ، الجهاز المركزي للتقييس والسيطرة النوعية ، بغداد.

➢ المواصفة القياسية العراقية رقم (45) لسنة 1984، ركام المصادر الطبيعية المستعمل في الخرسانة والبناء , الجهاز المركزي للتقييس والسيطرة النوعية ، بغداد.

➢ الدليل الاسترشادي المرجعي رقم 274 , فحوص الخرسانة و طرق تعيين كثافة الرسانة المتصلبة  , الجهاز المركزي للتقييس والسيطرة النوعية , 1992.

➢ سعيد, رفيق , دراسة الخصائص الميكانيكية لمتراكبات البولي اثيلين المدعم بدقائق مسحوق الصدف  , مجلة الهندسة والتكنولوجيا , المجلد 29, العدد 15 , 2011 .

➢ الخلف , يوسف , تكنولوجيا الخرسانة , الجامعة التكنولوجية , 1982.

➢ ليفون, ساكو, انشاء المباني  , مطبعة جامعة بغداد , ط 1 , 1983 .

## 9. المصادر الاجنبية

➢ American Concrete Institute Committee 211.1R-91 ,Properties for Normal , Heavyweight and Mass Concrete ,Reported by ACI committee 211,   ACI Manual of Concrete Practice.

➢ American Concrete Institute , Standard Practice for Making and Curing Concrete Test Specimens in the Laboratory, Annual Book of ASTM Standards C 192/C 192M -07 .

➢ British Standards Institution. BS 1881,Part 203, 1983, Recommendations for measurements of velocity of ultrasonic pulses in concrete .

➢ British Standards Institution. BS 1881,Part 116, 1989, Method for determination of compressive strength of concrete cubes" British standards institution .

➢ Kumar , B.V. Kiran., and Praka...,. .,2006, Use of Waste Plastics in Cement Concrete Pavement , PP. 1-6 .

➢ Batayneh , Malek., Marie , Iqbal.,and Asi, Ibrahim.,2007, Use of selected waste materials in concrete mixes  , Waste Management 27 , PP. 1870–1876 .

➢ Rahman , Md. Mostafizur., Islam, Md. Akhtarul., and Ahmed , ,Mainuddin., 2012 , Recycling of Waste Polymeric Materials as a Partial Replacement for Aggregate in Concrete " , International Conference on Chemical, Environmental and Biological Sciences (ICCEBS'2012) , PP. 99-102 .

➢ Naik et al., taken from Yadav,Ishwar Singh, 2008 , Laboratory Investigating Investigations of the Properties of Concrete Containing Recycled Plastic Aggregates , M.Sc. Thesis, Thapar University , India .

**الجدول (1) الخواص الفيزيائية للسمنت**

| حدود المواصفة العراقية( م.ق.ع /5/ 1984 ) | نتائج الفحص | الخواص الفيزيائية |
|---|---|---|
| لا تقل عن 2300 سم² / غم | 3255 | النعومة ( بطريقة Blaine ) سم² / غم |
| لا يقل عن 45 دقيقة<br>لا يزيد عن 10 ساعات | 2:10<br>4:45 | زمن التماسك<br>الابتدائي , ( دقيقة:الساعة )<br>النهائي , ( دقيقة:الساعة ) |
| لا تزيد عن 0.8 | 0.03 | السلامة ( الثبات ) بطريقة المحمم ( % ) |
| لا يقل عن 15 ميكا باسكال<br>لا يقل عن 23 ميكا باسكال | 22.31<br>28.61 | مقاومة الانضغاط ( ميكا باسكال )<br>3 أيام<br>7 أيام |

**الجدول (2) الخواص الكيميائية للسمنت**

| حدود المواصفة العراقية<br>( م.ق.ع /5/ 1984 ) | المحتوى % | الصيغة الكيميائية | الخواص الكيميائية |
|---|---|---|---|
| – | 62.10 | CaO | اوكسيد الكالسيوم ( % ) |
| – | 20,12 | SiO2 | اوكسيد السليكون ( % ) |
| – | 4,97 | Al2O3 | اوكسيد الالومنيوم ( % ) |
| – | 3.35 | Fe2O3 | اوكسيد الحديد ( % ) |
| محتوىSO3 ( % ) لا يزيد 2.8 عندما تكون نسبة ( C3A ) اكثر من 5 % | 2.5 | SO3 | الاملاح الكبريتية( % ) |
| لا يزيد عن 5 % | 1.86 | MgO | اوكسيد المغنسيوم ( % ) |
| لا تزيد عن 1.5 % | 0.32 | I.R. | المواد القابلة للذوبان ( % ) |
| لا يزيد عن 4 % | 3.74 | L.O.I. | الفقدان بالحرق ( % ) |
| 1.02 –0.66 | 0.94 | L.S.F. | عامل الاشباع الجيري ( % ) |
| المركبات الرئيسية % بموجب معادلات Bogue | | | |
| 54.52 | | | سليكات ثلاثي الكالسيوم ( C3S ) |
| 16.64 | | | سليكات ثنائي الكالسيوم ( C2S ) |

| | 7.51 | الومينات ثلاثي الكالسيوم ( C3A ) |
|---|---|---|
| | 10.18 | حديد الومينات رباعي الكالسيوم  ( C4AF ) |

الجدول (3 ) خواص الركام الناعم

| حدود المواصفة العراقية ( م.ق.ع /45 / 1984 ) | نتائج الفحص | الخواص الفيزيائية |
|---|---|---|
| – | 2.5 | الوزن النوعي |
| – | 3.1 | معامل النعومة |
| – | % 1 | الامتصاص |
| – | 1630 كغم/م³ | الكثافة الجافة المرصوصة |
| لا تزيد عن 0.5 % | 0.35 % | محتوى الأملاح الكبريتية |

الجدول (4 ) تدرج الركام الناعم

| حدود المواصفة العراقية ( م.ق.ع /45 / 1984 )  منطقة التدرج رقم ( 2 ) | النسبة المئوية العابرة وزنا | مقاس فتحات الغربال (ملم ) |
|---|---|---|
| 100 | 100 | 10 |
| 100−90 | 92.39 | 4.75 |
| 100−75 | 75.21 | 2.36 |
| 90−55 | 59.24 | 1.18 |
| 50−35 | 46.19 | 0.6 |
| 30−8 | 10.16 | 0.3 |
| 10−0 | 0.07 | 0.15 |

**الجدول ( 5 ) تدرج الركام الخشن**

| حدود المواصفة العراقية ( 14/5 ) ملم ( م.ق.ع /45 /1984 ) | النسبة المئوية العابرة وزنا | مقاس فتحات الغربال ( ملم ) |
|---|---|---|
| 100 | 100 | 20 |
| 90−100 | 94.5 | 14 |
| 50−85 | 57.34 | 10 |
| 0−10 | 0 | 5 |

**الجدول (6 ) خواص الركام الخشن**

| حدود المواصفة العراقية ( م.ق.ع /45 / 1984 ) | نتائج الفحص | الخواص الفيزيائية |
|---|---|---|
| – | 2.65 | الوزن النوعي |
| – | 0.5% | الامتصاص |
| – | 1700كغم/م³ | الكثافة الجافة المرصوصة |
| لا تزيد عن 0.1 % | 0.05 % | محتوى الأملاح الكبريتية |

**الجدول (7) الخصائص التقنية للملدن المتفوق المستخدم في البحث.**

| خواص الملدن المتفوق المستخدم | الخاصية الأساسية |
|---|---|
| اصفر فاتح | اللون |
| 1.05±0.02@ 25 C° | الكثافة النسبية |
| -3 C° | درجة الانجماد |

الجدول (8 ) خواص البولي ايثيلين ذو الكثافة المرتفعة و المنخفضة.

| | LPED | HPED | 13 | الخواص العامة للمنتج |
|---|---|---|---|---|
| | 17<br>14<br>0.29<br>500<br>( 0.94 –0.92 ) | 31<br>40<br>1.86<br>100<br>( 0.97–0.95 ) | | مقاومة الشد ( ميكا باسكال )<br>مقاومة الانثناء ( ميكا باسكال )<br>معامل المرونة ( كيكا باسكال )<br>نسبة الاستطالة عند القطع ( % )<br>الكثافة ( غم / سم³ ) |

الجدول ( 9 ) تفاصيل الخلطات المستخدمة .

| w/c | الملدن المتفوق لتر/ م³ | الماء لتر/ م³ | البولي ايثيلين ذو الكثافة المرتفعة ( نسبة استبدال حجمي من الرمل ) | | الرمل كغم/ م³ | الحصى كغم/ م³ | السمنت كغم/ م³ | رمز الخلطة |
|---|---|---|---|---|---|---|---|---|
| 0.37 | 4.365 | 182.4 | 0 | 0 | 820 | 748 | 485 | R |
| 0.37 | 4.365 | 182.4 | 0.025 | %5 | 779 | 748 | 485 | HDPE1 |
| 0.37 | 4.365 | 182.4 | 0.05 | %10 | 811.8 | 748 | 485 | HDPE 2 |
| 0.37 | 4.365 | 182.4 | 0.075 | %15 | 697 | 748 | 485 | HDPE3 |
| 0.37 | 4.365 | 182.4 | 0.025 | %5 | 779 | 748 | 485 | LDPE1 |
| 0.37 | 4.365 | 182.4 | 0.05 | %10 | 811.8 | 748 | 485 | LDPE 2 |
| 0.37 | 4.365 | 182.4 | 0.075 | %15 | 697 | 748 | 485 | LDPE3 |

**الجدول ( 10 ) نتائج فحص مقاومة الانضغاط للخرسانة الحاوية على البولي ايثيلين**

| مقاومة الانضغاط ( نيوتن/ملم² ) | | | |
|---|---|---|---|
| 60 | 28 | 7 | البولي ايثيلين ذو الكثافة المرتفعة |
| 60 | 47 | 43.35 | 0% |
| 54 | 43 | 40 | 5% |
| 48 | 40 | 38 | 10% |
| 47 | 38.6 | 34 | 15% |
| 60 | 28 | 7 | البولي ايثيلين ذو الكثافة المنخفضة |
| 45 | 31 | 28 | 5% |
| 42 | 28 | 25 | 10% |
| 40 | 26 | 21 | 15% |

**الجدول (11 ) نتائج فحص كثافة الخرسانة الحاوية على البولي ايثيلين**

| الكثافة ( كغم/م³ ) | | | |
|---|---|---|---|
| 60 | 28 | 7 | البولي ايثيلين ذو الكثافة المرتفعة |
| 2480 | 2470 | 2450 | 0% |
| 2467 | 2460 | 2448 | 5% |
| 2445 | 2440 | 2430 | 10% |
| 2420 | 2415 | 2410 | 15% |
| 60 | 28 | 7 | البولي ايثيلين ذو الكثافة المنخفضة |
| 2460 | 2442 | 2400 | 5% |
| 2421 | 2396 | 2370 | 10% |
| 2400 | 2380 | 2330 | 15% |

**الجدول (12) نتائج فحص سرعة الذبذبات فوق الصوتية للخرسانة الحاوية على البولي ايثيلين**

| سرعة الذبذبات فوق الصوتية ( كم/ثا ) | | | |
|---|---|---|---|
| 60 | 28 | 7 | البولي ايثيلين ذو الكثافة المرتفعة |
| 5.3 | 5.1 | 4.8 | 0% |
| 5 | 4.9 | 4.7 | 5% |
| 4.9 | 4.8 | 4.5 | 10% |
| 4.8 | 4.7 | 4.4 | 15% |
| 60 | 28 | 7 | البولي ايثيلين ذو الكثافة المنخفضة |
| 4.9 | 4.7 | 4.6 | 5% |
| 4.7 | 4.6 | 4.4 | 10% |
| 4.6 | 4.5 | 4.3 | 15% |
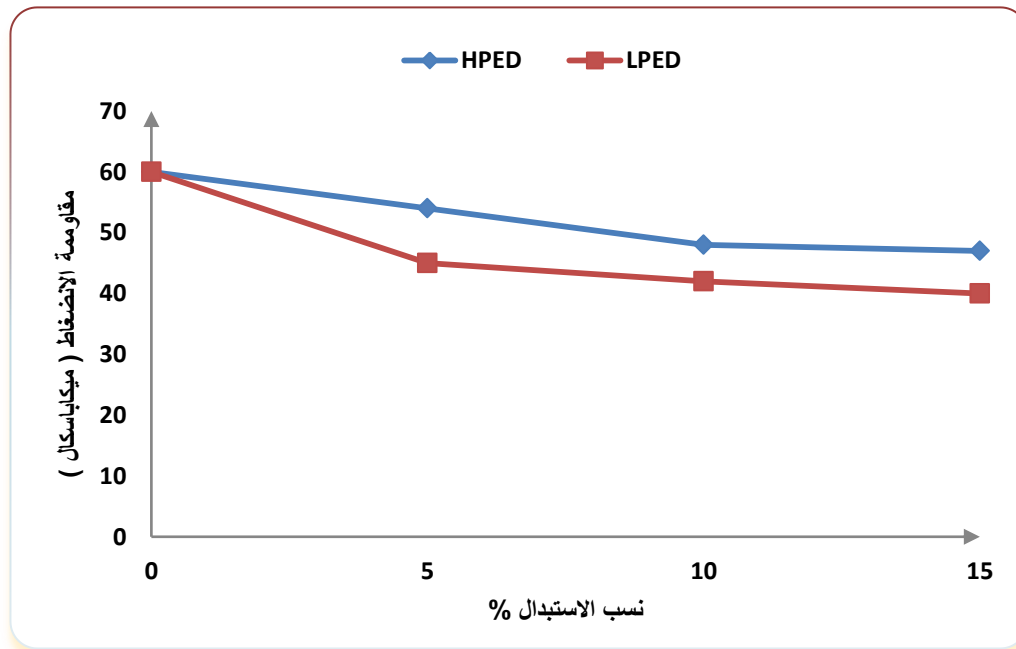


**الشكل (1) العلاقة بين نسب الاستبدال الحجمي للبولي ايثيلين مع مقاومة الانضغاط**
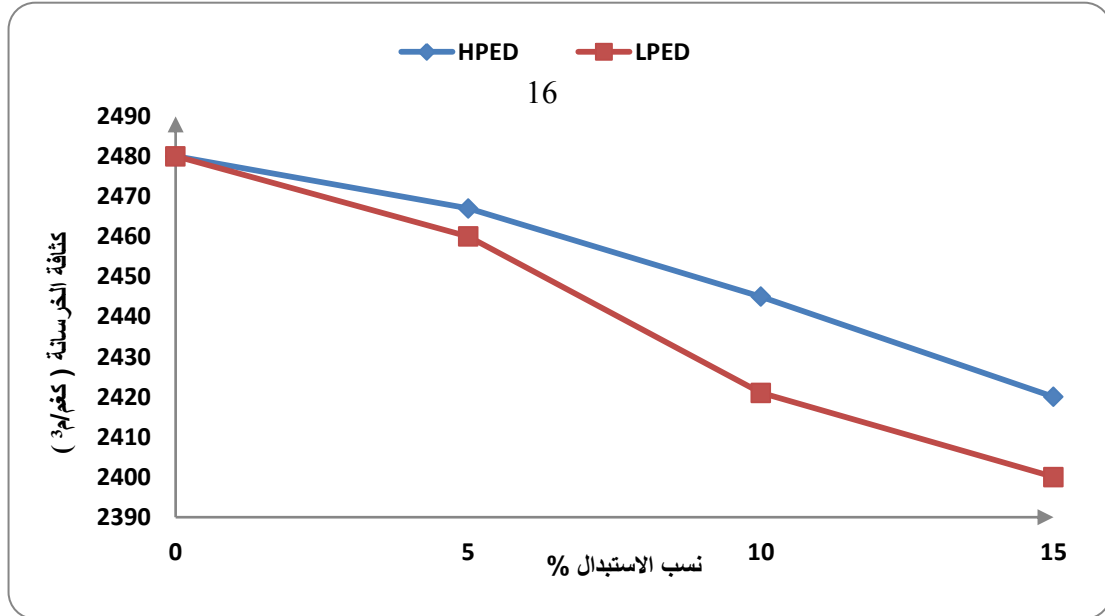
**الشكل (2) العلاقة بين نسب الاستبدال الحجمي للبولي ايثيلين مع كثافة الخرسانة**
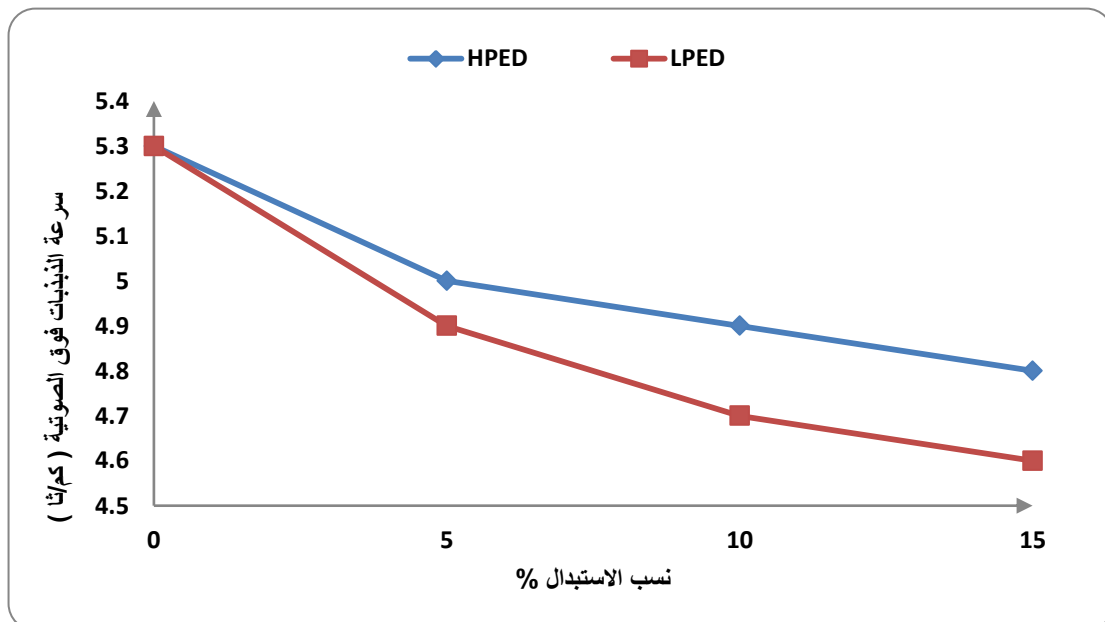


**الشكل (3) العلاقة بين نسب الاستبدال الحجمي للبولي ايثيلين  مع سرعة الذبذبات فوق الصوتية**